Ignition modeling in methane-oxygen rocket engines

Design and modeling of a methane-oxygen rocket engine igniter using reacting flows with computational fluid dynamics

C. Akkermans

Technische Universiteit Delft

TU Delft

Ignition modeling in methane-oxygen rocket engines

Design and modeling of a methane-oxygen rocket engine igniter using reacting flows with computational fluid dynamics

by

C. Akkermans

to obtain the degree of Master of Science
at the Delft University of Technology,
to be defended publicly on Thursday August 31, 2017 at 09:30.

Student number:	1356119
Project duration:	July 1, 2016 – August 31, 2017
Supervisor:	Ir. B.T.C. Zandbergen, TU Delft
Version:	1.0.1

An electronic version of this thesis is available at `http://repository.tudelft.nl/`.

TU Delft

I met a traveler from an antique land
Who said: Two vast and trunkless legs of stone
Stand in the desert... near them, on the sand,
Half sunk, a shattered visage lies, whose frown,
And wrinkled lip, and sneer of cold command,
Tell that its sculptor well those passions read
Which yet survive, stamped on these lifeless things,
The hand that mocked them and the heart that fed:

And on the pedestal these words appear:
'My name is Ozymandias, king of kings:
Look on my works, ye Mighty, and despair!'
Nothing beside remains. Round the decay
Of that colossal wreck, boundless and bare
The lone and level sands stretch far away.

- Percy Bysshe Shelley *1818*

Preface

At the start of the Msc thesis project you are told that the goal is to make a contribution to the field in which the thesis is to be done. In this manner the bar is set at an almost impossible level; how can a mere mortal soul ever hope to make a meaningful contribution to a field which was dominated by the smartest minds with virtually unlimited budget and a nuclear arms race to lose? The sheer volume of knowledge to be covered between rocket engine and igniter design, numerical methods, chemistry and fluid dynamics, and experimental validation was daunting from time to time. While the masters program itself provides a good foundation much of these topics is not covered.

Never the less I think I succeeded in finding a small niche in which some stones remain unturned and a few secrets are kept hidden. Above all this thesis became a personal journey into the deep waters of CFD with reacting flows and a fight to obtain what little publicly available information is available in the field of rocket engine igniter design.

The work of Poinsot and Veynante, both in the form of the book Theoretical and Numerical Combustion, as well as their work on laser ignition has been of great value in helping me understand the concepts required to perform my work. The standard works on computational fluid dynamics by Versteeg, and Ferziger and Peric were a great foundation and fall back.

Mister Zandbergen was ever helpful in reviewing my work and while sometimes his endless questions became a pain they surely kept me sharp leading to a better final work. His enthusiasm for the field of rocket engine design can be contagious from time to time. Mister van Zuijlen was helpful in providing pointers and clarifying for some of the challenges I ran into with computational fluid dynamics.

Verifying and validating my work proved to be highly challenging due to the lack of publicly available data. Design of experiments is difficult because no objective measures for quality for match between predicted and observed flow fields is available. A lot of the work being performed in this field by professionals seems to be based on vast amount of experience.

In the end I think I managed to scratch the surface on modeling ignition in rocket engines. Above all this work clearly underlines the missing links in modeling ignition and is perhaps the very first work in which the complete path to setting up such a model is fully documented.

C. Akkermans
Delft, August 2017

Contents

Summary

Achieving reliable and timely ignition is critical to the correct functioning of chemical rocket propulsion systems. Designing ignition systems and experimentally verifying correct ignition of a rocket propulsion system is both costly and time consuming. Being able to accurately model ignition offers to possibility to speed up and to reduce cost of the design and validation of rocket engine ignition systems.

Major aeronautical and space institutions such as NASA, DLR and Airbus have demonstrated the ability to model rocket engine ignition and/or the ability to leverage modeling tools improve ignition system design. Published literature is however limited and lacking in completeness regarding the implementation details of a model capable of accurately modeling ignition. Particularly the choice of chemistry modeling is insufficiently elaborated and presented conclusions are at times conflicting.

The goal of this work is to identify the effects of using different chemical reaction schemes, and to a lesser degree, the effect of using different chemistry models on the modeling of ignition in a LOX/CH4 rocket engine. In order to limit the scope and time required to produce meaningful results it is decided to limit the work to modeling ignition inside the rocket engine igniter which operates on gaseous methane and oxygen. In this manner the computational domain remains limited in size and complex effects such as atomization and vaporization can be omitted.

In order to simulate ignition an igniter design for an experimental LOX/CH4 rocket engine of Delft Aerospace Rocket Engineering is produced. The designed igniter is of the spark-torch type and aims to generate sufficient thermal power to ignite 10% of the main combustion chamber mass flow. Equilibrium chemistry is used to predict the thermal output of the igniter per unit mass allowing the igniter to be sized. The igniter design uses an automotive spark plug to initiate combustion and is connected to the main combustion chamber via a sonic throat. The design contains two planes of symmetry which can potentially be exploited to reduce the size of computational domain of the model.

The numerical model for ignition is implemented in ANSYS Fluent and makes use of the Fluent implementation of Reynolds Averages Navier Stokes (RANS) code. Turbulence is modeled using the two equation $\kappa - \epsilon$ turbulence model and radiation using the P-1 model. The gas state is either modeled as ideal gas or as real gas using the Peng-Robinson ideal gas model. Chemistry is modeled using one of the following methods: equilibrium chemistry based PDF methods using mixture ratio transport, solely finite rate chemistry, the Eddy Dissipation Model (EDM) or the Eddy Dissipation Concept (EDC) combined with finite rate chemistry. For cases using finite rate chemistry either a single step, two step and four step chemical kinetics model for the combustion of methane is used. Wall temperatures are assumed to be constant in order to model worst case thermal performance.

The model is applied to four different meshes, three of which exploit symmetry to reduce the size of the computational domain and one in which the full geometry is included. Of the former three meshes one includes inflow regions to enable modeling the injection orifices and one includes an outflow region beyond the sonic nozzle. The model is solver using the Semi-Implicit Method for Pressure Linked Equations (SIMPLE) and second order spatial discretization.

In order to answer the research question cases are run assuming both an ambient 1 bar exhaust pressure, and at an elevated exhaust pressure of 40 bar which represents conditions once the main combustion chamber has ignited. First cases are run and verified using solely cold flow after which subsequently the equilibrium chemistry based PDF model is employed, solely finite rate chemistry, EDM and finally EDC. The solely finite rate and EDC cases are in addition run with all of the different chemical kinetics schemes. All of these cases use the quarter geometry mesh exploiting symmetry and excluding extended inflow or outflow regions.

Cases employing a real gas model failed due to numerical instability and cases using the two and four step chemical kinetics models failed to converge to a stable solution. Due to the high required computation time the EDC cases are only simulated using ambient exhaust pressure. Transients simulations could not be performed due to excessive required computation time. Applying relaxation to the solver equations was frequently required to maintain numerical stability in the model.

Additional cases are run for verification and validation purposes and for sensitivity analysis. Grid independence of the solution is proven using a grid convergence study. The cold flow is positively verified against analytically predicted nozzle flow. All cases are checked for sanity by verifying conservation of mass. The assumption that symmetry can be exploited to reduce the size of the computational domain is checked and found valid for all except highly detailed flow features. Influence of inclusion of radiation modeling is verified to be negligible.

Chemistry is validated against two different equilibrium chemistry software packages and is found to not exceed upper limits. It is however shown that the equilibrium chemistry based PDF model does predict way lower than predicted temperatures due to incomplete combustion. Modeling of igniter injector conditions is shown to be highly inaccurate, demonstrating the need for using a real gas model instead of ideal gas. Finally two experimental validation approaches are proposed, one of which is simple and can be applied to the current igniter design, and one which is more involved using Schlieren photography and/or OH emission imaging with a windowed combustion chamber.

Using the obtained results it is concluded that using extended inflow regions is of importance to accurately modeling propellant injection. The model predicts favorable mixing near the spark plug electrode location. The influence of initial hardware temperature which is in other literature claimed to have a significant influence on ignition is shown to have limited influence on thermal power. The model predicts a thermal power of 23% to 82% of the design thermal power, depending on the exact chemical model selected. The equilibrium chemistry based PDF cases predict a very low thermal power due to incomplete combustion.

The flame shape and location of maximum temperature is shown to be highly dependent on the chemistry model being used. In addition it is shown that the two step chemical kinetics model behaves differently between the cases using solely finite rate chemistry and the cases using the EDC. These observations lead to the conclusion that the choice of the chemistry model highly influences the results both in terms of predicted power as the predicted flame shape.

The required computation time to produce converged solutions for the cases in which more complex chemistry models such as the EDC are used ranges in the dozens of hours on a modern PC. In order to simulate ignition transients much more powerful hardware will need to be used. Numerical stability is an issue with the more complex chemical models and real gas models and will need to be looked in to.

The lack of mention or explanation in literature of the numerical stability encountered, high computational cost, tuning of model coefficients for the EDM and EDC and differences in results between chemical models when used in context of rocket ignition underline the problem statement of this work. While no full answer to the posed research questions could be produced a clear and well documented road map is presented on the construction of a model for modeling ignition.

Glossary

AMG Algebraic Multi Grid - A technique used in Navier Stokes solvers to accelerate convergence using multiple grids of differing resolution.

CCD Charge-Coupled Device - A major semiconductor based technology for constructing imaging arrays for use in digital cameras.

Chemical kinetics A system of reaction equations and rate coefficients which are used in the chemical model.

Chemical scheme Synonymous to chemical kinetics.

Chemical model The model used to represent chemistry.

Combustion chamber Dedicated chamber where combustion of propellants is to take place. Major component of any rocket propulsion system.

CFD Computational Fluid Dynamics - The field of numerically solving fluid flows using computers.

CH4 Methane.

EBU Eddy Break Up - A model for capturing combustion in premixed turbulent flow in which infinitely fast chemistry is assumed.

EDM Eddy Dissipation Model - A model for capturing the effect of turbulent mixing on reacting flow. In the eddy dissipation concept infinitely fast chemistry is assumed. An extension to EBU for non premixed turbulent flow.

EDC Eddy Dissipation Concept - An extension to the EDM in which finite rate chemistry is assumed.

EMI Electro Magnetic Interference - The process of electronic radiation causing unintended interference in an electrical system.

GOX Gaseous Oxygen.

Hard start Start of a rocket propulsion system where excess propellant accumulated in the combustion chamber giving rise to an unindented pressure spike during ignition.

Hypergolic Property of two substances to react directly without the need for an external stimulus when coming into contact.

Igniter The part of an ignition system tasked with delivering the stimulus for ignition.

Ignition The state of combustion being established.

Ignition system The complete system tasked with delivering the stimulus for ignition including the igniter, controller and other supporting systems.

Kerosene Refined hydrocarbon fuel.

LES Large Eddy Simulation - A numeric technique in which all relevant scales of turbulence are completely simulated and only smaller turbulent quantities are averaged. This is in contrast to RANS in which all turbulent flow quantities are averaged.

LESTF Large Eddy Simulation Thickened Flame - A method to model flame in a LES simulation in which the flame boundary is thickened to ensure that the flame is properly captured.

LOX Liquid oxygen.

NCC National Combustion Code - NASA developed numerical model for simulation combustion in fluid flows.

PDF Probability Density Function, used to refer to chemistry models which use mixture fraction transport in conjunction with a statistical model to prepresent reacting flow.

Prechilling The process of lowering the temperature of hardware prior to commencing operations. Usually aimed to prevent boiling of cryogenic fluids.

Relaxation factor A factor used in the solution finding process of a numerical simulation which controls the magnitude of the calculated correction for each iteration.

RP-1 Rocket Propellant 1 - A refined form of kerosene used in rocket engines.

RANS Reynolds Averaged Navier-Stokes - A numerical technique in which the Navier-Stokes equations are solved by averaging all turbulent quantities.

SIMPLE Semi-Implicit Method for Pressure Linked Equations - Numerical procedure used for solving Navier-Stokes equations.

Thrust chamber Combustion chamber of a rocket propulsion system.

Turbulence model A model used to model turbulent flow quantities. Required in RANS based fluid dynamics models.

Under relaxation The practice of setting one or more relaxation factors to a value below one.

List of Figures

List of Tables

1 Introduction

The ignition system of rocket propulsion systems has proven to be a frequent source of failure in spaceflight in the past [52]. The launch of an Ariane 3 failed in 1985 after the second stage failed to ignite properly [16] dooming the two satellites on board. The total financial loss resulting from this failure is estimated at around EUR 1 billion [30].

The task of igniting a rocket is a difficult one. Ignition needs to be timed with sub-second precision while simply running the ignition system for longer periods prior to the required moment of ignition has problems of its own. Rocket engine walls in which no propellant is circulated are sensitive to heating and the engine needs to be cooled prior to start, which conflicts with an early start of the ignition system.

The requirement for sub-second timing of ignition is illustrated in Figure 1.1 in which the relation between the time t to the chamber pressure P relative to normal chamber pressure P_∞ is given [14]. A number of lines are drawn representing different ignition delays τ, each of them starting with a vertical ascent to the striped line which is the maximum pressure at ignition P_0. Key is the consideration that the horizontal time axis is scaled by the time propellants typically reside in the combustion chamber, typically referred to as the blowdown time t_c. This blowdown time is typically in the one to two microseconds range [14].

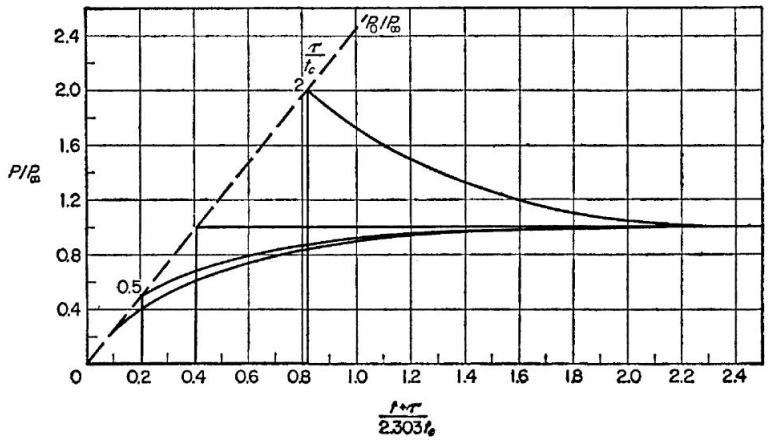

Figure 1.1: Ignition pressure P over operating pressure P_∞ ratio $\frac{P}{P_\infty}$ versus ignition delay τ plus time after ignition t over the blowdown time of combustion chamber t_c ratio $\frac{t+\tau}{2.303t_c}$. Showing effect of ignition delay on the chamber pressure. Source: [14]

Rocket engines are engineered with minimal margins in order to save mass and depending on type operate with chamber pressures well over 100 bar. Considering the short blowdown t_c time and these high operating chamber pressures P Figure 1.1 clearly implicates the grave results of delaying ignition. Failing to

achieve ignition within a time frame of equal magnitude to the millisecond chamber blowdown time will result in to much propellant having accumulated in the chamber causing explosive engine failure.

It should thus not come as a surprise that all the leading authors on rocket propulsion system design recognize the critical importance of attaining controlled and reliable ignition [17, p. 120] [44, p. 320] [45, p. 70]. The core problem statement of ignition is thus formulated as:

An improperly functioning ignition system can lead to further failures in a rocket propulsion system which lead to loss of the mission.

Because fairly little information on the design, modeling and testing of ignition systems was available within DARE and Delft TU, a literature study was performed to uncover these details behind ignition system design [3]. This document is a proposal to further the knowledge on ignition system design by investigating the effects of selecting different chemical models on modeling ignition.

1.1. Scope and context

At Delft Aerospace Rocket Engineering (DARE) students have gathered a lot of experience building and testing solid and hybrid rocket engines in the thrust range from tens of N to over ten kN [24]. In order to develop even higher performing propulsion systems DARE is now looking to expand their research and experience into liquid cryogenic propulsion systems. To this end a team of students within DARE of which the author of this work is a member is looking to design, build and test a small scale cryogenic liquid bi-propellant demonstrator engine [19]. A logically following step is the selection, design and testing of a suitable ignition system for this rocket engine.

The faculty of Aerospace Engineering of Delft TU has shown interest in liquid rocket propulsion technology before, for example in the Msc thesis work of M. Mostert [32]. This thesis aims to expand the knowledge on liquid rocket propulsion technology at both DARE and Delft TU. In addition it aims to provide a baseline model suitable for designing a spark torch ignition system for the 3 kN LOX/CH4 demonstrator engine being developed at DARE [19].

As part of the Msc Aerospace Engineering educational program at Delft TU students are required to complete a 7 month thesis which is preceded by a 12 week literature study on their thesis subject. The thesis subject is required to be a technical subject which is related to the program of study and should be of sufficient academic depth. Students are expected to be familiar with the concepts of rocket propulsion at the moment of starting their thesis [51].

1.2. Problem statement

In the introduction the case for the core problem statement was made in which the requirement for a functional ignition system is described. In the literature study which preceded this work the design methodology and models used to come to a functional ignition system were explored [3]. Due to the scope and context of this project the complete design of an ignition system is however considered to be an overly broad subject.

In the literature review it was demonstrated that one of the key design tools in ignition system design is the capability to model ignition itself [3]. Being able to model ignition with sufficient accuracy can save on highly expensive full scale ignition tests and can speed up rocket engine design.

An important component of these models for ignition is the model used to represent the chemistry combustion [3]. The literature review showed that various chemical models have been applied to model combustion, leading to very good results, but sometimes also to lesser results [3]. The multitude of models available and their differing detail in terms of species and reactions included raises the question of which chemical model is to be employed in an ignition model. A graphical sketch of this breakdown is shown in Figure 1.2.

An added complication is that the kinetics of the system itself need to be obtained and that those sources are slim and that the work of deriving the kinetics is not trivial [3] [35]. Following this breakdown and taking

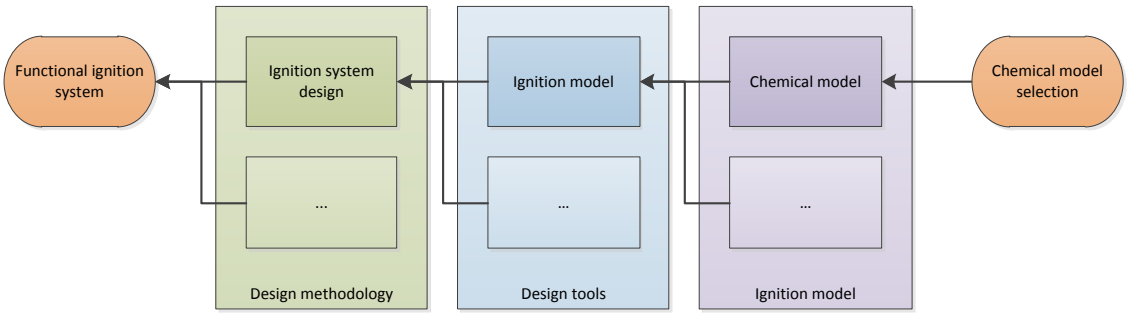

Figure 1.2: Breakdown of the core problem statement to chemical model selection.

the context of the design of a 3 kN LOX/CH4 demonstrator engine into account the problem of selecting a chemical model can be limited to models covering combustion of methane with oxygen. The problem statement for this proposal is then formulated as follows:

Selecting an appropriate chemistry model to represent combustion in the modeling of ignition of LOX/CH4 rocket propulsion systems is not possible due to a lack of comprehensive comparative studies on these chemistry models.

This work will thus start off with an attempt to address the presented problem statement. Performing a comparative study on the available chemistry models used in modeling ignition is however no easy feat as it means that a complete model for ignition needs to be designed. In order for such a model to have any value also an igniter design is required. For the study to have any value the resulting model must be verified and validated as well. The steps to providing a solution to the problem statement are thus numerous and reach far beyond evaluating solely the chemistry models themselves.

A more formal introduction of the research objective and questions is presented in Chapter 2. From those a thorough research setup is derived which acted as a guideline for most of the work performed in this study.

1.3. Challenges

In the literature study it was found that the only work in which a truly comprehensive overview is given on the construction of a numerical model for ignition is in the work of G. Lacaze, T. Poinsot, et al [26]. In addition the book Theoretical and Numerical Combustion by T. Poinsot and D. Veynante is, while being slightly dated at the moment of writing, an invaluable source of background information on modeling numerical combustion [35].

Beyond these two works there are some high quality papers which place focus on how to validate models for ignition as well on how to characterize ignition itself. The first of which is the work by M. Wohlhüter, C. Manfletti, et al [49]. The other is the work solely performed by C. Manfletti [29]. Finally there are various works by NASA and CIRA which provide some useful results on modeling ignition but in which the details on the implementation of the model are shallow at best. Virtually all other works which were identified are either highly outdated, provide little useful information on modeling ignition, use only analytical models, or focus on characterizing ignition instead of modeling ignition.

While the motives for disclosing so little information behind the aspects involved in modeling ignition can only be guessed upon, it does mean that attempting to construct exact such an model is unlikely to be an easy endeavor. In may thus during this work become clear that the initially set goals need to be adjusted or that unexpected challenges arise.

The impact of these challenges is primarily discussed in the Chapters 6 and 5 which respectively deal with verification and validation and the discussion of the results.

2

Research setup

This chapter formalizes the research setup based on the problem statement given in the introduction. A number of research questions are presented and the methodology using which it is attempted to answer these research questions is presented.

2.1. Research objective

In context of the given the problem statement from Section 1.2, the perceived role of the chemical scheme in modeling ignition and the lack of a comparative study on the different chemical schemes available, it is decided to perform an experimental study on the effects of choosing different chemical schemes for modeling ignition. The research objective of this study is formulated as follows:

The objective of this research is to characterize the effects of using different chemical reaction schemes on the modeling of ignition of LOX/CH4 rocket engine using a spark torch igniter by comparing numerical results from these different chemical schemes.

Before research questions are synthesized from the objective some simplifications and limitations need to be applied to the proposed project. These limitations are required in order to make the project fit the scope. Attempting to build an ignition model from scratch will be extremely time consuming. These limitations and their rationale are:

Existing CFD tools In order to limit the time required to develop the CFD model the aim is to use existing implementations of CFD solvers, turbulence models and turbulence chemistry interaction models. Using existing models avoids having to deal with a lot of the complexities of developing numerical implementations of these models.

Igniter ignition modeling only While ignition takes place both in the igniter and the combustion chamber it is chosen to solely model ignition in the igniter. On the one hand this limits the usability of the model, but on the other hand a spark-torch igniter is very much alike to a rocket engine itself. Since especially the chemical scheme used is under scrutiny in this study the conclusions can be extended to modeling ignition in main combustion chambers as well. Some thrust chambers are directly ignited by a spark, making them conceptually similar to a spark torch igniter. If combustion is accurately modeled in a spark torch igniter it is likely that as long as the propellant combination is the same the model can be extended to model combustion of a full thrust chamber as well by extending the computational domain to include the thrust chamber.

Solely gaseous propellants In case a common feed system is used, it is likely that the ignition system is supplied with liquid oxygen and/or liquid methane. Modeling would in this case require taking account droplet tracking, propellant atomization and vaporization which greatly complicates the model. Due to time constraints it is assumed that both propellants are fully gaseous. Figure 2.3 provides an illustration of the model components which can be omitted due to using solely gaseous propellants.

Default radiation models None of the studies reviewed during the literature study make any mention of the radiation model used [3]. While radiation is an important factor in the thermal design it is deemed unfeasible to also include a detailed evaluation of radiation modeling in this study.

2.2. Research questions

Working from the given research objective a number of research questions are formulated which further focus on the aspects of the used of different chemical schemes. Areas of focus are the general usability of the model in terms of computational cost as well as how the model fits in the larger picture. Next the difference between models is evaluated in relation to the requirements to which an ignition system is to be designed. Reason for doing so it that in the grander scheme of things an ignition model is to be used in the design of ignition systems. In this role the model should be able to tell if the design is either passing or failing the requirements. Finally attention is spent on verification and validation of the developed models as no numerical study would be complete without verification and validation.

In order to fully define the research questions some additional definitions are required. These definitions are as follows:

Ignition Ignition is defined as the state of the flow field reaching a point from where it is reasonable to assume that established flame will not go extinct without cutting propellant flow. This is when the flame is fully spanning the combustion chamber.

Total power The total thermodynamic power of the exhaust flow. This value is both for analytical verification as well as being a design parameter for the igniter.

Response time The time to which the igniter approaches stable operation, if ignition occurs. The igniter response time is a design parameter of major importance. Two measures of response time will be used: one will be the time until ignition is achieved the second is until 90% of the steady state power is produced by the igniter.

Minimum ignition energy The energy required to achieve ignite in a combustion chamber using a spark or laser pulse. Measured as the energy deposited into the gas, which is less than the energy in the

The research questions and corresponding subquestions are now formulated as follows:

1. What are the effects on required computational power from choosing different chemical schemes?

One of the first and foremost reasons not to use a chemical scheme of full fidelity is the associated computational cost. Truncating of simplifying the scheme reduces the computational cost. This does however raise the questions of how much computational time is saved by doing so. This research question aims to provide an answer to that question.

2. What are qualitative differences in the results arising from the use of different chemical schemes?

This research question is subdivided in subquestions in order to investigate different qualitative aspects of the predicted ignition behavior. These questions aim to identify any differences in the observed behavior of the model which are not easily described in numbers.

2.1. What are differences in flame front development?

From the literature study it was found that the flame front development is one of the key methods to validate a numerical model [3]. Any clear differences in the shape or manner in which the flame front develops between different chemical schemes would be a clear early indication of the effects the chemical scheme has on the results.

2.2. What is the effect on observed reliability of ignition?

Achieving reliable ignition is one of the key requirements and any differences in the observed reliability of ignition arising from picking different chemical schemes would be of interest. It is likely that the results of this question are coupled to the observed minimum required ignition energy as it was observed that ignition may take multiple sparks before being fully established [3]. Due to the stochastic nature of the spark (model) and turbulence determining the ignition reliability requires a Monte Carlo like approach in which a number of simulations under equal conditions need to be run to be able to derive a statistically relevant ignition reliability.

Especially the early stages of flame front development after the spark are of interest as this is the period in which any errors in the chemical model will have the largest effect on the initiation of the flame.

3. What are quantitative differences in results from different chemical schemes?

This research question will focus on the quantitative differences between different chemical schemes. The aspects focused on are related to the ignition system parameters which are listed in the literature review [3]. The subquestions formulated are as follows:

3.1. What are the differences in predicted igniter response time?

R ignition was determined to be one of the key requirements for any ignition system [3]. In case choosing different chemical schemes is found to have influence on the time it takes for ignition to take place this is likely to have a significant impact on how the requirement of quick and timely ignition is going to be satisfied.

3.2. What are the differences in predicted minimum required ignition energy required due to choosing different chemical schemes?

A key parameter when designing a spark-torch, direct spark or laser ignition system is determining the minimum required ignition energy [3]. The spark or laser pulse must at least deposit this amount of energy to start combustion. In case picking a different chemical scheme has any influence on this value it is of high importance to quantify this effect. Because the chemical scheme is fundamental to the combustion being modeled it is to be expected that picking different chemical schemes will have some effect on the minimum ignition energy.

3.3. How does the predicted bulk power compared to analytically predicted bulk power?

In non of the reviewed literature a clear relation between the analytical bulk power method and numerical results is drawn [3]. While one paper from DLR briefly touches upon this subject, no direct comparison is made [26]. As different chemical schemes will invariably have some effect on the predicted chemistry, it is of interest to see how well each chemical scheme compares to the analytical method.

In addition answering this subquestion is a verification step since any major discrepancies between analytical results and numerical results will be an indication of issues with the numerical code.

4. How do the results from different chemical schemes compare to experimental data?

While all of the previous research questions focus on the differences between the results obtained using different chemical schemes, a very important question is how these results compare to reality. In case the results do not very accurately match reality it is of interest to get a handle on the size of the error made. Validation is a key step when building models and is the final step before the developed model can be used in real world applications. Being able to answer this question does however depend on the availability of experimental data, which may be difficult to obtain.

From the literature review it can be concluded that key output parameters to compare with experimental data are high frequency pressure and temperature measurements [3]. If available flow field topology obtained using Schlieren or shadowgraph imaging can be used for comparison as well. Finally OH emission imaging may be used to compare numeric chemical activity with real world chemical activity.

5. How can the results be applied to improve the used ignition system design?

This research question aims to obtain an answer how the obtained results can be used in designing an ignition system for the demonstrator engine being developed by DARE. Does the model enable making any improvements to the igniter design used in the study? In this manner the link to the need from which this research proposal has arisen is completed.

2.3. Methodology

The research questions presented are to be answered by running experiments using numerical methods. The process of ignition is to be modeled using reacting flow computational fluid dynamics. The goals is to be able to describe relative differences by implementing different models and comparing results. From these results conclusions are to be drawn which allow answering the research questions.

Performing experiments numerically however does place a lot of importance on verification and validation of the employed numerical models. Verification can be performed against analytical models while validation can primarily be performed against experimental and results from other already validated numerical models.

Experimental data Full validation can be performed by comparing numerical results to experimental data obtained from actual ignition experiments. These experiments however require an instrumented combustion chamber and are only meaningful if equal propellant combinations are used. At Delft TU some of the instruments required are available but the combustion chambers and test sites are not. This complicates validation and requires looking for validation data outside Delft TU. Potential data sources are:

- The HYPROB program of CIRA
- Experiments performed on the M3 burner at DLR Lampoldshausen
- Vinci igniter from Aerospace Propulsion Products BV

Numerical data As an alternative to validation using experimental data it is possible to validate against numerical results from other already validated models. Specifically this would be the models identified in the literature review which performed well [3]. The NCC seems to be inactive and Rocflam-II is proprietary, making it unlikely that numerical data from both models can be obtained from them. The complete list of candidate sources identified is:

- NASA National Combustion Code (NCC)
- Airbus Rocflam-II
- DLR LES code

The degree to which data can be obtained and is useful will be further discussed in Chapter 6.

Verification Verification will primarily make use of the analytical methods which will be used to design the igniter baseline as well as equilibrium chemistry tools. Using equilibrium chemistry tools such as RPA Lite and NASA Chemical Equilibrium with Applications (CEA) bounds for which within the chemistry can be considered sensible can be derived.

2.4. Experimental set-up

This section outlines how the numeric experiments to be performed in this study are to be set up. In order to be able to employ the to be developed numerical model and in order to be able to generate representative data, an igniter design is required. As this study is part of a project aiming to produce an igniter and rocket engine, an igniter design is also a desirable outcome in the greater scheme of things. A first step in the study will be to produce a first order igniter design and accompanying ignition system. Only the igniter part of this

system is required to be detailed.

The next step is to generate the mesh and to compose the numerical model. From this point on it will be attempted to simulate flow, combustion and ignition in ever increasing complexity by progressively switching on more models. The initial simulations will all be steady state solutions while the work will cumulate in a full transient simulation of the ignition process. The resulting high level work breakdown structure is shown in Figure 2.1.

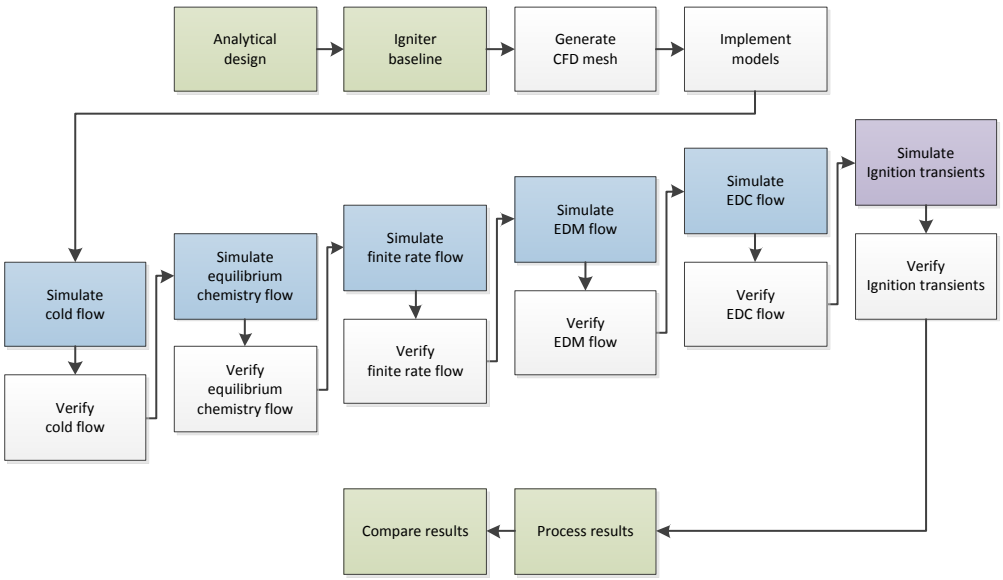

Figure 2.1: High level breakdown of model development approach.

The reason for conducting the simulation experiments in this sequence of increasing complexity is in order to allow for lessons learned from the simpler cases to be applied to the more complex cases. In addition it is expected that getting the numerical model to work correctly in the more complex cases will be difficult. By following an approach in which increasingly more submodels are included chances are higher that usable results are produced.

For each and every case verification and validation need to be covered. This results in the work breakdown shown in Figure 2.2. For some cases not all the verification steps need to be repeated as results are shared between cases.

The next subsections will discuss the steps shown in the work breakdown in Figure 2.2 in more detail and will elaborate on the experimental inputs and outputs.

2.4.1. Mesh geometry

The geometry of the computational domain must not only resemble an ignition device in shape, but must also account for various aspects which are required to ensure good numerical results. These aspects are shortly discussed:

Boundary conditions Appropriate boundary conditions need to be set. In the literature review it was shown that cold walls can have an distinct effect on whether ignition is achieved [3]. This indicates the need for proper boundary conditions in terms of for example temperature.

Wall treatment Near walls the mesh geometry needs to be adjusted in order to reproduce accurate flow conditions. Due to the inclusion of chemistry and the interaction of cold walls with chemistry, it is expected

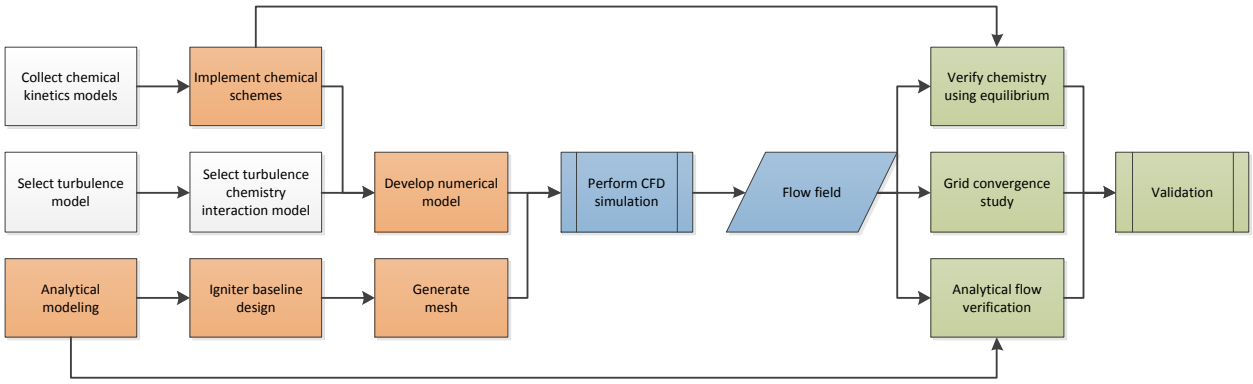

Figure 2.2: High level work breakdown structure. Legend: white are literature/study tasks, orange are programming and design tasks, green are verification and validation tasks, blue are data generation and processing tasks.

that wall treatment is very important in modeling ignition.

Flow development The flow from the injection elements is unlikely to have a uniform velocity distribution due to viscosity and friction. In order to numerically replicate this effect the flow geometry must allow for space for the flow to develop to real world conditions.

Outflow In order to obtain realistic outflow the geometry must accommodate a sufficiently large outflow region with suitable boundary conditions.

Spark region The region where the spark is deposited requires special attention as the mesh mush be sufficiently detailed to capture the spark and initial flame kernel formation.

2.4.2. Numerical CFD implementation

The core of the numerical implementation is the numerical flow solver. The goal is to use an existing CFD solver package to solve the flow. Two CFD packages have been identified which may be suitable for use in this study is ANSYS Fluent.

Fluent is a commercial toolbox for solving a wide range of numerical problems in fluid dynamics. As Delft TU possesses a license for ANSYS Fluent it is possible to leverage this commercial CFD package for this research. In addition ANSYS Fluent has been used in numerous other studies on rocket engine ignition suggesting that it is a good candidate [3] [38].

As Fluent is widely used it is expected that time can be saved on verifying and validating various model component. ANSYS has published a verification and validation report on Fluent which shall be evaluated in further detail in Chapter 6 [7].

2.4.3. Model components

After selecting the CFD solver package all the individual model components displayed in Figure 2.3 need to put to together. In case the CFD solver package does not have implementations of the respective model components they need to be implemented. Because of our earlier made simplification of assuming that all propellants are gaseous the model components required to represent two phase flow are not required and are grayed out in the figure. The model components are:

Transport equations Both the bulk of the mass as well as the transport of individual species through the computational domain needs to be modeled. These are expected to be implemented by the CFD solver package.

Gas state Density, temperature and pressure need to be related. Appropriate gas state equations are also expected to be implemented by the CFD solver package.

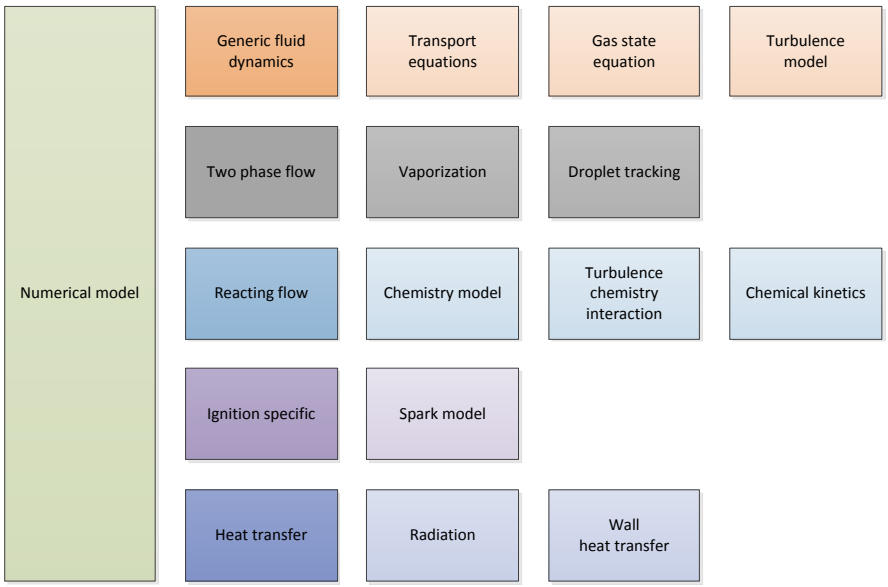

Figure 2.3: Graphical overview of building blocks for numerical model. Two phase flow will not be considered and is grayed out.

Turbulence model Turbulence will be modeled using the standard two equation $\kappa - \epsilon$ model. In case a RANS solver is used turbulence needs to be modeled. The literature review revealed that the two equation $\kappa - \epsilon$ model is typically used for combustion modeling in rocket propulsion devices. Thus this model will be used in this study as well.

Turbulence chemistry interaction The eddy dissipation model (EDM) and eddy dissipation concept (EDC) will be used to model interaction between turbulent flow and chemistry.

Chemistry The manner in which chemistry itself is modeled needs to be selected. This component can be closely linked to turbulence chemistry interaction and may or may not on the chemical scheme. Chemistry models to be evaluated are chemical equilibrium and Arrhenius finite rate chemistry.

Chemical scheme The chemical scheme models the rates of the actual individual chemical reactions and is one of the main points of interest of this study. In the literature a few have already been identified [3], but it may be worth while to try to obtain more. A very detailed chemistry model can be used as a baseline to benchmark other models against. So far the most detailed chemical scheme is the Sandia National Labs 1D flame with 7 reactions. Currently known flame models which are suitable or can be adapted for use in modeling combustion of oxygen and methane are:

- 1 step from Westbrook and Dryer [48]
- 2 step from Westbrook and Dryer [48]
- Multi step from Westbrook and Dryer [48]
- 4 step model by Jones and Lindstedt [35, p. 189] [20]
- Sandia National Labs 1D flame [12]

Spark model The spark energy deposition is modeled using the stochastic model presented in the literature review [3].

Radiation The P-1 radiation model will be used to approximate heat transfer via radiation.

Heat transfer The Euler equations are used to model heat conduction through the igniter walls.

Chapter 4 will introduce the various models in much greater details and will elaborate on the exact reason behind selecting them.

2.5. Experiment inputs and outputs

This section will shortly discuss the foreseen inputs and outputs of the experiment and their relevance. It is from the relation between the inputs and the outputs that the conclusions will have to be drawn which ultimately enable answering the research questions.

2.5.1. Inputs

The following inputs are the main parameters which will be varied during the experiment:

Chemical scheme The different chemical schemes to be used is one of the primary inputs. Their relevance should be clear from the research questions.

Spark energy The energy per spark has a crucial effect on whether ignition occurs. In addition it is a key design parameter for an ignition system [3].

Mixture ratio The mixture ratio is a known driver of the ignitability. Varying the mixture ratio yields insight in the required mixture ratio when designing an ignition system.

Wall temperature During the literature review it was found that some researchers noted a significant impact on performance based on hardware temperature [12] [21]. Varying wall temperature can potentially shed light on the effects on the igniter design being evaluated.

Exhaust pressure An igniter will have to operate at atmospheric pressures but will ultimately also have to cope with the engine starting up and attaining operating pressure. Igniter exhaust pressure shall thus be varied between these two limits.

Mesh The mesh resolution will need to be varied in order to perform a grid independence study.

Boundary conditions The type of boundary condition can be used to test the assumptions made while modeling the inflow elements of the igniter. By comparing the resulting inflow using a pressure boundary condition to the inflow from a mass-flow boundary condition the validity of the

The following inputs are to be held constant during all experiments except for cases of sensitivity analysis.

- Igniter geometry
- Propellant mass flow
- Propellant pressure
- Propellant temperature
- Spark energy deposition model
- Ambient temperature

2.5.2. Outputs

From the simulation the following outputs are either directly obtained or are to be derived. These outputs will be used to answer the research questions.

Computation time The computational time required for each simulation run is of interest to answering research question 1.

Computed flow A CFD simulation yields a complete view of the flow field including velocity, temperature, pressure, density and chemical species. From this flow field various derived results are computed.

Residuals The evolution of residuals over time in a CFD computation are the most important metric for assessing if the obtained solution has converged.

From the computed flow field the following quantitative and qualitative properties are derived. These results will be used to answer the earlier posed research questions. These outputs are:

Ignition A qualitative assessment on whether ignition occurred. As no formal definition of ignition is available ignition is defined as the state of the flow field reaching a point from where it is reasonable to assume that established flame will not go extinct without cutting propellant flow.

Total power The total thermodynamic power of the exhaust flow. This value is both for analytical verification as well as being a design parameter for the igniter.

Response time The time to which the igniter approaches stable operation, if ignition occurs. The igniter response time is a design parameter of major importance. Two measures of response time will be used: one will be the time until ignition is achieved the second is until 90% of the steady state power is produced by the igniter.

Pressure The minimum, maximum and steady state pressure of the igniter. Pressure is both an important igniter design parameter as well as a design driver for the igniter housing.

Flame development A qualitative assessment on flame development after ignition. Qualitative features of interest are the location of the flame and the shape and movement of the initial flame kernel after the spark. Literature review showed that measuring OH concentration and density gradients are proven manners of tracking the flame, which can also be applied in actual experiments [3].

Statistical results Due to the stochastic nature of the spark energy deposition model, it will be required to run multiple instances of each simulation case to collect sufficient data to derive statistically meaningful results. Examples are reliability of ignition and the minimum required spark energy. In order to give any indication of the reliability of the ignition and corresponding confidence interval it will be necessary to perform multiple simulations. Similar considerations apply for the minimum ignition energy.

2.6. Summary

The objective of characterizing the effects of using different chemical reaction schemes on the modeling of ignition of LOX/CH4 rocket engine using a spark torch igniter by using numerical results from these different chemical schemes was set. By defining research questions the exact aspects are defined in which differences are to be investigated in.

The study in this work is to be performed using numerical models. In order to save time an existing CFD solved package is to be used. The numerical model will consist out of transport equations, turbulence model, gas state equation, chemistry model, turbulence chemistry interaction model, chemical kinetics, spark model, radiation and wall heat transfer model. For some of these model multiple variants can be selected with the chemical kinetics model being one of the foremost.

With a numerical study verification and validation are important hence potential data sources for obtaining validation data and verification tools are identified. Finally the inputs and output and their significance for the study have been specified.

3

Igniter baseline design

The goal of the work documented in this chapter is to come up with a first order igniter design which is suitable for use in a numerical model. This chapter will elaborate on the design process and resulting igniter design, which shall be referred to as the igniter baseline design.

In order to come up with a successful design one must set requirements and select the igniter type. These two inputs are then used as starting points to perform a full design iteration of the igniter. First required heating power is derived from which the igniter propellant flows are set. Various methods for deriving the required heating power are discussed and their differences highlighted. The injectors and exhaust are then sized and finally the fully igniter body is designed.

It should be noted that the igniter design serves as a basis for the numerical model which will be developed next. The design of the igniter itself it not the primary deliverable in this study and this the time to be spent on the igniter design will be limited. Hence some details like analysis of thermal loads are skipped. In a study in which the igniter design is the primary deliverable the design cycle will be more involved and will likely include iterations.

3.1. Requirements

The first step in the design process of the igniter is definition of the requirements. Requirements for the igniter design follow primarily from the demonstrator engine specifications. The specifications of the demonstrator engine are listed in Appendix A. Other requirements follow from the context of the igniter being designed for use in a student project. The following requirements are given for the igniter design:

REQ-DESIGN-1 The igniter shall be able to establish combustion in the main engine combustion chamber.

REQ-DESIGN-2 The igniter shall not use any toxic or hazardous materials.
The use of toxic and excessively hazardous materials greatly complicates testing and use of the igniter. Because the igniter is intended to be used in context of a student project the use of such materials is even less desirable.

REQ-DESIGN-3 The igniter shall not require any new technological development.
The goal of the engine development project is to demonstrate the ability to develop a cryogenic rocket engine. Further complicating the project with the development of novel ignition techniques does not ease completing the project goal.

REQ-DESIGN-4 The igniter design shall use a structural safety factor of 2.
Because of the context of use in a student project and the intended use on an experimental engine extra safety is desirable. The use on an experimental engine means that the igniter may be subjected to unexpected conditions.

REQ-DESIGN-5 The igniter shall be reusable for at least 25 ignition cycles.
Igniter reusability is a requirement because the igniter is intended to be used in the development program of a rocket engine. A lot of tests will thus have to be performed. A non reusable igniter will complicate these tests and raise cost in terms of time and money due to a new igniter being needed for every test.

In order for the design to be usable as a basis for a numerical model some other requirements need to be specified as well. Essentially these requirements should be fulfilled when a full igniter design is produced. These requirements are:

REQ-MODEL-1 Internal geometry shall be defined such that a computational mesh can be generated from it.

REQ-MODEL-2 Inflow conditions must be derivable from the design.

REQ-MODEL-3 Outflow conditions must be derivable from the design.

Further requirements will be derived based on the igniter type selected in the next section.

3.2. Igniter type tradeoff

Before commencing on the design of the igniter a igniter type must be selected. Because the goal of this study is not necessarily to come up with the best igniter design only limited effort is spent on selecting a suitable igniter type. In the literature review which preceded this study a number of ignition methods were identified and described [3]. The following igniter types are considered:

Pyrotechnic Ignition system which relies on solid propellants to generate a hot gas stream used to ignite the propellants in the main combustion chamber.

Hypergolic Ignition system which uses either two igniter propellants which are hypergolic with each other or a single igniter propellant which is hypergolic with one of the main propellants to initiate combustion.

Spark plug Ignition system which solely relies on a spark plug to initiate combustion in the main combustion chamber.

Spark-torch Ignition system which uses a separate igniter combustion chamber with a spark plug to generate a hot gas stream, which in turn is used to ignite the propellants in the main combustion chamber.

Laser Ignition system which employs laser energy to ignite the propellants in the main combustion chamber.

Catalytic Ignition system which uses a catalyst to decompose igniter propellant into a a hot gas stream which is used to ignite the propellants in the main combustion chamber.

In the literature review the described ignition methods were compared based on four properties: technological readiness, reliability, suitability for reusable and restartable propulsion systems and their ease of handling. Cost, mass and size were omitted from the comparison because they require a more detailed design phase or are hard to estimate. For this study cost, mass and size are not directly of interest either. It is therefore decided to directly perform the igniter type trade-off based on the scores as assigned in the literature review.

From the earlier given requirements it follows that technological readiness, handling and reusability are the most important factors to consider. An overview of these scores is given in Table 3.1.

Based on the results in Table 3.1 it is concluded that a spark-torch based ignition system has the most favorable score on the selected properties. In addition the spark-torch excels on the aspects of technological readiness, handling and reusability which are part of the requirements. It is therefore decided to select the spark-torch type ignition system to further conduct this study.

Igniter type	Tech readiness	Reliability	Reuse and restart	Handling
Pyrotechnic	High	High	Low	Medium
Hypergolic	High	High	Medium-High	Low
Spark plug	High	Medium	Medium-High	High
Spark-torch	High	High	High	High
Laser	Medium	High	High	High
Catalytic	Medium-Low	High	High	Medium-High

Table 3.1: Comparison of igniter types based on selected properties [3].

The spark-torch igniter will be connected to the main combustion chamber via a tube and throat. Including a throat separates the igniter and main combustion chamber to some degree because disturbances are unable to propagate upstream in a supersonic flow. This separation is only to some degree because ignition transients may raise the main engine combustion chamber pressure to values above which sonic flow can exist. It is only in the detail design that this separation can be guaranteed.

Having selected an igniter type a number of extra requirements can be derived. Each of them is shortly discussed in the following list:

REQ-TYPE-1 The igniter shall be able to heat a sufficient fraction of the engine propellant flow above its auto ignition temperature to initiate combustion.
Spark torch igniters work by heating a fraction of the main engine propellant flow.

REQ-TYPE-2 The igniter shall provide the required power for one second.
The amount of time the intended power is delivered is set in a fairly arbitrary manner at this point. The modest size and absence of a pump should allow the feed system to develop to full flow fairly quickly. More detailed analysis is likely to yield a different required duty cycle.

REQ-TYPE-3 The igniter shall be connected to the main combustion chamber via a sonic throat.

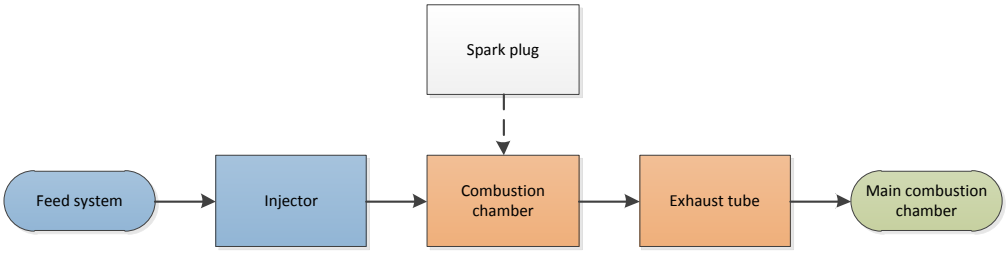

Figure 3.1: Schematic overview of the design process for the igniter baseline design.

The presence of a sonic throat allows one to directly determine an estimate of the minimum required igniter chamber pressure. By solving for the required chamber pressure using the critical pressure ratio from isentropic flow one can derive the required igniter pressure from the engine chamber pressure:

$$\frac{p_t}{p_c} = \left(\frac{2}{\gamma-1}\right)^{\frac{\gamma}{\gamma-1}} \quad \Longrightarrow \quad p_c = p_t \left(\frac{2}{\gamma-1}\right)^{\frac{\gamma-1}{\gamma}} \tag{3.1}$$

As a initial estimate the specific heat capacity ratio γ is taken to equal 1.2. The exact cannot be determined directly as it depends on the actual composition of the exhaust flow and its temperature. Both are unknown at this moment. Taking $\gamma = 1.2$ and yields and setting the throat pressure p_t equal to the pressure of the main combustion chamber yields a required igniter chamber pressure of $7.086{\cdot}10^6$ MPa.

3.3. Required power

One of the key requirements of the ignition system is the required power. A spark-torch igniter functions by heating (part of) the engine propellant flow to a temperature sufficient to initiate combustion. In order to put a figure to this requirement it must be determined how much propellant must be heated and to what temperature. This section will aim to answer both questions.

3.3.1. Propellant fraction

The first question to be answered when determining the actual required power of an igniter, is the fraction of the propellant flow in the main combustion chamber which is to be ignited by the igniter. During the literature study it was found that generally not the full propellant flow is ignited. There is however no clear consensus on how much of the propellant flow should be ignited or how to determine this fraction.

Because of this it is decided to try to determine the fraction of the power required to heat the full propellant flow delivered by already existing igniters. Due to the time consuming nature of looking up ignition system specifics and the lack of detailed data on ignition systems, some assumptions are made:

Autoignition It is assumed that for all engines considered it is sufficient to raise (a fraction of) the main combustion chamber propellant flow to the auto ignition temperature of the fuel used. Selected auto ignition temperature are listend in Table 3.2.

Perfect heating It is assumed that the heating of the main combustion propellant flow by the igniter exhaust propellant flow is perfect.

Propellant state It is assumed that the main combustion chamber propellants are injected at the boiling temperature at atmospheric pressure. In reality this temperature may be different due to high injection pressure and in order to avoid supercriticality of the propellants.

Igniter power In case the igniter heating power is not specified it is assumed that the heating power of the igniter is equal to the lower heating value of the fuel mass flow used in the igniter.

Temperature		**Conditions**	
Kelvin	Celsius		
839	566	Hydrogen auto ignition temperature at 1 atm pressure.	[40]
828	555	Methane auto ignition temperature in oxygen atmosphere at 1 atm pressure.	[25]

Table 3.2: Selected auto ignition temperatures for various propellants.

For rocket engines of which the exact propellant mass flow is not readily available the propellant mass flow $\dot{m}$ can be estimated using ideal rocket theory:

$$F = g_0 I_{sp} \dot{m} \quad \Longrightarrow \quad \dot{m} = \frac{F}{g_0 I_{sp}} \tag{3.2}$$

Using the given assumptions the fraction of the full power delivered by each igniter is listed in Table 3.3. From the results it can be concluded that usually a relatively small portion of the complete propellant flow in the main combustion chamber is ignited.

It should be noted however that in this short investigation no attention was paid to how exactly the main propellants are heated by each of the igniters. It may be the case that specific portions of the propellant flow are heated or that the desired target temperature is different than the previously selected autoignition temperatures. Still the results do provide an indication of the typical power level of an igniter.

Engine			Igniter			Fraction	
Name	Propellants	Power [kW]	Type	Propellants	Power [kW]		
HYPROB			Spark-torch		64		[8]
Vinci	LOX/LCH4	35927	Catalytic	H2O2	440	0.0122	[21] [23]
Vinci	LOX/LCH4	35927	Spark-torch		440	0.0122	[10] [23]
LE-7	LOX/LH2	542584	Spark-torch	GOX/GH2	22971	0.00512	[51]
LE-7 Preburner	LOX/LH2	377158	Spark-torch	GOX/GH2	38000	0.101	[51]
LE-5	LOX/LH2	63516	Spark-torch	GOX/GH2	1320	0.0208	[51]
LE-5 Preburner	LOX/LH2		Spark-torch	GOX/GH2	120		[51]
SSME RS-25	LOX/LH2	1048191	Spark-torch	GOX/GH2	51529	0.0492	[51]

Table 3.3: Overview of reviewed rocket engines, their igniters, igniter output power, power required to heat the main combustion chamber propellant stream to autoignition temperature and the fraction of this power delivered by the igniter.

From the results it is concluded that aiming to heat 5% of the main combustion chamber propellant flow to its autoignition temperature is likely a good starting point. Except for the LE-7 Preburner igniter all reviewed ignition systems deliver a lower power level, suggesting that 5% is a safe estimate.

In order to account for the large number of uncertainties in the design process of an ignition system a safety factor of 2 is added to the required igniter power. This brings the desired power output to 10% of the power required to heat the full propellant flow to autoignition temperature.

1	Igniter design	Required propellant fraction

Table 3.4: Validation items.

3.3.2. Thermodynamic calculation

In order to determine the temperature to which the propellants need to be raised at which auto-ignition occurs the work of Shchemelev [41] is used. Shchemelev reports that oxygen-methane mixtures readily self ignite at temperatures above 510 degrees Celsius at atmospheric pressure, with the exact auto ignition temperature depending on the vessel size and mixture ratio.

The works of Zabetakis [50] and Kuchta [25] are considered standard works on explosion and flammability limits. Zebetakis reports an auto ignition temperature of methane air mixtures of around 540 degrees Celsius at atmospheric pressure. Kuchta reports an auto ignition temperature of 555 degrees Celsius of oxygen-methane mixtures at atmospheric pressure.

At elevated pressures the auto ignition temperature tends to decrease [46]. While no predictions on the relation between pressure and auto ignition temperature are made, the described relation makes using the atmospheric auto ignition temperature a safe choice. The exact mixture ratio at which the main propellant flow will ignite is not known due to turbulent mixing, causing local deviations from the overall mixture ratio. Nor is there a firm relation between the auto ignition temperature and mixture ratios available. Therefore the required temperature of the propellants for ignition is assumed to be equal to the highest reported auto ignition temperature as a safe estimate. This temperature equals 828 K. The results are summarized in Table 3.5.

In order to ensure ignition it is decided to set the requirement that the igniter should be able to heat a fraction of the propellant mass flow above its auto ignition temperature. The total energy per unit mass Q required is determined by summing the difference in enthalpy at the injection state and autoignition state of each of the propellant components multiplied by their respective fraction:

$$Q = \sum_i n_i \Delta H_i = \sum_i n_i \left(H_t - H_{ref}\right)_i \tag{3.3}$$

Where n_i is the propellant fraction, H_t the enthalpy at the target (autoignition) temperature and H_{ref} the

Temperature		Conditions	
Kelvin	Celsius		
783	510	40% oxygen, 59% methane by volume. No pressure specified.	[41]
813	540	In air at 1 atm pressure.	[50]
828	555	In oxygen atmosphere at 1 atm pressure.	[25]
828	555	Selected auto ignition temperature	

Table 3.5: Reported and selected auto ignition temperatures for methane.

enthalpy at the reference (injection) state of the propellant. Substituting fractions n_i for mass flows $\dot{m}_i$ in kgs^{-1} results in an expression for the required power P in Js^{-1}:

$$P = \sum_i \dot{m}_i \Delta H_i = \sum_i \dot{m}_i \left(H_t - H_{ref}\right)_i \tag{3.4}$$

As the methane fuel will be used to regeneratively cool the engine prior to being injected into the combustion chamber, it is likely that the methane will have vaporised or is in supercritical conditions once it is injected into the chamber. This assumption may however not be valid at engine start, due to the fact that there is no combustion in the main chamber yet and that the engine is to be prechilled prior to start. For ignition it is thus assumed that both the methane and oxygen will be in the liquid phase and need to undergo a phase change. The properties of the propellants at injection are summarized in Table 3.6.

It is assumed that heating occurs under constant pressure conditions at chamber pressure. Since the rocket engine chamber is exposed to the atmosphere the pressure inside the chamber is considered to be constant. In reality the propellants will experience a pressure drop as they move downstream in the chamber. Determination of this exact pressure drop is left for future work. The enthalpy values are then obtained from the NIST Chemistry WebBook [2].

Using the assumption of heating under constant pressure and the discussed relations the required power is determined. The results of this calculation are listed in the lower half of Table 3.6.

Parameter	Unit	Value
Oxidizer temperature	K	90
Oxidizer phase	-	liquid
Fuel temperature	K	111
Fuel phase	-	liquid
Oxygen heat of vaporization	$Jmol^{-1}$	$213{\cdot}10^3$
Methane heat of vaporization	$Jmol^{-1}$	$509{\cdot}10^3$
Auto ignition temperature	828	K
Oxidizer enthalpy at injection	Jkg^{-1}	$-1.32{\cdot}10^5$
Oxidizer enthalpy at autoignition	Jkg^{-1}	$7.96{\cdot}10^5$
Fuel enthalpy at injection	Jkg^{-1}	$5.70{\cdot}10^4$
Fuel enthalpy at autoignition	Jkg^{-1}	$2.57{\cdot}10^6$
Power required	Js^{-1}	$62.9{\cdot}10^3$
Power required after design factor	Js^{-1}	$126{\cdot}10^3$

Table 3.6: Propellant properties at the injector face at engine start and corresponding required ignition power.

3.4. Igniter propellant flow

The igniter will burn propellants at stoichiometric ratio in order to generate the maximum amount of heat. The molar mixture ratio is determined by assuming the following reaction equation for complete combustion of methane. From the molar mixture ratio the mass mixture ratio is derived. The results are summarized in Table 3.7.

$$CH_4 + 2\,O_2 \longrightarrow CO_2 + 2\,H_2O \tag{3.5}$$

In order to be able to determine the desired igniter propellant flows an estimate of the power delivered per unit of propellant mass burned in the igniter is required. The starting point for estimating the power delivered is the state of the propellants at injection into the igniter chamber. The pressure at injection is set equal to the pressure of the main combustion chamber in order to ensure that no reverse flow will occur under normal operating conditions.

Feeding the igniter propellant from the main propellant feed system has the theoretical advantage that no separate feed system is required. As the igniter is to use gaseous propellants this however means that the propellants will likely have to be heated in order to gasify them prior to injection into the igniter combustion chamber. It is assumed that the propellants are heated to exactly the boiling temperature at injection pressure. The resulting propellant states are summarized in Table 3.7.

Parameter	**Unit**	**Value**
Oxygen molar mass	$gmol^{-1}$	31.9988
Methane molar mass	$gmol^{-1}$	16.0425
Molar mixture ratio (O/F)	-	2
Mass mixture ratio (O/F)	-	3.99
Injection pressure oxygen	P	$4{\cdot}10^6$
Injection pressure methane	P	$4{\cdot}10^6$
Injection temperature oxygen	K	147.56
Injection temperature methane	K	186.1
Injection phase oxygen	-	gas
Injection phase methane	-	gas

Table 3.7: Propellant properties at the main combustion chamber injector face at engine start.

With the fuel oxidizer ratio set and the propellant state defined at injection the question of how much propellant is required can be answered. To provide an answer to this question an estimate on the delivered amount of energy per unit mass of propellant is required. The following subsections will aim to answer this question.

3.4.1. Adiabatic flame temperature

The most straight forward method for estimating the delivered energy per unit mass of propellant is calculating the adiabatic flame temperature. In this method it is assumed that all energy released is solely employed for heating the combustion products [47, p. 349] [51]. In this application complete combustion of methane is assumed:

$$CH_4 + 2\,O_2 \longrightarrow CO_2 + 2\,H_2O \tag{3.6}$$

The adiabatic flame temperature is subsequently obtained by calculating the available heat from the combustion of the propellants using Hess's law:

$$\Delta H = \sum_p \left(n\Delta_f H\right)_p - \sum_r \left(n\Delta_f H\right)_r \tag{3.7}$$

Where ΔH_f is the heat of formation, n the molar fraction, r denotes a reactant and p denotes a reaction product. From the available heat the adiabatic flame temperature itself can be determined.

The required heat Q to raise the temperature of a mixture of substances from an initial reference temperature T_{ref} to a target temperature T_i equals the sum of the difference in internal energy of each of the substances:

$$Q = \sum_j n_j (H_i - H_{ref})_j \tag{3.8}$$

If the pressure in the combustion chamber is considered constant, the required heat Q to raise the temperature of a substance can be determined using:

$$Q = \sum_j n_j \int_{T_{ref}}^{T_i} Cp_j(T) dT \tag{3.9}$$

Where the specific heat coefficient Cp_j of each specie should be considered to be a function of temperature. For the specific heat coefficient Cp_j it is common for a fit to the Shomate equation to be published, which allows determination of isobaric specific heat capacity. The Shomate equation is defined as follows [2]:

$$Cp = A + BT + CT^2 + DT^3 + \frac{E}{T^2} \tag{3.10}$$

Equating the heat released by the combustion of the propellants to the heat required to heat the resulting reaction products allows one to determine solve for the temperature. Doing so one finds an adiabatic flame temperature of 5142.9 K. The values used and results are summarized in Table 3.8. The values for the heat of formation used were obtained from the NIST JANAF Themochemical Tables [13].

Parameter	**Unit**	**Value**	
$\Delta_f H^{gas}$ CH_4	$kJmol^{-1}$	74.6	[2]
$\Delta_f H^{gas}$ CO_2	$kJmol^{-1}$	-393.51	[2]
$\Delta_f H^{gas}$ H_2O	$kJmol^{-1}$	-241.8	[2]
ΔH	$kJmol^{-1}$	-802.510	
Adiabatic flame temperature	K	5142.9	

Table 3.8: Propellant properties at the injector face at engine start

The high temperature found is an indication that the result is inaccurate. When calculating the adiabatic flame temperature it is assumed that all energy released by the combustion is used to heat the reaction products. In reality the four following effects are expected to have a significant impact on the flame temperature:

Dissociation At high temperatures (typically above 3000 K) dissociation of the reaction products occurs. Dissociation is endothermic and will thus lower the resulting flame temperature.

Incomplete combustion It is assumed that the propellants are fully combusted. In reality combustion may be incomplete due to fuel and oxidizer flows not being fully mixed. The energy released may thus be lower.

Kinetic energy Part of the energy liberated by combustion will be used to accelerate the reaction products through the igniter exit tube.

Thermal losses The igniter body itself will soak up thermal energy causing effective flame temperature to drop.

Using a chemical equilibrium program can largely address these discussed shortcomings, resulting in a more realistic flame temperature.

3.4.2. Chemical equilibrium power

In order to determine the energy delivered per unit of mass of propellant burned, the enthalpy change resulting from the combustion can be determined using a chemical equilibrium software tool like RPA or NASA's CEA [36] [33]. Using chemical equilibrium the exact exhaust composition is predicted. For each specie in the exhaust flow the heating power per unit mass is determined, after which the total heating power per unit mass can be determined.

The igniter heating power P_i above the reference temperature K is then determined using the equation:

$$P_i = \dot{m}_i(H_i - H_{ref}) \tag{3.11}$$

Where H_i is the enthalpy of the gas leaving the igniter in kJkg^{-1}, H_{ref} is the enthalpy of the gases at the reference temperature in kJkg^{-1} and $\dot{m}_i$ is the mass flow of gas leaving the igniter in kgs^{-1}. Extending this equation for a mixture of multiple species:

$$P_i = m_i \sum_j n_j \frac{1000}{M_j}(H_i - H_{ref})_j \tag{3.12}$$

Where M_j is the molar mass of the species in gmol^{-1} and n_j the molar fraction of the species.

Taking the auto ignition temperature as the reference temperature and working out this equation for all the major species in the exhaust flow as predicted by the chemical equilibrium software yields the results as shown in Table 3.9. RPA-Lite was used in this study for determining the chemical equilibrium power of the igniter exhaust. The full input file used and complete detailed output file as generated by RPA-Lite can be found in Appendix C.

Species	ΔH **[kJ/mol]**	**Molar frac**	**Molar mass M [g/mol]**	ΔH **[kJ/kg]**
H2O	126.6	0.4885	18.02	7027
CO2	143.6	0.1660	44.01	3263
CO	86.44	0.1253	28.01	3086
H2	82.21	0.0469	2.016	40779
O2	90.89	0.0635	32.00	2840
OH	82.76	0.0767	17.01	4866
O	50.37	0.0156	16.00	3148
H	50.16	0.173	1.008	49762
Total	114.2	0.9998	23.32	7737

Table 3.9: RPA-Lite predicted exhaust composition. $\frac{At}{Ae}$ = 1.1

From the calculated total enthalpy change above the reference temperature the heating power delivered by the igniter can be calculated. From this value the required igniter exhaust mass flow can be determined. From the total igniter exhaust mass flow the mass flows of the oxidizer and fuel given can be determined from the O/F ratio:

$$r = O/F = \frac{m_{ox}}{m_f} \quad \Longrightarrow \quad m_{ox} = \frac{O/F\,m}{1 + O/F} \qquad m_f = \frac{m}{1 + O/F} \tag{3.13}$$

Using the results from the chemical equilibrium software and the relations given the results given in Table 3.10 are obtained.

3.5. Injector design

For the injector design a pressure drop of 20% compared to the target injection pressure is assumed. A 20% injection pressure drop is presented as a rule of thumb to avoid combustion instabilities in main combustion chambers [17, p. 113]. Unsurprisingly an injector pressure drop of this magnitude is observed in various rocket engine designs [44, p. 272]. While a main combustion chamber is different from the igniter combustion chamber a similar pressure drop is assumed as a design starting point.

Parameter	Unit	Value
Chamber flame temperature	K	3509
Heating power	$kJkg^{-1}$	7737
Required exhaust mass flow	kgs^{-1}	0.01625
Oxidizer mass flow	kgs^{-1}	0.01299
Fuel mass flow	kgs^{-1}	0.003259

Table 3.10: Required igniter exhaust mass flow and propellant mass flows.

2	Igniter design	Exhaust propellant flow temperature
3	Igniter design	Heating efficiency of igniter exhaust propellant flow

Table 3.11: Validation items.

Predicting the flow and pressure drop in the injector is complex and arguably an expertise on itself. Due to the propellants being in gaseous form during injection compressibility effects will be present in the injector orifice flow. With the propellants close to their boiling temperature changes in temperature and pressure due to flow topology in the injector elements may cause condensation and other two phase flow effects. Analyzing these phenomena however is outside the scope of part of the study and it therefore omitted. Validation of the effect of these phenomena is however in order.

For incompressible hydraulic flow a simple relation for predicting injection velocity v_i in ms^{-1} from pressure drop Δp in Nm^{-2} and density ρ in kgm^{-3} is presented by some authors [51] [44, p. 278]:

$$v_i = C_d \sqrt{\frac{2\Delta p}{\rho}} \tag{3.14}$$

Obviously this relation will not yield very accurate results because it is tailored to hydraulic incompressible flow and due to the complexities of injector flow mentioned before. For the sake of limited amount of time available and the lack of more suitable yet simple relations, the results from this relation are used as a first order estimate. From the obtained injection velocity the required injector area A_i can be determined:

$$\dot{m}_i = v_i \rho A_i \quad \Longrightarrow \quad A_i = \frac{\dot{m}_i}{v_i \rho} \tag{3.15}$$

In order to check if the predicted injection velocities are realistic it can be checked if the predicted injection velocity exceeds the choked / critical flow velocity. The choked flow velocity is also of interest during startup, as the pressure drop over the injector orifices will be very large at this moment. Working from the equation as given by Zandbergen [51] and substituting in the ideal gas law results in:

$$\begin{aligned} \dot{m} &= \frac{p_0}{RT_0}\sqrt{\gamma RT_0}A\left(\frac{2}{\gamma+1}\right)^{\frac{\gamma+1}{2(\gamma-1)}} \\ &= p_0 A\sqrt{\frac{\gamma}{RT_0}\left(\frac{2}{\gamma+1}\right)^{\frac{\gamma+1}{\gamma-1}}} \\ &= A\sqrt{\gamma\rho_0 p_0\left(\frac{2}{\gamma+1}\right)^{\frac{\gamma+1}{\gamma-1}}} \end{aligned} \tag{3.16}$$

Introducing the discharge coefficient C_d and solving for the velocity yields:

$$v = C_d\sqrt{\frac{\gamma p_0}{\rho_0}\left(\frac{2}{\gamma+1}\right)^{\frac{\gamma+1}{\gamma-1}}} \tag{3.17}$$

For the discharge coefficient a conservative value of $C_d = 0.65$ is assumed. The discharge coefficient depends on the shape of the injection orifices. As the shape of the injection orifices not only depends on the

design choices but also on the manufacturing process and limits therein, it is hard to put a solid number to the discharge coefficient at this moment in time. The value selected is a value in the lower end of the spectrum of discharge coefficients typically encountered [44, p. 279].

Using the selected discharge coefficient and the discussed relations the injection velocity and area is solved for both the fuel and oxidizer. The results are summarized in Table 3.12.

Parameter	**Unit**	**Value**
Injector pressure drop	Pa	$0.8{\cdot}10^{6}$
Injector discharge coefficient C_d	-	0.65
Fuel injection velocity	ms^{-1}	88.51
Fuel injection choked flow velocity	ms^{-1}	102.8
Fuel injection area	m^2	$4.263{\cdot}10^{-7}$
Fuel injection orifices	-	4
Fuel injection orifice diameter	m	$3.68{\cdot}10^{-4}$
Fuel injection density	$kgm^{-3]}$	86.3
Oxidizer injection velocity	ms^{-1}	61.07
Oxidizer injection choked flow velocity	ms^{-1}	72.43
Oxidizer injection area	m^2	$1.174{\cdot}10^{-6}$
Oxidizer injection orifices	-	4
Oxidizer injection orifice diameter	m	$3.25{\cdot}10^{-3}$
Oxidizer injection density	$kgm^{-3]}$	181.3

Table 3.12: Igniter oxidizer and fuel injection velocity and area.

3.5.1. Injection stream momentum

The igniter will use a doublet injector type configuration where the fuel and oxidizer sprays are made to collide. A sketch of the injection geometry is given in Figure 3.2. A straight forward kinetic relation can be derived for the momentum of the resulting jet [44, p. 280] [17].

The resulting momentum of the collided jet is of interest because it enables a rough prediction of the flow patterns resulting from propellant injection. This in turn is of interest because one will want to prevent injected propellant streams from directly impinging with the igniter walls. Failing to do so is likely going to result in thermal problems due to the flame being very close to the walls. Another potential problem would be impingement of an oxidizer rich propellant stream on the wall which may cause excessive oxidation of the wall material. Using the kinetic relation:

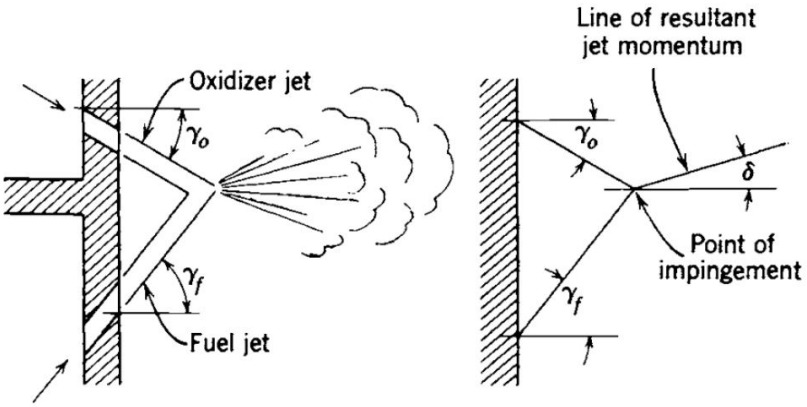

Figure 3.2: Schematic of doublet injector impingement and relation between angles. Source: [44].

$$tan(\delta) = \frac{\dot{m}_o v_o sin(\gamma_o) - \dot{m}_f v_f sin(\gamma_f)}{\dot{m}_o v_o cos(\gamma_o) - \dot{m}_f v_f cos(\gamma_f)} \tag{3.18}$$

Where v is the injection velocity, $\dot{m}$ the mass flow, γ the injection angle and δ the angle of the momentum of the resulting jet all with their standard SI units. The o and f subscript respectively indicate oxidizer and fuel. In the injector it is generally undesirable to have any off axis momentum in the resulting jet, allowing one to set $\delta = 0$. Doing so significantly simplifies the relation:

$$\dot{m}_o v_o \sin(\gamma_o) = \dot{m}_f v_f sin(\gamma_f) \quad \Longrightarrow \quad sin(\gamma_o) = \frac{\dot{m}_f v_f}{\dot{m}_o v_o} sin(\gamma_f) \tag{3.19}$$

Using the previously determined required propellant injection velocities one will come to the conclusion that due to the high oxygen injection stream momentum it is not feasible to lay out the injector orifice pairs in a 'classical' fashion as depicted in Figure 3.2. It is therefore decided to align the oxidizer injection stream with the chamber axis.

	Igniter design	Do CFD results predict injector stream wall impingement?

Table 3.13: Validation items.

3.5.2. Injector orifice placement

The injector is laid out as 4 sets of injection orifices around the central sparkplug electrode. Oxygen is injected along the spark plug in the vertical direction. Methane is injected in horizontal direction a downstream from the oxygen jet in such a manner that the jets impinge. Placing injection ports around the electrode is hoped to ensure even mixing around the electrode. Layout of the sets of injection orifices in a symmetrical manner is hoped to result in symmetrical flow patterns. In addition the symmetry can in theory be exploited to save on computational cost in simulating the igniter.

A similar configuration of injection ports around the spark electrode is found in some other igniter designs [39] [10].

	Igniter design	Do CFD results predict symmetrical flow patterns?
	Igniter design	Do CFD results predict recirculation around the spark plug electrode?
	Igniter design	Do CFD results predict mixing around the spark plug electrode?

Table 3.14: Validation items.

3.6. Thermal management

Thermal management of spark-torch igniters is an issue. Like any combustor wall the interior of a spark-torch igniter will be subject to very high heat fluxes [35, p. 365]. With spark-torch igniters being somewhat similar to rocket engines and rocket engines requiring extreme measures to cool the chamber and nozzle it should come to no surprise that similar cooling methods are applied to spark-torch igniters as well.

The two methods which are commonly used are:

Film Some igniter designs make use of film cooling by injecting fuel in such a manner that it forms a relatively cool boundary layer along this igniter wall.

Cooling jacket Most of the igniters described in studies make use of what can be described as a cooling jacket [37].

As mentioned in the introduction the goal of this design process is to come up with a first order design in a limited amount of time. The design of the cooling system requires more detailed analysis and essentially follows from the first design iteration. It is in this first design iteration that the thermal power of the igniter is set. Because of the limited scope of the design process in this work it is decided to not spend any further attention to thermal management at this point.

3.7. Spark plug

The igniter is started using a spark plug, hence a spark plug must be selected. Making a well founded spark plug selection is probably worthy of a study in its own as the shape, materials and location of the spark plug likely all influence its performance. In addition it was found that actual technical information on spark plugs is fairly difficult to come by.

Because of this reason only qualitative requirements are given for the spark plug and a spark plug is selected based on the NGK catalog as it was found to provide a quick overview of the spark plugs available.

Fuel compatibility As the igniter operates on the combustion of methane and oxygen it is assumed that a spark plug suited for operating an LNG engine is likely to perform best. The LNG mixture is largely composed of methane.

High temperature As temperature in the igniter will become very high a spark plug designed to operate at high temperature is desired. Spark plugs with tips manufactured out of iridium are readily sold and are claimed to tolerate high temperatures.

Small size As the spark plug will be located in the same assembly as the igniter injector a small size is preferred. This is expected to make placement of the spark plug easier.

The spark plug selected is the NGK 5344 IFR6D10 Laser Iridium and is shown in Figure 3.3. Its specifications are listed in Table3.15. No specific reason for selecting except for that it complies with the requirements stated pretty well and is readily available in Europe. Ideally smaller spark plug would be selected but no smaller models with similar properties were identified at this stage.

Parameter	Unit	Value
Thread diameter	mm	14.0
Thread reach	mm	19.0
Electrode gap	mm	1.0

Table 3.15: NGK 5344 IFR6D10 Laser Iridium spark plug specifications.

Figure 3.3: NGK Laserline spark plugs. Source: http://www.ngk.de

3.8. Physical dimensioning

With all the major design choices made all these elements need to be physically accommodated. In addition some physical dimensions need to be selected for the throat, exhaust tube and chamber. This section will elaborate on the choices made regarding these physical dimensions.

3.8.1. Throat

As described earlier the igniter will be connected to the main combustion chamber via a tube and throat. The chemical equilibrium program provides an estimate of the throat mass flux Q_t in $\mathrm{kgm^{-2}s^{-1}}$. Using conservation of mass, the throat area A_t in $\mathrm{m^2}$ can simply be determined using:

$$A_t = \frac{\dot{m}_i}{Q_t} \tag{3.20}$$

Where $\dot{m}_i$ is the igniter mass flow in $\mathrm{kgs^{-1}}$. The resulting throat and exit dimensions are summarized in Table 3.16.

Parameter	**Unit**	**Value**
Throat mass flux	$\mathrm{kgm^{-2}s^{-1}}$	2236.8
Area ratio $\frac{A_e}{A_t}$	-	1.1
Throat area	$\mathrm{m^2}$	$7.266{\cdot}10^{-6}$
Throat diameter	m	0.003042
Exit area	$\mathrm{m^2}$	$7.993{\cdot}10^{-6}$
Exit diameter	m	0.00319

Table 3.16: Igniter throat and exit dimensions.

From a manufacturing point of view it is questionable if the throat can be manufactured as designed. A 3 millimeter throat is probably perfectly manufacturable, but the diverging section of the nozzle is diverging so small that it will require tailored tooling. It is however questionable if the diverging section is truly necessary. Its purpose is to guarantee the presence of a sonic throat. By including a diverging section the location of the sonic throat is fixed. This fixing of the location does however not serve any of the igniter requirements and only model requirements. The throat may thus be omitted in the final design.

3.8.2. Chamber

The combustion chamber needs to be able to accommodate the injection ports and sparkplug as well as providing sufficient volume to allow for proper mixing and combustion of the propellants.

In rocket engine design the required chamber length is driven by the requirement of the propellants to sufficiently mix and react prior to entering the nozzle. This required length is usually captured as the L* value [17]. The L* value is heavily dependent on the propellant combination and injection method used. No known L* values have been found for GOX/CH4 propellant combinations as used in this igniter.

	Igniter design	Do the propellants sufficiently react prior to leaving the igniter combustion chamber?

Table 3.17: Validation items.

The chamber width is selected such that the centerline of the oxidizer injection ports are spaced about 10 mm away from the sparkplug. An overview is given in Figure 3.6.

3.8.3. Chamber walls

The minimum required wall thickness of the igniter chamber is calculated by treating the igniter as a pressure vessel and assuming that it is thin walled. The required thickness to cope with the hoop stress is found using:

$$\sigma_y = \frac{pr}{t} \implies t_{min} = \frac{pr}{\sigma_y} \tag{3.21}$$

Where r is the radius in m, t the wall thickness in m, p the pressure in Pa and σ the stress in Pa. By substituting in the yield stress σ_y and solving for the thickness the minimum required thickness is found. Analogous to the hoop stress the axial stress is determined as follows:

$$\sigma_y = \frac{pr}{2t} \implies t_{min} = \frac{pr}{2\sigma_y} \tag{3.22}$$

Using the von Mises yield criterion the required wall thickness to cope with the equivalent tensile stress resulting from the combined stresses can be determined:

$$\sigma_v = \sqrt{\sigma_1^2 - \sigma_1\sigma_2 + \sigma_2^2} = \sqrt{\frac{p^2r^2}{t^2} - \frac{p^2 - r^2}{2t^2} + \frac{p^2r^2}{4t^2}} = \sqrt{\frac{3}{4}}\frac{pr}{t} \implies$$
$$t_{min} = \sqrt{\frac{3}{4}}\frac{pr}{\sigma_y} \tag{3.23}$$

For the igniter body Inconel 625, which is a so called nickel-base alloy is selected as a material because of its tolerance to high temperatures [17, p. 50]. No detailed selection procedure for the igniter body material is performed. Performing a detailed trade-off for the igniter body material may be part of a future study. One aspect of interest is for example the difficulty of machining Inconel due to its hardness.

The properties of Inconel 625 are listed in Table 3.18.

Parameter	**Unit**	**Value**	**Comments**
Density	kgm^{-3}	8.44	
Tensile yield strength	Pa	$290{\cdot}10^6$	At elevated temperature of 650 degrees Celcius, annealed prior to test

Table 3.18: Inconel 625 properties. Source: [1]

Parameter	**Unit**	**Value**
Igniter design safety ratio	-	1.5
Igniter safety pressure	Pa	$10.49{\cdot}10^6$
Required wall thickness	mm	0.69

Table 3.19: Igniter chamber pressure and resulting required wall thickness

3.8.4. Exhaust tube

The igniter chamber is connected to the combustion chamber via a tube. The tube provides a standoff from the main combustion chamber assembly as well as transport of the exhaust flow into the combustion chamber. The required length of this tube is not known at this moment of time and is dependent on the final engine design. Thus an arbitrary value of 4 centimeters is used for this study.

3.9. Summary

The Spark-Torch concept was selected for use in the igniter design because it enables the use of non-toxic propellants, eases handling, can be made reusable and is as a concept both proven and reliable.

Selecting the required power proved highly challenging due to the fact that there is no information available on what fraction of the main combustion chamber propellant flow should be ignited. Based on a survey of existing igniters it was decided that aiming to ignite 10% of the main propellant flow is a safe estimate.

Determining the required igniter propellant flow rate from the required power highly depends on the chemistry assumed and on the ignition temperature of the main propellant flows. Assuming equilibrium chemistry the required power including safety factors is estimated at 126 kW which can be delivered by a total igniter propellant flow of 32 gs^{-1}.

Sizing the injection ports is challenging due to the lack of adequate analytical design tools for high velocity discharge flow from orifices. An attempt was made by approximating the flow by assuming incompressible flow and verifying if the condition of choked flow is not violated. Further validation on these choices will however be required. It was decided to inject both the oxidizer and fuel via 4 injection orifices each, which are arranged in doublet like setting.

Finally a spark plug was selected and the igniter exhaust and body were sized by assuming sonic throat flow in the exhaust and by modeling the igniter body as a pressure vessel where it is assumed that the igniter body is fabricated out of Inconel 625. The resulting igniter design is symmetrical in two planes.

The resulting igniter design is presented in schematic form in the Figures 3.4, 3.5 and 3.6. The key design parameters are listed in Table 3.20.

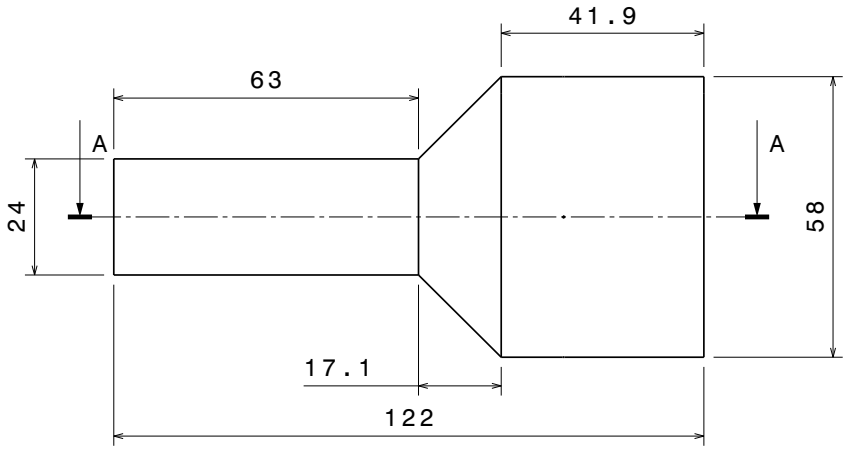

Figure 3.4: Igniter design top view

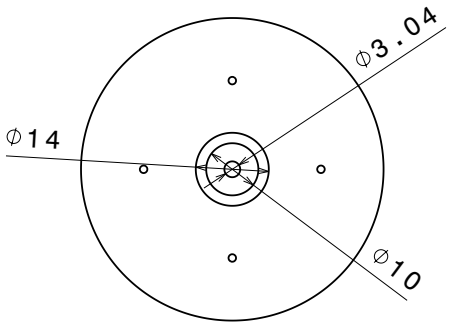

Figure 3.5: Igniter design side view

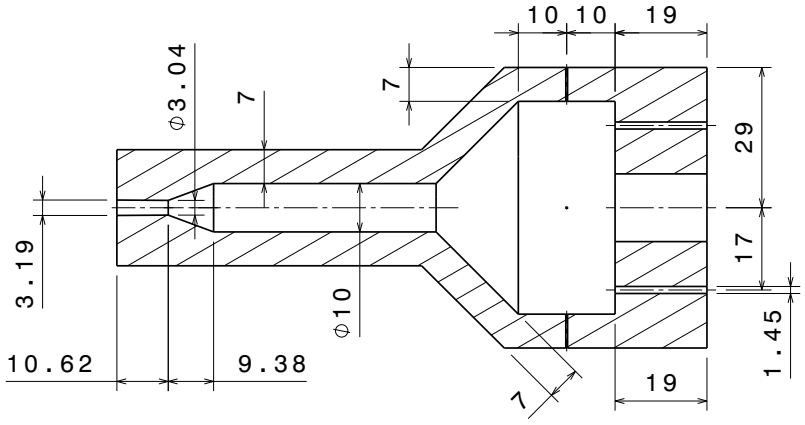

Figure 3.6: Igniter design side view section A-A

Parameter	Unit	Value	Comments
Igniter type	-	Spark-torch	
Molar mixture ratio (O/F)	-	2	
Mass mixture ratio (O/F)	-	3.99	
Fuel mass flow	kgs^{-1}	0.003259	
Fuel injection orifices	-	4	
Fuel injection orifice diameter	m	$3.68 \cdot 10^{-4}$	
Oxidizer mass flow	kgs^{-1}	0.01299	
Oxidizer injection orifices	-	4	
Oxidizer injection orifice diameter	m	$3.25 \cdot 10^{-3}$	
Throat mass flux	$kgm^{-2}s^{-1}$	2236.8	
Area ratio $\frac{A_e}{A_t}$	-	1.1	
Throat area	m^2	$7.266 \cdot 10^{-6}$	
Throat diameter	m	0.003042	
Exit area	m^2	$7.993 \cdot 10^{-6}$	
Exit diameter	m	0.00319	
Exhaust tube length	m	0.04	
Envelope size	m x m	0.058 x 0.122	Tubular shape
Spark plug	-	NGK 5344 IFR6D10 Laser Iridium	
Wall material	-	Inconel 625	

Table 3.20: Igniter design summary.

4

Computational model

With the baseline igniter design presented in the previous chapter this chapter describes the setup and rationale behind the computational model used to model ignitionl.

The full igniter model is comprised of a number of elements which are listed in Figure 4.1. Some of these elements are true models in the sense that they attempt to model physics. Others are elements which are inputs to the model equations which are derived from the igniter baseline design. Finally some elements deal with the numerics required to obtain a solution from the model.

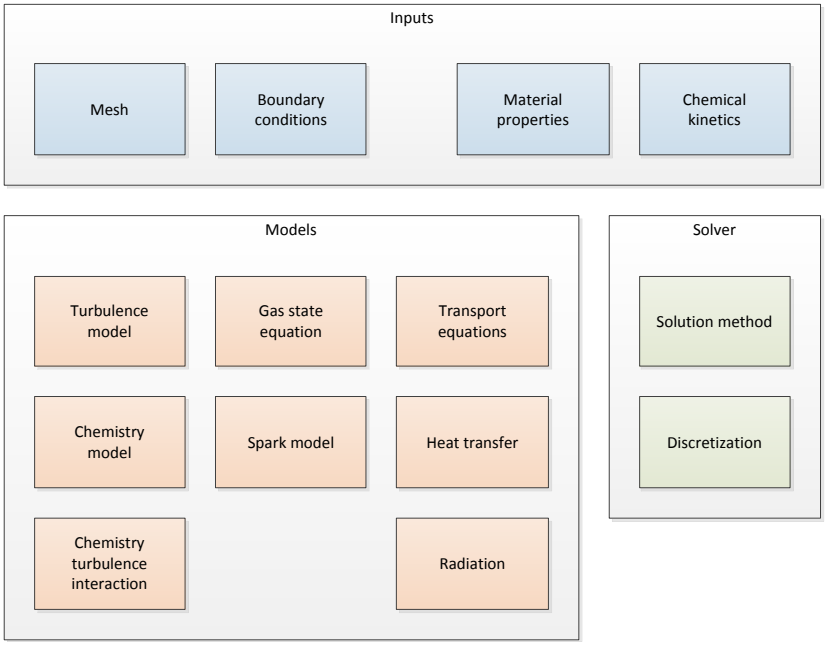

Figure 4.1: Graphical overview of building blocks for numerical model.

For most of these model elements different implementations can be used depending on the exact ignition case being simulated and the desired accuracy. In this chapter each of these elements is discussed in detail.

4.1. Mesh

In order to perform a numerical simulation using a finite volume method a grid or mesh is required. Typically a 3 dimensional grid is referred to as a mesh. This mesh divides the geometry of interest up in small volumes

referred to as cells, from which the finite volume method derives its name. In doing so it forms the computational domain in which the model equations are to be solved. In order to do so a geometry is required from which the mesh can be generated, and decisions need to made on the desired cell size and cell shape. Finally locations and methods of refinement need to be selected to ensure mesh quality.

4.1.1. Geometry

From the igniter baseline design geometry needs to be created which is suitable for use in a CFD simulation. Essentially this boils down to defining the volume in which the flow is going to be solved. The geometry is therefore equal to the enclosed volume of the igniter design. The main geometries used are shown in Figure 4.2. In addition to the three main geometries in which symmetry is exploited used also a full geometry is used to generate a mesh in which symmetry is not exploited. The nomenclature used to indicated these four different geometries is:

Quarter The regular quarter igniter geometry with truncated in- and outflow regions in which two planes of symmetry are used.

Full The full geometry which is equal to four quarter geometries fused together. Has truncated in- and outflow regions.

Inflow Equal to the quarter geometry with exception of the extended inflow regions. The extended inflow region are labeled A and B in Figure 4.2.

Outflow Equal to the quarter geometry with exception of an extended outflow region. The extended outflow region is labeled D in Figure 4.2.

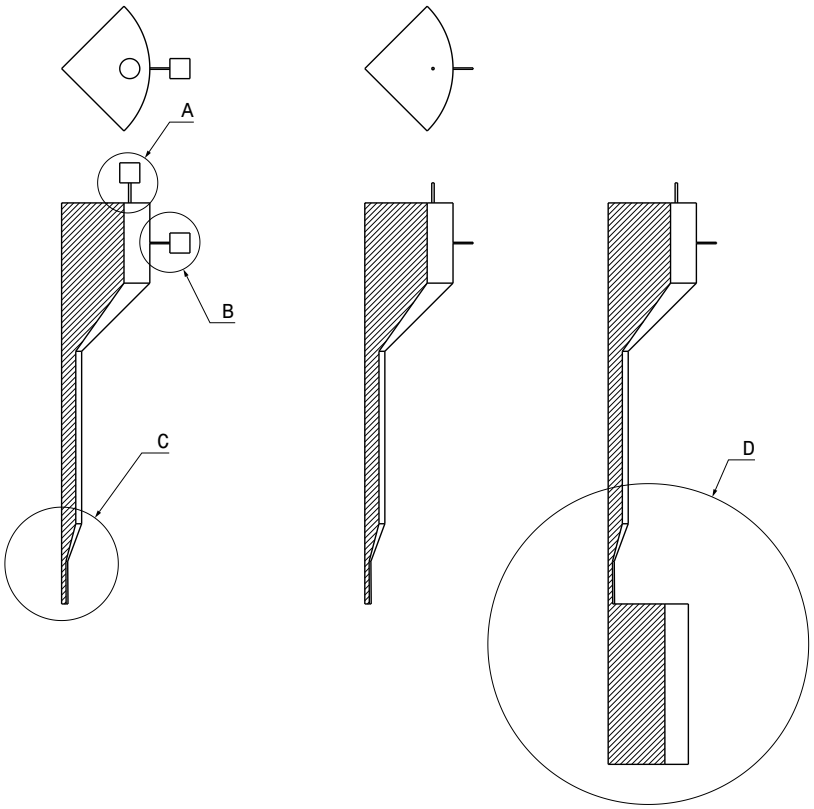

Figure 4.2: Projections of the main CFD geometries used. Planes of symmetry on geometry are drawn hatched. Geometry names from left to right: quarter, inflow and outflow.

Inflow region In order to obtain realistic results the flow in the inflow areas must be allowed to sufficiently develop before the flow enters the region of interest. In a real world flow the velocity distribution of the flow out of an orifice will be lower on the edges than in the center. The flow requires some distance to develop into a realistic flow from the inlet boundary, thus the geometry of the inflow region must account for this.

In order to asses the accuracy of the predicted discharge through the orifices a further extension of the inflow region is required to include the manifold via which the propellants are distributed. For the purpose of the baseline design the propellant manifolds are simply modeled as the sockets to where the propellant feed lines are connected. It is assumed that the manifolds are circular and have diameter of 5 mm. A detailed sketch of the used inflow regions is given in Figure 4.3.

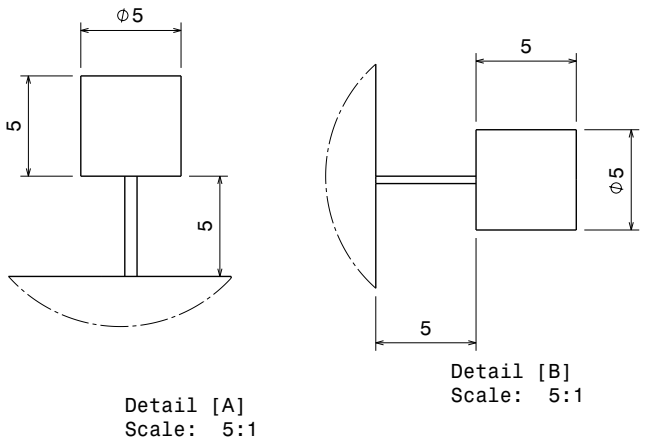

Figure 4.3: Detail sketches of the inflow region of CFD geometry

	Model	Do CFD results differ between a full inflow region and a truncated inflow?

Table 4.1: Validation items.

Outflow region Due to the presence of a sonic throat in the exhaust of the igniter it should in theory be possible to truncate the outflow region to a simple outflow boundary. As the throat is sonic no information is transferred upstream of the throat meaning that truncation of the outflow region has no effect on the solution in theory. Truncating the outflow region reduces mesh size and thus saves computational time. In addition the management of a proper outflow region can be problematic due to interaction of the exhaust jet with the relatively stationary environment and recirculation induced by the exhaust jet.

In practice there are however a few issues with this assumption, necessitating the use of a proper outflow region in some cases. These issues are:

- During startup or cold flow conditions the flow may be subsonic in the throat, which requires a proper outflow region in order to produce meaningful results. Effects of the diverging section of the nozzle will propagate upward of the flow direction.
- At solution initialization the flow may not be sonic, hence information can travel upstream. This potentially can cause issues with convergence as the solver must first establish supersonic flow before the solution will converge to a meaningful result [18].
- As the function of the throat is only to ensure choked flow and not to accelerate to flow, the expansion ratio is limited. Boundary layer growth may make the exact location of the sonic throat uncertain, both in the real world and in numerical cases.

Because of these issues both a geometry with a complete outflow region and one with a truncated outflow region will be used. A detail sketch of the outflow regions is given in Figure 4.4.

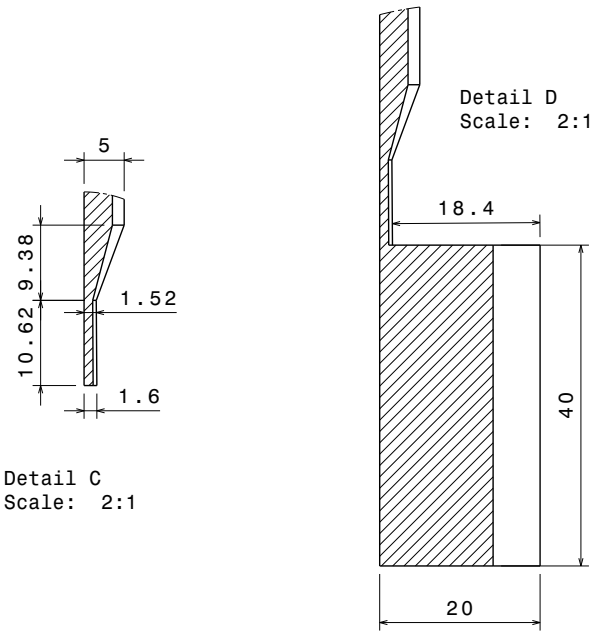

Figure 4.4: Detail sketches of the outflow region of CFD geometry

	Model	Do CFD results for sonic flow differ between a full outflow region and a truncated outflow?

Table 4.2: Validation items.

Symmetry As indicated in Chapter 3 the igniter design has two planes of symmetry. This symmetry can in theory be leveraged to significantly reduce the mesh size and thus computational cost of the numerical model. Literature however indicated that reducing geometry size by exploiting symmetry may give rise to different flow patterns [3]. Care must thus be taken that not only the predicted flow patterns are symmetrical, but also that the change from full to partial geometry exploiting symmetry does not induce and significantly different results.

	Meshing	Do CFD results differ between full geometry and reduced geometry exploiting symmetry?

Table 4.3: Validation items.

Spark plug For the numerical model it is decided not to model the spark plug geometry. Reasons for not doing so are:

- The spark plug geometry itself will be small in relation to the total igniter volume.

- The spark plug is located in the center of the igniter. It is expected that this region will only have a circulating flow and the consequently and disturbances in this region will only influence the global flow field to a small degree.
- No detailed schematics of the selected spark plug could be found. It would need to be measured after having been physically acquired making modeling it at this stage difficult.

4.1.2. Mesh generation

The mesh is largely automatically generated as a unstructured tetrahedral mesh using the ANSYS Fluent meshing program. The exact functioning of this program is beyond the scope of this work. This subsection will however shortly describe the controls used to control the mesh generation process. The primary settings used in the ANSYS Fluent meshing program are shown in Figure 4.5.

Display	
Display Style	Body Color
Defaults	
Physics Preference	CFD
Solver Preference	Fluent
Relevance	0
Sizing	
Use Advanced Si...	On: Curvature
Relevance Center	Coarse
Initial Size Seed	Active Assembly
Smoothing	Medium
Transition	Slow
Span Angle Center	Fine
Curvature Norma...	Default (18.0 °)
Min Size	Default (5.622e-005 m)
Max Face Size	Default (5.622e-003 m)
Max Size	Default (1.1244e-002 m)
Growth Rate	Default (1.20)
Minimum Edge L...	2.893e-004 m
Inflation	
Use Automatic In...	None
Inflation Option	Smooth Transition
Transition Ratio	0.272
Maximum Layers	5
Growth Rate	1.2
Inflation Algorit...	Pre
View Advanced ...	No

Figure 4.5: Primary settings as used in the ANSYS Fluent meshing program.

Cell size control The cell size of the generated mesh is primarily controlled by applying a global 'body sizing' control the overall minimum cell size is controlled. This minimum cell sizing is specified as a distance. The settings used are shown in Figure 4.6

Scope	
Scoping Method	Geometry Selection
Geometry	1 Body
Definition	
Suppressed	No
Type	Element Size
Element Size	1.e-003 m
Behavior	Soft
Curvature Normal Angle	Default
Growth Rate	Default
Local Min Size	Default (5.622e-005 m)

Figure 4.6: Settings as used on the body sizing control in the ANSYS Fluent meshing program.

Mesh refinement In order to resolve the flow with sufficient precision mesh refinements are applied. Mesh refinements are also applied to increase mesh quality. Mesh refinements were applied at the following locations:

Injector inflow The inflow orifice is shaped like a circular pipe and is therefore suitable to be meshed as a structured mesh.

Injector outflow The outflow orifice is shaped like a circular pipe and is therefore suitable to be meshed as a structured mesh.

Wall treatment For accurate modeling of boundary layers it is of importance to appropriately treat walls in the mesh. The common approach is to progressively refine the mesh as the wall is approached. The use of so called wall functions by CFD solvers relax the requirement of mesh refinement near the walls [18]. In case a slip-wall boundary condition is applied to the wall the requirement for wall treatment vanishes as no boundary layer will form in the first place.

Program sizing control The ANSYS Fluent meshing program is set to automatically control cell size as a function of distance to curvature. This is referred to as 'Advanced Size Function' in Figure 4.5.

In order to achieve the desired wall treatment all outward facing faces were included in a so called 'inflation' control. The settings as used in this inflation control are displayed in Figure 4.7.

Scope	
Scoping Method	Geometry Selection
Geometry	1 Body
Definition	
Suppressed	No
Boundary Scoping Method	Geometry Selection
Boundary	11 Faces
Inflation Option	Smooth Transition
Transition Ratio	Default (0.272)
Maximum Layers	5
Growth Rate	1.2
Inflation Algorithm	Pre

Figure 4.7: Settings as used on the inflation control in the ANSYS Fluent meshing program.

4.1.3. Mesh quality

Once the mesh is generated it is of importance to verify the quality of the resulting mesh. A low quality mesh can drastically slow convergence of the solution, induces excessive dissipation in the final solution, or can even directly induce numerical instabilities [5] [15, p. 341]. This section will discuss the metrics used to assess mesh quality and how they are applied in this work.

Skewness Skewness is a measure of how well the shapes of the face or cells used deviate from their ideal shapes. Highly skewed cells or faces cause problems during interpolation and therefore have a detrimental impact on the numerical results. Two types of skewness are typically used to determine mesh quality: volumetric and equiangular skewness [5].

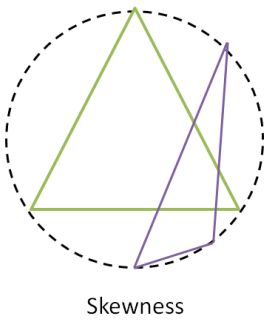

Figure 4.8: Illustration of volumetric skewness of a triangle. Source: Wikipedia

One measure of the skewness is based on the volume or area covered by an element relative to the optimal area or volume that could be covered. This skewness is referred to as the volumetric skewness, of which an illustration is given in Figure 4.8. The volumetric skewness is defined as follows:

$$SKEW_{volume} = \frac{V_{opt}}{V_{cell}} V_{opt} \tag{4.1}$$

Where V_{opt} is the optimal cell volume or face area and V_{cell} the actual volume of the cell or area of the face considered.

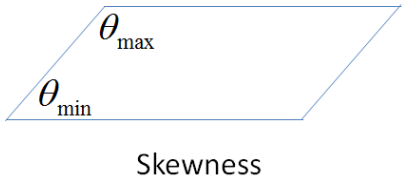

Figure 4.9: Illustration of angles used to determine equiangular skewness for a quad. Source: Wikipedia

Another measure of the skewness is based on the angles found within the face or cell compared to the expected angles in the equiangular form of the type of cell or face used. An illustration of the angles used in determining this equiangular skewness is given in Figure 4.9. The equiangular skewness is defined as follows:

$$SKEW_{angle} = max\left(\frac{\theta_{max} - \theta_e}{180 - \theta_e}, \frac{\theta_e - \theta_{min}}{\theta_e}\right) \tag{4.2}$$

Where θ_{max} is the largest angle in the face or cell, θ_{min} the smallest angle in the face or cell and θ_e the expected angle for an equiangular face or cell.

Both measures of skewness yield a score between 0 and 1, where 0 represents optimal quality and 1 the worst quality. Typical judgment for different scores are given in Table 4.4.

Skewness value	**Quality**
0.00 - 0.25	Excellent
0.25 - 0.50	Very good
0.50 - 0.80	Good
0.80 - 0.95	Acceptable
0.95 - 0.98	Poor
0.98 - 1.00	Unacceptable

Table 4.4: Cell skewness quality scoring.

Aspect ratio or cell stretch The aspect ratio is a measure to which individual cells are stretched. Highly stretched cells pose numerical problems and will invariably also have suboptimal skewness [5]. A sketch of the aspect ratio is given in Figure 4.10.

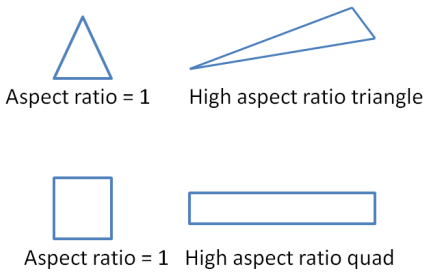

Figure 4.10: Illustration of high and low aspect ratio faces. Source: Wikipedia

Orthogonality The orthogonal quality of a mesh is of importance because highly non-orthogonal meshes cause trouble with interpolation. The orthogonal quality score used is defined as the minimum of the normalized dot product between two vectors. Perfect orthogonality is indicated by a 0 score where the two vectors are perfectly aligned. In the worst case the resulting score is 1 where the two vectors are exactly orthogonal. The orthogonal quality is calculated as follows:

$$min\left(\frac{A_i \dot{f}_i}{|A_i||f_i|}, \frac{A_i \dot{c}_i}{|A_i||c_i|}\right) \tag{4.3}$$

Where A_i is the face normal vector, f_i is the vector which points from the cell centroid to the face centroid, and c_i the vector which points from the cell centroid to the adjacent cell centroid. A graphical illustration of the vectors used is given in Figure 4.11. The typical judgments attributed to the various scores are listed in Table 4.5.

Orthogonal quality value	Quality
0.000 - 0.001	Unacceptable
0.001 - 0.140	Poor
0.140 - 0.200	Acceptable
0.200 - 0.690	Good
0.700 - 0.950	Very good
0.950 - 1.000	Excellent

Table 4.5: Cell orthogonal quality scoring.

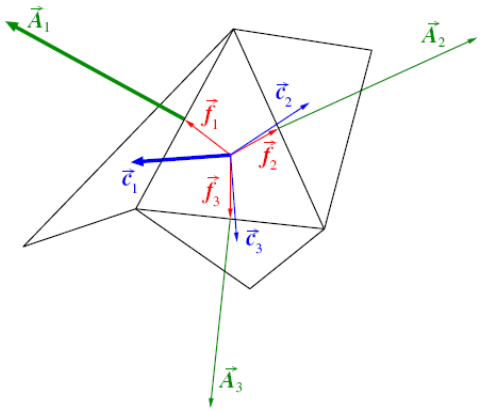

Figure 4.11: Illustration of vectors used to determine orthogonal quality of a cell [5].

Checking mesh quality in ANSYS Fluent The mesh quality can be checked in ANSYS Fluent by issuing the command **/mesh/ quality**. An example of the output of this command is given below.

```
Mesh Quality:

Minimum Orthogonal Quality = 1.53804e-02 (cell 17262 on zone 3)
(Orthogonal Quality ranges from 0 to 1, where values close to 0 correspond to low quality.)

Maximum Ortho Skew = 7.70254e-01 (cell 10800 on zone 3)
(Ortho Skew ranges from 0 to 1, where values close to 1 correspond to low quality.)

Maximum Cell Squish Index = 7.70254e-01 (cell 10800 on zone 3)
(Cell Squish ranges from 0 to 1, where values close to 1 correspond to low quality.)

Maximum Cell Equivolume Skewness = 9.84620e-01 (cell 17262 on zone 3)
(Cell Equivolume Skewness ranges from 0 to 1, where values close to 1 correspond to low quality.
```

```
Maximum Aspect Ratio =  2.01202e+01 (cell 8780 on zone 3)

Minimum Expansion Ratio =  1.60097e-01 (cell 17125 on zone 3)
```

In order to get a more detailed report on the number of low quality mesh elements the command **/mesh/repair-improve report-poor-elements** is used. An example of the output of this command is given below.

```
Skewness exceeded 0.98 at 1 cells on thread ID = 3.
Skewness exceeded 0.98 at 1 cells on thread ID = 3.
Poor Mesh Element Statistics:
 Identified     0 faces with too small area.
 Identified     0 faces adjacent to negative volume cells.
 Identified     0 faces adjacent to bad quality cells.
```

4.1.4. Results

In this subsection the resulting meshes are presented. By providing a graphical representation of the generated meshes it becomes visible how the discussed mesh features and detailing turn out in the final mesh. Figures 4.12 and 4.13 display the mesh as generated for the quarter geometry without extended inflow and outflow domains. Figures 4.14 and 4.15 display the mesh as generated for the quarter geometry including an extended inflow domain. Figure 4.16 displays the same quarter geometry mesh but in this instance with an extended outflow domain. Figures 4.17 and 4.18 finally show the full geometry mesh.

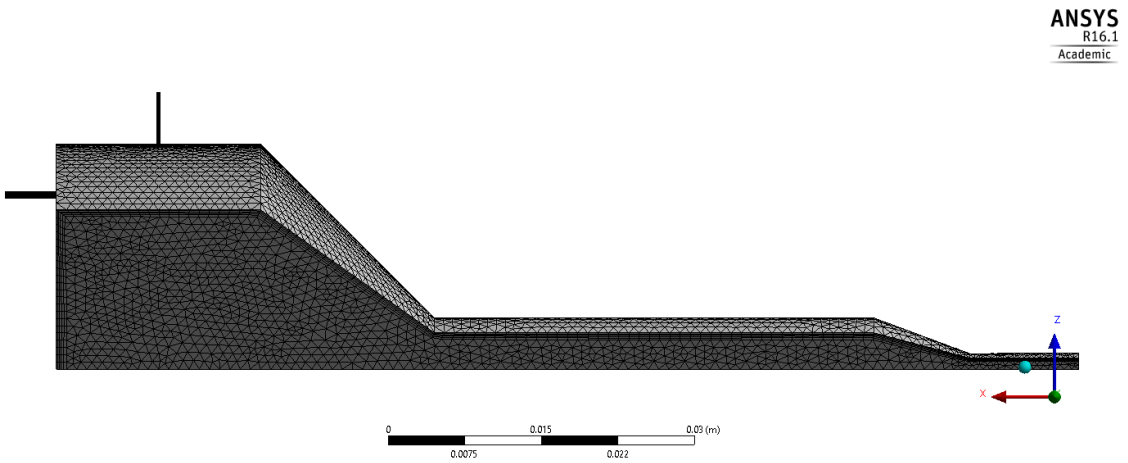

Figure 4.12: Quarter geometry mesh side view.

The primary statistics and quality scoring based on the orthogonality and skewness as discussed in Section 4.1.3 for each of the generated meshes are presented in Tables 4.6 and 4.7. Based on these metrics it is concluded that the meshes are of acceptable quality.

Name	**Nodes**	**Max aspect**	**Skewness**			
			Min	**Max**	**Avg**	**Std**
Quarter	54220	16.431	0	0.87866	0.25153	0.13857
Quarter inflow	57652	15.682	0	0.89814	0.24892	0.14218
Quarter outflow	70483	16.227	0	0.89622	0.25191	0.16303
Full	199370	18.432	0	0.885	0.2378	0.1381

Table 4.6: Mesh statistics and skewness scoring for generated meshes.

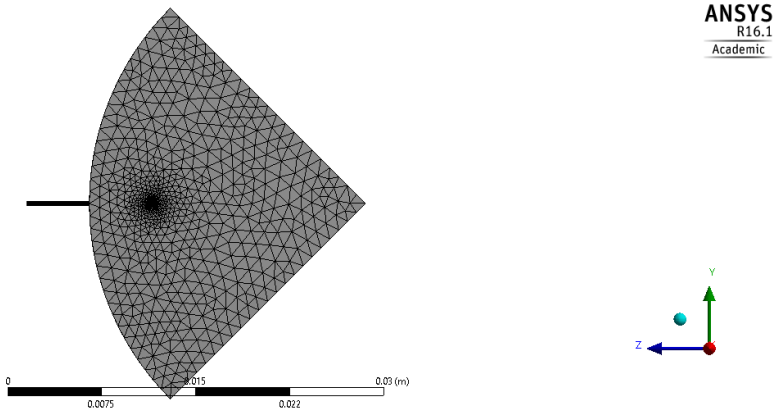

Figure 4.13: Quarter geometry mesh top view.

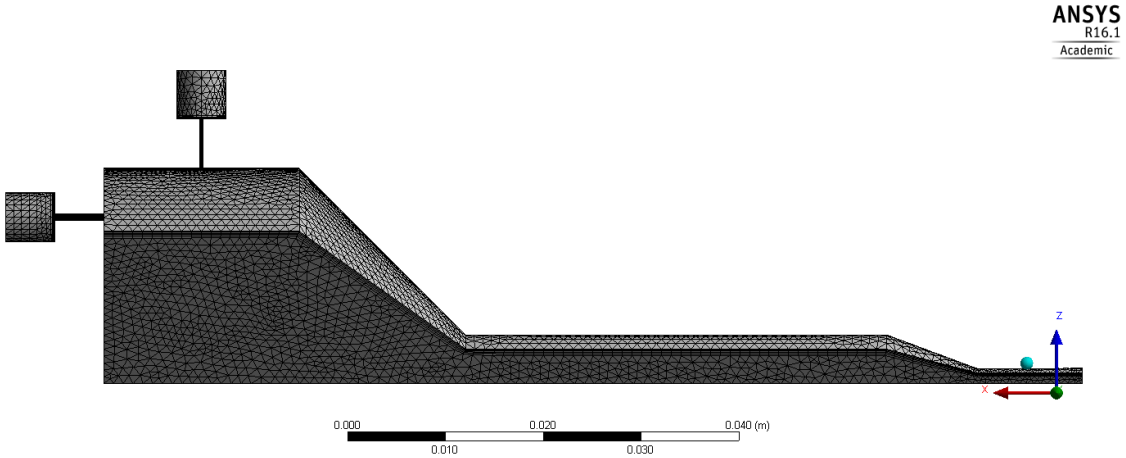

Figure 4.14: Quarter geometry mesh with inflow side view.

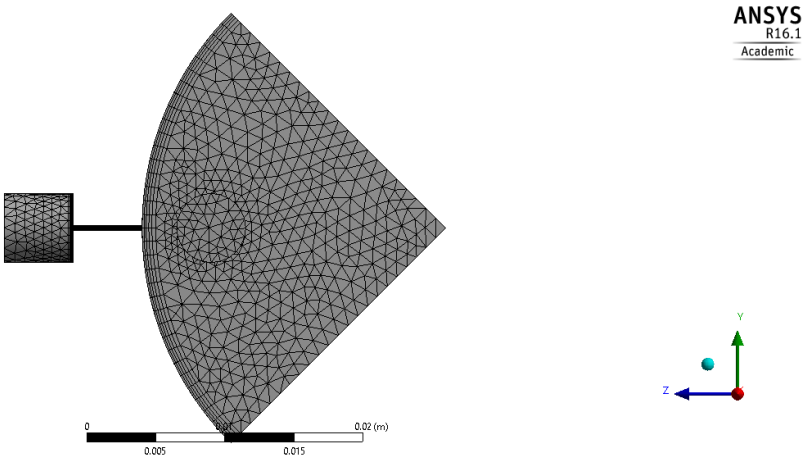

Figure 4.15: Quarter geometry mesh with inflow top view.

4.2. Boundary conditions

Part of any numerical simulation are boundary conditions. The boundary conditions must not only represent the physical world, but must also be numerically compatible. This section will elaborate on the boundary

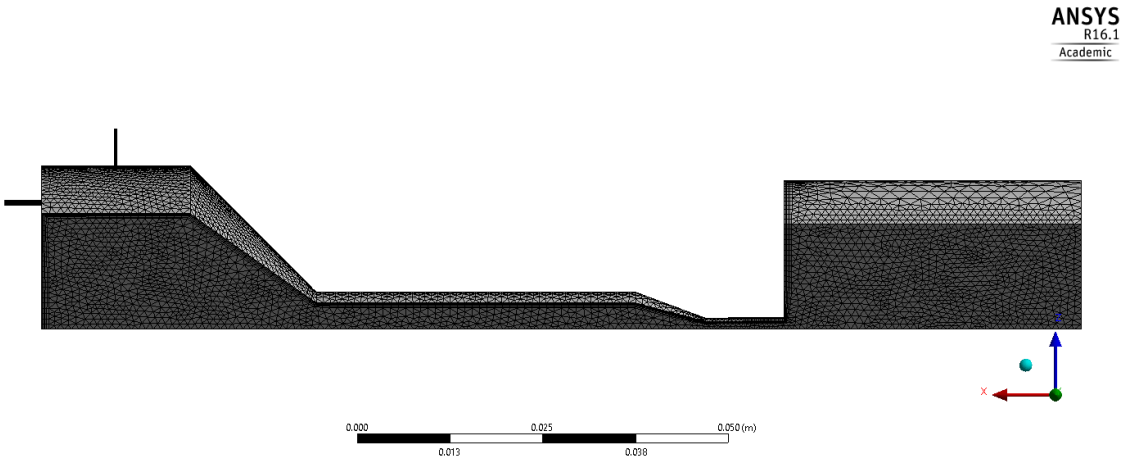

Figure 4.16: Quarter geometry mesh with outflow side view.

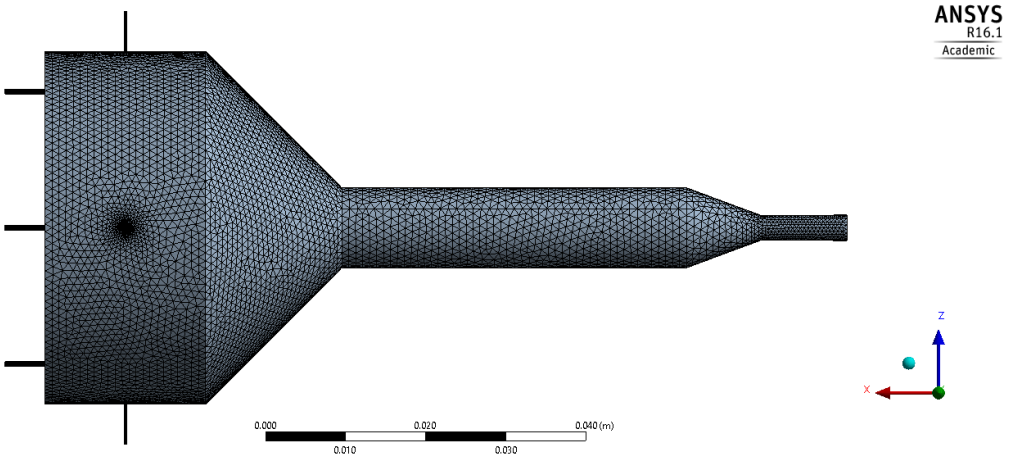

Figure 4.17: Full geometry mesh side view.

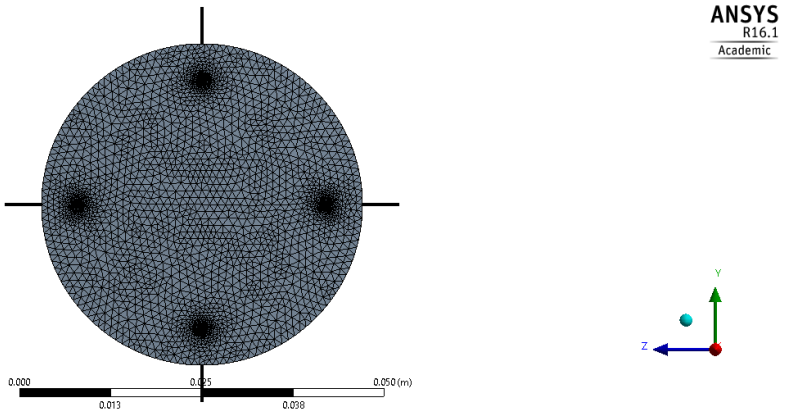

Figure 4.18: Full geometry mesh top view.

conditions used in this work.

Name	Orthogonal quality			
	Min	Max	Avg	Std
Quarter	0.19077	0.99989	0.85516	0.09944
Quarter inflow	0.10186	0.99989	0.85262	0.10566
Quarter outflow	0.17195	0.9999	0.85046	0.10448
Full	0.18032	0.99993	0.8585	0.10027

Table 4.7: Mesh orthogonal quality scoring for generated meshes.

4.2.1. Inlet

For the inflow boundaries at the oxidizer and fuel injection elements two different types of boundary conditions will be used depending on the case. For both types of inlets the species concentration and temperature are defined. The exact location of the inflow boundaries in both the regular and extended inflow geometry are shown in Figure 4.19. The two types of boundary conditions used are:

Mass flow inlet In a mass flow inlet a target mass flow is specified. The CFD solver will force the exact specified mass flow into the computational domain. As a result the pressure near the boundary will vary accordingly. This type of boundary condition is highly suitable for the type of problem used in this study because it allows precise mixing control in the igniter.

Pressure inlet When using a pressure inlet only the pressure is specified, the resulting mass flow follows from the development of the flow field. This type of inlet boundary condition is suitable for predicting the mass flow through the injection orifices given their geometry and given a feed system pressure.

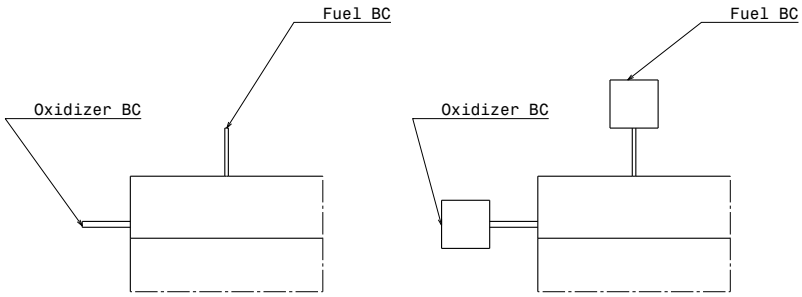

Figure 4.19: Detailed location of inflow boundaries in regular and extended inflow geometry.

4.2.2. Outlet

For the outlet a pressure boundary condition is used which enables outflow. In principle only the pressure is specified on such a boundary. In case a large outflow region is used it is likely that inflow over the outflow boundary will occur due to recirculation. For this reason it is of importance that also a species composition and temperature are specified. The location of the boundaries is indicated in Figure 4.20.

When flow becomes locally super sonic on the boundary it is no longer sensible to specify a boundary condition as no information can travel upstream. Fluent implements this behavior by not using the specified pressure as soon flow becomes locally super sonic [5]. All values are then extrapolated from the flow itself.

4.2.3. Walls

Most of the boundaries of the model are made out of various types of walls. Heat transfer along these walls is treated separately in Section 4.2.4. The location of the primary walls is illustrated in Figure 4.21. The various types of wall boundary conditions are:

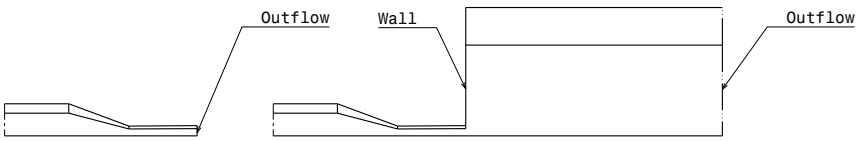

Figure 4.20: Detailed location of boundaries in outlet region for both regular and extended outflow geometry.

No slip wall All physical walls in the model are treated as regular no slip walls unless stated otherwise.

Slip wall In the nozzle a slip wall boundary condition is applied. Effectively this means that no boundary layer in terms of velocity is generated in the nozzle. The reason for using this kind of boundary is that the absence of a boundary layer ensures the nozzle throat location is fixed. In reality the sonic throat will likely be located somewhere between the geometric throat and the end of the exhaust tube. For the purpose of the numerical simulation this is however undesirable as it may falsify the assumption of the presence of a sonic throat before the truncated outflow region. Hence a slip wall is used to fix the nozzle location.

Symmetry In order to exploit the aforementioned symmetry in the model appropriate boundaries must be specified at the planes of symmetry. CFD software provides ready made boundary conditions for this purpose. Regular symmetry boundary conditions are however not suited for problems which include gravity normal to the symmetry or flow swirling into the symmetry boundary. As flow in this problem is generally expected to develop along the plane of symmetry this should not be a problem. Still it remains of importance to inspect the results due to symmetry.

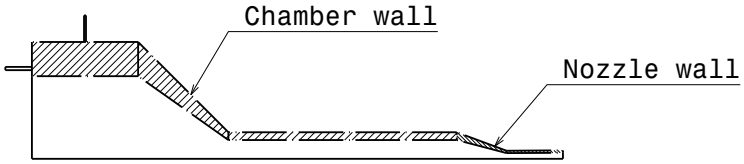

Figure 4.21: Detailed location of walls in geometry.

4.2.4. Heat transfer

Rocket engines experience extreme heat fluxes and rocket engine like devices like an igniter are thus no exception. In addition literature research indicated that hardware temperatures can have a significant impact on igniter performance [3]. On the other hand being able to cope with the thermal load on the ignition system can be a driving requirement following from REG-DESIGN-5. It is therefore necessary to consider heat transfer in the computational model.

- The relevant actuation period of the igniter is relatively short. While some ignition systems are kept active for the whole duration of the engine operating time it is only during the first few seconds of operation that the igniter performance is of importance. The amount of time available to transfer heat from the igniter interior to the igniter hardware is thus short.

- At the start of ignition the igniter hardware will be at ambient temperature. Because the igniter relies on gaseous propellants it is expected that prechilling is not required.
- In the given igniter design no active cooling method is foreseen. It is difficult to determine before hand how much heat is transferred from the igniter hardware away via radiation and convection because this will depend on the full propulsion system design. It is thus assumed that the ignition hardware will act like a heat sink.
- The impact of heat transfer on the igniter performance is most significant when the ignition system is started. As the ignition system heats up the amount of heat lost diminishes.

Because of these reasons it is assumed that the worst case scenario during which the largest amount of heat absorbed by the walls can be modeled by specifying a fixed wall temperature. In this manner the obtained results represent a conservative estimate in terms of thermal performance. In case of transient simulations more detailed modeling of the heat transfer may be required. The heat flux to the wall is then calculated by Fluent using the following equation [5]:

$$q = h_f \left(T_f - T_w\right) + q_{rad} \tag{4.4}$$

Where h_f is the coefficient for the convective heat flux as determined by Fluent, T_f the fluid temperature, T_w the wall temperature and q_{rad} the radiative heat flux.

4.3. Radiation model

In this study the so called P-1 radiation model was used to model radiation. The P-1 radiation model is a simplistic radiation model based on the more general P-N radiation approximation model [31, p. 496]. No other studies make any mention of the radiation model used, leaving no obvious choice for a radiation model [3]. The P-1 radiation model is computationally cheap and its primary drawback is its loss of accuracy of modeling optically thin media.

ANSYS Fluent provides an implementation of this model [6]. The radation flux q_r is modeled as follows in the P-1 radation model:

$$q_r = -\frac{\nabla G}{3(a+\sigma_s) = C_{\sigma_s}} \tag{4.5}$$

Where a is the absorption coefficient, σ_s the scattering coefficient, C the linear anisotropic phase function, and G the incident radiation.

4.4. Governing equations

The model proposed makes use of a set of conservation equations used to model compressible fluid flow. These equations are commonly referred to as the Navier-Stokes equations. While the full format derivation of these equations is outside the scope of this work, each of them shall be treated shortly in this section. These equations not only form the basis of the fluid dynamics model, but they are also the anchor point for many other parts of the model.

The starting point is commonly referred to as the Reynolds transport theorem, which states that for some intensive property ϕ the sum of the change in the volume Ω must be equal to what is transported over the boundary of this volume $\partial\Omega$ and what is created or consumed inside the volume [15]:

$$\text{change} = \text{transport} + \text{created}$$

$$\frac{d}{dt}\int_\Omega \phi dV = \int_{\partial\Omega} \phi \vec{u}\cdot\vec{n} dA + \int_\Omega s dV \tag{4.6}$$

Where s is the source term, $\vec{u}$ the flow velocity and $\vec{n}$ the surface normal vector. Using the divergence theorem one can rewrite this integral to:

$$\frac{d}{dt}\int_\Omega \phi dV = \int_\Omega \nabla\cdot(\phi\vec{u}) dV + \int_\Omega s dV \tag{4.7}$$

Using Leibniz's rule one can then combine all integrals:

$$\int_{\Omega}\left(\frac{d}{dt}\phi+\nabla\cdot(\phi\vec{u})+s\right)dV=0 \tag{4.8}$$

Dropping the integral yields the general conservation equation which is used to derive not only the common conservation equations seen in all CFD applications, but also for quantities like turbulent energy and species transport:

$$\frac{d}{dt}\phi+\nabla\cdot(\phi\vec{u})+s=0 \tag{4.9}$$

Momentum equation The conservation of momentum is obtained by taking $\phi=\rho\vec{u}$ and by recognizing that this equation essentially equals Newton's second law of motion. The source terms are there fore set to the force exerted by the pressure p, the force exerted by viscosity $\vec{\tau}$ and a term for other forces acting on the fluid $\vec{F}$ [35, p. 13] [6] [15]:

$$\frac{\partial}{\partial t}(\rho\vec{u})+\nabla\cdot(\rho\vec{u}\vec{u})=-\nabla p+\nabla\cdot\vec{\tau}+\rho\vec{F} \tag{4.10}$$

Continuity equation Conservation of mass is a fairly straight forward law. Mass can neither be created or destroyed in the system forcing one to set the source term to zero. The conservation of mass is also referred to as continuity and the corresponding equation is then formulated as follows by taking $\phi=\rho$ [35, p. 13] [6] [15]:

$$\frac{\partial\rho}{\partial t}+\nabla\cdot(\rho\vec{u})=0 \tag{4.11}$$

Energy equation Conservation of energy for compressible and reacting flows is again obtained in a similar manner by setting $\phi=\rho E$. The exact formulation of the energy equation tends to differ from author to author [15] [35]. In this work the formulation as used in the ANSYS Fluent software is used. The work done by pressure p is included on the left hand side, and the diffusion and of source term are included on the right hand side [6]:

$$\frac{\partial}{\partial t}(\rho E)+\nabla\cdot\left(\vec{u}\left(\rho E+p\right)\right)=-\nabla\cdot\left(\sum_{j}h_{j}J_{j}\right)+s \tag{4.12}$$

4.5. Turbulence modeling

For turbulence modeling the $\kappa-\epsilon$ turbulence model is used. The $\kappa-\epsilon$ model is one of the most widely employed turbulence model in the industry and is implemented in ANSYS Fluent [5] [47, p. 67]. The reason for using the $\kappa-\epsilon$ model in this study is the fact that it was identified as the dominant model used to model turbulence in rocket engine igniter studies [3]. Leading authors also mention the $\kappa-\epsilon$ turbulence model to be one of the most validated models, making the selection of this model a safe choice [47, p. 67]. Evaluation of the specific performance of this turbulence model and comparison to other turbulence models is outside of the scope of this study.

The $\kappa-\epsilon$ turbulence model is a so called two equation turbulence model which introduces two extra quantities and corresponding equations to model turbulence: κ denotes the turbulent kinetic energy per unit mass, and ϵ denotes the dissipation rate [47, p. 67]. These two quantities are modeled as follows were for both quantities use is made of the earlier derived general conservation equation:

$$\frac{\partial(\rho k)}{\partial t}+\frac{\partial(\rho k u_i)}{\partial x_i}=\frac{\partial}{\partial x_j}\left[\frac{\mu_t}{\sigma_k}\frac{\partial k}{\partial x_j}\right]+2\mu_t E_{ij}E_{ij}-\rho\epsilon \tag{4.13}$$

$$\frac{\partial(\rho\epsilon)}{\partial t}+\frac{\partial(\rho\epsilon u_i)}{\partial x_i}=\frac{\partial}{\partial x_j}\left[\frac{\mu_t}{\sigma_\epsilon}\frac{\partial\epsilon}{\partial x_j}\right]+C_{1\epsilon}\frac{\epsilon}{k}2\mu_t E_{ij}E_{ij}-C_{2\epsilon}\rho\frac{\epsilon^2}{k} \tag{4.14}$$

The constants $C_\mu,\sigma_\kappa,\sigma_\epsilon,C_{1\epsilon}$ and $C_{2\epsilon}$ are model constants which can be adjusted. Finally μ_t is the eddy viscosity, which is defined as follows:

$$\mu_t = \rho C_\mu \frac{k^2}{\epsilon} \tag{4.15}$$

4.6. Chemistry

For most chemistry modeling it is fundamental that the transport of species in the flow is modeled. Species transport for every specie Y_i is modeled using the general conservation equation, yielding the following equation [6]:

$$\frac{\partial(\rho Y_i)}{\partial t} + \nabla \cdot (\rho \vec{u} Y_i) = -\nabla \cdot \vec{J}_i + R_i + S_i \tag{4.16}$$

Where R_i is the reaction rate, J_i the diffusion flux of the species, and S_i is an optional source term. The attentive reader will notice that this transport equation looks surprisingly familiar to the transport equations introduced in Section 4.4. The ANSYS Fluent implementation of modeling diffusion can be found in the ANSYS Theory guide [6].

Chemistry models can primarily be divided in categories based on how the reaction rate of chemistry itself is modeled and how mixing and the interaction between mixing and turbulence and chemistry is modeled. A graphical overview in the form of a matrix of the various chemistry models discussed in this section is shown in Figure 4.22.

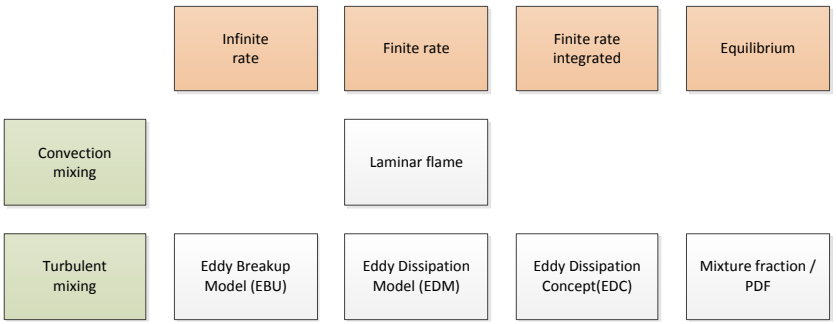

Figure 4.22: Matrix illustrating the relation between the rate of reaction of chemistry and the interaction between turbulence and mixing.

Finite/infinite rate and equilibrium In order to accurately model chemistry one needs to decide if the chemistry of interest can be treated as finite rate chemistry or infinite rate. In finite rate chemistry the reaction rate of each reaction is assumed to be dependent on a number of different factors and thus not all of available species need to completely react. In infinite rate chemistry it is assumed that all available species immediately react. In equilibrium chemistry the rate of chemistry is not directly modeled it is instead assumed that chemistry has always progressed to and equilibrium state. Finite rate integrated is a label for an approach which combines the characteristics of finite rate and equilibrium chemistry.

Mixing and turbulence In order for most chemical reactions to be able to take place different substances must be mixed. In turbulent flows mixing will only occur due to diffusion, but also due to the formation of eddies. In a RANS simulation like applied in the model used in this work only average flow quantities are calculated, thus some mixing model is required.

Transport At the start of this chapter species transport was named as an import component of modeling chemistry. Some models do however not model the transport of actual species but assume that the chemical composition can be represented by some other variables.

The following subsections will elaborate on each of the chemistry and mixing models used in this study.

4.6.1. Mixture fraction based equilibrium chemistry

In mixture fraction based chemistry, also referred to as Probability Density Function (PDF) based chemistry, it is assumed that the species fractions, temperature and density of the flow solely depend on the mixture fraction f and the enthalpy H [35, p. 327] [6]. Chemistry itself is assumed to be infinitely fast. Instead of modeling the transport of all individual species, only the transport of mixture fraction f is modeled. Using the general conservation equation introduced in Section 4.4 and taking $\phi = \rho\bar{f}$:

$$\frac{\partial}{\partial t}\left(\rho\bar{f}\right) + \nabla\cdot\left(\rho\vec{u}\bar{f}\right) = \nabla\cdot\left(\frac{\mu_l+\mu_t}{\sigma_t}\nabla\bar{f}\right) + s \tag{4.17}$$

Where σ_t is a model constant and s an optional source term. The mixture fraction f is subsequently defined as:

$$f = \frac{Y_i - Y_{i,ox}}{Y_{i,fuel} - Y_{i,ox}} \tag{4.18}$$

Where Y_i is the specie concentration and the subscript ox denotes the oxidizer while $fuel$ denotes the fuel.

The key issue with equilibrium chemistry is that in a RANS simulation the turbulent flow quantities are averaged. Effectively this implies that turbulent mixing is not modeled. For this purpose a mixture variance f'' is modeled which is dependent on predicted flow turbulence. This enables the mixture fraction based chemistry to be coupled to turbulence models like the $\kappa-\epsilon$ model. The conservation equation for the mixture fraction variance f'' is formulated as follows:

$$\frac{\partial}{\partial t}\left(\rho\bar{f''}\right) + \nabla\cdot\left(\rho\vec{u}\bar{f''}\right) = \nabla\cdot\left(\frac{\mu_l+\mu_t}{\sigma_t}\nabla\bar{f''}\right) + C_g\mu_t\cdot\left(\nabla\bar{f}\right)^2 - C_d\rho\frac{\epsilon}{\kappa}\bar{f''} + S \tag{4.19}$$

Where C_g and C_d are model constants and S an optional source term. The model constants as used in ANSYS Fluent are listed in Table 4.8.

Variable	Value
σ_t	0.85
C_d	2.0
C_g	2.86

Table 4.8: Mixture fraction model constants for ANSYS Fluent [6].

In a non adiabatic or compressible flow it is not acceptable to assume that the species fractions, temperature and density solely depend on the mixture fraction. They will also depend on the enthalpy H. Generalizing this dependency allows definition of a mapping function ϕ_i which maps each of these quantities from the local f and H:

$$\phi_i = \phi_i(f, H) \tag{4.20}$$

The final piece of the puzzle is to relate the instantaneous mixture ratio to the averaged mixture ratio f as predicted by they Reynolds averaged simulation. This is usually accomplished by using a probability density function $p(f)$. Because the real shape of this PDF is unknown an assumed shape is used. In ANSYS Fluent this PDF is a function of both the average mixture ratio f and the mixture ratio variance f'' [6].

In order to speed up the computation it is possible to generate lookup tables for each of the dependent quantities. Calculation of equilibrium chemistry is relatively expensive in terms of computational time. Using a lookup table avoids having to perform this calculation for every cell in the grid for every iteration. Two examples of these tables as generated using ANSYS Fluent are shown in Figure 4.23a and 4.23b.

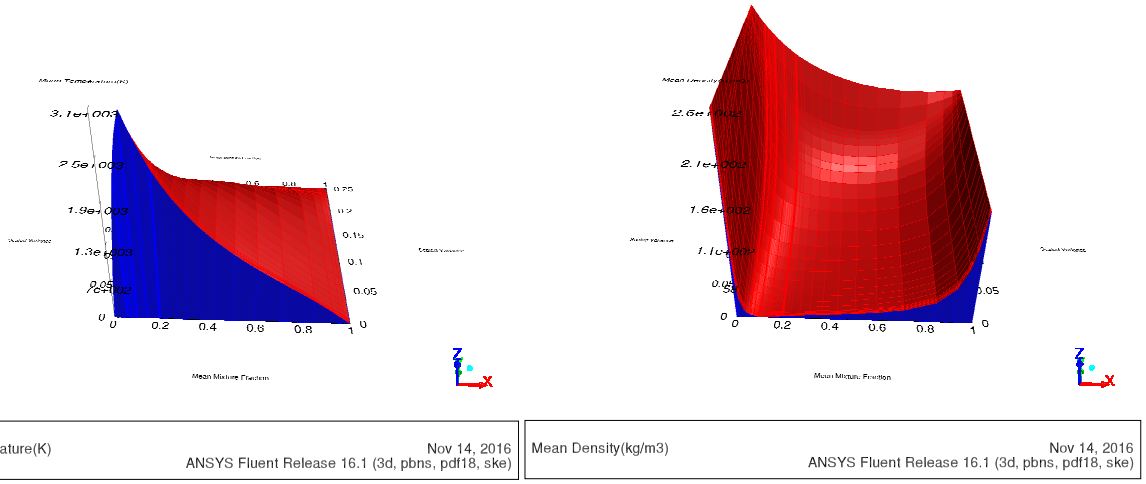

(a) Temperature - from 0 to 3100 K on the Z axis, the mean mixture fraction on the X axis and mixture variance on the Y axis.

(b) Density - from 0 to 200 kgm^{-1} on the Z axis, the mean mixture fraction on the X axis and mixture variance on the Y axis.

Figure 4.23: Examples of equilibrium chemistry tables mapping mixture ratio and enthalpy to other state variables.

The maximum number of species considered while generating the equilibrium chemistry tables is set to 20.

4.6.2. Arrhenius and chemical kinetics

The Arrhenius equation is commonly used to derive the reaction rate for specific reactions and is generally well known from the field of chemistry. When used in standalone form there is no coupling with turbulence and mixing is solely convective. This type of setup is commonly referred as a laminar flame model.

In chemistry the reaction rate r of a reaction involving N reactants is usually formulated as follows:

$$r = k \prod_{i=1}^{N} [X_i]^{a_i} \tag{4.21}$$

Where $[X_i]$ is the molar concentration of the i-th reactant, k is the reaction rate constant and a_i the order to which the rate depends on the i-th reactant. This reaction rate constant is modeled using the Arrhenius equation [3]:

$$k = Ae^{-\frac{E}{RT}} \tag{4.22}$$

The modified Arrhenius equation introduces an explicit temperature dependence [35] [3]. The equation is then formulated as follows:

$$k = AT^n e^{-\frac{E}{RT}} \tag{4.23}$$

Where A is the pre-exponential factor in s^{-1}, T the temperature in K, n the dimensionless temperature dependence factor, E the activation energy in Jmol^{-1} and R the gas constant in Jmol^{-1}K^{-1}.

In order to use the Arrhenius equation one however needs a set of reaction equations and corresponding constants. This chemical kinetics model, or chemical scheme, typically takes the form of a table which lists which reactions between which species are modeled and the parameters of the kinetics of these reactions [35] [3]. Such a model is sometimes also referred to as a global reaction model.

Four examples of kinetic schemes for the combustion of methane with oxygen which were observed in literature are list in Tables 4.9, 4.10, 4.11, 4.12 [3].

Table 4.9: Oxygen - methane single step chemical scheme proposed by Westbrook and Dryer [48]. Activation energy E in kcal/mol.

#	Reaction	A	n	E	Order
1	$CH_4 + 5\,O_2 \rightleftharpoons CO_2 + 4\,H_2O$	$1.3{\cdot}10^8$	1.0	$4.84{\cdot}10^1$	$[CH_4]^{-0.3}[O_2]^{1.3}$

Table 4.10: Oxygen - methane two step chemical scheme proposed by Westbrook and Dryer [48]. Activation energy E in kcal/mol.

#	Reaction	A	n	E	Order
1	$CH_4 + 3/2\,O_2 \longrightarrow CO + 2\,H_2O$	$2.8{\cdot}10^9$	0.0	$2.0{\cdot}10^5$	$[CH_4]^{-0.3}[O_2]^{1.3}$
2	$CO + 1/2\,O_2 \longrightarrow CO_2$	$4.0{\cdot}10^{14}$	0	$1.7{\cdot}10^5$	$[CO]^1[H_2O]^{0.5}[O_2]^{0.25}$
2	$CO + 1/2\,O_2 \longleftarrow CO_2$	$5{\cdot}10^8$	0	$1.7{\cdot}10^5$	$[CO_2]^1$

Table 4.11: Oxygen - methane chemical scheme proposed by Jones and Lindstedt [35, p. 189] [20]. Activation energy E in J/kmol.

#	Reaction	A	n	E	Order
1	$2\,CH_4 + O_2 \rightleftharpoons 2\,CO + 4\,H_2$	$4.4{\cdot}10^{11}$	0.0	$3.00{\cdot}10^4$	$[CH_4]^{-0.5}[O_2]^{1.25}$
2	$CH_4 + H_2O \rightleftharpoons CO + 3\,H_2$	$3.0{\cdot}10^8$	0.0	$3.00{\cdot}10^4$	$[CH_4][H_2O]$
3	$2\,H_2 + O_2 \rightleftharpoons 2\,H_2O$	$2.5{\cdot}10^{16}$	-1.0	$4.00{\cdot}10^4$	$[H_2]^{0.5}[O_2]^{2.25}[H_2O]^{-1}$
4	$CO + H_2O \rightleftharpoons CO_2 + H_2$	$2.75{\cdot}10^9$	0	$2.00{\cdot}10^4$	$[CO][H_2O]$

Table 4.12: Oxygen - methane chemical scheme based on truncated Sandia National Labs 1D flame model [12]. Units of activation energy E not specified in source.

#	Reaction	A	n	E
1	$CH_4 + 2\,O_2 \rightleftharpoons CO_2 + 2\,H_2O$	$6.70{\cdot}10^{11}$	0.0	$4.84{\cdot}10^4$
2	$H_2 + O_2 \rightleftharpoons H_2O + O$	$5.00{\cdot}10^{12}$	1.0	$4.80{\cdot}10^4$
3	$H_2 + O \rightleftharpoons H + OH$	$2.50{\cdot}10^{14}$	0.00	$6.00{\cdot}10^3$
4	$H + O_2 \rightleftharpoons O + OH$	$4.00{\cdot}10^{14}$	0.00	$1.80{\cdot}10^4$
5	$CO + OH \rightleftharpoons CO_2 + H$	$1.51{\cdot}10^7$	1.28	$-7.58{\cdot}10^2$
6	$O_2 + H_2O \rightleftharpoons 2\,O + H_2O$	$5.00{\cdot}10^{18}$	0.00	$1.12{\cdot}10^5$
7	$CO + H_2O \rightleftharpoons CO_2 + H_2$	$5.50{\cdot}10^4$	1.28	$-1.00{\cdot}10^3$

In order to obtain some idea of the flame temperatures predicted by the models listed in Tables 4.9, 4.10, 4.11, 4.12 [3] it is decided to use the NASA Chemical Equilibrium with Applications (CEA) program to predict these temperature using chemical equilibrium [33].

The temperatures are predicted by instructing CEA to only consider the species which appear in the chemical kinetic schemes. The combustion temperatures are calculates at three pressure levels which are found in the igniter system during operation. As CEA cannot represent the propellants at the exact temperature at injection in the igniter slightly different initial temperatures had to be used. This results in an enlarged uncertainty in the predicted flame temperatures. The corresponding CEA inputs and output can be found in Appendix D and the obtained flame temperatures are presented in Table 4.13.

Table 4.13: Flame temperatures as predicted using equilibrium chemistry with the NASA CEA for the presented chemical kinetic schemes.

Scheme	**Pressure**		
	70 bar	40 bar	1 bar
1-step Westbrook-Dryer	5103.17	5103.17	5103.17
2-step Westbrook-Dryer	4099.88	4049.95	3789.77
4-step Jones-Lindstedt	3894.7	3822.35	3360.38
Sandia National Labs	3705.42	3633.49	3189.94

4.6.3. Eddy Breakup Model (EBU)

In the Eddy Breakup Model it is assumed that the reaction rate is solely dependent on the turbulent mixing and that chemistry is infinitely fast in all other aspects [35, p. 226]. This dependence on turbulent mixing is modeled by estimating a turbulent mixing time τ_t from the turbulent energy ϵ and turbulent dissipation κ:

$$\tau_t = \frac{\kappa}{\epsilon} \tag{4.24}$$

Because in the Eddy Breakup Model it is assumed that combustion is instantaneous once mixed, chemistry can effectively be considered to be single step. Only a progress variable f which progressed from 0 (unmixed) to 1 (full mixed) needs to be tracked [35, p. 225].

$$\bar{k} = C\bar{\rho}\frac{\sqrt{\bar{f''^2}}}{\tau_t} = C\bar{\rho}\frac{\epsilon}{\kappa}\sqrt{\bar{f''^2}} \tag{4.25}$$

Where $\bar{f''^2}$ is the variance of the mass fraction of the mass fraction of the reactant.

Potential problems when running multiple step schemes in EBU due to all reaction rates being equal as they are solely dependent on mixing [6]. This fact make the EBU fundamentally unsuited for schemes containing more than two steps to model for example radicals. The EBU is not separately implemented in Ansys Fluent, but is still explained because it forms the basis for other turbulence chemistry interaction models.

4.6.4. Eddy Dissipation Model (EDM)

The Eddy Dissipation Model (EDM) extends the concept of the EBU by assuming that chemistry is still primarily limited by mixing but that different types of eddies govern mixing and that actual species transport is modeled [28]. This enables the EDM to model chemistry and mixing in much more detail. Central to the EDM is the notion of the existence of non premixed flow regions and premixed flow regions.

In non premixed flow regions there will be separate eddies of each of the reactants. It is the rate of dissipation of these eddies which governs the mixing and thus limits chemistry. Each of the reactants however requires the presence of the other reactants to be able to react, leading to a set of equations of the one yielding the lowest value is limiting. The reaction rate r_i for each of the reactants Y_i is formulated as follows:

$$r_i = A\frac{\bar{Y}_i}{s}\frac{\epsilon}{\kappa} \tag{4.26}$$

Where A is a model constant, and s is the ratio of reactant needed for the reaction. In most literature the presence of only an oxidizer and a fuel are assumed and the s is then taken as the stoichiometric ratio for the given reactant in the propellant combination.

In premixed flow regions where all reactants are present in the eddies the EDM assumes that reaction rates are limited by dissipation of eddies of hot reaction products which spread the flame. This reaction rate r as limited by the dissipation of each of the reaction products Y_j is formulated as:

$$r_j = AB\frac{\bar{Y}_j}{1+s}\frac{\epsilon}{\kappa} \tag{4.27}$$

Where B is another model constant. Again in most literature it is assumed that only a single reaction product is present, yielding a single equation. The actual reaction rate r as predicted by the EDM is then given as the minimum of the full set of equations:

$$r = min\left(r_0, ..., r_i, r_j\right) \tag{4.28}$$

The model constants A and B are to be experimentally determined and represent the manner in which the eddies dissipate and also model progression of chemistry itself. They are usually set to $A = 0.5$ and $B = 4$ [28]. Little literature on the tuning of these model parameters is known, but a common extension on the EDM, which is also used in this study, is to limit the reaction rate as predicted by the EDM by the reaction rate as predicted using Arrhenius's Law. In this manner the chemistry becomes finite rate without having to tune the model constants. It is unknown to what degree the validity of this assumption, but it does appear to be the norm in many implementations of the EDM.

While the EDM does extend EBU to include finite rate chemistry it still suffers from the fundamental flaw that in locations where chemistry is not limited by Arrhenius's law for the rates of all modeled reaction rates in the EDM itself. In case multiple reactions are used chances a high that at least in some locations predicted reaction rates for the modeled reactions end up to be equal [6]. This fact make the EDM largely unsuited for modeling multi step chemistry schemes.

4.6.5. Eddy Dissipation Concept (EDC)

The Eddy Dissipation Concept (EDC) further extends the concept of the EDM introducing finite rate chemistry [27]. Central to the EDC is the notion that turbulent energy is transformed into heat at four different levels of flow structure where every deeper level represents finer grained flow structures. It is only in the finest flow structures that chemistry is modeled.

The full derivation for the EDC is quite lengthy and extends beyond the scope of this study. Central is however the notion that chemistry limited both by Arrhenius' Law and the mixing between the bulk of the flow and the fine flow structures. Because of this approach complex chemical schemes can be used to model chemistry.

The reactions in the fine structures are integrated over a time scale τ^* in order to simulate the finite rate reactions progressing. The volume considered in which the chemical reactions are integrated equals ${\epsilon^*}^3$. While this integration in time arguably leads to better results it is also much more computationally expensive compared to the earlier discussed models.

In the Ansys Fluent implementation the time scale τ^* and scale ϵ^* are defined as follows [6]:

$$\begin{aligned} \tau^* &= 0.4082\left(\frac{\nu}{\epsilon}\right)^{\frac{1}{2}} \\ \epsilon^* &= 2.1377\left(\frac{\nu\epsilon}{\kappa^2}\right)^{\frac{1}{4}} \end{aligned} \tag{4.29}$$

Where κ and ϵ are the turbulent quantities which are modeled using the $\kappa - \epsilon$ model.

4.7. Equation of state

In a pressure based solver the pressure is calculated from the density and temperature. One thus needs an equation of state to relate the pressure of the gases in the model to the density. A very common used manner of modeling gas is by using the ideal gas assumption. In the extreme environment of a rocket engine these assumptions may however be questionable. This section will further elaborate on the gas models used.

4.7.1. Ideal gas

As mentioned the ideal gas assumption is one of the most commonly used methods for modeling gas. The two most important assumptions made for ideal gases are:

- There are no intermolecular forces between the gas molecules.

- The volume of the molecules is negligible compared to the volume occupied by the gas.

Under ideal gas a few other more minor assumptions are made. These can be found in virtually any work on gas dynamics. The state equation for ideal gas is defined as follows:

$$pV = nRT \tag{4.30}$$

Where R is the gas constant in $\mathrm{Jmol^{-1}K^{-1}}$, p the pressure in Pa, n the number of moles, V the volume in $\mathrm{m^3}$, and T the temperature in K. The simplicity of the equation of state for ideal gas makes usage of it computationally cheap and thus a prime candidate for use in a computational model.

4.7.2. Real gas

It is however questionable if the ideal gas assumption is valid in the context of this work. In the injector orifices pressures are very high and the state of the injected methane and oxygen may be close to the critical point. Exactly because of this reason other studies indicated that a real gas equation was used [3]. In these cases the authors opted to use the Peng Robinson ideal gas equation.

Specifically the low temperature and high pressures are known to break down the assumption that the volume of the molecules is negligible compared to the volume occupied by the gas, causing the compression factor to be non constant and not equal to 1. In case conditions approach the critical point the assumption of no intermolecular forces between the gas molecules also breaks down.

In order to address these issues it is decided to also use the Peng Robinson ideal gas equation in the model. There are other real gas models, but the prevalence of the Peng Robinson model in comparable works and the fact that ANSYS Fluent offers a ready made implementation are the basis for selecting this real gas model [6]. A detailed trade-off between real gas models is beyond the scope of this study.

The Peng Robinson gas model is defined as follows [34]:

$$p = \frac{R\,T}{V_m - b} - \frac{a\,\alpha}{V_m^2 + 2bV_m - b^2} \tag{4.31}$$

$$\begin{aligned} a &= \frac{0.45724\,R^2\,T_c^2}{p_c} \\ b &= \frac{0.07780\,R\,T_c}{p_c} \\ \alpha &= \left(1 + \kappa\left(1 - \left(\frac{T}{T_c}\right)^{0.5}\right)\right)^2 \\ \kappa &= 0.37464 + 1.54226\,\omega - 0.26992\,\omega^2 \end{aligned} \tag{4.32}$$

Where T_c is the critical temperature, ω the acentric factor, R the universal gas constant, V_m the molar volume in $\mathrm{m^3}$, p_c the critical pressure in Pa.

Beyond all the theoretical advantages of using a real gas model there is also a price to pay in terms of complexity. The use of a real gas equation like the Peng Robinson equation also does not come for free in terms of computational cost; it is much more expensive than the standard ideal gas equation. This computational cost is mainly lodged in the fact that many more computational steps are required to solve the Peng-Robinson equation compared to the Ideal gas equation.

4.8. Material properties

In the developed model various properties of the fluids are required. Examples are the heat capacities and molar masses. These properties do not only need to be resolved, but also need to be offered in a format usable by the solver.

In this work the database of materials properties supplied with ANSYS Fluent is used [6]. As only simple and fairly commonly used materials are used: namely methane, oxygen, hydrogen, water, carbon-dioxide and carbon-monoxide there is no need to devote extra attention to the properties of these materials. As the database is supplied with ANSYS Fluent itself, using the covered materials is straight forward.

4.9. Spark energy deposition model

A validated model for energy deposition assumes that the spark energy is distributed normally in space and time [26]. This model has been shown to be valid for both laser and electrical sparks. The energy deposition is modeled as an extra source term $\dot{Q}$ in the energy equation:

$$\dot{Q}(x,y,z,t) = \frac{\epsilon_i}{4\pi^2\sigma_r^3\sigma_t} e^{-\frac{1}{2}\left(\frac{r}{\sigma_r}\right)^2} e^{-\frac{1}{2}\left(\frac{t-t_0}{\sigma_t}\right)^2} \tag{4.33}$$

Where r is the distance to the center, t_0 the time at which the deposited energy attains its maximum, ϵ_i the total deposited energy of the spark, and σ_r and σ_t are respectively the spatial and temporal widths of the spark.

Using this model does require one to determine the spatial and temporal width as well as the total deposited energy of the spark. Determining the widths of a laser focus region is straight forward as it is the result of the laser pulse length and focal region. For a spark these properties may be more difficult to predict.

4.10. Discretization scheme

In order to solve the different differential equations used in this model (and any CFD simulation) a spatial discretization scheme is required. In the model both first order and second order upwind discretization schemes will be employed. For both schemes the Taylor series expansion of a function ϕ around the point a can be considered:

$$\phi(a) = \phi(a) + \frac{\phi'(a)}{1!}(x-a) + \frac{\phi''(a)}{2!}(x-a)^2 + O(3) \tag{4.34}$$

The fact that the value from the upwind node is used is reflected in the name of this discretization scheme. Upwind refers to the direction in relation to the flow velocity direction.

First order upwind For the first order upwind discretization scheme only the first term is considered, hence the name first order. For this first term the upwind value of the upwind node is used in the implementation of this discretization scheme by ANSYS Fluent [6]. When for example the value of ϕ at the cell face ϕ_f is to be interpolated, the value of the upwind node is used ϕ as the sole term to be filled in truncated Taylor expansion:

$$\phi(a) = \phi(a) + O(1) \quad \Longrightarrow \quad \phi_f = \phi \tag{4.35}$$

Second order upwind For the second order upwind scheme the first and second terms of the Taylor expansion are considered. Using the same example as for the first order scheme where the face value ϕ_f is to be interpolated the value of the upwind node is used ϕ by ANSYS Fluent [6]. This time however also the gradient $\Delta\phi$ is substituted for the local derivative of ϕ' and $(x-a)$ is substituted by the vector $\vec{r}$ which is defined as the vector from the upwind node to the face center:

$$\phi(a) = \phi(a) + \frac{\phi'(a)}{1!}(x-a) + O(2) \quad \Longrightarrow \quad \phi_f = \phi + \Delta\phi \cdot \vec{r} \tag{4.36}$$

From the Taylor expansion it follows that this scheme is more accurate than the first order scheme. In practice the use of the gradient can cause problems. Very steep gradients can arise shortly after initialization or near natural flow phenomena. It is not unthinkable that the interpolated value becomes insensible when local gradients are very steep. The most straight forward example of such an insensible value is when the gradient is so steep that the interpolation result becomes negative. Due to this effect use of a second order upwind discretization scheme can induce numerical instability.

4.11. Solution method

With the model and discretization methods specified in the preceding sections of this section a method to numerically solve problems is required. In theory it is possible to find a solution by discretizing all governing equations described and setting up a single linear system which is then directly solved. Such direct methods are however computationally and storage wise expensive. Because of this reason sequential methods are preferred in which each of the governing equations is solved in sequence.

In this study the Semi-Implicit Method for Pressure Linked Equations (SIMPLE) algorithm was used. As the name implies SIMPLE is a so called pressure based method, in contrast with density based methods. The SIMPLE algorithm was originally developed for incompressible flows but is also applicable to compressible flows. Using the SIMPLE algorithm the different governing equations are iteratively solved by solving these equations separately.

The key concept of SIMPLE is that assumes that the correct pressure field consists out of an uncorrected pressure and a pressure correction term [6] [15]. The velocity is likewise assumed to be separable in an uncorrected term and a correction term:

$$\begin{aligned} p &= p^* + p' \\ u &= u^* + u' \end{aligned} \tag{4.37}$$

Where p and u are the corrected pressure and velocity fields, p^* and u^* are the uncorrected pressure and velocities, and p' and u' are the corresponding corrections. These corrected pressure and velocity fields are then substituted in the momentum and continuity equation. Finally a so called pressure correction equation is obtained by solving for the unknown pressure correction term p'.

The full formal derivation of the SIMPLE algorithm is beyond the scope of this work. A high level flow diagram of the SIMPLE solution method is however shown in Figure 4.24. The operations performed in each step are:

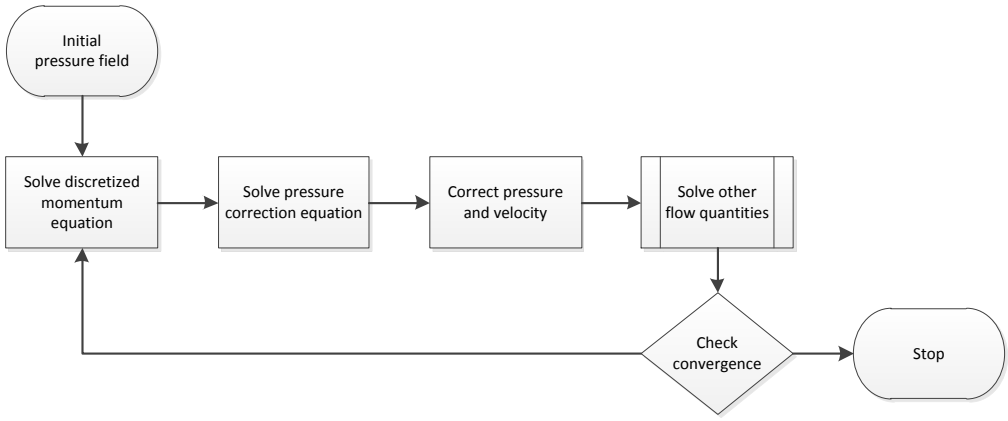

Figure 4.24: Flow diagram of the SIMPLE solution method.

Initial pressure field In order to start the solution loop an initial uncorrected pressure field is required. This is a 'guessed' pressure field, and is typically obtained from the initialization settings of the CFD software.

Solve discretized momentum equation Using the current uncorrected pressure the uncorrected velocities are obtained by solving the discretized momentum equation.

Solve pressure correction equation Because the obtained uncorrected velocities need to satisfy the discretized continuity equation one can calculate the required velocity corrections, yielding the corrected velocity

field. Using this corrected velocity field the corrected pressures are then obtained. This step is typically encapsulated in the pressure correction equation.

Correct pressure and velocity The corrected velocity fields p^{k+1} and u^{k+1} are obtained by applying the obtained corrections.

Solve other flow quantities During this step other flow quantities are solved. Examples are species transport, energy and turbulence quantities.

Check convergence In case the solution has sufficiently converged no further iterations are performed. Is convergence is not reached the current pressure field is assumed to be the uncorrected pressure field for the next iteration. More attention is spent on assessing convergence in Section 5.2.

Large pressure corrections can cause issues with convergence, which is why an relaxation factor α is introduced in the update step of the pressure field. More attention will be spent on these relaxation factors in Section 5.3.1. The new pressure and velocity field to be used in the next iteration $k+1$ are calculated using:

$$\begin{aligned} p^{k+1} &= p^* + \alpha p' \\ u^{k+1} &= u^* + u' \end{aligned} \tag{4.38}$$

In contrast to the pressure correction the velocity correction does not include a relaxation term. This is due to the fact that the corrected velocity is required to satisfy the continuity equation. Including a relaxation term would be nonsensical: only the corrected velocity satisfies the continuity equation.

In order to further speed up the solution process a method referred to as the Algebraic Multi Grid (AMG) is used in which multiple different grids of increasing coarseness are used to solve the same problem. Explanation of this method is beyond the scope of this work. More information can be found in the ANSYS Fluent manual [6].

Other solution methods such as PISO and variants to the SIMPLE algorithm such as SIMPLER and SIMPLE-C exist [6]. As a comparison between solution methods is outside of the scope of this work they will not be treated in further detail.

4.12. Summary

In this chapter the need and rationale for selecting different model components were extensively treated. The computational model is completed by specifying the mesh and boundaries and by selecting and introducing appropriate discretization and solver techniques.

Four computational meshes four different meshes were generated and checked for quality. One quarter and one full geometry mesh in order to asses the influence of exploiting symmetry, a mesh with extended inflow and a mesh with extended outflow. While the resulting mesh quality was not optimal the quality is sufficient for the purpose of this study.

For inlet region a mass-flow type boundary will be used. To verify predicted discharge coefficients the inlet boundaries can be changed to pressure boundaries. For the nozzle wall a slip wall boundary is used to ensure that the sonic throat is located at the desired location. For the outflow region a pressure boundary is used. Heat transfer is modeled using heat equation and radiation using the P-1 model.

The primary governing equations are introduced which relate the change in a transported quantity to the transport over a control volume and the creation in that control volume. Using those equations momentum, mass, energy, species, turbulent kinetic energy and turbulence dissipation are transported. For turbulence the widely used two equation $\kappa - \epsilon$ model is used.

For chemistry either the Eddy Dissipation Model (EDM), the more complex Eddy Dissipation Concept (EDC), or a chemical equilibrium method can be used which models the transport of a mixture fraction ratio. The EDM can optionally be paired with finite rate chemical schemes while the EDC requires one to function.

The EDM can only effective model single step chemistry while the EDC can work with more complex multi-step chemical schemes. Finally four of these required chemical schemes were presented.

Two gas models are proposed: the widely used ideal gas equation which is computationally cheap and the Peng-Robinson real gas equation which is computationally more expensive but which is capable of accurately representing liquid and supercritical phases.

Finally the discretization schemes and solution method were introduced. An iterative solution method which independently solves pressure and velocity called SIMPLE will be used. The use of relaxation factors in controlling numerical stability is explained as well as the role of the discretization method in maintaining numerical stability.

5
Experiments

This chapter presents the practical methodology of obtaining the results, a condensed overview of the cases run and a discussion of specific observations while running individual cases. With the model fully specified in the previous chapter a strategy is required in order to produce the numerical results. Specifically the initial values need to be selected and considerable effort needs to be spent to keep the solution from becoming unstable.

As iterations of the solution are produced by the solver one needs to asses if the solution can be considered to have converged. The rationale and method behind this assessment is presented in Section 5.2.

This chapter concludes with an overview of all the cases simulated for this study. In this overview the configuration and convergence of each case is given. Finally the most interesting cases are discussed in terms of observations during the solution process. For each case it applies that full printouts of the flow fields are available in Appendix H.

The implications of the results produced will be discussed in Chapter 7.

5.1. Initialization

Proper initialization of the solution is a crucial part in the solution process. While in theory the final solution should be independent of the initialization given that the solution is converged practice paints a different picture. The reasons that initialization is of importance are:

Convergence speed When a solution is initialized in a state close to the final solution convergence will naturally be much quicker as fewer iterations are required to attain the correct solution.

Divergence In case the solution is initialized to a non physical or extreme state divergence may occur during the first few iterations. If one would for example initialize the complete solution as an explosive mixture gradients may become so steep that the solution becomes invalid due to numerical errors.

Non unique solutions In special problems where for example super sonic flow is present more than one solution may be valid. Initializing the solution in the correct state ensures that the solution converges to the right solution. Another example is reacting flow which is initialized at a low temperature preventing combustion from starting.

In order to initialize the solution as correctly as possible three sets of initial values were used. These three sets are listed in Table 5.1. Depending on the exact models used some minor variations to these sets were made.

5.2. Convergence

When solving a flow using a numerical model one aims to achieve a state of convergence where the found solution does no longer change between consecutive iterations and that residuals are zero [47]. Due to limited

Parameter	Unit	Chemistry		
		Very hot	Hot	Cold
Pressure	Pa	7.00E+06	7.00E+06	7.00E+06
X velocity	ms^{-1}	-200	-200	-20
Y velocity	ms^{-1}	0	0	0
Z velocity	ms^{-1}	-100	-100	-10
CH4	-	0	0	0.2
O2	-	0	0	0.8
Temperature	K	3000	2000	300

Table 5.1: Used sets of initialization values depending on the expected temperature.

machine precision and limited precision in the model it is very likely that true convergence will be achieved. Luckily true convergence is not required in order to end up with a good representation of the flow. What then the exact criteria for convergence should be is rather fuzzy. None the less one can state that a stable solution must have been found and that residuals should have sufficiently decreased. Recommended criteria for convergence are found in CFD manuals [5] and follow from experience working in the field of CFD [18]. Key criteria are:

- Residuals should decrease a factor of $\cdot 10^3$ from the initial solution.
- The residual of the energy equation should be around $1 \cdot 10^{-6}$ or smaller.
- Residuals should be stable over iterations. Residuals which are still in motion indicate that the solution has not yet finished converging.
- Local fluctuations may prevent convergence to be observed in the residuals. In case these local fluctuations are minor or periodic the solution may still be considered to be converged despite the residuals not having reached the usual criteria for convergence. Such local fluctuations may represent physical fluctuations or be of numerical nature [18].

Beside the criteria of convergence based on the residuals there are also a few other indicators of a non converged or bad solution:

Reversed flow Incorrect boundary conditions or wrong solutions may cause reverse flow on some types of boundaries. Usually this is a very clear indication that the solution is not converging or not converging correctly. On the other hand reversed flow is to be expected when including a very large outflow boundary.

Limits exceeded Limits are applied to certain variables to aid convergence and stability [5]. These limits prevent values like temperature from assuming nonsensical values during the solution process. A solution is generally not considered to have converged if limits are still being exceeded. Naturally this requires the limits set to be truly nonsensical.

5.2.1. Integral terms

Despite residuals having become small or having decreased significantly it may be hard to judge convergence solely on their behavior. Oscillations in the flow or unstable flow features may cause residuals to never become truly small and an otherwise well solved flow may exhibit large residuals due to local effects. One should not forget that the residuals are not per se the quantity of interest in a solution but that the quality and stability of the solution itself are the properties which are desired to be maximized. It would thus be helpful to have additional means of assessing the quality and stability of the found solution.

So called integral terms can be an effective manner to monitor the quality and stability of the solution [5] [18]. Solely monitoring the residuals may thus lead to one to prematurely conclude that a solution has converged or may suggest that a solution never converges. A number of integral terms were defined and monitored during the solving processes performed in this work. Each of the integral terms monitored is shortly discussed in this section.

Exhaust mass flow The total exhaust mass flow is of interest because it is together with the temperature one of the key features of an operating igniter. In case the exhaust mass flow stabilizes one of the primary outputs of the solution has essentially been established.

Average exhaust temperature Together with the total exhaust mass flow the exhaust temperature is the other key feature of an operating igniter. Because of this reason this is also an important factor to evaluate when determining if convergence has occurred. A stable exhaust temperature can also be an indicator that the predicted chemistry is fairly steady state; unstable exhaust temperatures would suggest that either the predicted chemistry is not stable or that the solver is having issues due to predicted physical combustion instabilities. The average exhaust temperature is taken as the mass averaged temperature across the exhaust boundary.

Average internal fluid temperature The mass averaged temperature taken over a plane at $x = 0$ was used to determine the internal temperature. The average temperature should in theory be an indication of how mixing and combustion is developing inside the combustion chamber.

Average exhaust velocity With rising temperature and mass flow also the exhaust velocity is expected to increase. Together with the exhaust mass flow the velocity

Oxidizer and fuel inlet mass flow The oxidizer inlet mass flow is of interest because fluctuations are an indication of instabilities. If the mass flow being fed into the system is not constant it is unlikely that the rest of the system is oblivious to these fluctuations. In cases where a pressure inlet boundary is used the inlet mass flow is of interest to verify the predicted injector discharge rate.

Oxidizer and fuel inlet pressure Likewise to the oxidizer inlet mass flow the oxidizer inlet pressure is of interest for cases where a mass flow boundary condition is used for the inlet.

In the research performed in this study the integral terms proved to be invaluable in determining the convergence of solutions. Frequently the residuals either stopped converging or became very small while the motion of the integral terms had not yet stabilized. In these cases the integral terms either indicated that the while the fit was perhaps not very good a flow field was established, or that while residuals were small the flow field was still developing.

5.3. Solution strategy

During this work it was found that performing a CFD simulation is seldom a manner of starting a simulation and returning a few hours later to collect the results. Even though the problem seems well posed numerical instabilities can arise, requiring under-relaxation to be applied. Over applying under-relaxation makes the solution converge very slowly necessitating a lot of 'playing around' with the relaxation factors. This section describes the general strategy used to obtain solutions.

The ANSYS Fluent user manual suggests to first solve for the flow field without solving the energy equation [5]. This is however deemed problematic as the energy equation is intimately related with the flow chemistry and the fact that the flow is unlikely to be supersonic without combustion taking place. Simply disabling the energy equation will yield a vastly different flow field, defeating the concept of first solving for an approximate flow field before switching on the energy equation.

The strategy used during this work was to impose limits to prevent numerical instabilities from growing while keeping relaxation factors at a level at which the solution process was fully stable. This often required momentarily lowering the relaxation factors during the first 50 to 100 iterations.

5.3.1. Relaxation factors

Relaxation factors are introduced in the solver to provide additional control over stability and convergence speed. The notion of relaxation factors was already introduced as a fundamental part of the numerical solution method presented in Section 4.11. The concept of relaxation factors is however generalized and applied to almost all state variables for which the model solves.

The general formulation of an relaxation factor α in the update equation for a variable ϕ is as follows [6]:

$$\phi = \phi_{old} + \alpha\Delta\phi \tag{5.1}$$

Where $\Delta\phi$ is the calculated required change in ϕ. In case $\alpha < 1$ the variable in question is under-relaxed. Under-relaxation improves stability because extreme changes are not propagated as quickly, but also do slow convergence as desired changes are propagated less quickly. Still this makes the relaxation factors an important tool when calculating complicated flow problems such as supersonic and reaction flows [5].

During the execution of the numerical experiments for this work the following values for the relaxation factors were used:

Pressure under-relaxation At 0.4

Energy equation under-relaxation At 0.8 or 0.9

Radiation P1 model under-relaxation At 0.8 or 0.9

Momentary bumping of relaxation factors Bumping relaxation factors to higher values for a few iterations was used to test if integral terms really were stable.

5.3.2. Limits

Limits are another tool in the solver designed to provide additional control over numerical stability. Using limiters one can enforce upper and lower bounds of the values of the flow variables being solved for. By imposing these limits unrealistic and extreme values which are predicted during iterations can be prevented damped preventing them from being propagated to the following iterations. The following limits were used during the solution process:

Maximum absolute temperature The analytically derived adiabatic flame temperature provides an upper bound to the temperature. Any significantly higher temperatures are numerical artifacts or pseudo transients originating from the solution process.

Minimum absolute temperature Temperatures below the freezing points of the propellants are nonsensical as they should not only not occur in the system but also cannot be represented by the model.

Maximum absolute pressure The injection pressure should be the location of the highest pressure. Any pressures significantly higher than the injection pressure are numerical artifacts or pseudo transients originating from the solution process.

Based on the described rationale the limit values listed in Table 5.2 were imposed on the solver.

Parameter	Unit	Limit
Maximum absolute temperature	K	5500
Minimum absolute temperature	K	50
Maximum absolute pressure	Pa	$1{\cdot}10^8$

Table 5.2: Used sets of limit values imposed on the solver.

5.3.3. Discretization scheme

By selecting a first order discretization scheme instead of a second order discretization scheme stability and speed can be traded against accuracy. The schemes themselves have been introduced in Section 4.10.

In this study all calculations were performed using the second order upwind discretization scheme. While the gains in computational speed offered by using a first order discretization scheme may have been welcome, no improvements in numerical stability were observed for trouble cases. As using first order discretization schemes results in a loss of accuracy in the solution no further effort was put in exploring the use of employing a first order discretization scheme.

5.4. Case overview

In order to answer the research questions a number of cases were run which all have a different combination of model components, boundary conditions and mesh configurations. The results from these cases are in the following chapters leveraged to perform verification and validation as well as answering the research questions. In this section an overview of the cases is presented.

The case naming convention used is as follows:

Mesh type (optional)	**Kinetics**	**Exhaust Pressure**	Mesh size (optional)	Other conditions (optional)

The cases follow the buildup of experiments as discussed in Section 2.4 of which a compact schematic representation is shown in Figure 7.1 to present the cases run. Using this buildup a philosophy of gradually increasing complexity is followed. First the cold flow cases are discussed, next the equilibrium chemistry cases and finally the cases using more complex finite rate chemistry. The attentive reader will note that no transient cases are presented in this chapter. The reason for this will be further discussed in Chapter 7.

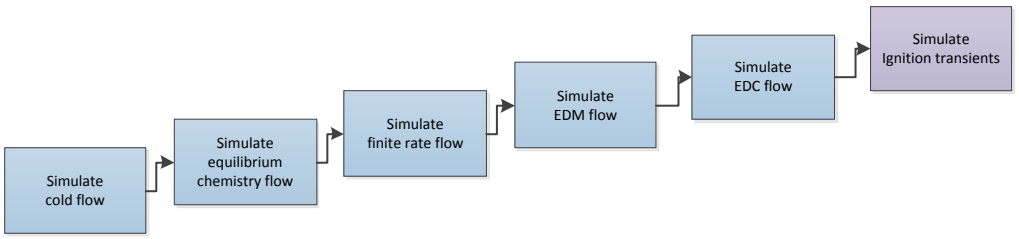

Figure 5.1: High level breakdown of model development approach which is used as guideline for introducing cases.

5.4.1. Cold flow

The cold flow cases serve as the foundation for this work and are of interest because they model the state of the igniter prior to ignition within the igniter. The two primary cold flow cases are ColdFlowStart and ColdFlowPressure of which the first one assumes ambient exhaust conditions and the latter one assumes high back pressure.

The cold flow cases will be used for a grid convergence study, hence there are a number of cases which only differ in mesh size used: ColdFlowPressure08, ColdFlowPressure15, ColdFlowPressure20 and ColdFlowPressure30. All assume a high main chamber pressure and hence high exhaust pressure. There is no specific reason for using high exhaust pressure instead of ambient, this choice was arbitrary.

In order to verify the assumption that symmetry can be used to reduce the size of computational domain by using only quarter geometry a cold flow case using the full geometry is run, named FullColdFlowStart. In order to assess the impact of using a real gas model a single cold flow case is run which uses a real gas model instead of the ideal gas model: ColdFlowAmbientReal.

In order to verify the accuracy of the analytical method to size the injection orifices two cases are included in which the full injector geometry is modeled. The mesh used is referred to as the extended inflow mesh. In one case a mass flow boundary condition is used, in the other a pressure inflow boundary. These two cases are referred to as InflowColdFlowMassStart and InflowColdFlowPressureStart.

5.4.2. Equilibrium chemistry

Of the equilibrium chemistry cases again the two main cases only differ in the type of exhaust pressure prescribed where EquilibriumAmbient uses ambient exhaust pressure and EquilibriumPressure assumes a high back pressure. In the cases which include chemistry the cases which assume a high back pressure are of interest because they represent the functioning of the igniter after the main engine combustion chamber has

ignited.

For the equilibrium chemistry cases the effect of including an extended outflow region is assessed using the OutflowEquilibriumPressure case. The influence of the wall temperature is assessed using the EquilibriumAmbientHotWall case in which the wall temperature will be elevated to 598 Kelvin. In order to verify the assumption that radiation modeling is of little influence is tested using the case EDMAmbientNoRad where radiation modeling is completely disabled.

5.4.3. Finite rate chemistry

In order to be able to assess the influence the act of coupling chemistry to turbulence modeling itself has a number of cases are run in which the same chemical kinetics schemes are used which will later be used for turbulence coupled chemistry except that they are used without turbulence coupling.

For the finite rate chemistry cases which do not use any coupling of chemistry with turbulence both both a case with ambient exhaust pressure and high back pressure are run. The FiniteRate1StepAmbient and FiniteRate1StepPressure both make use of the Westbrook Dryer single step chemical kinetics scheme.

More complex chemical kinetics schemes are used in the FiniteRate2StepAmbient and FiniteRate4StepAmbient ambient cases in which respectively the Westbrook Dryer two step and Jones Lindstedt 4 step chemical schemes are used. Because it was not possible to attain converged solutions no attempt was made to repeat these cases with an elevated back pressure.

5.4.4. Turbulence coupled chemistry

For the finite rate chemistry cases which do couple chemistry with turbulence both the Eddy Dissipation Model (EDM) and Eddy Dissipation Concept (EDC) are used. For the EDM the two usual cases which assume ambient exhaust pressure and high back pressure are run which are respectively named EDMAmbient and EDMPressure.

The EDM cases will be used for a grid convergence study, hence there are a number of cases which only differ in mesh size used: EDMAmbient08, EDMAmbient15, EDMAmbient20 and EDMAmbient30. All assume ambient exhaust pressure. There is no specific reason for using ambient exhaust pressure instead of high exhaust pressure, this choice was arbitrary.

For the EDC cases only cases for which ambient exhaust pressure is used are run. In addition the mesh size was increased from 0.001 to 0.002 to limit the required computation time. Both the Westbrook Dryer single step and two step chemical kinetics schemes are used for which the cases are respectively named EdcWd1StepAmbient and EdcWd2StepAmbient.

5.4.5. Overview

In the case overview the following abbreviations are used to indicate the type of models, boundary conditions, and meshes used. In addition various other key properties are indicated using these abbreviations. The case overview including the case configuration itself is presented in Table 5.3 and Table 5.4.

Inflow Denotes the type of inflow region included in the mesh used to model the injector elements.

- **Truncated** Only a short straight section of the diameter of the actual injector orifice is used.
- **Full** A full inflow area modeling a complete injector element is used.

Mesh Denotes the geometry used to generate the mesh.

- **Quarter** Only a quarter geometry was used exploiting symmetry in the igniter design.
- **Full** The full geometry was used.

Inflow type Denotes the type of boundary condition applied on the inflow region.

- **Mass flow** A boundary condition prescribing the amount of mass per unit of time entering the domain is used.

Pressure A boundary condition prescribing the pressure is used.

Outflow Denotes the type of outflow region included in the mesh used to model the exhaust.

Truncated Only the converging-diverging section of the nozzle is included in the mesh.

Full Both the converging-diverging section of the nozzle as well as a larger volume representing part of the main engine combustion chamber is included in the mesh.

Mesh size The value used as input for the mesh size control.

Pressure The pressure prescribed at the outflow boundary.

Kinetics The type of chemical model and accompanying chemical kinetics used.

Cold Cold flow in which only species transport is modeled.

Equilibrium Equilibrium chemistry combined with PDF methods in which mixture variance transport is modeled.

Finite rate Chemistry which does not use any turbulence coupling but which does use a finite rate chemical kinetics scheme.

EDM Eddy dissipation model which assumes complete combustion.

EDC Eddy dissipation concept combined with a chemical kinetics scheme.

WD 1 step The 1 step chemistry kinetics scheme proposed by Westbrook and Dryer.

WD 2 step The 2 step chemistry kinetics scheme proposed by Westbrook and Dryer.

JL 4 step The 4 step chemistry kinetics scheme proposed by Jones and Lindstedt.

State The equation of state used for modeling gas.

Iterations Abbreviated as 'Iter.' indicates the number of solution iterations computed for the case.

5.5. Selected cases

The next sections will discuss several cases of interest. This discussion does not cover the results obtained from any cases but rather the observations or challenges met while running the cases themselves. In addition the reasoning behind the convergence judgment attributed to these case sis discussed. A full overview of the results and residuals of all cases can be found in Appendix H.

5.5.1. EdcWd1StepAmbient

In this case the Eddy Dissipation Concept was used in conjunction with a single step combustion model from Westbrook and Dryer which resulted in a vastly higher computational time required to achieve a converged solution compared to other cases run. After about 8 hours and 900 iterations both the residuals and integral terms have stabilized while small oscillations remain as can be observed in Figure 5.2 and Figure 5.3.

In order to limit the computational time required the mesh size was increased to 0.002 from 0.001 in order to decrease the number of cells. While this simplification will result in reduced spatial resolution it is assumed that the mesh is not of significant influence to the overall results as was shown in Section 6.2.3.

Because both the integral terms and residuals are no longer displaying any movement outside of the oscillations the solution is assumed to have converged. The remaining oscillations may be the result of oscillations arising in the simulated physics such as unstable flow patterns.

5.5.2. EdcWd2StepAmbient

The case where the Eddy Dissipation Concept was used in conjunction with the 2 step combustion model from Westbrook and Dryer was a particularly troublesome one. After 26 hours of computation no convergence was attained and no sign of imminent convergence was visible. The solution finding process was halted at this point due to a lack of time.

Case	Inflow	Mesh	Inflow	Outflow	Mesh size	Kinetics
ColdFlowStart	Truncated	Quarter	Massflow	Truncated	0.001	Cold
ColdFlowPressure	Truncated	Quarter	Massflow	Truncated	0.001	Cold
ColdFlowPressure15	Truncated	Quarter	Massflow	Truncated	0.0015	Cold
ColdFlowPressure20	Truncated	Quarter	Massflow	Truncated	0.002	Cold
ColdFlowPressure30	Truncated	Quarter	Massflow	Truncated	0.003	Cold
ColdFlowPressure08	Truncated	Quarter	Massflow	Truncated	0.0008	Cold
FullColdFlowStart	Truncated	Full	Massflow	Truncated	0.001	Cold
InflowColdFlowMassStart	Full	Quarter	Massflow	Truncated	0.001	Cold
InflowColdFlowPressureStart	Full	Quarter	Pressure	Truncated	0.001	Cold
ColdFlowAmbientReal	Truncated	Quarter	Massflow	Truncated	0.001	Cold
EquilibriumAmbient	Truncated	Quarter	Massflow	Truncated	0.001	Equilibrium
EquilibriumPressure	Truncated	Quarter	Massflow	Truncated	0.001	Equilibrium
OutflowEquilibriumPressure	Truncated	Quarter	Massflow	Full	0.001	Equilibrium
EquilibriumAmbientHotWall	Truncated	Quarter	Massflow	Truncated	0.001	Equilibrium
FiniteRate1StepAmbient	Truncated	Quarter	Massflow	Truncated	0.001	WD 1 step
FiniteRate1StepPressure	Truncated	Quarter	Massflow	Truncated	0.001	WD 1 step
FiniteRate2StepAmbient	Truncated	Quarter	Massflow	Truncated	0.001	WD 2 step
FiniteRate4StepAmbient	Truncated	Quarter	Massflow	Truncated	0.001	WD 4 step
EDMAmbient	Truncated	Quarter	Massflow	Truncated	0.001	EDM, 1 step
EDMAmbient15	Truncated	Quarter	Massflow	Truncated	0.0015	EDM, 1 step
EDMAmbient20	Truncated	Quarter	Massflow	Truncated	0.002	EDM, 1 step
EDMAmbient30	Truncated	Quarter	Massflow	Truncated	0.003	EDM, 1 step
EDMAmbient08	Truncated	Quarter	Massflow	Truncated	0.0008	EDM, 1 step
EDMAmbientNoRad	Truncated	Quarter	Massflow	Truncated	0.001	EDM, 1 step
EDMPressure	Truncated	Quarter	Massflow	Truncated	0.001	EDM, 1 step
EdcWd1StepAmbient	Truncated	Quarter	Massflow	Truncated	0.002	EDC, WD 1 step
EdcWd2StepAmbient	Truncated	Quarter	Massflow	Truncated	0.002	EDC, WD 2 step

Table 5.3: Case overview part 1 showing used inflow region, full or partial geometry, type of inflow boundary, outflow region, mesh size and chemical kinetics.

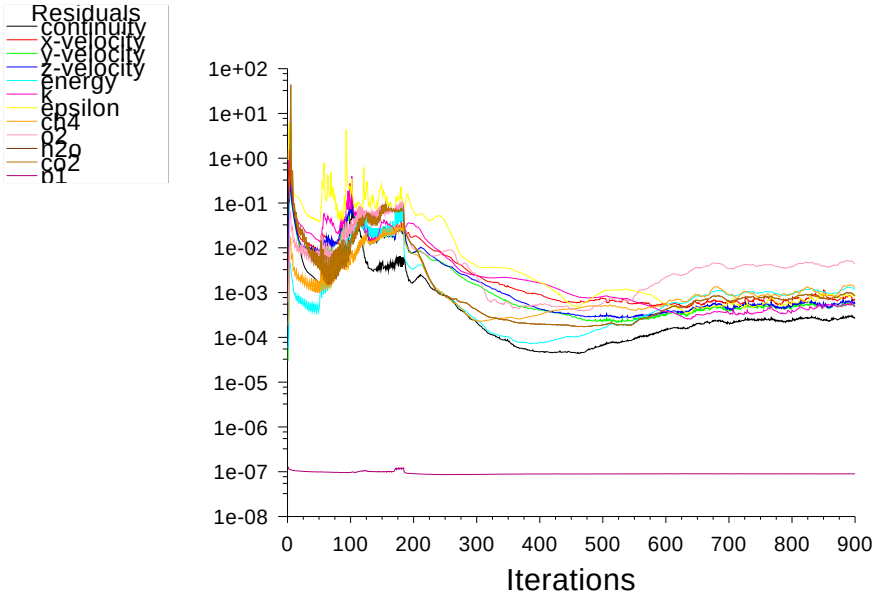

Figure 5.2: Convergence history of scaled residuals for EdcWd1StepAmbient case.

Case	State	Exhaust pressure	Iter.	Residuals	Integrals
ColdFlowStart	Ideal	1.00E+05	600	Converged	Stable
ColdFlowPressure	Ideal	4.00E+06	600	Converged	Stable
ColdFlowPressure15	Ideal	4.00E+06	500	Converged	Stable
ColdFlowPressure20	Ideal	4.00E+06	500	Converged	Stable
ColdFlowPressure30	Ideal	4.00E+06	500	Converged	Stable
ColdFlowPressure08	Ideal	4.00E+06	600	Converged	Stable
FullColdFlowStart	Ideal	1.00E+05	500	Converged	Stable
InflowColdFlowMassStart	Ideal	1.00E+05	500	Converged	Stable
InflowColdFlowPressureStart	Ideal	1.00E+05	500	Converged	Stable
ColdFlowAmbientReal	Real	1.00E+05		No convergence	No convergence
EquilibriumAmbient	Ideal	1.00E+05	2500	Questionable, energy at 1e-4	Stable
EquilibriumPressure	Ideal	4.00E+06	3300	Questionable, energy at 1e-4	Stable but oscillating
OutflowEquilibriumPressure	Ideal	4.00E+06	2000	Questionable, large oscillations.	Stable.
EquilibriumAmbientHotWall	Ideal	1.00E+05	2000	Questionable, energy at 1e-4	Stable
FiniteRate1StepAmbient	Ideal	1.00E+05	1200	Questionable	Stable, minor oscillations
FiniteRate1StepPressure	Ideal	4.00E+06	1200	Questionable	Stable, minor oscillations
FiniteRate2StepAmbient	Ideal	1.00E+05	1200	Not converged	Questionable, oscillations
FiniteRate4StepAmbient	Ideal	1.00E+05	700	Not converged	Not converged
EDMAmbient	Ideal	1.00E+05	1300	Converged, minor oscillations	Stable, minor oscillations
EDMAmbient15	Ideal	1.00E+05	1500	Converged	Stable
EDMAmbient20	Ideal	1.00E+05	1000	Converged, small oscillations	Stable
EDMAmbient30	Ideal	1.00E+05	1300	Converged	Stable but small long period oscillations
EDMAmbient08	Ideal	1.00E+05	1200	Converged, small oscillations	Stable
EDMAmbientNoRad	Ideal	1.00E+05	1250	Converged	Stable
EDMPressure	Ideal	4.00E+06	Unkn.	Converged, minor oscillations	Stable, minor oscillations
EdcWd1StepAmbient	Ideal	1.00E+05	900	Converged, minor instabilities	Stable, minor instabilities
EdcWd2StepAmbient	Ideal	1.00E+05	970	Questionable, still decreasing	Unstable

Table 5.4: Case overview part 2 showing used equation of state, exhaust pressure [Pa], number of iterations performed, residual convergence and integral term convergence.

In order to limit the computational time required the mesh size was increased to 0.002 from 0.001 in order to decrease the number of cells. While this simplification will result in reduced spatial resolution it is assumed that the mesh is not of significant influence to the overall results as was shown in Section 6.2.3. Required computation time was further limited by only updating chemistry every 2 or 3 iterations. This does case some noise like behavior in the residuals.

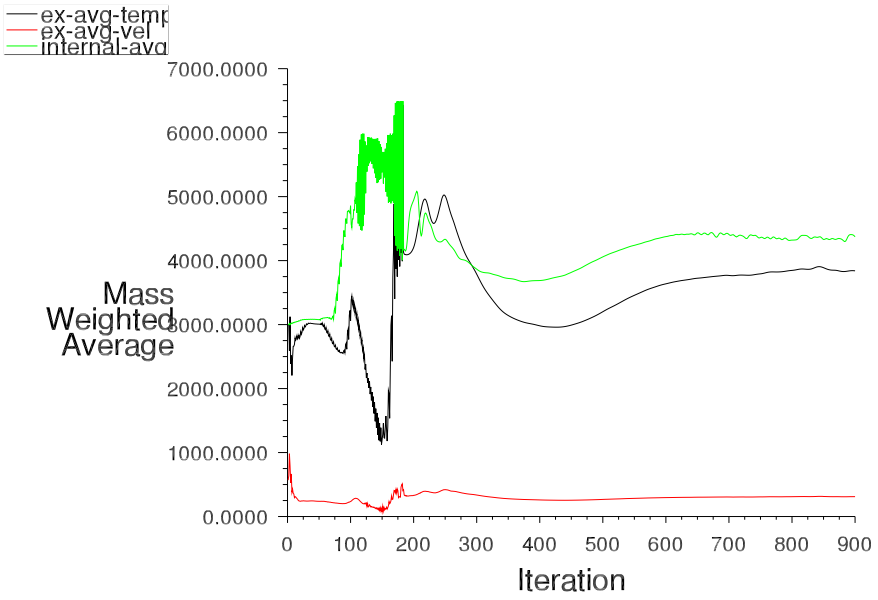

Figure 5.3: Convergence history of integral quantities for EdcWd1StepAmbient case.

Initially chemistry was updated every 5 iterations, but this resulted in very high fluctuations in the size of residuals. The chemistry update was accordingly set to every 3 iterations, resulting in significantly improved stability of residuals as can be seen in Figure 5.4. After 800 iterations chemistry update interval was changed to every single iteration in the hope to make the solution converge.

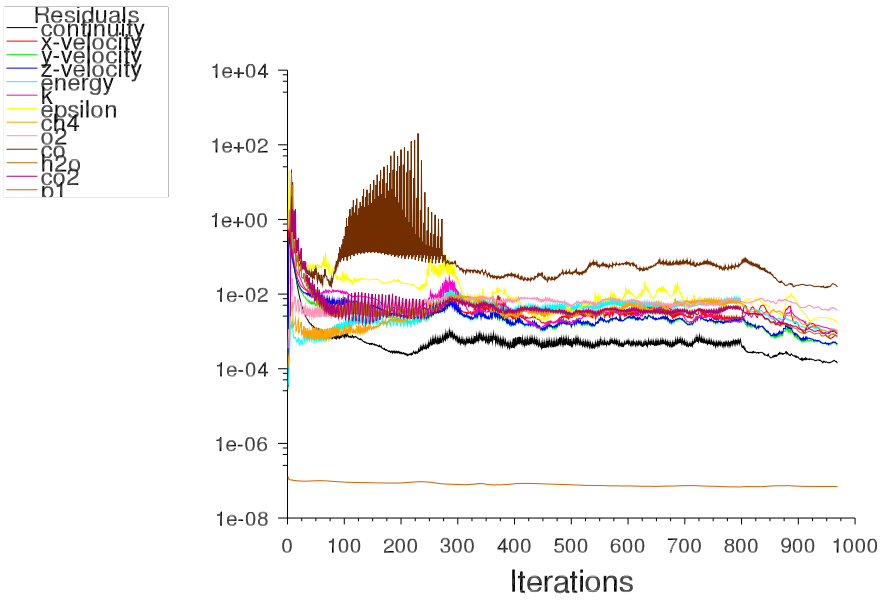

Figure 5.4: Convergence history of scaled residuals for EdcWd2StepAmbient case.

The residuals are still decreasing when the solution process was halted, suggesting the solution had not yet fully converged. Integral terms are shown to be heavily fluctuating up until the halting as is visible in Figure 5.5. Because of these reasons it is concluded that from a point of view of convergence the results from this solution are not usable.

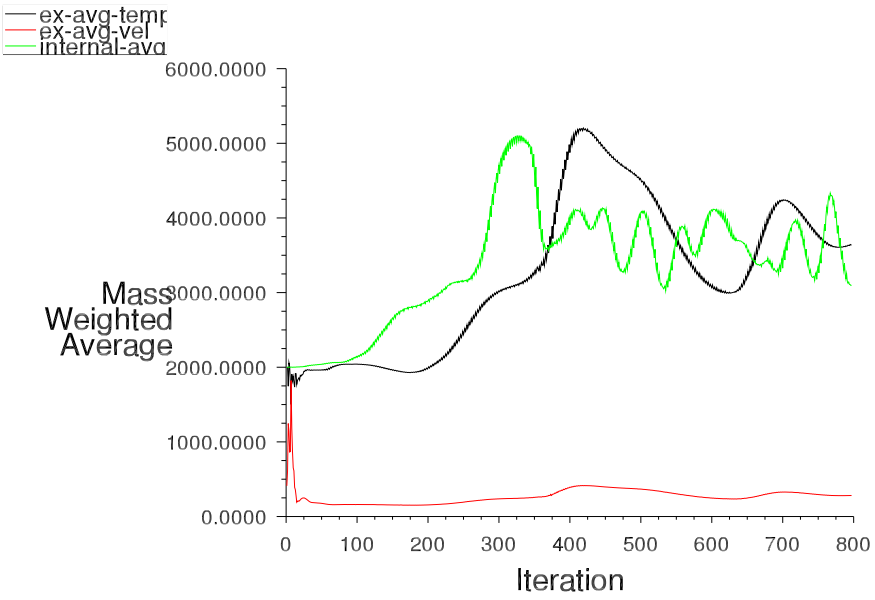

Figure 5.5: Convergence history of integral quantities for EdcWd2StepAmbient case.

5.5.3. ColdFlowAmbientReal

The real gas case failed to produce any meaningful results. It was impossible to attain convergence. The solution did not seem to converge beyond a certain point and frequent numerical excursions prevented a large number of iterations from reliably being run. Even measures such as extreme under-relaxation and switching to a first order discretization method did not result in the model becoming numerically stable. An example of the residual behavior is shown in Figure 5.6.

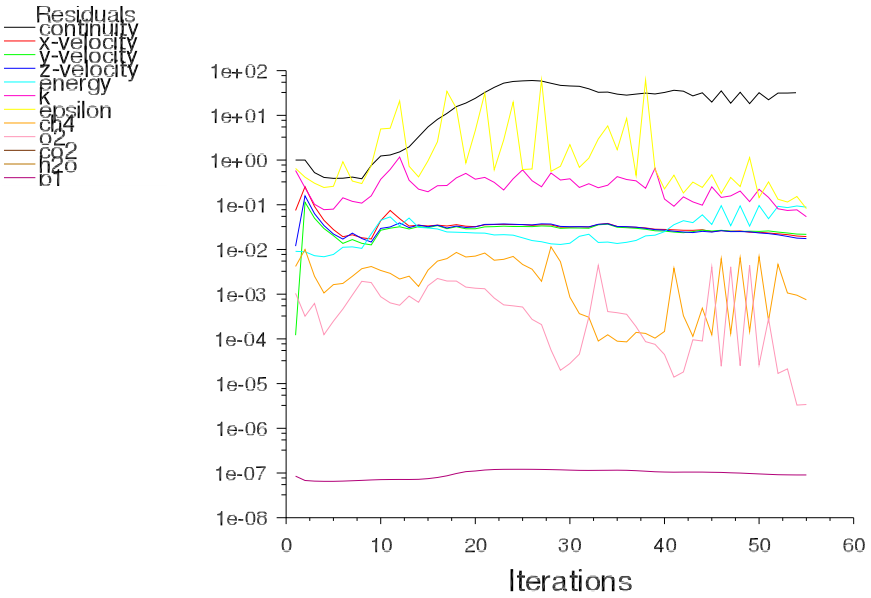

Figure 5.6: Residual plot of the ColdFlowAmbientReal case in which the Peng-Robinson real gas model is used but which is numerically unstable.

The increase in computation cost of using the real gas model instead of using the ideal gas model was found to be very significant. Individual iterations took about an order of magnitude more time to be calculated as compared to cases which used a similar model configuration with the ideal gas model.

5.5.4. OutflowEquilibriumPressure

The case where equilibrium chemistry was used in conjunction with mixture fraction transport in an extended outflow region shows interesting convergence behavior. Initially the residuals shown in Figure 5.7 appear to be converging well. After about 800 iterations instabilities in the residuals develop. One could interpret this as a signal that the solution is not converging.

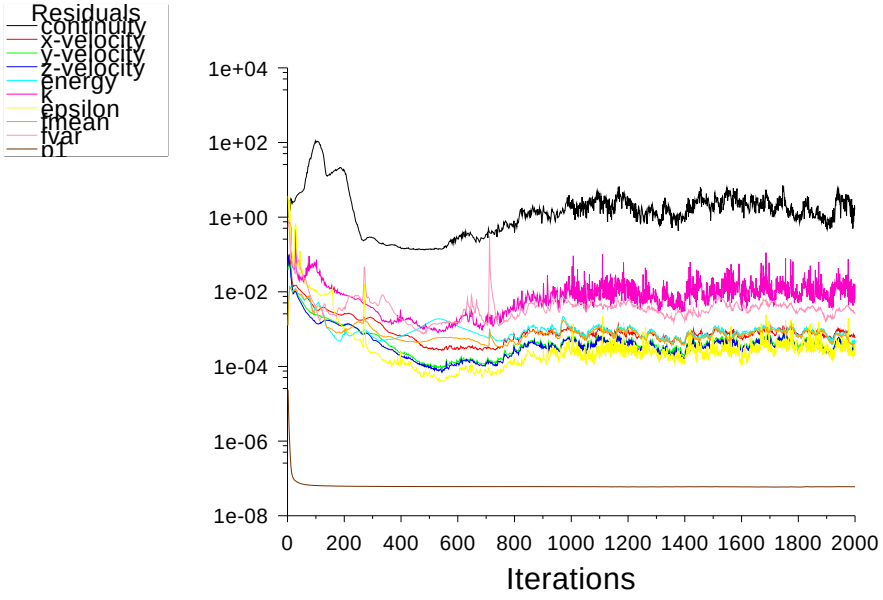

Figure 5.7: Convergence history of scaled residuals for OutflowEquilibriumPressure case.

Judging by the integral terms shown in Figure 5.8 the solution is however still converging. After 2000 iterations the averaged internal temperature is stable, suggesting that the solution has converged.

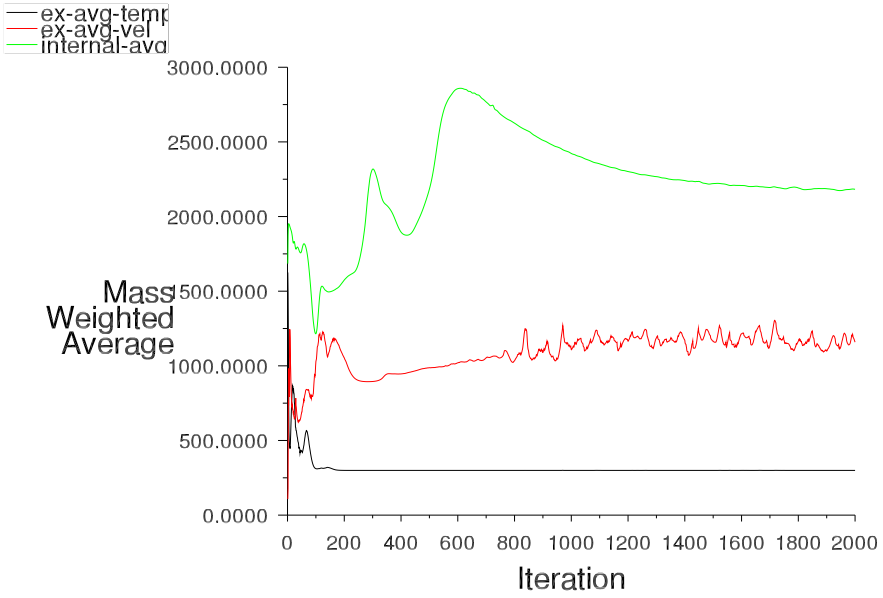

Figure 5.8: Convergence history of integral quantities for OutflowEquilibriumPressure case.

Judging by the velocity plot shown in Figure 5.9 the velocity field looks pretty much as expected in the igniter interior. The exhaust jet however looks undeveloped. Based on these findings it is assumed that the solution has converged in the interior region and is hence usable only for evaluating the properties of the flow

field internal to the igniter.

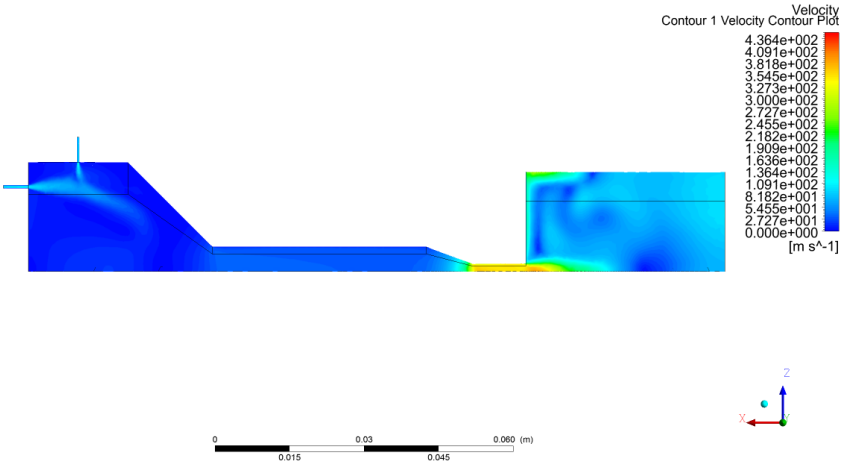

Figure 5.9: Velocity contour plot for OutflowEquilibriumPressure case.

5.5.5. FiniteRate2StepAmbient

The case were solely finite rate chemistry using the Westbrook and Dryer 2 step chemical kinetics scheme is used proved extremely unstable under the first hundred or so iterations. The relaxation factors for the individual species had to be set to a value of 0.5 for the first dozens of iterations to prevent the solution from blowing up directly. The relaxation factors could be stepped up to a value of 1.0 at 0.1 increments per 50 iterations. Concurrently temperatures had to be limited to 5500 to further preserve numerical stability. This behavior can be observed in the integral quantity plot shown in Figure 5.10.

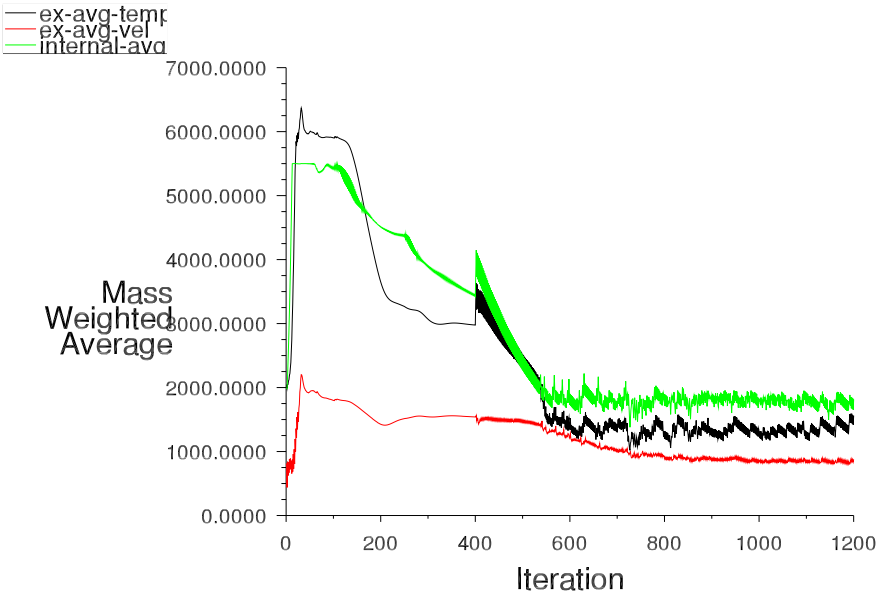

Figure 5.10: Convergence history of integral quantities for FiniteRate2StepAmbient case.

After stabilizing the internal and exhaust temperatures steadily dropped and developed oscillations as can been observed in Figure 5.10. At the same moment the residuals plot showed residuals growing a lot as can be observed in Figure 5.11. Because of the unexpected and the odd behavior of both the residuals and

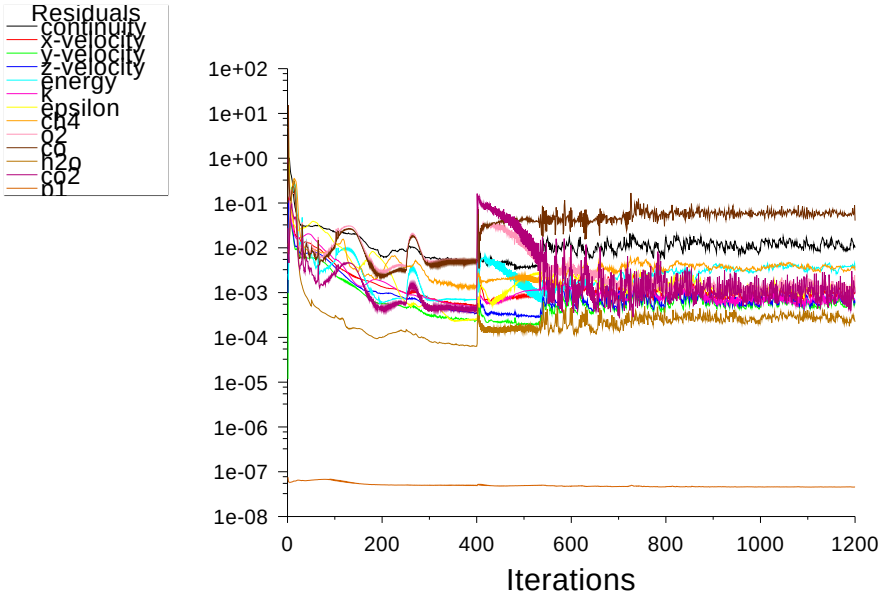

Figure 5.11: Convergence history of scaled residuals for FiniteRate2StepAmbient case.

integral quantities it is assumed that this case has not converged and is thus not usable.

5.5.6. FiniteRate4StepAmbient

The case were solely finite rate chemistry using the Jones Lindstedt 4 step chemical kinetics scheme is used did not predict a stable flame. Numerical stability and convergence behavior was however found to be good. The energy equation was under relaxed at a factor of 0.8 for the first 50 iterations, after that point relaxation was no longer required.

The solver however quickly started to converge on a solution which seemed to contain only a very low temperature flame. While the case does not simulate transient flow this behavior can be interpreted to be analogous to predicting flame extinction. This phenomena is clearly visible in the integral quantity plot shown in Figure 5.12 during the first several hundred iterations. Attempts to initialize the case at elevated temperatures did not change this behavior.

Because neither the residuals nor the integral quantities show any indication of convergence it is concluded that this case has not converged. Neither is there any indication which suggests that the solution will at some moment in time converge.

Computation time required stated to notably rise compared to the other finite rate chemistry cases, which is attributed to the more complex chemical kinetics scheme used in this case.

5.6. Summary

In this chapter the need for proper initialization of the solution prior to the solving process is discussed and the used initialization values are given.

After initialization it is the goal to obtain a converged solution. Convergence is primarily scored by a sufficient decrease of the residuals and the stabilization of integral terms at realistic values. Integral terms used are exhaust mass flow, average exhaust temperature, average internal temperature, average exhaust velocity, and inlet mass flow and pressure. Local fluctuations, either being of numerical origin or of physical origin can however prevent residuals from decreasing to the desired level.

In order to prevent numerical instabilities and to arrive at a converged solution relatively quickly relax-

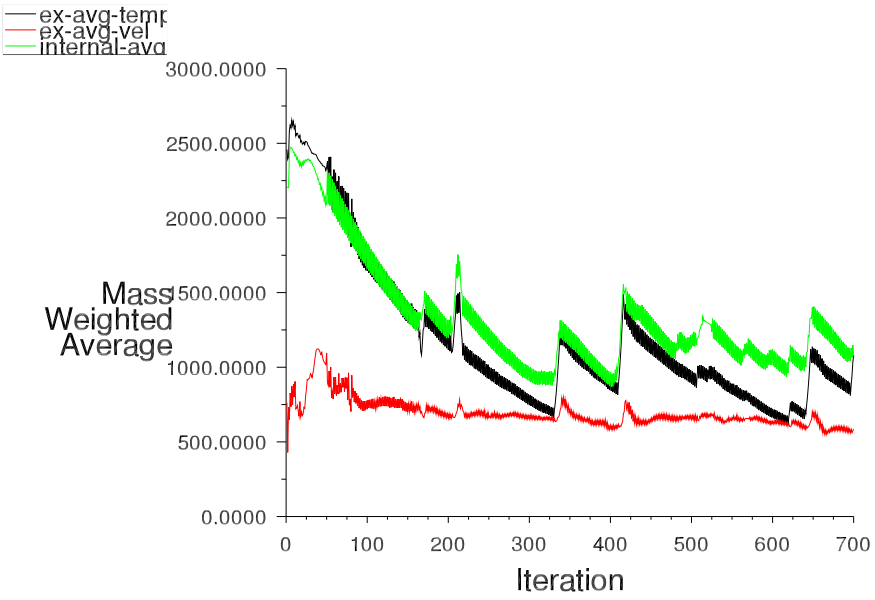

Figure 5.12: Convergence history of integral quantities for FiniteRate4StepAmbient case.

ation factors and limits are used. Pressure, energy and radiation relaxation factors are under-relaxed meaning that they are set to values below 1 in order to preserve stability.

Finally it was described how troublesome it was to attain convergence for cases which included more detailed chemistry in conjunction with the EDC. The case in which a real gas equation was used to model fluid state it was impossible to attain a solution as the model was too unstable.

6

Verification and validation

In this chapter the verification and validation of the presented model is treated. The practice of verification and validation of model is an important step in proving to which degree the outputs of this model are correct and usable. For the purpose of this study the following definitions of verification and validation are used:

Verification The process of checking if a product is working as intended. In the context of this work the verification process focuses mainly on testing if the model produces sensible results under the assumptions made.

Validation The process of checking if a product is solving the correct problem. In the context of this work the validation process focuses on testing if the model is capable of sufficiently predicting rocket engine ignition.

In this chapter it is attempted to provide an answer to the questions posed by verification and validation. A first step to verification and validation is deriving criterion which define positive or negative validation and verification results. These criterion are derived in the introduction. Following the verification and validation of the model are explored in depth. Finally some time is spent on evaluating existing validation studies of ANSYS Fluent.

Chapter 7 will discuss the implication of the verification and validation results and will explore methods to address any issues uncovered during verification and validation.

6.1. Introduction

In order to perform verification and validation one is required to define what precision or deviation between results from different methods is considered acceptable. In order to generate meaningful acceptable errors it is required to relate the influence of errors between different variables. Thermal power is for example dependent on the error in the predicted temperature are well as mass flow. This section aims to provide values for the acceptable errors.

For resolving the relations between the maximum errors of various variables it is assumed that the predicted or measured value $\hat{x}$ is a combination of the actual value x and a corresponding error e_x. In addition it is assumed that errors are small in general and that multiplied errors of the form $e_x e_y$ can thus be neglected. In order to ease computations an approximation is used for the relative error of the quotient of two variables containing errors. These assumptions are summarized as follows:

$$\begin{aligned} \hat{x} &= x + e_x \\ e_x e_y &\approx 0 \\ z &= \frac{x}{y} \\ \frac{e_z}{z} &= \frac{(x+e_x)y - x(y+e_y)}{x(y+e_y)} \approx \frac{e_x y - x e_y}{xy} \approx \frac{e_x}{x} - \frac{e_y}{y} \end{aligned} \tag{6.1}$$

Using this maximum error theory it is attempted to derive the maximum allowable error in various key output parameters while taking the thermal power P and heat flux q as starting points. The reason for taking the thermal power and heat flux as starting points is that these two values are driving design requirements. A maximum allowable error in these values is set from the design process and here it is attempted to obtain a handle on the resulting maximum errors in other variables on which these two primary outputs depend.

The thermal power P delivered is a function of the mass flow $\dot{m}$ and the change in enthalpy H. Using this definition the relative error in thermal power can be decomposed:

$$\begin{aligned} P &= \dot{m}\Delta H \\ \frac{e_P}{P} &= \frac{e_{\dot{m}}}{\dot{m}} + \frac{e_{\Delta H}}{\Delta H} \end{aligned} \tag{6.2}$$

In rocket engine design the assumption that chemical processes operate under constant pressure is frequently made [51]. This allows specification of the change in enthalpy solely as a function of the temperature change ΔT and specific heat capacity C_p. Using this assumption the following decomposition of the relative error in enthalpy is obtained:

$$\begin{aligned} \Delta H &= C_p \Delta T \\ \frac{e_{\Delta H}}{\Delta H} &= \frac{e_{C_p}}{C_p} + \frac{e_{\Delta T}}{\Delta T} \end{aligned} \tag{6.3}$$

The heat capacity of a gas composed of multiple species of which the number of molecules in the mixture is n is given as follows. It is assumed that the heat capacity is sufficiently well known such that the error in it is small enough to be neglected. It can then be shown that the relative error in the heat capacity depends on the weighted sum of the relative errors in the composition of the mixture:

$$\begin{aligned} C_p &= \frac{\sum_i \left(C_{pi} n_i\right)}{\sum_i n_i} \\ \frac{e_{C_p}}{C_p} &\approx \frac{e\left(\sum_i (C_{pi} n_i)\right)}{\sum_i (C_{pi} n_i)} - \frac{e\left(\sum_i n_i\right)}{\sum_i n_i} = \frac{\sum_i (e_{c_{pi}} e_{n_i})}{\sum_i (C_{pi} n_i)} - \frac{\sum_i e_{n_i}}{\sum_i n_i} \end{aligned} \tag{6.4}$$

While the individual errors e_{n_i} in the fraction of each of the species is certainly not zero, the total individual error contributions are dampened by the denominator $\sum_i n_i$. In addition not all of these individual errors can have the same sign as this would result in an over prediction of the mass flow, which is fundamentally constrained. It is assumed that the relative error in the heat capacity is much larger than the error in the mixture fractions. Using these two assumptions allows one to further simplify the expression for the relative error in the specific heat capacity:

$$\begin{aligned} e_{c_{pi}} &\gg e_{n_i} \\ \frac{\sum_i e_{n_i}}{\sum_i n_i} &\approx 0 \\ \frac{e_{C_p}}{C_p} &\approx \frac{\sum_i e_{c_{pi}}}{\sum_i (C_{pi} n_i)} \end{aligned} \tag{6.5}$$

Combining all the above derivations of the maximum error allows one to express the maximum relative error of the thermal power as a function of all these individual terms:

$$\frac{e_P}{P} = \frac{e_{\dot{m}}}{\dot{m}} + \frac{\sum_i e_{c_{pi}}}{\sum_i (C_{pi} n_i)} + \frac{e_{\Delta T}}{\Delta T} \tag{6.6}$$

The heat flux q is primarily governed by Fouriers law. In reality the heat flux is also dependent on the radiation, but as modeling radiation is not a primary focus of this study this contribution is ignored while

determining allowable errors. Applying the maximum error theory to Fouriers law allows one to decompose the dependence of the error as follows:

$$\begin{aligned} q &= h_f \Delta T \\ \frac{e_q}{q} &= \frac{e_{h_f}}{h_f} + \frac{e_{\Delta T}}{\Delta T} \end{aligned} \tag{6.7}$$

Using the derived relations between maximum errors one can now attempt to create a coherent system of maximum errors. In section 3.3.2 it was determined that a design factor of 2 was applied to the required power. Based on that factor it is decided that the maximum tolerable relative error in the output power shall be 0.25. This allows for another 0.25 to account for other effects in the worst case scenario.

For this purpose only that the exhaust is solely the result of the complete combustion of methane, which is governed by the following reaction equation which was also used to derive the adiabatic flame temperature. Depending on the chemical model used the number of resulting species may be larger, but also in those cases CO2 and H2O will likely be the primary constituents of the exhaust flow. Also H2O has a very large specific heat coefficient which gives it even more weight in the total maximum error. For simplicity thus only CO2 and H2O are considered.

$$CH_4 + 2\,O_2 \longrightarrow CO_2 + 2\,H_2O \tag{6.8}$$

The heat capacities are assumed to have a maximum error of about 0.025. As it was shown in Section 3.4 equilibrium chemistry predicts a chamber temperature of around 3500 K. The heat capacity at that temperature will be used for the purpose of determining the maximum allowable error as equilibrium chemistry should predict a fairly accurate chamber temperature [51]. The results are displayed in Table 6.1.

Parameter	**Unit**	**Value**		
		CO2	**H2O**	
n	-	0.33	0.66	
Cp	$\mathrm{Jmol^{-1}K^{-1}}$	62.80	57.07	[2]
$n \cdot Cp$	$\mathrm{Jmol^{-1}K^{-1}}$	20.72	36.67	
e_{Cp_i}	$\mathrm{Jmol^{-1}K^{-1}}$	1.57	1.43	

Table 6.1: Presumed errors for the heat capacity at T = 3500 K.

The thermal conduction coefficient is assumed to be known very well with only a maximum relative error 0.01 as this is a constant which can be measured relatively easily in laboratory settings. Combing all the known errors and the desired errors in the primary output allows one to set up the following system of maximum allowable errors shown in Table 6.2. The relative error in temperature $\frac{e_{\Delta T}}{\Delta T}$ is allowed to have a larger error than the relative error in mass flow because one of the primary difficulties of this study is in modeling chemistry. This invariably means that the relative error in predicted mass flow is to be smaller.

Relative error in	**Value**
m	0.05
ΔT	0.15
Cp	0.051
P	0.251
h	0.01
q	0.11

Table 6.2: Completed system of maximum allowable relative errors.

6.2. Verification

In order to perform verification the models results are compared to analytically derived values and a number of key model assumptions such as symmetry are asserted. In addition a grid convergence study is presented which is an important verification step in the design of numerical models.

6.2.1. Mass conservation

In a numerical model dealing with the transport of fluids producing a steady state solution it is to be expected that fluxes through the computed domain are in balance. As the fundamental conservation laws of physics state that neither mass nor energy can be created or disappear in a closed system these laws should also hold for the computational domain. Any deviation from these laws are either indicative of a badly converged solution, bad physics or serious numerical errors.

Verification of this fundamental law is thus an important tool to test the sanity of the produced solutions. To this end a table containing the mass flows at the inlets, throat and exit for each of the simulation cases is created. The resulting table is listed as Table 6.3.

	Inlet	**Exhaust flow**		**Throat flow**	
Case	**Flow**	**Flow**	**Relative**	**Flow**	**Relative**
ColdFlowStart	4.06E-03	4.06E-03	0.00%	3.97E-03	2.29%
ColdFlowPressure	4.06E-03	4.11E-03	-1.17%	4.11E-03	-1.17%
FullColdFlowStart	1.55E-02	1.62E-02	-3.98%	1.58E-02	-1.69%
InflowColdFlowMassStart	4.06E-03	4.06E-03	0.10%	3.97E-03	2.17%
InflowColdFlowPressureStart	7.81E-03	7.90E-03	-1.15%	7.73E-03	0.94%
EquilibriumAmbient	4.06E-03	4.04E-03	0.64%	3.93E-03	3.37%
EquilibriumPressure	4.06E-03	4.05E-03	0.20%	4.00E-03	1.63%
FiniteRate1StepAmbient	4.06E-03	4.07E-03	-0.15%	3.97E-03	2.31%
FiniteRate1StepPressure	4.06E-03	4.05E-03	0.32%	3.96E-03	2.52%
FiniteRate2StepAmbient	4.06E-03	4.11E-03	-1.10%	3.59E-03	11.61%
FiniteRate4StepAmbient	4.06E-03	3.31E-03	22.76%	3.27E-03	24.03%
EDMAmbient	4.06E-03	4.05E-03	0.27%	3.94E-03	2.96%
EDMPressure	4.06E-03	4.08E-03	-0.49%	3.99E-03	1.67%
EdcWd1StepAmbient	4.06E-03	4.06E-03	-0.05%	4.01E-03	0.97%
EdcWd2StepAmbient	4.06E-03	4.06E-03	0.02%	4.01E-03	1.21%

Table 6.3: Tabulated results from mass flow conservation check per simulated case. All units in kgs^{-1} unless otherwise indicated.

From the results listed in Table 6.3 it is concluded that for most cases flux conservation is observed very well. No commonly used criteria for flux conservation is known, and small deviations are expected due to the possibility of presence of cyclic phenomena in the flow. In order to reach the target maximum error of 10% on the predicted mass flow the criteria for conservation of mass flow through the model is set at 2.5%. This allows for the majority of the error to originate in modeling errors of the inlets. The EquilibriumAmbient, FullColdFlowStart, EDMAmbient and FiniteRate show a significant deviation from the flux conservation requirement.

No clear reason could be identified for the deviation from the mass conservation requirement of the said cases. Assuming that the numerical model itself is correct two straight forward reasons can be suggested: the solutions may not have fully converged due to an insufficient number of iterations having been calculated. Another possibility is that the solution is unable to fully converge due to periodic flow phenomena. These phenomena may prevent the model from reaching steady state flow conditions. Future study will however be required to identify an exact cause.

The cases FiniteRate2StepAmbient and FiniteRate4StepAmbient for which it was already concluded that the solution had not converged extremely large deviations from the requirements of mass conservation are observed. It is thus concluded that these cases do not pass verification.

6.2.2. Cold flow

For the cold flow case with ambient back pressure the major flow quantities can analytically be approximated fairly well. The igniter chamber is modeled as a pressure vessel with constant volume for which a mass balance is set up. For this mass balance a constant inflow of propellants and outflow via a sonic throat in which chocked flow is assumed. The pressure in the chamber is derived from the enclosed mass using the ideal gas law. For simplicity heat transfer is not modeled but is assumed that the propellants will be warmed to a temperature which is midway between the injection temperature and the initial hardware temperature of 298 K. The propellant temperature in the combustion chamber is therefore set to a constant temperature of 200 K.

The chocked nozzle flow is modeled using the equation from Zandbergen [51]:

$$\dot{m} = \frac{\sqrt{\gamma R T_c}}{p_c A_t} \left(\frac{2}{\gamma + 1} \right)^{\frac{\gamma+1}{2(\gamma-1)}} \tag{6.9}$$

Where T_c is the chamber temperature, p_c the chamber pressure, γ the specific heat ratio, and A_t the throat area. The specific heat ratio γ is determined using the mixing law.

The chamber pressure p_c is determined by calculating the density ρ_c according to the contained propellant mass in the chamber. Using the ideal gas equation the and chamber temperature T_c the pressure is determined. The chamber density ρ_c is calculated by dividing the contained propellant mass by the chamber volume V_c:

$$\rho_c = \frac{m_c}{V_c} \tag{6.10}$$

The enclosed propellant in the chamber m_c is determined by numerically finding the equilibrium value at which inflow and outflow balance. A schematic overview of the model is shown in Figure 6.1.

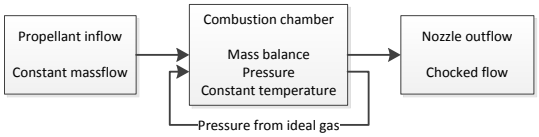

Figure 6.1: Schematic overview of the analytical model of the igniter for the purpose of predicting flow quantities in cold flow cases.

From the chamber pressure p_c and the known nozzle geometry the exhaust pressure can be determined. It is assumed that no shock waves are present in the exhaust flow. Zandbergen provides an expression for relating the pressure ratio $\frac{p_e}{p_c}$ to the exhaust area ratio ϵ [51]:

$$\frac{A_e}{A_t} = \epsilon = \Gamma \left(\frac{2\gamma}{\gamma - 1} \left(\frac{p_e}{p_c} \right)^{\frac{2}{\gamma}} \left(1 - \left(\frac{p_e}{p_c} \right)^{\frac{\gamma-1}{\gamma}} \right) \right)^{-0.5} \tag{6.11}$$

Because this expression is hard to invert a numerical solution is determined using Newtons method.

The chamber volume V_c is determined by modeling the combustion chamber as a set of cylinders and truncated cones. The nozzle section and injection ports are not included in the chamber volume. The code used to calculate these results is listed in Appendix G. The results of this analytical approach are summarized in Table 6.4. The values as predicted by the model are summarized in Table 6.5.

As can be seen from the results presented in Table 6.4 and Table 6.5 the predicted chamber pressure matches within 10% and both approaches predict chocked flow. The analytically predicted exhaust pressure deviates by about 25% from the model predicted exhaust pressure. The model predicted chamber temperature is close to the assumed chamber temperature.

These results are considered positive because the analytical approach made use of large assumptions. The differences in predicted chamber pressure and exhaust pressure can be explained by the presence of a boundary layer which decreases the effective throat area and nozzle expansion ratio resulting in higher model predicted pressures.

Quantity	Units	Value	
Chamber volume V_c	m^3	$1.66 \cdot 10^{-5}$	
Chamber temperature T_c	K	200	
Cp methane	$Jmol^{-1}K^{-1}$	33.51	[2]
Cp oxygen	$Jmol^{-1}K^{-1}$	29.11	[2]
Chamber pressure p_c	Nm^{-2}	$8.21 \cdot 10^5$	
Nozzle flow	-	Chocked	
Exhaust pressure p_e	Nm^{-2}	$2.72 \cdot 10^5$	

Table 6.4: Analytically obtained flow quantities for cold igniter flow with ambient back pressure.

Quantity	Units	Value
Chamber pressure	Nm^{-2}	$9.36 \cdot 10^5$
Chamber temperature	K	207
Nozzle flow	-	Chocked
Exhaust pressure	Nm^{-2}	$3.50 \cdot 10^5$

Table 6.5: Model predicted flow quantities for cold igniter flow with ambient back pressure in ColdFlowAmbient case.

6.2.3. Grid convergence study

In a grid convergence study it is checked if the obtained results are not the result of mesh or grid features. The quality of the mesh can be a detrimental effect on the both the convergence rate and the numerical results obtained [15, p.341]. A number of mesh quality metrics were discussed in section 4.1.3 which can be applied before performing any numerical studies. A grid convergence study is done by performing numerical studies and is the last step in either ruling out or quantifying the influence of the mesh itself on the obtained solution.

A grid convergence study is performed by performing the same numerical simulation using a progressively refined mesh and comparing the obtained results. In this manner one can effectively quantify the sensitivity of the solution to the mesh fineness. For a high quality mesh the results should not significantly differ as a function of fineness of the mesh used. Naturally a certain amount of detail is required in the mesh in order to predict any meaningful flow patterns while an overly refined mesh is expensive in terms of computational effort required to obtain a solution.

The parameters of interest are wall heating, exhaust temperature, exhaust velocity, exhaust mass flow and inlet pressures. The reason for selecting these parameters is that fact they are used to assess convergence and the fact that the exhaust temperature and mass flow, wall heating and inlet pressures are key output parameters of the model. The wall heating is calculated the total heat transfer through the walls of the igniter. The criterion for acceptable convergence are taken from the maximum errors derived in Table 6.2 with the difference being that now the variance between results is used instead of the difference between the actual and predicted results.

Cold flow The first grid convergence study was performed on the cold flow. The results are listed in Table 6.6 and Table 6.7. From these results it can be concluded that the solution for cold flow is independent of the mesh. No straight forward trends are visible in the parameters scored suggesting that no relation to the mesh resolution and if they are present they must be very small.

Eddy dissipation model The second grid convergence study was performed on the reacting flow case which employs the eddy dissipation model. The results are listed in Table 6.8 and Table 6.9.

The cases with a base grid size of 0.003 m and 0.0008 m stand out in the fact that the predicted heat flux is roughly a factor 2 different from the heat fluxes predicted in the other cases. The inlet pressures also show a difference albeit the magnitude of the difference is a lot smaller than the difference between other

Case	Grid size [m]	Cells	Wall heating [W]
ColdFlowPressure08	0.0008	75683	317.14
ColdFlowPressure	0.001	54220	317.05
ColdFlowPressure15	0.0015	38107	323.48
ColdFlowPressure20	0.002	34581	326.08
ColdFlowPressure30	0.003	33037	325.3

Table 6.6: Tabulated results from grid convergence study on cold flow case.

	Exhaust			Inlet pressure	
Case	Temp [K]	Velocity [ms^{-1}]	Flow [kgs^{-1}]	O [Pa]	F [Pa]
ColdFlowPressure08	228.2	36.40	0.004028	4303000	4156000
ColdFlowPressure	229.8	37.22	0.004110	4312000	4156000
ColdFlowPressure15	229.2	36.88	0.004061	4302000	4157000
ColdFlowPressure20	229.9	37.03	0.004065	4308000	4158000
ColdFlowPressure30	229.8	36.99	0.004060	4359000	4159000

Table 6.7: Tabulated results from grid convergence study on cold flow case.

cases. What is especially interesting to note is that both the EDMAmbient08 and EDMAmbient30 cases predict roughly equal values. This suggests that there may be two stable solutions to the problem.

Because the EDM cases predict two distinct sets of values and the values from the individual cases in these sets differ very little it is assumed that there are indeed two different stable solutions. While the presence of two stable solutions is something to take into account when processing results it is not an indication of a grid dependency. Answering the question of why there are two stable solutions and how they arise is a task for future work.

While the results of the grid convergence study for the cases using the eddy dissipation model are less robust than the cold flow cases it is still concluded that the grid size does not have any significant effect on the obtained resolution.

6.2.4. Flame temperature

The adiabatic flame temperature as calculated in Section 3.4.1 provides an upper bound for the temperatures to be expected in the CFD model. Because the adiabatic flame temperature per definition is the highest achievable flame temperature, temperatures above it are deemed unrealistic. Higher flame temperatures would require additional energy beyond the chemical energy which is available from the combustion of the propellants.

At the other end of the spectrum are chemical equilibrium methods which take into account effects such as dissociation and which were introduced in Section 3.4. Due to the simplicity of most chemical models it is assumed that they will predict temperatures higher than the chemical equilibrium temperature because these simpler models cannot accurately represent dissociation. Model variants using equilibrium chemistry are however assumed to predict temperatures lower than the analytically obtained chemical equilibrium temperature.

To this end all the recorded flame temperatures are listed in Table 6.10. From this table it is concluded that none of the predicted flame temperatures exceed the analytically predicted temperature for complete combustion. This is considered to be a positive result. In addition the cases leveraging equilibrium chemistry indeed predict flame temperatures below the analytically predicted equilibrium flame temperature. Methods using simple chemical models in turn yield a higher estimated flame temperature.

It is interesting to note that the cases using solely finite rate chemistry FiniteRate1StepAmbient and FiniteRate1StepPressure show an increase in the predicted flame temperature with an increase in pressure. Such

Case	Grid size [m]	Cells	Wall heating [W]
EDMAmbient08	0.0008	75721	-25854
EDMAmbient	0.001	54220	-12787
EDMAmbient15	0.0015	38125	-13528
EDMAmbient20	0.002	34603	-13148
EDMAmbient30	0.003	33007	-25186

Table 6.8: Tabulated results from grid convergence study on eddy dissipation model case.

	Exhaust			Inlet pressure	
Case	Temp [K]	Velocity [ms^{-1}]	Flow [kgs^{-1}]	O [Pa]	F [Pa]
EDMAmbient08	3370	1473	0.004049	4582000	4457000
EDMAmbient	3459	1487	0.004051	4338000	4262000
EDMAmbient15	3392	1476	0.004058	4425000	4288000
EDMAmbient20	3419	1481	0.004058	4426000	4291000
EDMAmbient30	3403	1488	0.004055	4614000	4483000

Table 6.9: Tabulated results from grid convergence study on eddy dissipation model case.

an effect is normally expected in equilibrium chemistry as increased pressure reduces dissociation while these cases only make use of single step chemistry. While for the other finite rate chemistry cases FiniteRate2StepAmbient and FiniteRate4StepAmbient it was already concluded that they are probably not converged they also predict very low flame temperatures compared to the other cases.

It is however remarkable that the model predicted equilibrium chemistry flame temperatures are over 1300 K below the values predicted by RPA. Investigating the model predicted exhaust flows reveals the equilibrium chemistry cases predict an exhaust flow containing almost 10% CH4 by mass. The full predicted exhaust composition of each case can be found in Appendix F. Leaving that much methane non combusted can easily explain a large fraction if not all of the temperature difference with RPA predicted values.

Another manner of verifying chemistry is by using the flame temperatures calculated using NASA's Chemical Equilibrium with Applications (CEA) program and comparing those to the model predicted flame temperatures. Calculation of the expected flame temperature for each of the chemical kinetics schemes used was already performed in Section 4.6.2. In Table 6.11 each of the predicted flame temperatures is compared to the corresponding model predicted flame temperature.

As already noted in Section 4.6.2 the NASA CEA predicted flame temperatures are not fully accurate due to CEA's inability to correctly represent the propellant injection conditions, but nevertheless the NASA CEA flame temperatures do serve as a rough upper bound of the expected flame temperatures.

It is interesting to note that only the Westbrook-Dryer 2 step chemical scheme used in conjunction in the EdcWd2StepAmbient case exceeds the CEA predicted flame temperature. Investigating the exhaust composition which is fully listed in Appendix F reveals about 2.5% of CH4 by mass. The fraction of CO in the exhaust stream is negligible. Based on these results one would expect a flame temperature close to but slightly lower than predicted by the single step chemical scheme using the EdcWd1StepAmbient case. This does however not answer the question as to why the predicted flame temperature exceeds the CEA predicted flame temperature. Given the fact that the EdcWd2StepAmbient case is not considered to have fully converged no conclusions are drawn from this observation.

Again it stands out that the FiniteRate2StepAmbient and FiniteRate4StepAmbient cases predict very low flame temperatures compared to CEA predicted flame temperatures. While a low flame temperature technically is not something which is considered incorrect they are remarkable. Another things which stands out is that using the same chemical kinetics scheme the EdcWd2StepAmbient predicts a much higher flame temperature than the FiniteRate2StepAmbient case.

Case	Temperature			Comments
	Throat	Exhaust	Chamber	
Analytical			5143	Complete combustion
Equilibrium RPA Pressure	3352	3241	3509	Chemical equilibrium temperature
EquilibriumAmbient	1916	1726	2190	
EquilibriumPressure	1982	1924	2185	
FiniteRate1StepAmbient	3988	3561	4269	
FiniteRate1StepPressure	4040	3865	4397	
FiniteRate2StepAmbient	1489	1229	1718	
FiniteRate4StepAmbient	1054	928	1084	
EDMAmbient	3885	3459	4187	
EDMPressure	3967	3826	4186	
EdcWd1StepAmbient	4017	3846	4321	
EdcWd2StepAmbient	3969	3813	4355	

Table 6.10: Tabulated flame temperatures in K at different locations in the flow field compared to analytically obtained values for these locations.

Case	Temperature			CEA Temperature
	Throat	Exhaust	Chamber	
EDMAmbient	3885	3459	4187	5103
EDMPressure	3967	3826	4186	5013
FiniteRate1StepAmbient	3988	3561	4269	5103
FiniteRate1StepPressure	4040	3865	4397	5103
FiniteRate2StepAmbient	1489	1229	1718	4049
FiniteRate4StepAmbient	1054	9285	1084	3633
EdcWd1StepAmbient	4017	3846	4321	5103
EdcWd2StepAmbient	3969	3813	4355	4049

Table 6.11: Tabulated flame temperatures in K at different locations in the flow field compared to NASA CEA predicted flame temperature at 40 bar pressure.

6.2.5. Gas state

In Section 4.7 the used models for modeling the gas state were presented and it was pointed out that based on the literature study it is questionable if the ideal gas assumption is valid in the modeling of rocket engine ignition [3]. Hence also a real gas model was included as a second option for modeling the gas state. In this section it is attempted to asses the need and relevance of using a real gas model instead of the ideal gas model.

The approach taken is to compare the density, temperature and pressure at the oxygen and methane inlets predicted at the inlet against analytically calculated values. For the analytically calculated cases the model predicted pressure and temperature taken as the variables of interest. The results are shown in Table 6.12 for fuel inlet and Table 6.13 for the oxidizer inlet.

The cases considered are both the start and pressure variants for the cold flow, equilibrium chemistry and eddy dissipation model cases. These distinct cases are of interest because the cold and hot flow are expected to yield very different internal pressures due to combustion being present or absent. The PDF / equilibrium chemistry variant is distinct from the two other cases because it does not directly use an equation of state but uses a precalculated table to determine density as a function of mixture ration and enthalpy. All other cases with reacting flows use the ideal gas law directly in the solver algorithm to obtain the density.

From the results obtained it can be concluded that the predicted density is usually an order of magnitude

Case	**Value**	**Density** [kgm^{-3}]	**Temperature** [K]	**Pressure** [Pa]	**Phase**
ColdFlowStart	Model	3.20E+01	1.74E+02	2.87E+06	
	Analytical	3.00E+02	1.74E+02	2.87E+06	liquid
	Corrected	5.07E+01	1.76E+02	2.87E+06	gas
ColdFlowPressure	Model	4.63E+01	1.80E+02	4.31E+06	
	Analytical	2.88E+02	1.80E+02	4.31E+06	liquid
	Corrected	9.64E+01	1.89E+02	4.31E+06	gas
EquilibriumAmbient	Model	5.14E+01	1.76E+02	3.31E+06	
	Analytical	2.96E+02	1.76E+02	3.31E+06	liquid
	Corrected	6.05E+01	1.81E+02	3.31E+06	gas
EquilibriumPressure	Model	7.02E+01	1.80E+02	4.60E+06	
	Analytical	2.91E+02	1.80E+02	4.60E+06	supercritical
	Corrected	8.50E+01	1.95E+02	4.60E+06	supercritical
EDMAmbient	Model	7.63E+01	1.10E+02	4.34E+06	
	Analytical	4.28E+02	1.10E+02	4.34E+06	liquid
	Corrected	1.01E+02	1.89E+02	4.34E+06	gas
EDMPressure	Model	8.71E+01	1.10E+02	4.98E+06	
	Analytical	4.29E+02	1.10E+02	4.98E+06	supercritical
	Corrected	2.40E+02	1.10E+02	4.98E+06	supercritical

Table 6.12: Fluid properties at the fuel (methane) inlet as predicted by the model and analytically calculated values.

below the analytically calculated density. The most likely cause is easily identified when investigating the state of the gas and taking into account that the ideal gas model can only accurately represent the gas phase. In order to test this assumption a second density is derived at a slightly elevated temperature compared to the model predicted temperature. These results are listed under the label **Corrected** in Tables 6.12 and 6.13. In most cases dropping to the gas phase yields a density figure which is much closer to the model predicted density. This is in accordance to what one would expect when evaluating PT plots of the boiling point of methane and oxygen as shown in Figure 6.2.

Case	Value	Density	Temperature	Pressure	Phase
ColdFlowStart	Model	6.84E+01	1.33E+02	2.37E+06	
	Analytical	8.82E+02	1.33E+02	2.37E+06	liquid
	Corrected	9.46E+01	1.37E+02	2.37E+06	gas
ColdFlowPressure	Model	1.12E+02	1.43E+02	4.16E+06	
	Analytical	8.01E+02	1.43E+02	4.16E+06	liquid
	Corrected	2.04E+02	1.50E+02	4.16E+06	supercritical gas
EquilibriumAmbient	Model	9.76E+01	1.40E+02	3.28E+06	
	Analytical	8.22E+02	1.40E+02	3.28E+06	liquid
	Corrected	1.43E+03	1.44E+02	3.28E+06	gas
EquilibriumPressure	Model	1.34E+02	1.43E+02	4.59E+06	
	Analytical	8.08E+02	1.43E+02	4.59E+06	liquid
	Corrected	2.34E+02	1.53E+02	4.59E+06	gas
EDMAmbient	Model	1.86E+02	8.80E+01	4.26E+06	
	Analytical	1.16E+03	8.80E+01	4.26E+06	liquid
	Corrected	2.06E+02	1.51E+01	4.26E+06	gas
EDMPressure	Model	2.14E+02	8.85E+01	4.92E+06	
	Analytical	1.16E+03	8.85E+01	4.92E+06	supercritical
	Corrected	3.09E+02	8.85E+01	4.92E+06	gas

Table 6.13: Fluid properties at the oxidizer (oxygen) inlet as predicted by the model and analytically calculated values.

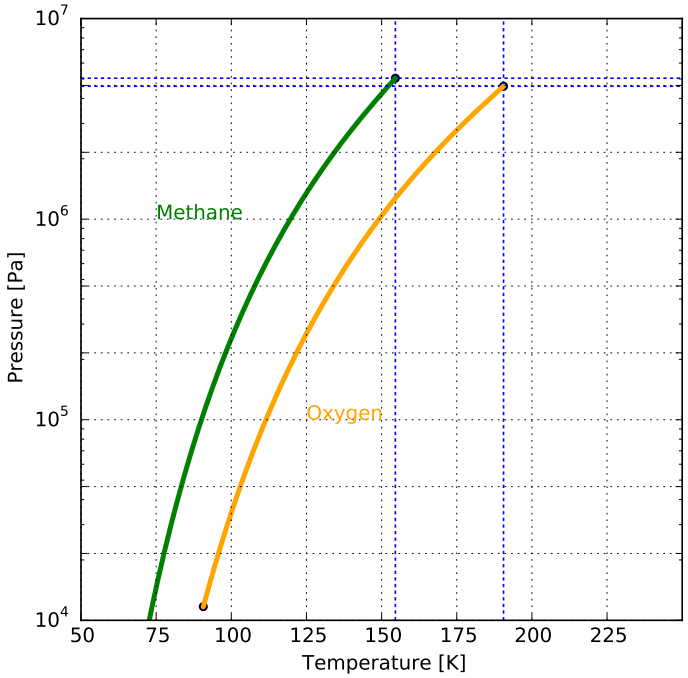

Figure 6.2: PT diagram for the boiling point of methane and oxygen. The upper dots represent the critical point and the lower dots represent the triple points. Data obtained from Coolprop [9].

Taking into account that the density is given by dividing mass by volume and assuming that enclosed mass is a proxy for the predicted mass flow and assuming that the volume is known very well one finds that the maximum allowable error for density is equal to maximum allowable error in mass flow. This means that the maximum allowable error in density is equal to 5% as was specified in Table 6.2. All results far exceed this criterion.

The conclusion of this verification step is that for the inlet conditions the model yields values which highly

deviate from analytically predicted values. The model is thus in its current form not suitable for predicting inlet and injection conditions.

6.2.6. Full versus partial geometry

In section 4.1 it was mentioned that the symmetry of the igniter design potentially can be exploited to compute the flow only in a quarter of the geometry and use the results as representative for the full geometry. Doing so is expected to roughly reduce computational time by a factor four. The key question that however arises is how valid the assumption is that the quarter geometry results are representative for the full geometry results. This section aims to verify this assumption.

First of all is should be noted that as most of the mesh is generated as an unstructured mesh it is not possible for the solution to be exactly symmetric. The full geometry mesh is not simply equal to four quarter geometry meshes. For all practical purposes these differences are however expected to be small. As the grid convergence study from Section 6.2.3 yielded a positive result the predicted results should be largely independent of the mesh.

Integral quantities A first check is to determine if integral quantities between the full and partial geometry match. If there is a clear discrepancy between these numbers it would be a very strong indicator that both geometries do not yield similar flow fields.

In order to asses this the mass flows, exhaust temperature and velocity, pressures and total wall heat flux for both the partial and full geometry were evaluated and compared. The results are listed in Table 6.14. Due to the difference in geometry some values of the full geometry case are to be expected to be four times as large as for the partial geometry. This effect has been accounted for in the relative column.

Quantity		Unit	ColdFlowAmbient	FullColdFlowStart	Relative
Flow	Fuel	kgs^{-1}	8.14E-04	3.26E-03	0.00%
	Oxidizer	kgs^{-1}	3.25E-03	1.30E-02	-0.02%
	Exhaust	kgs^{-1}	4.06E-03	1.62E-02	-0.36%
Exhaust	Velocity	ms^{-1}	3.28E+02	3.38E+02	3.04%
	Temperature	K	1.79E+02	1.79E+02	0.17%
Pressure	Chamber	Pa	936000	932000	-0.43%
	Fuel inlet	Pa	2868000	2963000	3.21%
	Oxidizer inlet	Pa	2368000	2434000	2.71%
Heat flux		Wm^{-2}	296.95	1222.2	2.81%

Table 6.14: Tabulated integral quantities of both partial and full geometry results.

From the results in Table 6.14 it can be concluded that predicted velocities, temperatures and pressures inside the igniter are within a small margin of each other when either predicted using a full or partial geometry. The small remaining differences may have arisen due to the solution not being fully converged yet.

Flow patterns Another manner of assessing whether the assumption that full and partial geometries yield similar flow fields is by checking if the flow field in the full geometry is symmetric. If it is not, then obviously it is not possible to reproduce the flow field using a partial geometry which exploits symmetry. In addition to comparing the full and partial geometry case, it is also of interest to compare the flow fields on the two symmetry planes in the full geometry cases.

The velocity fields of the flow in the full geometry case are plotted in Figure 6.3 for the XZ plane and in Figure 6.4 for the XY plane. It is interesting to note that while the flow field looks highly symmetric in the XY plane it clearly does not when evaluating it in the XZ plane. In the XZ plane a recirculation region developed in the lower right corner of the chamber. This recirculation region is not observed in the upper right corner in

the chamber. The flow in the center of the chamber appears to be flowing in the upward direction to the left when viewed in the XZ plane. In addition the flow is seen to enter the exhaust tube under an upward angle.

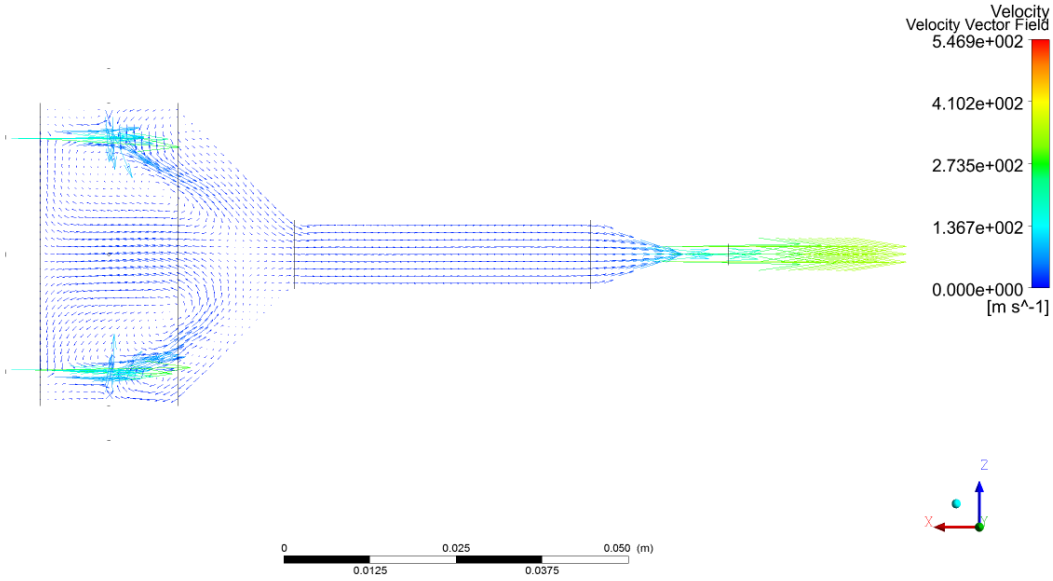

Figure 6.3: Velocity field for full geometry cold flow case in XZ plane.

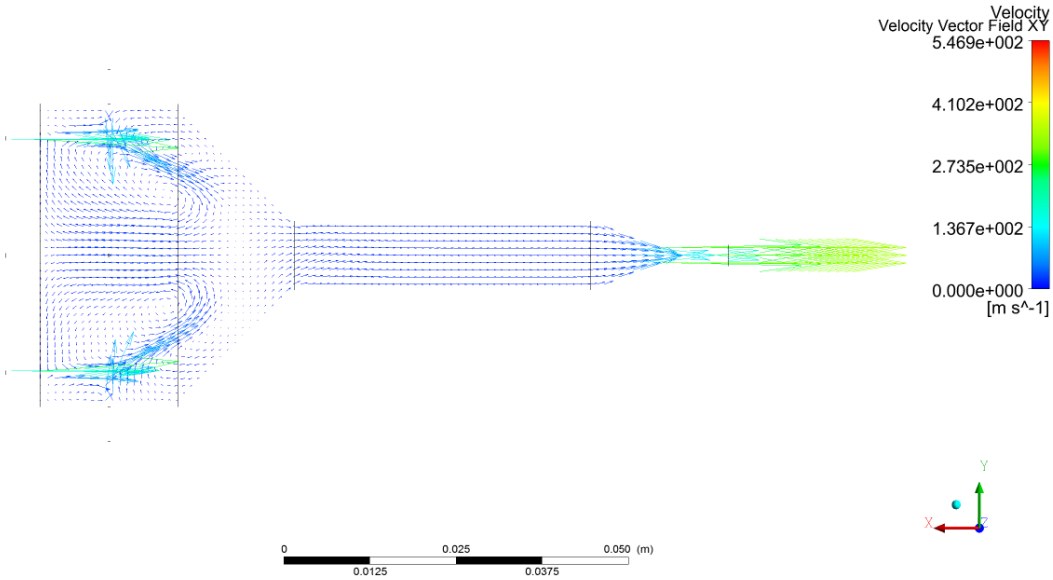

Figure 6.4: Velocity field for full geometry cold flow case in XY plane.

Comparing the partial geometry velocity field as plotted in Figure 6.5 with the velocity fields 6.5 reveals that the partial geometry shows a much stronger recirculation in the area that would normally be the center of the igniter chamber.

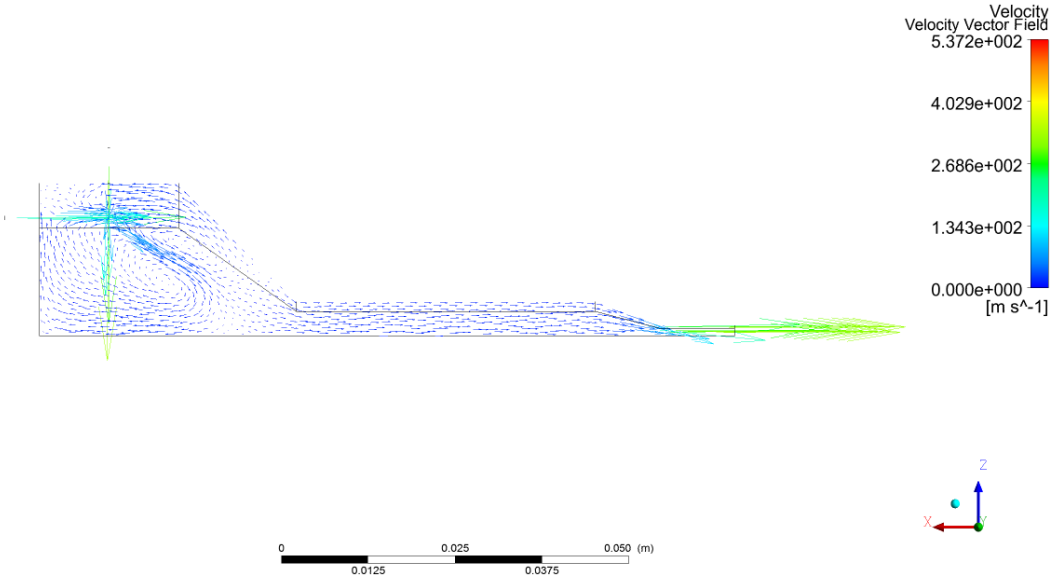

Figure 6.5: Velocity field for partial geometry cold flow case in XZ plane.

All three flow velocity fields show very similar behavior in the latter parts of the exhaust tube. Flow velocities are comparable and all oriented towards the exhaust. The few very large vectors drawn in the plots arise due to comparatively large velocity in the injection ports.

Another manner of assessing the flow symmetry is by measuring the total mass transport over the symmetry plane. This value is calculated by multiplying the local density and local velocity component normal to the plan and taking the integral over the plane. The results are shown in Table 6.15. In order to provide some sort of context to the magnitude of the calculated cross plane mass flow, the mass flow is also expressed as a fraction of the exhaust mass flow. In addition the cross plane mass flow is expressed as a fraction of half the fuel mass flow, which is the injector mass flow aimed at the symmetry plane.

Plane	**Mass flow**	**Mass flow fraction**	**Mass flow fuel fraction**
Plane XZ	$3.913 \cdot 10^{-5}$	0.00242	0.0240
Plane XY	$1.375 \cdot 10^{-4}$	0.00849	0.0845

Table 6.15: Calculated mass flow over symmetry planes. Units in kss^{-1}.

The results in Table 6.15 underline the asymmetry between the two planes of symmetry. Based on these results it is concluded that using partial geometry is sufficient for predicting the bulk performance figures of an igniter as the integral quantities differ very little. For predicting detailed phenomena such as ignition it remains necessary to evaluate both the full and partial geometry. The flow fields between partial and full geometry differ and non symmetrical flow patterns are observed.

6.2.7. Turbulence model

In this study the standard ANSYS Fluent provided implementation of the $\kappa - \epsilon$ model was used as explained in Section 4.5. As the selection of the turbulence model itself is set to be outside of the scope of this study and given that an existing implementation of this very model is used, verification of this model is skipped. As none of the comparable studies on rocket engine ignition make any mention of direct verification of their turbulence model there is also no obvious paths to take in verifying the turbulence model [3].

Standard works on computational fluid dynamics do however note that the $\kappa - \epsilon$ model is one of most widely used and most validated turbulence models available [47, p. 72] [15, p. 296]. Some further attention is spent on the general verification and validation of ANSYS Fluent are made in Section 6.3.1.

6.2.8. Radiation model

In this study the standard ANSYS Fluent provided implementation of the P-1 radiation model was used as explained in Section 4.3. Because the focus of this study on the effects of the choice of chemistry model and the limited time available it is decided to skip verification of the used radiation model.

Because none of the other study make any mention of the use of a radiation model this does raise the question as to what the influence of the use of any radiation model is on the results. It is therefore decided to do a comparative study to verify if the influence of the use of a radiation model is indeed small, as is suggested by the fact that it is not mentioned in other studies.

In order to verify this assumption the EDM case with ambient pressure is simulated twice; once including the P-1 radiation model and once without including any radiation model. Of these two cases the key integral quantities are compared to asses the impact of not using any radiation model. The EDM case is selected because it predicts high combustion temperatures. High temperatures are expected to make the effect of absence or presence of a radiation model more pronounced. In addition the EDM case is computationally cheap.

Quantity		**Unit**	**EDMAmbient**	**EDMAmbientNoRad**	**Relative**
Flow	Fuel	kgs^{-1}	$8.14{\cdot}10^{-4}$	$8.14{\cdot}10^{-4}$	0.00%
	Oxidizer	kgs^{-1}	$3.25{\cdot}10^{-3}$	$3.25{\cdot}10^{-3}$	0.00%
	Exhaust	kgs^{-1}	$4.05{\cdot}10^{-3}$	$4.02{\cdot}10^{-3}$	-0.67%
Exhaust	Velocity	ms^{-1}	$1.49{\cdot}10^{-3}$	$1.50{\cdot}10^{-3}$	0.54%
	Temperature	ms^{-1}	$3.46{\cdot}10^{-3}$	$3.49{\cdot}10^{-3}$	0.86%
Pressure	Chamber	Pa	4162000	4150000	-0.29%
	Fuel inlet	Pa	4170000	4151000	-0.46%
	Oxidizer inlet	Pa	4164000	4150000	-0.34%
Heat flux		Wm^{-2}	12787	9808	-30.37%

Table 6.16: Tabulated integral quantities of EDM cases at ambient pressure comparing the inclusion of radiation modeling and omission of radiation modeling.

The results of this comparison are displayed in Table 6.16. The results show very little difference between including the P-1 radiation model and omitting radiation altogether. The sole quantity in which the effect is significant is in the total heat flux over the walls, which decreases by 30% when no radiation is modeled. This is not surprising as radiation is one of the prime methods by which heat is transferred. It is therefore concluded that for the purpose of modeling ignition and combustion itself radiation modeling is indeed not of significant influence. For the purpose of modeling heat transfer radiation modeling is however required.

6.3. Validation

Proper validation of the developed numerical model is challenging in the sense that the experiments are required to be conducted are rather sophisticated. Never the less literature research demonstrated that such experiments are entirely feasible [3]. Figure 6.6 presents an overview of the flow field quantities generated by the numerical model and their relation to different experimental techniques.

In any validation effort the maximum allowable errors derived at the beginning of this chapter in Section 6.1 and Table 6.2 shall be used as starting criterion for assessing if validation succeeds.

Direct validation using experimental data from previously conducted experiments from third parties is deemed unfeasible. The challenges in obtaining this data due to igniter design being a closely guarded corporate secret and general scarcity of comparable studies make it very difficult to obtain suitable data [3].

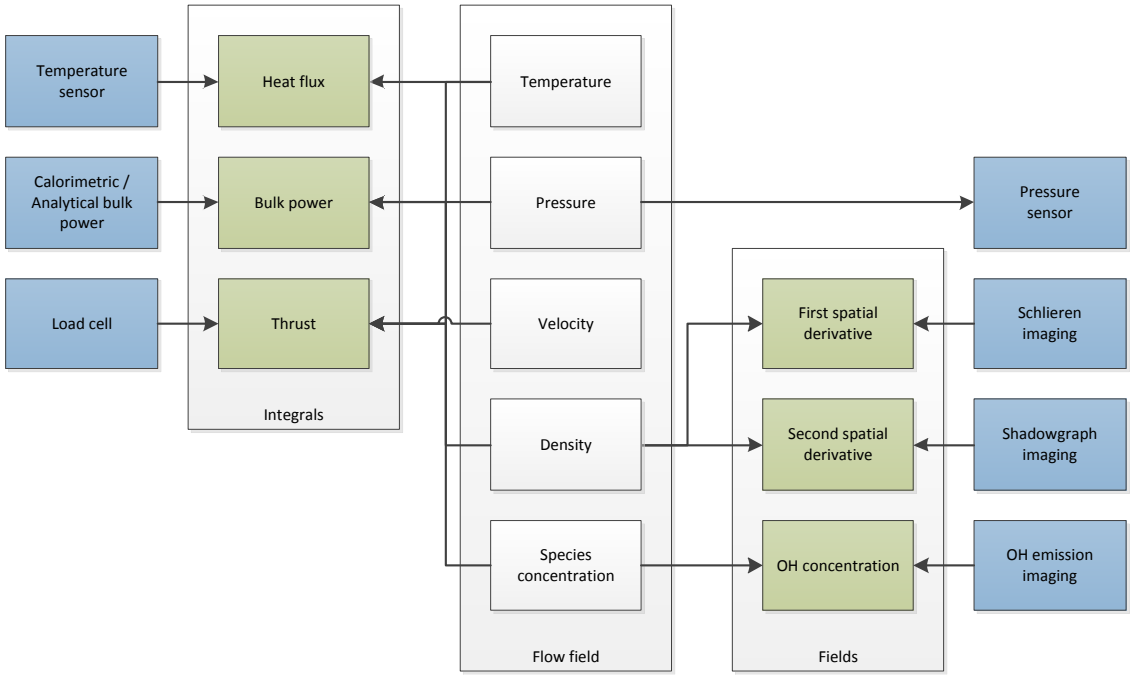

Figure 6.6: Schematic overview of experimental methods (blue) and their relation to derived properties (green) of the flow field generated from the numerical model (grey).

Validation using other experimental data would only be helpful in case data from an experiment using very similar near critical inlet conditions and roughly similar geometry could be obtained. No such cases are known to the author.

6.3.1. ANSYS Fluent

In this work it is generally assumed that all the codes implemented by ANSYS fluent are validated. This essentially clears most of the mathematical models used and their implementation of verification and validation. It would however be foolish not to discuss and investigate this assumption in more detail as the effect of this assumption can be detrimental to the results of this work. This section will briefly explore the relevant verification and validation of the ANSYS Fluent code, what is validated and what is missing.

While the number of validation and verification cases presented by ANSYS is significant, the number of relevant cases for this study is highly limited. Only two presented cases involve turbulent non-premixed combustion and neither combines this with compressible let along supersonic flow. The two relevant cases are:

VMFL025: Turbulent Non-Premixed Methane Combustion with Swirling Air [7]

In the VMFL025 case turbulent reacting flow with a swirl is validated. The non-premixed combustion model is used in combination with both radiation and heat transfer. The verification manual describes the test case as follows:

> Air and Methane enter as separate streams into an annular chamber. Air issues as a swirling jet and also as a separate co-flowing stream with axial velocity. Both the air streams are free of methane. Species mixing and combustion take place in the axisymmetric chamber. Radiative heat transfer is taken into account.

The obtained solution is validated against experimental data. This validation reveals that flow swirl is predicted fairly well, but velocity, temperature and CO2 concentration is off by around 20% at the points published. These values are outside the maximum allowable error ranges set at the start of this chapter.

VMFL049: Combustion in an Axisymmetric Natural Gas Furnace [7]

In the VMFL049 case turbulent reacting flow is validated. The eddy dissipation model with $\kappa-\epsilon$ turbulence model is used to model combustion. The verification manual describes the test case as follows:

> Non-premixed combustion in a natural gas fired furnace is modeled. The axisymmetric flow field is modeled by a 3° cylindrical domain. Fuel jet consists of natural gas modeled as 90% Methane and 10% Nitrogen by mass.

The solution agrees very well with experimental data points published. Both the measured temperature and CH4 fraction follow the predicted curve within a margin of a few percent. While detailed results are missing the notion of predicted temperatures being off only a few percent from measured values compares favorably with the maximum acceptable criterion of 15% set at the start of this chapter.

Missing verification and validation Based on fact that the documented validations of ANSYS Fluent it is concluded that a large part of the ANSYS Fluent code employed in this work is for practical purposes to be considered unvalidated. This underlines the need for a dedicated set of experiments to validate the model.

6.3.2. Validation approach

During the presentation of the model it was noted that the general conservation equation plays a key role. The other key role is played by the chemistry. The premise offered by the different conservation equations; that these quantities are conserved provide an appealing handle for performing validation. If one can demonstrate that these quantities are indeed conserved a major validation step is completed. This approach is illustrated as the left hand set of the relations between the flow field, integral properties and experimental methods as sketched in Figure 6.6.

The second validation approach would ideally leverage the fact that the numerical model produces a complete 3D flow field. Given that this flow field is detailed enough one can attempt to compare the obtained field to the experimentally observed flow field. One can split this approach in comparing qualitative flow field properties such as the presence of shocks or expansion waves and comparing quantitative properties. This approach does require fairly involved measurement techniques, but does allow a much deeper validation. This approach is illustrated as the right hand set of the relations sketched in Figure 6.6.

Based on the two formulated approaches as well as based on the results from the literature review two validation approaches are presented in this section: a simple and an advanced approach. These two approaches have also been observed to be used for validating similar studies [3].

6.3.3. Simple experimental

In the simple experimental approach the goal is to validate if the model correctly predicts global outcomes such as if ignition is achieved using certain combinations of initial conditions. Examples of such experiments are the testing of a catalytic igniter at TNO [21] and the testing of a LOX/Methane igniter at NASA [11].

Beside the more simple nature of the setup required to perform this experiment as major advantage is that the actual igniter design can be used with only minor modifications for placement of the required sensors. This not only allows the model itself to be validated but also allows validation of the model in the context of this exact igniter design and the simultaneous validation of the igniter design itself.

For this experiment the following sensors are to be placed:

Chamber pressure sensor Chamber pressure is a key parameter as ignition will cause a distinct rise in chamber pressure. Care must be taken to place the pressure sensor port away from areas where flow velocities are high, or else provisions must be taken to be able to measure both the static and dynamic pressure. The area around the spark plug is the preferred location for the pressure port.

Chamber temperature sensor Predicted flame temperature is key output parameter of the model and ignition is characterized by a sharp rise in temperature. By placing a thermocouple inside the exhaust tube

or combustion chamber a lower bound value for the chamber temperature can be obtained. The temperature reading will be a lower bound because it will be inside the boundary layer which is likely to have a lower temperature than the gas in the central chamber. The area around the spark plug is the preferred location for the thermocouple.

Chamber wall temperature sensor Thermal loss is of interest because it is expected to significantly impact igniter performance. Measuring the chamber wall allows characterization of the thermal losses as well as derivation of the heat flux which can be used to validate the model.

Theoretically one could also derive the chamber pressure by measuring thrust produced by the igniter using ideal rocketry theory. Combining the thrust measurement with the measured chamber pressure, one can derive the effective exhaust velocity. This allows one to solve for the chamber pressure. Doing so however requires estimations of the nozzle quality and thermal losses. In addition one will need to assume a value for the average molecular mass, which will not be constant due to equilibrium chemistry in the cooling exhaust flow. Due to these challenges it is concluded that using this method it is not feasible to obtain an sufficiently accurate estimate for the chamber temperature.

Using the output of the numerical model the measurements for the physical sensors can easily be matched by interpolating the values of interest at the exact location of the physical sensor.

6.3.4. Advanced experimental

The goal of the proposed advanced experimental method is to verify the correctness of both the chemical model and the fluid dynamics model on small scales in time and space. The outputs of the computational model are inherently available on small scales in time and space. Ideally one would want to directly compare these values against experimental observations.

Fitting a combustion chamber with a window on both sides enables imaging of various flow field characteristics. A schematic representation of such an setup as used at DLR is given in Figure 6.7. Such an setup allows for simultaneous Schlieren imaging as well as OH emission imaging. Typical sensor equipment used and equipment required for such an setup was studied in the literature review which preceded this work [3].

Figure 6.7: Schematic representation of imaging setup of experimental 400N thruster at DLR [49].

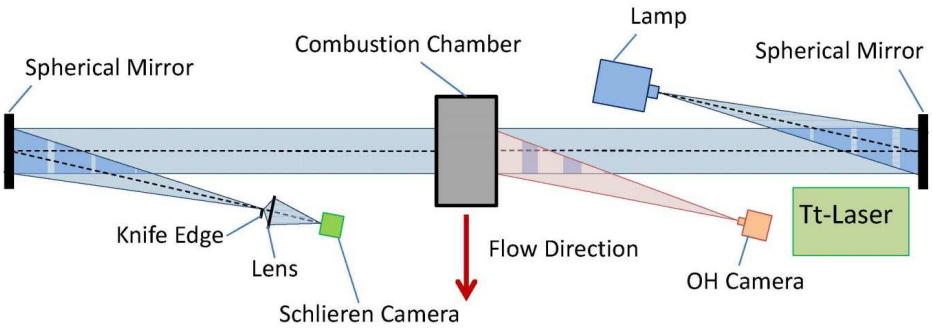

Because the combustion chamber needs to be fitted with windows is is very unlikely that the current igniter design can directly be validated in this manner. The size of the igniter chamber will make it challenging to fit windows. The high operating pressures will make it challenging to design windows capable of withstanding these pressures. In order to conduct the experiments required for validating the model a different combustion chamber shall thus have to be designed.

Another key difficulty with this experimental approach is the lack of objective and quantifiable scoring mechanisms. It is very unlikely that a numerical model is will exactly reproduce the experimental data. Because the full flow field is to be compared this prevents on from simply subtracting predicted values from measured values; the resulting field is going to be equally difficult to score for correctness. Scoring is therefore primarily based on visual inspection and comparison of the flow fields.

Schlieren imaging With Schlieren imaging information on the density gradient is obtained as it yields the spatial distribution of the derivative of the refractive index field ∇n. Density gradients in the flow are caused by flow features and by chemical reactions which rapidly release energy into the flow changing the pressure and density accordingly.

An example in which the results from Schlieren imaging are compared to the results obtained from a numerical model is given in Figure 6.8. In this particular study from DLR the pressure field was derived from the Schlieren imaging and compared to the numerically obtained pressure field [26].

Figure 6.8: Example of Schlieren imaging of cold flow obtained from experiment (top) compared to the pressure distribution (bottom). Source: [26]

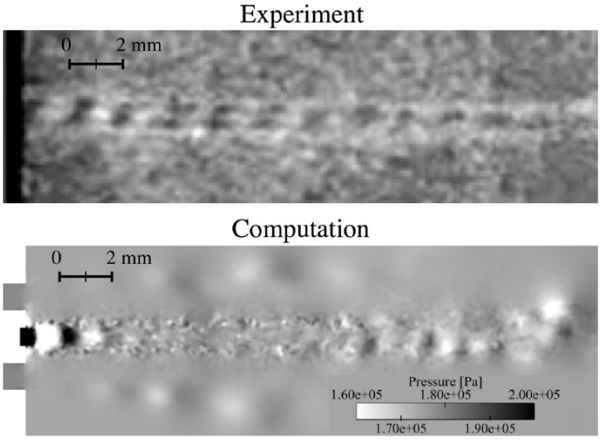

For this work the following flow features are to be compared using Schlieren imaging:

Injector jets The injector jets bring along strong density gradients as is visible in the density plot obtained from the numerical model show in Figure 6.9. Using Schlieren imaging to compare the location of the density gradients allows validation of the injector jet flow topology.

Flame front location In steady state situations the flame front location should match the flame front location of the numerical model.

Flame spreading The spreading of the flame can be captured by taking multiple Schlieren images in consecutive manner, which can be compared against transient simulations.

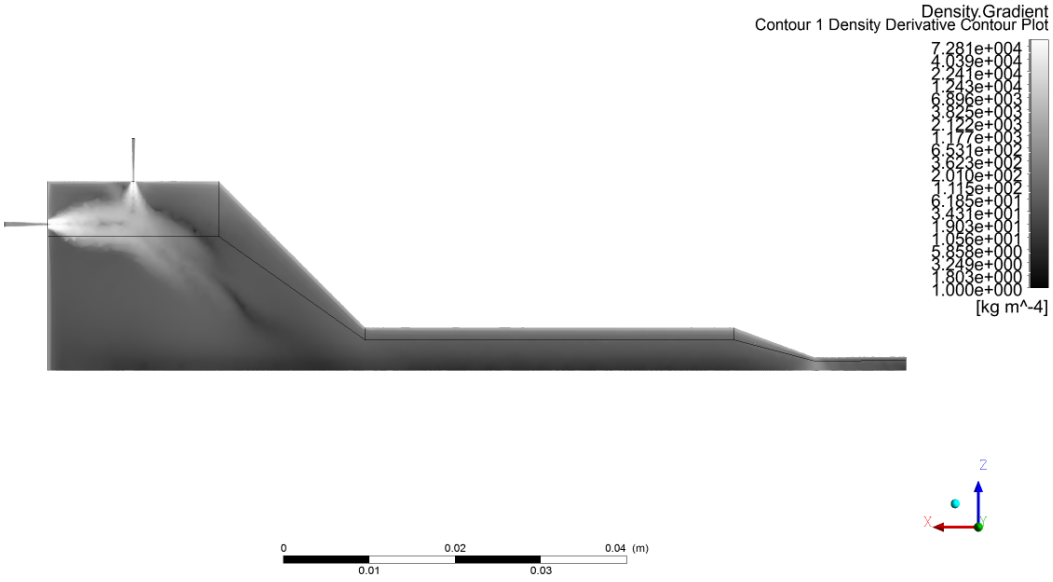

Figure 6.9: Density gradient plot of EDMAmbient case which reacting cold flow with ambient exit conditions.

Shortcomings Due to time constraints and a lack of facilities and equipment no detailed experiments supporting validation have been performed in the context of this work. Because a tailored combustion chamber is to be designed and used for this experimental approach this method cannot be used to directly validate the designed igniter. Only the numerical model itself can be validated in this manner.

6.4. Summary

In order to perform verification a quantification for what is considered a positive verification result is required. To this end the maximum acceptable deviations from analytically derived quantities were derived.

The grid convergence study yielded highly positive results, indicating that the solution is independent of the grid at the chosen grid resolution and further underlining the conclusion that the quality of the generated mesh is sufficient. Flame temperatures were found to not exceed the analytically predicted adiabatic flame temperatures which is another key verification. Likewise mass conservation is usually observed to hold for converged cases, but there are some outliers. These outliers can be explained by the presence of multiple stable solutions in the model.

The cases using solely finite rate chemistry combined with multi-step chemical schemes were found to no pass verification. This result is not entirely unexpected as the cases were judged to not have converged.

The prediction of the fluid state in the inlet regions is found to be highly deviant from analytically predicted values. The need for a real gas model is clear as the fluids in the inlet are often in a supercritical or fluid state. The ideal gas model prevents results from being accurate. In addition it is suspected that numerical errors lead to density over prediction in other cases. In order to correctly model the flow in the injector and inflow region a real gas model is required. The numerical instability of both the real gas model and ideal gas model need to be further investigated.

The validity of the assumption that the full geometry flow can be represented by only partial geometry by exploiting symmetry has proven to be fairly acceptable. While the integral results match very well, the flow fields differ. For modeling ignition itself the full flow field will need to be simulated. The validity of the assumption that modeling radiation is not significantly influential on the results was positively verified, with the exception that for modeling heat transfer to the igniter hardware radiation does have a significant influ-

ence.

Both a simple and advanced experimental method have been suggested to fully validate the model. While the advanced experimental model allows for a more fundamental validation it cannot be done using an actual igniter design. As ANSYS Fluent itself is insufficiently validated experiments are required to be able to put any value to the results generated by the model.

With the conclusion of this chapter it is clear that the model behaves very well on a number of aspects, but that the modeling of inlet conditions is troublesome. Some more work is definitely required to make the model fully usable for modeling ignition, part of which are validation experiments. The criterion and setups of both a simple and advanced experiment were presented where the simple experiment has the advantage that it can be used to validate the actual igniter design.

7

Results and discussion

This chapter aims to present the results obtained in this study and to reflect on these results. While the originally proposed goal of simulating ignition was not achieved a lot of valuable lessons are learned and a great deal of insight is achieved in modeling combustion using CFD in rocket engine like devices. It is in this chapter that these lessons learned and insights are discussed. From this discussion a list of recommendations for future work is derived.

First the results as obtained from the experiments presented in Chapter 5 are presented. In this discussion it is attempted to formulate answers to the research questions using the basic numerical results obtained from the experiments. Next the various observations made while setting up the model and conducting the experiments are discussed. Finally reflection on the research of this work is performed.

In this section the results as obtained from the experiments are evaluated and used to derive answers to the research questions. The structure of this section is made to match the buildup of experiments as discussed in Section 2.4 of which a compact schematic representation is shown in Figure 7.1. First the cold flow cases are discussed, next the equilibrium chemistry cases and finally the cases using more complex finite rate chemistry.

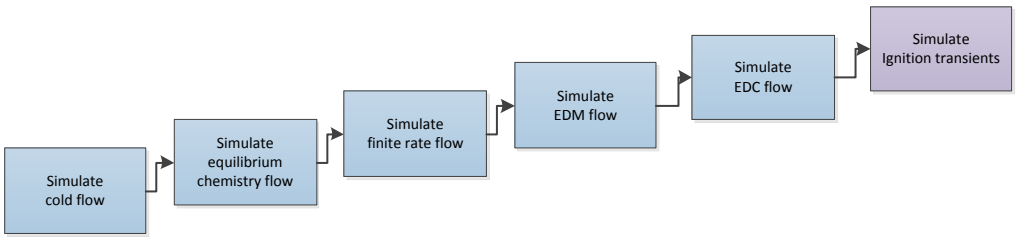

Figure 7.1: High level breakdown of model development approach which is used as guideline for discussing results.

7.1. Cold flow cases

The cold flow cases are in terms of model complexity the most simple cases. The results from these cases can be used to assess the injection conditions and to verify the assumption that simulating an extended inflow region can produce more realistic results. The cold flow cases also offer a glimpse in the conditions prior to ignition of the igniter, allowing testing of the mixing in the igniter chamber.

7.1.1. Inflow

In Section 3.5 of the baseline design it was explained that modeling the injector flow of the propellants is challenging and that a CFD analysis can potentially offer much better predictions of the actual inflow. Unfortunately verification described in Section 6.2.5 revealed that the quality of the prediction of the conditions in

the inflow regions is insufficient. Despite this fact it is still of interest to see if the results match predictions from the baseline design in any way.

The results are listed in Table 7.1 for the fuel injector and in Table 7.2 for the oxidizer injector. The pressure is measured near the inlet boundary condition. The pressure drop is measured from near the inlet boundary to interface of the orifice with the igniter combustion chamber.

Case	**Inflow**	**BC type**	**Back p.**	**Pressure** [Pa]	**Mass flow** [kgs^{-1}]	**Pres. drop** [Pa]	**Velocity** [ms^{-1}]
Analytical	N/A	N/A	Pressure	$7.79{\cdot}10^{6}$	$8.14{\cdot}10^{-4}$	$8.00{\cdot}10^{5}$	$8.85{\cdot}10^{1}$
ColdFlowStart	Truncated	Mass flow	Ambient	$2.87{\cdot}10^{6}$	$8.14{\cdot}10^{-4}$	$2.46{\cdot}10^{5}$	$2.69{\cdot}10^{2}$
InflowColdFlowMassStart	Extended	Mass flow	Ambient	$4.60{\cdot}10^{6}$	$8.14{\cdot}10^{-4}$	$1.96{\cdot}10^{6}$	$2.59{\cdot}10^{2}$
InflowColdFlowPressureStart	Extended	Pressure	Ambient	$7.79{\cdot}10^{6}$	$1.38{\cdot}10^{-3}$	$3.35{\cdot}10^{6}$	$2.62{\cdot}10^{2}$

Table 7.1: Summarized results of fuel injection flow properties.

Case	**Inflow**	**BC type**	**Back p.**	**Pressure** [Pa]	**Mass flow** [kgs^{-1}]	**Pres. drop** [Pa]	**Velocity** [ms^{-1}]
Analytical	N/A	N/A	Pressure	$7.79{\cdot}10^{6}$	$3.25{\cdot}10^{-3}$	$8.00{\cdot}10^{5}$	$6.11{\cdot}10^{1}$
ColdFlowStart	Truncated	Mass flow	Ambient	$2.37{\cdot}10^{6}$	$3.25{\cdot}10^{-3}$	$2.43{\cdot}10^{5}$	$1.79{\cdot}10^{2}$
InflowColdFlowMassStart	Extended	Mass flow	Ambient	$3.97{\cdot}10^{6}$	$3.25{\cdot}10^{-3}$	$1.81{\cdot}10^{6}$	$1.77{\cdot}10^{2}$
InflowColdFlowPressureStart	Extended	Pressure	Ambient	$7.79{\cdot}10^{6}$	$6.43{\cdot}10^{-3}$	$3.60{\cdot}10^{6}$	$1.79{\cdot}10^{2}$

Table 7.2: Summarized results of fuel injection flow properties.

Comparing the analytical values from the baseline design to the ColdFlowStart case reveals that the model predicted pressure drop is about a factor 3 lower than the design pressure drop. At the same time the model predicted injection velocity is roughly a factor three higher than the design injection velocity and the model predicted pressure at the inlet boundary is about a factor three lower than analytically predicted.

Extended inflow Specifically for the purpose of modeling injector flow a number of cases were simulated in which an extended inflow region was modeled. By extending the inflow region the flow is allowed to develop prior to entering the injection orifices, potentially yielding a more realistic flow. The meshes used for this purpose were presented in Section 4.1. In order to realize such an potentially more realistic flow field one would need to apply a pressure boundary condition instead of a mass-flow boundary condition.

The question now is whether the same mass-flow and pressure drop are observed irrespective of whether a mass-flow or pressure inlet boundary are used and whether the use of an extended inflow region results in different pressure drop and/or mass-flows being predicted. Comparing the InflowColdFlowMassStart and InflowColdFlowPressureStart indicate that the type of boundary condition used has a profound effect on the predicted flow. The reason can simply be that the injector orifice is larger than required resulting in a large mass-flow in case a mass-flow boundary is applied. In this work it is however not possible to draw any conclusions due to the fact that verification of the modeling of the gas state failed.

7.1.2. Mixture ratio

In Section 3.5.2 it was explained that the injector orifices are placed in such a manner as to ensure proper mixing around the spark plug electrode location. The ColdFlowStart case which models non reacting flow with ambient exhaust conditions is used to verify the assumption of the orifice placement leading to good mixing.

The model predicts an O2 mass fraction of 0.8001 and CH4 fraction of 0.1993 at the spark plug electrode region. This equates to a mass O/F ratio of 4.01 which is very close to the design mass O/F ratio of 3.99 calculated in Section 3.4. The model thus positively confirms the assumption that the injector orifice placement leads to good mixing around the spark plug electrode.

7.2. Equilibrium chemistry cases

The cases combining equilibrium chemistry with mixture ratio variance transport are a step up in complexity compared to the cold flow cases. By including chemistry investigating the effect of boundary changes on the igniter performance becomes possible and the first predictions on the thermal power of the igniter can be produced.

7.2.1. Influence of initial temperature

Studies by NASA indicated the initial hardware temperature is detrimental to the operation of the igniter [12] [11]. In these works it is suggested that cold hardware might result in the initial flame being extinguished due to too much heat being extracted from the growing flame. While in the cases run no transient simulations were performed this observation does raise the question as to what the influence of cold or hot walls are on the results as predicted by the model.

Using the case **EquilibriumAmbientHotWalls** an attempt was made to characterize the effects of hot walls. In this particular case the wall temperature was raised from 298 to 598 Kelvin. The resulting wall heat flux and thermal power for a quarter igniter geometry are given in Table 7.3.

Case	**Wall temperature** [K]	**Exhaust temperature** [K]	**Exhaust power** [Js^{-1}]	**Wall heat transfer** [Js^{-1}]
EquilibriumAmbient	298	1737	$7.18 \cdot 10^6$	$1.29 \cdot 10^5$
EquilibriumAmbientHotWalls	598	1828	$7.13 \cdot 10^6$	$1.21 \cdot 10^5$

Table 7.3: Comparison of predicted exhaust thermal power and wall heat transfer for hot and cold walls for a quarter geometry igniter model.

While the results show an increase in wall heat transfer for the case with cooler walls, the predicted thermal heating power is higher for the case with colder walls. The rise in heat transfer is as expected as a larger temperature difference should yield a larger heat flux. Accordingly the predicted exhaust temperature is higher for the case with the hot wall case compared to the cold wall case. The predicted exhaust heating power is however lower for the hot wall case than for the cold wall case.

This seemingly contradictory result of higher predicted exhaust temperature but lower exhaust heating power for the hot wall case suggests that some other effect is at play. With a change in exhaust temperature of about 5% the effect of wall temperature does seem to be significant. With wall heat transfer making up a little under 2% compared to the exhaust heating power and the difference in wall heat transfer between both cases being small, it is clear that the wall heat transfer itself cannot explain the exhaust temperature difference.

Based on the results presented in Table 7.3 it is therefore concluded that the influence of wall temperatures does have some significant effect on model predictions, but as the effect of a hotter wall is not simply a higher exhaust power, the mechanism behind it is unclear. Further investigation is required to determine the manner in which the wall temperature affects the predicted results.

7.2.2. Outflow

In Section 4.1 it was asserted that in case a sonic throat is present in the exhaust flow the exhaust region can be truncated without affecting the predicted upstream flow. While this assertion follows directly from fundamental aerodynamics it is of interest if this effect is correctly reproduced by the model. The location of the throat cannot be specified exactly due to meshing and boundary layer presence.

In order to verify the assumption the EquilibriumPressure cases which combined equilibrium chemistry with an elevated exhaust pressure is simulated using both an extended and truncated outflow region. The integral values as predicted by both model variants are summarized in Table 7.4.

Case	**Location**	**Velocity** [ms^{-1}]	**Temperature** [K]	**Pressure** [Pa]	**Massflow** [lgs^{-1}]
OutflowEquilibriumPressure	Throat	$3.484 \cdot 10^{2}$	$1.892 \cdot 10^{3}$	$3.999 \cdot 10^{6}$	$4.222 \cdot 10^{-3}$
EquilibriumPressure	Throat	$3.486 \cdot 10^{2}$	$1.982 \cdot 10^{3}$	$3.946 \cdot 10^{6}$	$3.997 \cdot 10^{-3}$
OutflowEquilibriumPressure	Chamber	$1.233 \cdot 10^{1}$	$2.156 \cdot 10^{3}$	$4.456 \cdot 10^{6}$	N/A
EquilibriumPressure	Chamber	$1.329 \cdot 10^{1}$	$2.185 \cdot 10^{3}$	$4.390 \cdot 10^{6}$	N/A

Table 7.4: Summarized integral results of equilibrium chemistry cases using both a truncated and extended outflow region.

While performing the simulation of the case with the extended outflow region it was found that the numerical stability worsened compared to the case using the truncated inflow region. No probably causes for this could be identified, but experts suggested that the type of boundary condition used may have been a suboptimal choice [18]. While the boundary used does not necessarily produce incorrect results, it is known to be numerically less stable for large outflow regions like the one used in this particular case.

From the results in Table 7.4 it is concluded that while a truncated outflow region does indeed largely result in the same predictions for the flow upstream of the throat the difference can amount to 5% of the flow quantities. Especially the differences in predicted mass-flow are unexpected and hint at an unstable solution of the case containing the extended outflow region. The mass flow for a quarter geometry igniter is slightly over $4 \cdot 10^{-3}$ kg/s, which makes the OutflowEquilibriumPressure violate the conservation of mass.

This discrepancy can be due to an insufficiently converged solution, or due to a flow which is actually unstable. The fact that the residuals do not decrease and that some integral terms show instabilities hint at an unstable flow pattern. While the sonic throat does seem to decouple the interior from the exterior there are still some changes visible in the interior values as predicted by the model. In case high precision is demanded the simulation of an outflow domain is more realistic.

7.3. Detailed chemistry cases

The cases including finite rate chemistry are the most complex cases short of the transient cases. These are also the cases where the computational cost significantly started to rise. The cases in which the EDC was used the required amount of computational time rose to over 8 hours when using single step chemical kinetics. For two step chemical kinetics the solution failed to fully converge even after 28 hours of computing.

Effectively this made combining the EDC with the more complex chemical kinetic schemes introduced in Section 4.6.2 unfeasible due to the required computational time. This also means that answering the research questions which relate to the comparison of different chemical kinetics schemes largely cannot be answered.

A few short attempts were made to evaluate the effects of using more detailed chemical kinetics schemes in combination with the EDC. In these cases not only the computational time required per iteration further rose but also numerical stability became an increasingly large problem. These two issues prevented any of such cases from being run. Hence they are not further presented nor discussed in this work.

The cases in which the EDM is used however yielded good results in terms of usability. And while the EDM cannot be combined with chemical kinetics involving more than a single reaction, the results can still be compared to the results from cases using EDC and equilibrium chemistry.

7.3.1. Power

During the baseline design phase discussed in Chapter 3 it was determined that the heating power is one of the key requirements of the igniter. In this section the thermal power as predicted using the model for the

various cases is evaluated.

The first step in evaluating the predicted thermal power is to calculate the thermal power. In order to calculate it a similar approach to the one taken in Section 3.4 is used. The predicted chemical composition of the exhaust flow and the predicted exhaust flow temperature are the primary inputs. For the cases where a chemical scheme is used these values can be extracted directly from the solution as species transport is modeled. For the equilibrium chemistry cases the mixture fraction and enthalpy are used as inputs to obtain the predicted chemical composition.

A summary of the calculated thermal powers is given in Table 7.5. Fully worked out calculations can be found in Appendix F. Note that the due to a quarter geometry being simulated the total predicted heating power is factor 4 larger than the exact thermal power of the model predicted exhaust flow. In addition the fraction of the predicted heating power compared to the design power is given.

Case	**Power** [kJs^{-1}]	**Fraction of design**
EquilibriumAmbient	$2.87 \cdot 10^4$	22.79%
EquilibriumPressure	$3.28 \cdot 10^4$	26.07%
EDMAmbient	$8.58 \cdot 10^4$	68.06%
EDMPressure	$9.95 \cdot 10^4$	78.95%
EdcWd1StepAmbient	$1.04 \cdot 10^5$	82.45%
EdcWd2StepAmbient	$1.01 \cdot 10^5$	80.16%
FiniteRate1StepAmbient	$8.74 \cdot 10^4$	69.37%
FiniteRate1StepPressure	$9.88 \cdot 10^4$	78.41%

Table 7.5: Summary of predicted thermal power for different model cases. Both total thermal power given and the fraction the total predicted heating power is of the design value.

A known difficulty in calculating the thermal power is the effect of conversion of kinetic energy in the exhaust flow. As the exhaust flow would collide with the propellant flow in the main combustion chamber at least part of the igniter exhaust flow should undergo an near adiabatic increase in temperature as the flow is slowed down. The degree in which this effect affects the thermal power is impossible to tell at this point. It is both dependent on the mixing process of the igniter exhaust flow and main engine propellant flow and the resulting change in temperature will drive chemical process altering the igniter exhaust flow composition. In this work the it is assumed that this effect is negligible for the purpose of comparing bulk power.

The results presented in Table 7.5 are somewhat surprising. As the design thermal power was calculated using equilibrium chemistry one would expect the finite rate chemistry models to predict a higher thermal power due to their inability to fully represent dissociation. All model predicted values are however significantly less than the design thermal power, including the non equilibrium chemistry ones. One potential cause for this discrepancy is heat loss through the walls, but it will be shown in Section 7.2.1 that heat loss is minimal. All predicted powers are outside the allowable error bounds set in Section 6.1.

Inspection of the composition of the exhaust stream of the EquilibriumAmbient and EquilibriumPressure cases reveals a presence of CH4 of 10.1% by mass. Leaving this much methane non combusted will invariably impact thermal performance. Other cases did not show a large concentration of CH4 in the exhaust stream. What is interesting is that the FiniteRate1StepAmbient and FiniteRate1StepPressure case predict absolutely zero CH4 in the exhaust stream while all other cases at least predicted trace amounts of CH4 in the exhaust stream.

The relative differences between the individual cases are more or less as expected. Using more detailed chemistry results in a lower predicted thermal power because dissociation is predicted more correctly, which is for example the case in the cases where the EDC is combined with either a single step or a two step chemical scheme. The two step chemical scheme yields a slightly lower thermal power than the single step chemical

scheme.

Increasing pressure results in an increased thermal power. This is in line with expectations as the effect of dissociation is reduced with pressure and this fact is one of the reasons why rocket engines are typically operated at high pressures [51]. In the the most extreme end of the spectrum of the results are the cases which used equilibrium chemistry for which as expected the lowest thermal power is predicted.

It does stand out that the EDC is predicted higher temperature and bulk power than the EDM. One would expect the EDC to predict lower temperature as chemistry is bound by a finite rate. In addition the EDC is conceptually closer related to the equilibrium chemistry method because chemistry is integrated over time allowing the reactions to attain chemical equilibrium more closely. This should lead to dissociation becoming more pronounced, yet predicted temperatures and power are higher.

7.3.2. Flame shape

The shape of the flame is frequently used to quantify the quality of combustion models as was described in Section 6.3.4. In section 3.5 it was also explained that the flame should not impinge with the walls as this is expected to induce excessive thermal loads on the igniter.

While the model predicted flames at the moment cannot be compared to experimentally measured flames it is still of interest to compare the flames between the cases as this can reveal differences between the different chemistry models used. In addition the requirement of the flame to not impinge with the chamber walls can be checked. In order to do so a contour plot of the flame temperature is used. The flames are compared based on relative temperature differences within the case.

For the cases which assume ambient exhaust pressure the temperature contour plots are displayed in Figure 7.2. All four flames show an equal pattern of relatively cool injection streams colliding and heating up as they react. The flame in of the FiniteRate1StepAmbient case stands out because it appears to be longer than the other flames, taking a longer distance to reach full temperature. The EDM and EDC cases predict the highest temperatures in the central region of the combustion chamber while the other two cases predict the highest temperatures along side the flow of cool gases. The flame from the EquilibriumAmbient case appears to make a lower angle to the horizontal than the other three cases.

The EDAmbient case predicts a hot spot near the wall at the fuel injection port which if correct can be important to take into account in the thermal design. In other cases this hot spot is empty or not very pronounced. Literature makes mention of similar large differences in the predicted flame structure in a rocket engine like context depending on the chemistry models [38].

For the cases which assume high exhaust pressure the temperature contour plots are displayed in Figure 7.3. The EDM case again predict the highest temperature in the central igniter combustion chamber region while the other cases predict the highest temperature along side cool gas region. Both the FiniteRate1StepPressure and EDMPressure cases predict a hot spot near the wall at the fuel injection port while the EquilibriumPressure case does not. Again the equilibrium chemistry predicted flame appears to have a lower angle to the horizontal than the other cases.

Comparing the ambient and high pressure cases reveal that the change in pressure has a most pronounced effect on the flame shape on the cases employing finite rate chemistry without turbulence coupling. The elevated pressure seems to significantly shorten the flame structure and a hot spot near the wall at the fuel injection port is formed.

While it is hard to draw any conclusions from these comparisons as not validation data is available it can be concluded that the choice in chemistry model between the models presented is detrimental to the success of accurately modeling combustion in the igniter. The hot spots which are predicted by some models and different locations of maximum temperature will have a detrimental effect on the thermal load on the igniter.

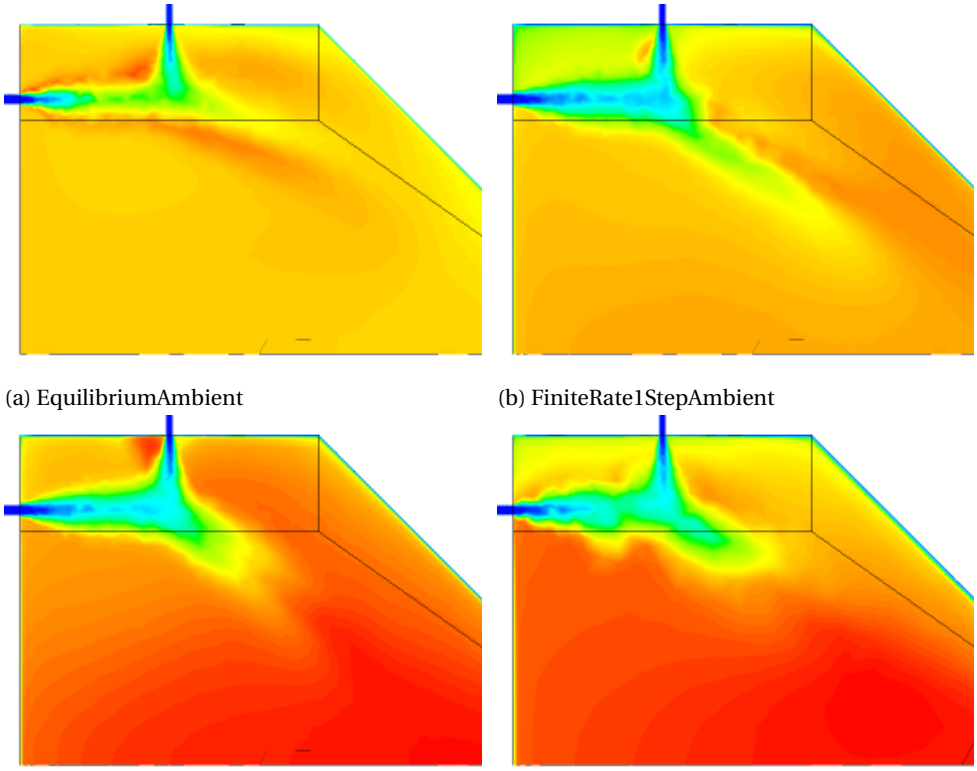

(a) EquilibriumAmbient (b) FiniteRate1StepAmbient

(c) EDMAmbient (d) EdcWd1StepAmbient

Figure 7.2: Zoomed in contour plots of temperature in the igniter combustion chamber for different cases under ambient exhaust pressure. Full figures including legends and scales can be found in Appendix H.

7.4. Transient cases

For the transient cases it was envisioned to simulate full ignition transients using the different chemistry models. Unfortunately both the required computational time as well as the limited time in terms of man hours allocated for this study prohibited implementation of these transient cases. In addition there remain significant issues with modeling the injection conditions and numerical stability which would need to be resolved before running transient cases would effectively become feasible.

It is thus largely impossible to provide answers to the research questions which relate to the ignition transient. This study however did yield a lot of insight in the process of building parts of a model which is capable of simulating transients. The associated observations, insights and limits are further discussed in Section 7.6.

7.5. Influence of chemistry

This section will discuss the influences of the choice in which chemistry is modeled on the results. Specifically the influences beyond the predicted thermal power are discussed.

2 step Westbrook Dryer While the FiniteRate2StepAmbient case which combines the 2 step Westbrook Dryer chemical kinetics scheme with solely finite rate chemistry is considered to not have converged it does provide an interesting observation. As already noted in Section 5.5.5 the produced solutions seem to indicate that a relatively low temperature flame is predicted. This contrasts with the EdcWd2StepAmbient case which is exactly the same case with the exception that the EDC is used instead of solely finite rate chemistry but which does suggest a much higher flame temperature. While the solutions for both cases cannot be considered to be fully converged and the FiniteRate2StepAmbient case failed to pass verification it is remarkable that two cases which use the same chemical kinetics scheme suggest to predict such differing flame temperatures.

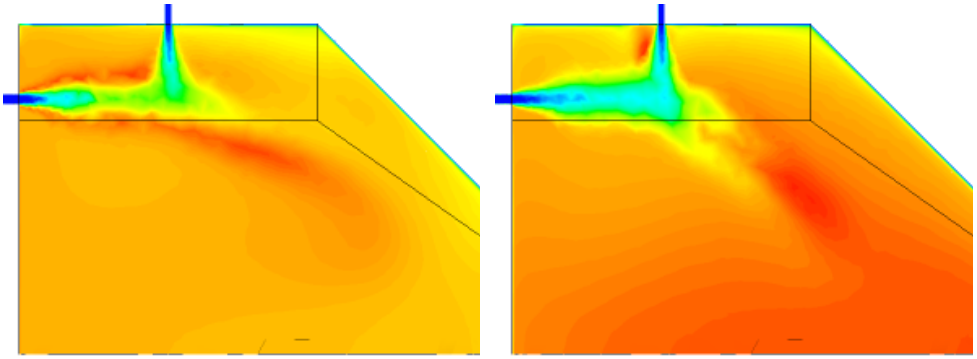

(a) EquilibriumPressure

(b) FiniteRate1StepPressure

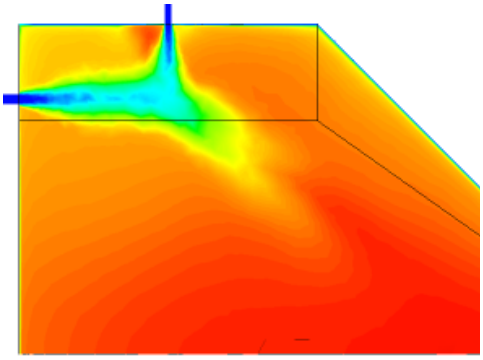

(c) EDMPressure

Figure 7.3: Zoomed in contour plots of temperature in the igniter combustion chamber for different cases under high exhaust pressure. Full figures including legends and scales can be found in Appendix H.

Complete combustion Comparing the exhaust compositions as listed in Appendix F reveals another interesting observation. For the cases FiniteRate1StepAmbient, FiniteRate1StepPressure and EDM cases the exhaust is predicted to contain no CH4 at all, while the EDC cases predict a CH4 content between 1.0 and 2.5% by mass. The equilibrium cases predict a CH4 content of around 10% by mass.

This difference in predicted CH4 content of the different chemistry models is remarkable. Given that there is sufficient oxygen provided and the flame temperature sufficiently high one would expect all the CH4 to react. In addition it is remarkable that the cases using solely finite rate chemistry predict no CH4 content while EDC does predict CH4 in the exhaust stream despite using the exact same chemical kinetics scheme.

The conclusion of this section is that the results produced in this study indicate that not only the chemical kinetics scheme is of influence to the predicted igniter performance but that also the manner in which this chemical kinetics scheme is employed has a significant influence on the results.

7.6. Observations

Now some observations made while developing, verifying and using the model are discussed. While the observations can generally not be supported using numbers they are valuable as one of the goals of this work was to determine how rocket engine ignition can be simulated. It are these observations which are valuable lessons to anyone attempting to develop a similar model.

7.6.1. Numerical stability

In this work it has not been a secret that achieving numerical stability was a challenge. While tools to improve numerically stability are provided in the form of limits and relaxation factors, it is worth taking a closer look at the manifestation of these instabilities. Because these instabilities quickly result in exceptions in the solver

it is difficult to capture them.

Inlet instabilities One case in which the growing of such an instability was successfully captured is the ColdFlowPressure case. The instabilities were observed in the fuel inlet and plots of the fields are shown in Figure 7.4. Before the instabilities developed the solution was converging nicely, with convergence being close.

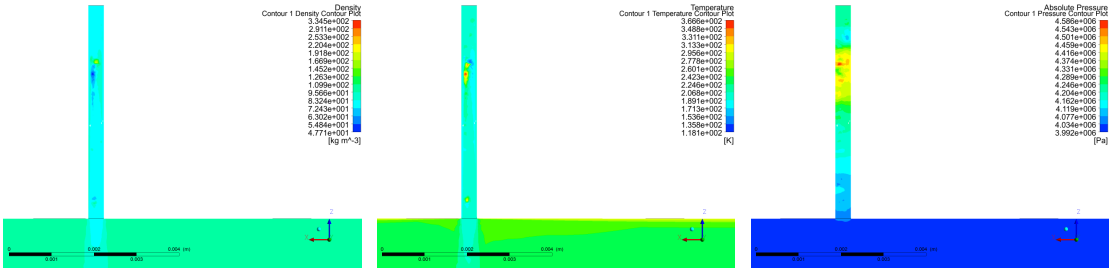

(a) Density (b) Temperature (c) Pressure

Figure 7.4: Example of developing numerical instabilities in fuel inlet in the ColdFlowPressure case

Examining the plots from Figure 7.4 suggest that these instabilities manifest themselves in the form of local increases in temperature leading to a decrease in density and an increase in pressure. Temperature rises from near cryogenic levels to over 350 Kelvin while density halves in value.

No straight forward reason for the appearance of these instabilities could be found. The fact that they however only appear in the inlet regions where the fluids are near their critical point suggest that problems in modeling this state may be part of the underlying cause.

Real gas The fact that in at least some cases instabilities arose in the inlet regions potentially points to problems modeling these inlet conditions. Because modeling of the gas state near critical conditions is not possible using the ideal gas equation and the ideal gas equation is used in the majority of the cases run, this is one the first likely suspect.

A potential solution is to use a real gas equation, which was introduced in Section 4.7. In Section 6.2.5 the predicted gas states were verified and compared to analytically derived results which did reveal large deviations between predicted gas states and analytically derived gas states. While this illustrates the necessity of using a more detailed model for the gas state is also raises the question whether the observed deviations can explain the numerical instabilities.

Based on the data in Table 6.12 and Table 6.13 it becomes clear that the ideal gas model under predicts densities in all cases except for cold flow cases with atmospheric exhaust pressures. Because this suggests that the ideal gas state predicts less steep gradients, it seems unlikely that the instabilities are due to inaccurate modeling of the gas state.

Another manner of assessing whether improving the gas model reduces numerical instabilities is by using the real gas model proposed in Section 4.7. Unfortunately stability of the cases run using this model was so bad that no meaningful results could be obtained. This fact seems to suggest that using a real gas equation worsens numerical stability instead of improving it. The need for more accurate gas modeling thus remains but the use of the ideal gas equation is not considered to be a cause for the observed numerical instabilities.

Full and partial geometry During the solution finding process it was noticed that for the full geometry mesh no under-relaxation was required. This is remarkable in the sense that it was presumed that there would be no difference between full and partial geometry. Naturally the resulting models are not exactly similar due

to the presence of symmetry boundary conditions in the partial geometry model. Also the exact layout of the mesh will be likely be different due to the fact that an automatically generated unstructured mesh is used.

These two differences in the model are then also two potential causes for this change in numerical stability. The mesh quality statistics as presented in Section 4.1.4 do not reveal any major differences in quality between the full and partial geometry meshes. More in depth analysis of the mesh quality is however required before the mesh can be ruled out as a factor in this difference.

At this point the evidence for difference in numerical stability between the full and partial geometry meshes are only anecdotal is nature. A more in depth analysis of this difference is required to draw any solid conclusions. Such an analysis is however of interest due to the time penalty associated with under-relaxation. If a fixable root cause is found solutions can be obtained more quickly.

Solutions from literature With the manifestation of these instabilities the question arises of how other groups dealt with them. Unfortunately only two papers by NASA mention the use of a 'Jameson operator (a blend of 2nd and 4th-order dissipation terms)'to maintain numerical stability [12] [11]. No information is however given on the exact implementation of this operator nor on the exact influence it has on numerical stability. The fact that other works make no further mention of numerical stability or problems with it which were encountered is hence surprising given the wide prevalence of numerical instabilities encountered in this work.

7.6.2. Solution speed

The speed at which the solution was determined became a problem when working with more detailed chemical models. Especially the eddy dissipation concept was found to be very computationally expensive. An overview of the computation time per case is given in Table 7.6. These figures are not very exact and indicative only as it is difficult to reliably measure the computing time.

From the results presented in Table 7.6 it can be concluded that as long as relatively simple models for chemistry such as the EDM, equilibrium chemistry or solely finite rate chemistry are used the computational cost is only marginally higher than simulating cold flow. The number of iterations required to obtain a converged solution does significantly increase. The more complex EDC stands out due to its extreme computational cost compared to the other chemistry models.

Based on these results it is clear that computation speed needs to be increased in order to be able to simulate transient flows. Several methods can be leveraged to increase computation speed:

Parallelization Determination of the solution can be sped up by parallelizing the solution process [15, p. 356]. ANSYS Fluent implemented its solver in such a way that the availability of multiple processing units in a single computer system can be leveraged. During this work up to 4 concurrent processing units were employed to solve the solution. Specialized processing units such as the Intel Xeon offer up to 24 processing units per processing module and multiple modules can be installed in a single computer system. Leveraging such hardware can further increase the speed of the solution process.

GPGPU General purpose processors are not optimized for executing floating point calculations. Using a highly optimized processing unit has the potential to significantly increase the solution process. Graphics processing unit (GPU) designs have over the last two decades evolved into highly efficient floating points calculation units. Derivatives of these GPU's which are suited for performing general purpose computations are referred to general purpose GPU's (GPGPU) and can be leveraged to attain significant speedups in CFD computations [43]. ANSYS Fluent can leverage the presence of a GPGPU in a computer system, but this functionality was not used in this work due to the lack of such a unit.

Computing cluster By distributing the work load over a cluster of multiple computer systems one can theoretically obtain further speed ups. Modern super computers are typically comprised of thousands of computer systems each equipped with several GPGPU modules. Leveraging such a cluster can theoretically further speed up the solution process. Increasing parallelization to such massive levels does however come at an extreme cost in terms of software complexity and the speed up attained is limited by the nature of the problem being solved. ANSYS Fluent has facilities built in to leverage computing clusters, but its use in this particular scenario is unclear without further research.

Case	Iterations	Computing time	
		Total [hours]	**Per iteration** [seconds]
ColdFlowStart	600	0.5	3.0
ColdFlowPressure	600	0.5	3.0
ColdFlowPressure08	600	0.75	4.5
ColdFlowPressure15	500	0.5	3.6
ColdFlowPressure20	500	0.5	3.6
ColdFlowPressure30	500	0.25	1.8
FullColdFlowStart	500	2	14.4
InflowColdFlowMassStart	500	0.5	3.6
InflowColdFlowPressureStart	500	0.75	5.4
EquilibriumAmbient	2700	3	4.0
EquilibriumPressure	3300	3	3.3
EquilibriumAmbientHotWall	2000	Unknown	Unknown
OutflowEquilibriumPressure	2000	Unknown	Unknown
FiniteRate1StepAmbient	1200	1.5	4.5
FiniteRate1StepPressure	1200	1.5	4.5
FiniteRate2StepAmbient	1200	1.5	4.5
FiniteRate4StepAmbient	700	1.25	6.4
EDMAmbient08	1200	Unknown	Unknown
EDMAmbient	1300	Unknown	Unknown
EDMAmbient15	1500	Unknown	Unknown
EDMAmbient20	1000	Unknown	Unknown
EDMAmbient30	1300	Unknown	Unknown
EDMAmbientNoRad	1250	2	5.8
EDMPressure	Unknown	1.5	Unknown
EdcWd1StepAmbient	900	8	32.0
EdcWd2StepAmbient	970	26	96.5

Table 7.6: Overview of the number of iterations and computing time per case and iteration. Numbers are indicative only as accurately measuring the actual computing time is difficult.

7.6.3. Model improvements

Based on the work done in this study it became evident that model improvements are possible and in some cases required. These potential and required improvements will be discussed in this section. Some of these improvements directly follow from the verification and validation or from the discussion of the results. Others follow from observations made while implementing various models and new insights from literature.

Gas state Verification of the predicted injection conditions as presented in Section 6.2.5 clearly demonstrated the need to more accurately model the gas state. Unfortunately the Peng-Robinson real gas equation induced severe numerical stability issues as discussed in Section 5.5.3. There are other real gas equations and it may be worth while to investigate their use and numerical stability.

Chemical kinetics The kinetic schemes used to model chemical reactions in this study were all fairly short. Reasons for not including more detailed kinetic schemes in this study were the required high computation time and the difficulty in achieving stable results with these more detailed kinetic schemes. Using more detailed kinetic schemes has however the potential to increase accuracy. Reasons for using a more detailed chemical scheme are:

Dissociation species At high temperatures (T > 2000 K) dissociation of the combustion products is to be expected [51]. Kinetic schemes of limited detail simply will not be able to model the dissociation due to the lack of details. In case no dissociated species are modeled the model will obviously not be able to model dissociation of these species.

Reversible chemistry As the propellants and combustion products flow through the igniter, exhaust tube and finally the exhaust nozzle they are expected to undergo compression and expansion. This compression and expansion will bring along temperature changes. In addition heat will be given off to the walls leading to cooling of the combustion products. Both of these effects mean that the mixture may cool down significantly. This cooling is known to bring changes in chemical composition of the exhaust stream [44, p. 150].
This effect can only be accurately captured by a kinetic scheme in case reversible reactions are accurately modeled. With the limited number of reactions modeled in the schemes used the accuracy of representation of these effects is questionable.

Flame detail More detailed kinetic schemes can reveal more detail in the flame structure because they contain more steps in chemistry enabling the combustion process itself to be resolved in more detail.

The observation that more complex chemical kinetics schemes increase numerical instability is an issue which will need to be investigated. It is not inconceivable that the schemes themselves represent highly dynamic systems which induce steep gradients which in turn cause interpolation errors. One could for example attempt to use more robust discretization methods.

Literature research performed at the end of this work revealed that some authors have published improved versions of the chemical kinetics schemes used in this work [4]. The claimed improvements are both in the field of making the kinetic schemes represent combustion more accurately as well as adjustments which make numerical computations more easy and stable. These kinetic scheme variants may be viable replacement for the variants used in this work.

Chemistry models The EDM as presented in Section 4.6.4 is coupled with finite rate chemistry. The EDM however also contains two model constants A and B which according to the author in part capture the progression of chemistry and need to be obtained experimentally [28]. In the default ANSYS Fluent implementation values for A and B are provided independent of the actual chemistry represented. A quick survey of literature revealed that the model parameters A and B are usually not tuned.

This situation seems contradictory in the sense that determining the values for the model coefficients is skipped while still provisions are taken to tune chemistry in other ways by for example introducing finite rate chemistry using Arrhenius' Law. While this approach seems straight forward no information was found on the effects and potential disadvantages. Further study is thus warranted.

Radiation modeling Verification of the influence on modeling radiation as presented in Section 6.2.8 showed that radiation has as expected a highly limited influence on the predicted thermal performance of the model. For a future developed model it is thus recommended to either completely exclude radiation modeling to save computational time. In case it is desired to evaluate the wall heat load one would need to investigate the modeling of radiation in more detail as radiation does have influence on the predicted wall heat transfer.

Mesh quality Tables 4.6 and 4.7 suggest that mesh quality is acceptable but not necessarily good. Overall quality is good, but there are definitely not so high quality elements present. Inferior quality meshes may complicate convergence and can degrade the quality of the solution in general.

In future work an attempt can be made to improve the quality of the mesh. ANSYS Fluent provides tools to address mesh quality by locally modifying mesh topology [5].

- Reducing cell size reduces interpolation errors.
- Aligning cells with flow direction reduces numerical dissipation.
- Reducing cell size increases spatial resolution of the solution.

Turbulence modeling As turbulence is an important piece of the computational model it is of interest to see if turbulence modeling can be improved. All studies evaluated during the literature study employed the $\kappa - \epsilon$ turbulence model and paid limited attention to the reasoning behind using this model [3]. While all chemistry models used in this research depend on modeling turbulent energy κ and dissipation rate ϵ limit the choice in turbulence models there are more two equation turbulence models widely used [**?**]. The $\kappa - \epsilon$ turbulence model itself also has variants which claim improved performance and which are also implemented in ANSYS Fluent [42] [5].

Because turbulence is a major input to the chemistry models this raises the question what the effect of the turbulence model itself is on the predicted chemistry. This question cannot be answered in this work but can be an interest stating point for future study. Conversely one can ask the question whether if there are indications of turbulence modeling being insufficient. Only if these indications are present it is meaningful to attempt to improve turbulence modeling. This last questions hall however also have to be investigated separately as the intricacies of modeling turbulence are outside the scope of this work.

7.7. Research setup

With the bulk of the work completed some reflection is performed on the research setup as originally presented in Chapter 2. The first and foremost is checking if all research questions have been answered. Next some reflection on the setup of the research plan itself is done. Last some reflection is performed on the conclusions drawn in this work.

7.7.1. Research questions

In order to check if all research questions have been answered each of the research sub questions is considered and a brief summary of the results is given.

1. What are the effects on required computational power from choosing different chemical schemes?

This work demonstrated that there certainly is a very large influence on the computational time from the chosen chemical scheme. Unfortunately it was not possible to measure the time required in a repeatable manner due to the challenges with numerical stability. In addition there are a lot of other factors which influence the required computational time such as the gas model used and the discretization scheme.

In terms of applicability it is questionable what the relevance of this question is. While from an high level perspective it is very interesting to know about the computational cost the actual required computing time to find a solution is not necessarily solely dependent on the time it takes to compute a single iteration. The number of iterations required to arrive at a stable solution was observed to vary widely. This means that the effective required total time to compute a solution may relate itself to completely different parameters.

Still is can be concluded that in general the cases using the EDM are solved the quickest, with Equilibrium chemistry being a second and the EDC being vastly slower. Non reacting flow is naturally even quicker than EDM cases and is also solved more quickly due to reduced model complexity lowering the required number of iterations.

2.1. What are differences in flame front development?

This question could not be answered due to the omission of transient simulations. Analysis of the steady state flames did however reveal large differences in the predicted flame structure between different chemistry models. Some models predicted hot spots near walls while others did not and there were differences in how the models reacted to pressure differences. One can only conclude that these differences will find they way in transient flame front developments as well.

2.2. What is the effect on observed reliability of ignition?

This question could not be answered due to the omission of transient simulations.

3.1. What are the differences in predicted igniter response time?

This question could not be answered due to the omission of transient simulations.

3.2. What are the differences in predicted minimum required ignition energy required due to choosing different chemical schemes?

This question could not be answered due to the omission of transient simulations.

3.3. How does the predicted bulk power compared to analytically predicted bulk power?

The model structurally predicts lower bulk power compared to the analytically predicted bulk power. Surprisingly this observation also holds for comparison against the analytically predicted bulk power using equilibrium chemistry against non equilibrium chemistry based results. This is however due to the predicted large amount of uncombusted CH4 in the exhaust stream.

4. How do the results from different chemical schemes compare to experimental data?

While all of the previous research questions focus on the differences between the results obtained using different chemical schemes, a very important question is how these results compare to reality. In case the results do not very accurately match reality it is of interest to get a handle on the size of the error made. Validation is a key step when building models and is the final step before the developed model can be used in real world applications. Being able to answer this question does however depend on the availability of experimental data, which may be difficult to obtain.

From the literature review it can be concluded that key output parameters to compare with experimental data are high frequency pressure and temperature measurements [3]. If available flow field topology obtained using Schlieren or shadowgraph imaging can be used for comparison as well. Finally OH emission imaging may be used to compare numerically predicted chemical activity with real world chemical activity.

5. How can the results be applied to improve the used ignition system design?

Given the quality of the results it is hard to actually apply them to improve the ignition system design without first performing extensive validation experiments. As performing validation experiments largely undercuts the purpose of setting up a model for modeling rocket engine ignition perhaps the best approach would be to aim to use models like the one presented in this work to improve an ignition system or engine design after the first hot fire tests.

7.7.2. Reflection

With the conclusion of this work reflection on the research setup is performed. In this chapter it has been explained that challenges with numerical stability and required computational time prevented part of the research questions from being answered. Hence the initial research plan and feasibility are reevaluated and critical questions regarding the conclusion of this work are presented in this chapter.

Would it have been better to first reproduce other experimental results? In theory it surely would have been easier to first attempt to reproduce other results as it would have avoided much of the hassle with verification and validation. It has however proven to be very difficult to obtain detailed information and data on experiments performed at other organizations. The scientific work published on the work at other organizations was already shown to be lacking in the literature review [3]. This work further underlines the amount of information required to setup a combustion model demonstrating the lack of relevant information in other works even more.

A further complicating factor is that the nature of the flow changes with conditions, potentially rendering the model incorrect for one case with it being correct for the reference case. Examples are different Reynolds

numbers which result in the flow developing in a different manner, which will have consequences in the predicted combustion in case a turbulence interaction model is used.

In that regard it becomes highly questionable if attempting to reproduce data from other experiments would be easy let alone useful.

Was the research plan overambitious? Based on the fact that due to time shortages it was not possible to implement spark modeling and the fact that it was not possible to extend the transient simulations it is concluded that the research plan was overambitious. While this it a pity in the sense that it is large not possible to answer the posed research questions it does underline the validity of the initial problem statement.

Is it even computationally feasible to simulate an ignition transient? Given the fact that even simulating the cases using the EDC with a reduced mesh resolution and even a fairly simple chemical kinetics scheme on what is currently considered to be moderately powered workstation and that the obtained solution was still not completely converged suggests that the computational cost of simulating an ignition transient are enormous by all standards. For a transient simulation an roughly equal number of iterations will have to be spent on each time step simulated, quickly driving the required computational time in the span of months.

While the suggestions from Section 7.6.2 can yield significant increases in computational power available, the computational cost will exponentially rise when more detailed chemical kinetics schemes are used. Extending the domain simulated beyond the igniter would raise computational cost even further.

This line of reasoning suggests that simulating ignition of a full rocket engine using moderately detailed chemistry requires computational power which is only offered by contemporary super computers. Simulating an ignition transient may thus be on the brink of being computationally feasible but reducing the problem to a 2D problem may be an easier path to obtaining meaningful results.

Was the extreme computational cost not mentioned in any of the literature? None of the literature reviewed made any comment on the high computational cost required to simulate rocket engine ignition. This is surprising because this work suggests that the computational cost may be so high that the computational power required is of extraordinary levels. In that light it is remarkable to no mention was made of the computers used to perform the simulation.

7.8. Summary

In this chapter it is proven that using extended inflow regions to verify orifice mass-flow and pressure drop yielded results vastly different from the analytically predicted values. While no solid conclusions can be drawn from the numbers due to failed verification of the modeling of the gas state at injection conditions, the large differences do underline the importance of modeling the inflow area before the injection orifice. Truncating the outflow region to the nozzle has limited effects in terms of the predicted flow quantities while using an extended outflow region induces extra numerical problems.

The model does confirm the assumption that the chosen injection orifice placement yields good mixing around the spark plug electrode region.

The model predicted bulk power in the range of 23% to 82% of the analytically predicted bulk power. The equilibrium chemistry cases were found to contain a significant amount of methane in the exhaust stream, explaining the low predicted temperature and bulk power. These results suggest that the actual igniter power is below the analytically obtained design value. The igniter design power will need to be increased in order to conform to the minimum required bulk power.

The influence of initial temperature and hardware temperature on bulk power was found to be minimal. While no direct parallel can be drawn this does contrast with the results mentioned in literature where the hardware temperature had a detrimental influence on igniteability.

Predicted flame structure and the location of maximum temperature were shown to highly depend on the chemistry model selected. Some models predicted the presence of hot spots near walls and models reacted differently to changes in pressure. Combined with the observation that thermal power depends on the model choice this leads to the conclusion that chemical models selection is of high influence to the results.

Due to the lack of time, higher than expected computational cost and numerical instability it was not possible to extend the model to predict transient flows. Due to this it is not possible to answer all research questions. The fact that setting up the model was more difficult than anticipated does however underline the initial problem statement, making the results from this work all the more valuable.

It is also revealed that the manifestation of the numerical instabilities which are mentioned in Chapter 5 may be linked to the inlet conditions. The fact that at least some of the instabilities manifest together with the discrepancies in predicted gas state underline the need for the use of a real gas model. Unfortunately the use of a real gas model only increased numerical instability.

The model can be improved by using more detailed chemical kinetics schemes, increasing mesh quality and evaluating the choice of turbulence model and investigating the tuning of the various coefficients used in the chemistry models. The high computational cost of the model can potentially be negated by employing novel computing methods using GPGPU's and distributed computers.

8

Conclusion

This work set out with the goal of comparing the results of using different chemical kinetic schemes in context of modeling rocket engine ignition. To fit the time and effort available it was decided to limit the work to modeling ignition in a LOX/CH4 rocket engine igniter. In order to do so a rocket engine igniter had to be designed and a computational model for rocket engine ignition had to be developed. A key difficulty is the number of parts required to build such a model and the limited amount of information available on the construction of such a model. In this work an approach to designing and igniter and computational model for rocket engine ignition is presented.

Primarily analytical methods were used for designing the igniter where the primary requirement is to ignite a fraction of the main combustion chamber propellant flow. The fraction of main combustion chamber propellant flow to ignite was set to 10% by mass by evaluating the flow fraction ignited by other igniters and applying a safety factor. The injector orifices are sized such that the choked flow conditions are not violated but the used design method can be improved.

Constructing a computational mesh from the igniter model is found to be fairly straight forward and the mesh quality can be verified using commonly used metrics. Composing the computational model is fairly straight forward once the models are selected. The real challenge after composing the model is dealing with numerical instabilities. Relaxation factors and artificially imposed limited derived from physics are the two main tools for dealing with these instabilities.

Verification underlined the need to use a real gas model instead of an ideal gas model. Unfortunately using a real gas model induces numerical instability so high that the model becomes unusable. Unfortunately this also rendered the results useless in context of verifying the injector mass flow and pressure drop. Modeling of radiation was shown to have a negligible influence on the predicted thermal power, meaning it can be omitted for most purposes. Positive verification results were achieved for the grid convergence study, chemistry and the assumption that symmetry can be exploited to reduce the size of the computational domain.

Validation proved impossible to achieve in this work due to the required hardware and instrumentation. Reproducing results from other studies is equally problematic due to the confidential nature of the results.

All chemical models predict a lower bulk power than the power predicted using analytical methods. This is surprising because the analytical methods relies on equilibrium chemistry which typically already yields a conservative flame temperature. Because of this it is recommended to increase the design power of the igniter. The relation between different chemical models is more or less as expected with equilibrium chemistry based methods yielding the lowest bulk power estimates. What stands out is that the EDC which conceptually is more closely related to equilibrium chemistry methods yields the highest predicted bulk power. It was found that the equilibrium chemistry cases predicted the presence of methane in the exhaust, contributing to the lower than expected predicted bulk power.

The flame structure and predicted locations of maximum heat differ between the chemical models. Different chemical models also react differently to pressure differences. It is therefore concluded that without validation the predictions of the fine predictions of the flame structure are not usable.

The required computation time to produce a steady state solution while using the EDC with even a fairly simple chemical kinetics scheme such as the Westbrook-Dryer 2-step scheme is large. Because of this it is questionable if it is computationally feasible to model the ignition transient in a domain larger than the igniter itself using more detailed chemical kinetic schemes as the computational cost would explode.

Above all this work underlined the difficulty of designing a numerical model for modeling rocket engine ignition. Given the limited amount of information available, the issues encountered with the used model, the difficulty of validation and extreme computation cost it is considered unlikely that rocket engine ignition can be fully simulated in the near future. Detailed models for ignition are then perhaps better applied to improving an igniter design after the initial hot fire tests as the test results can be used for validation of a developed model.

9

Recommendations

With the conclusion of this work a number of recommendations are formulated. These recommendations are grouped by their aim; some are aimed at getting the model to work for transient simulations, others are aimed at improving model fidelity and speed, and others at validating the model.

Model stability and transient simulations The following recommendations are aimed at improving the model stability and improvements required to extend the model to model transient simulations:

- The flow instabilities which arose in the inlet regions need to be further studied. Alleviating them can significantly improve numerical stability reducing the need for under-relaxation which in turn leads to faster convergence.
- Two papers from NASA mentioned employing a 'Jameson operator' to maintain numerical stability. In case numerical stability can be guaranteed it solution speed can again be improved due to a further reduced need for under-relaxation. Guaranteed numerical stability can also make the model a lot easier in use.
- More powerful computational hardware needs to be used. This work demonstrated that the model is computationally expensive making it impossible to model igniter transient cases on normal CPU's. Distributed computers and GPGPU technology are expected to make the model usable.
- In order to use more complex chemical kinetic schemes it must be investigated why more complex schemes increase numerical instability.

Model fidelity and speed The following recommendations are aimed at improving model fidelity and improving speed by reducing computational cost:

- Igniter design symmetry can be exploited to reduce computational cost. Using symmetry does however seem to slightly increase numerical instability and the flow patterns were shown not to be fully symmetry. It must be further investigated if the symmetry assumption is valid for modeling the ignition transient.
- Include inflow regions in the model to accurately model injection. The influence of the inflow region on modeling the ignition transient can be further investigated. If it would be possible to accurately model inflow without the inflow regions the mesh size can be reduced improving speed.
- Radiation modeling was shown to have a negligible influence on predicted thermal power. For the modeling of thermal loading of the igniter hardware radiation was shown to be of interest. As the current radiation model was selected fairly arbitrary more work needs to be put in selecting and tuning the radiation model.
- It was shown that in order to accurately represent the injection conditions a real gas model is required. The Peng-Robinson real gas equation does however severely effect numerical stability. Work needs to be done to select and implement a numerically stable real gas model.

Validation The following final recommendations are aimed at methods to validate the model and to make the model more correctly represent reality:

- The model is currently insufficiently validated and the validation of ANSYS Fluent was shown to be insufficient as well for modeling ignition. The suggested approach is to use this ignition model to improve an igniter design. The initial tests of the igniter design can double as validation experiments for the ignition model. More fundamental validation experiments require highly specialized equipment.
- The tuning constants for the EDM model must be investigated to yield more accurate results. None of the works comparable to this work reviewed in the literature study make any mention of the used tuning constants. According to literature tuning the EDM constants requires experiments to be conducted.
- The equilibrium chemistry based methods predict a large presence of methane in the exhaust flow. The cause of this needs to be investigated as one would expect all of the methane to be combusted under the used mixture ratio.
- There are more sophisticated variants of the used $\kappa - \epsilon$ turbulence model available and these models are widely used. Their and potential gains can be further studied to improve the modeling of turbulence.

Bibliography

[1] Special metals inconel alloy 625, 2016 . URL http://asm.matweb.com/search/SpecificMaterial.asp?bassnum=NINC33.

[2] Nist chemistry webbook, 2016. URL http://webbook.nist.gov/chemistry/. NIST Standard Reference Database Number 69.

[3] C. Akkermans. Ignition systems for non-hypergolic liquid bipropellant rocket propulsion systems. Technical report, Delft Technical University, 2016.

[4] Jimmy Andersen, Christian Lund Rasmussen, Trine Giselsson, and Peter Glarborg. Global combustion mechanisms for use in cfd modeling under oxy-fuel conditions. *Energy & Fuels*, 23(3):1379–1389, 2009. doi: 10.1021/ef8003619.

[5] *ANSYS Fluent User's Guide*. ANSYS, Inc., release 15.0 edition, 2013.

[6] *ANSYS Fluent Theory Guide*. ANSYS, Inc., release 15.0 edition, 2013.

[7] *ANSYS Fluid Dynamics Verification Manual*. ANSYS, Inc., release 15.0 edition, November 2013.

[8] Francesco Battista, Michele Ferraiuolo, Adolfo Martucci, Ainslie French, Pietro Roncioni, Manrico Fragiacomo, Vito Salvatore, and Leonardo De Rose. Design and testing of a gox/gch4 igniter for small scale rocket engine thrust chambers. 2013.

[9] I Bell, S Quoilin, J Wronski, and V Lemort. Coolprop: an open source reference-quality thermophysical property library, orc 2015 conference, 2015, 2015.

[10] F Bouquet. Development status of the ignition system for vinci. In *38th AIAA/ASME/SAE/ASEE Joint Propulsion Conference & Exhibit*. 2002. doi: 10.2514/6.2002-4330.

[11] Kevin Breisacher and Kumud Ajmani. Lox/methane main engine igniter tests and modeling. In *44th Joint Propulsion Conference, AIAA–2008–4757*, 2008. doi: 10.2514/6.2008-4757.

[12] Kevin Breisacher and Kumud Ajmani. Lox/methane main engine glow plug igniter tests and modeling. Technical report, NASA Glenn Research Center; Cleveland, OH, United States, 2009.

[13] Malcom W Chase. National institute of standards and technology (us), nist-janaf thermochemical tables 1985. NIST Standard Reference Database 13, 1985. URL http://kinetics.nist.gov/janaf/.

[14] J Ducarme, Melvin Gerstein, and Arthur Henry Lefebvre. *Progress in Combustion Science and Technology: International Series of Monographs in Aeronautics and Astronautics*, volume 1. Elsevier, 2014.

[15] Joel H Ferziger and Milovan Peric. *Computational methods for fluid dynamics*. Springer Science & Business Media, 2012.

[16] David M Harland and Ralph Lorenz. *Space systems failures: disasters and rescues of satellites, rocket and space probes*. Springer Science & Business Media, 2007.

[17] Dieter K Huzel and David H Huang. *Modern engineering for design of liquid-propellant rocket engines*, volume 147. AIAA, 1992. doi: 10.2514/5.9781600866197.0000.0000.

[18] Dr. ir. A.H. (Sander) van Zuijlen. Personal conversation, October 2016.

[19] Ralph Huijsman Christ Akkermans Luka Denis Filipe Barreiro Adriaan Schutte Angelo Cervone Barry Zandbergen Jeroen Wink, Rob Hermsen. Cryogenic rocket development at delft aerospace rocket engineering. 2016.

[20] WP Jones and RP Lindstedt. Global reaction schemes for hydrocarbon combustion. *Combustion and flame*, 73(3):233–249, 1988. doi: 10.1016/0010-2180(88)90021-1.

[21] Wouter A Jonker, Alfons EHJ Mayer, and Barry TC Zandbergen. Development of a rocket engine igniter using the catalytic decomposition of hydrogen peroxide. *Green Propellant for Space Propulsion*, 2006.

[22] Robert J Kee, Fran M Rupley, and James A Miller. Chemkin-ii: A fortran chemical kinetics package for the analysis of gas-phase chemical kinetics. Technical report, Sandia National Labs., Livermore, CA (USA), 1989.

[23] Oliver Knab, Anton Fröhlich, Dag Wennerberg, and Wolfgang Haslinger. Advanced cooling circuit layout for the vinci expander cycle thrust chamber. *AIAA Paper*, 4005, 2002.

[24] Tobias Knop, Jeroen Wink, Ralph Huijsman, Robert Werner, Johannes Ehlen, Stefan Powell, Barry Zandbergen, and Angelo Cervone. Failure mode investigation of a sorbitol-based hybrid rocket flight motor for the stratos ii sounding rocket. In *51st AIAA/SAE/ASEE Joint Propulsion Conference*, page 4133, 2015.

[25] Joseph M Kuchta. Investigation of fire and explosion accidents in the chemical, mining, and fuel-related industries. *Bull./US. Dep. of the interior Bureau of mines*, 1985.

[26] Guilhem Lacaze, Bénédicte Cuenot, Thierry Poinsot, and Michael Oschwald. Large eddy simulation of laser ignition and compressible reacting flow in a rocket-like configuration. *Combustion and Flame*, 156 (6):1166–1180, 2009. doi: 10.1016/j.combustflame.2009.01.004.

[27] B Magnussen. On the structure of turbulence and a generalized eddy dissipation concept for chemical reaction in turbulent flow. In *19th Aerospace Sciences Meeting*, page 42, 1981. doi: 10.2514/6.1981-42.

[28] Bjørn F Magnussen and Bjørn H Hjertager. On mathematical modeling of turbulent combustion with special emphasis on soot formation and combustion. In *Symposium (international) on Combustion*, volume 16, pages 719–729. Elsevier, 1977. doi: 10.1016/S0082-0784(77)80366-4.

[29] Chiara Manfletti. Laser ignition of an experimental cryogenic reaction and control thruster: Ignition energies. *Journal of Propulsion and Power*, 30(4):952–961, 2014. doi: 10.2514/1.B35115.

[30] A.G.M. Mareé, H.M. Sanders, and H.F.R. Schöyer. Process for igniting a rocket engine and rocket engine, May 25 2005. URL `http://www.google.com/patents/EP1533511A1?cl=en`. EP Patent App. EP20,030,078,614.

[31] Michael F Modest. *Radiative heat transfer*. Academic press, 2013.

[32] Maurits Mostert. Preliminary design and development testing of a liquid oxygen-methane thruster. Master's thesis, Delft Technical University, 2007.

[33] CEA NASA. Nasa computer program for calculating of the chemical equilibrium with applications. *NASA Glenn Research Center, Cleveland, OH*.

[34] Ding-Yu Peng and Donald B Robinson. A new two-constant equation of state. *Industrial & Engineering Chemistry Fundamentals*, 15(1):59–64, 1976. doi: 10.1021/i160057a011.

[35] Thierry Poinsot and Denis Veynante. *Theoretical and numerical combustion*. RT Edwards, Inc., 2005.

[36] Alexander Ponomarenko. Rocket propulsion analysis (rpa), 2017. URL `http://www.propulsion-analysis.com`.

[37] GA Repas. Hydrogen-oxygen torch ignitor. Technical Report NASA-TM-106493, NASA, 1994.

[38] Pietro Roncioni, Daniele Cardillo, Mario Panelli, Daniele Ricci, Marco Di Clemente, and Francesco Battista. Cfd modelling and simulations of the hyprob regenerative lox/ch4 thrust chamber. In *5th European Conference For Aeronautics And Space Sciences (EUCASS)*, 2013.

[39] Sanders D Rosenberg. Ignition system for oxygen/hydrogen auxiliary propulsion systems. *Acta Astronautica*, 10(1):19–30, 1983.

[40] Safety and Health Division (SHD). *Glenn Research Center Safety Manual*. Glenn Research Center, 2016. URL `https://www.grc.nasa.gov/smad-ext/wp-content/uploads/sites/82/gsm-manual.pdf`.

[41] GV Shchemelev, VU Shevchuk, MP Mulyava, and FB Moin. Self-ignition of methane - oxygen mixtures at atmospheric pressure. *Combustion, Explosion, and Shock Waves*, 10(2):202–205, 1974. doi: 10.1007/BF01464178.

[42] Tsan-Hsing Shih, William W Liou, Aamir Shabbir, Zhigang Yang, and Jiang Zhu. A new k-e eddy viscosity model for high reynolds number turbulent flows. *Computers & Fluids*, 24(3):227–238, 1995. doi: 10.1016/0045-7930(94)00032-T.

[43] Christopher Stone, Earl Duque, Yao Zhang, David Car, Roger Davis, and John Owens. Gpgpu parallel algorithms for structured-grid cfd codes. In *20th AIAA Computational Fluid Dynamics Conference*, page 3221, 2011.

[44] George P Sutton and Oscar Biblarz. *Rocket Propulsion Elements*. John Wiley & Sons, 2001.

[45] Martin JL Turner. *Rocket and spacecraft propulsion: principles, practice and new developments*. Springer Science & Business Media, 2008.

[46] F Verplaetsen and Frederik NORMAN. Influence of process conditions on the auto-ignition temperature of gas mixtures. 2008.

[47] Henk Kaarle Versteeg and Weeratunge Malalasekera. *An introduction to computational fluid dynamics: the finite volume method*. Pearson Education, 2007.

[48] Charles K Westbrook and Frederick L Dryer. Simplified reaction mechanisms for the oxidation of hydrocarbon fuels in flames. *Combustion science and technology*, 27(1-2):31–43, 1981. doi: 10.1080/00102208108946970.

[49] M Wohlhüter, VP Zhukov, and C Manfletti. Numerical analysis of laser ignition and flame development in a subscale combustion chamber. *Aerospace Science and Technology*, 7:517–531, 2014.

[50] Michael George Zabetakis. Flammability characteristics of combustible gases and vapors. Technical report, DTIC Document, 1965.

[51] B.T.C. Zandbergen. *Thermal Rocket Propulsion*. Delft University of Technology, 2010.

[52] B.T.C. Zandbergen. *Aerospace Design & Systems Engineering Elements*. Delft University of Technology, 2015.

A

Engine specifications

This appendix contains the key specifications of the cryogenic methane oxygen rocket engine being developed at Delft Aerospace Rocket Engineering (DARE).

Parameter	Unit	Value
Thrust (sea level)	N	3000
Chamber pressure	Pa	$40{\cdot}10^5$
Oxidizer	-	O_2 (oxygen)
Fuel	-	CH_4 (methane)
Mass flow oxidiser	kgs^{-1}	0.72
Mass flow fuel	kgs^{-1}	0.23
Mass O/F ratio	-	3.13
Oxidizer injection phase	-	liquid
Oxidizer injection temperature	K	90
Fuel injection phase	-	liquid
Fuel injection temperature	K	111.6

Table A.1: Demonstrator engine design specifications

B

Measurement locations

This appendix specifies the measurement locations and measurement techniques as used for the model results. A listing of the locations is given in Table B.1. The color codes in the listing Table correspond to the colored planes shown in Figure B.1. The methods by which various quantities are determined is listed in Table B.2.

Name	**Location**	**Color**
Exhaust	Plane of outflow boundary	Green
Throat	Plane at nozzle throat	Blue
Chamber	Plane at top of converging chamber section	Purple
Fuel inlet	Plane of fuel inflow boundary	
Fuel inlet chamber interface	Plane of fuel injector orifice at chamber interface	
Oxidizer inlet	Plan of oxidizer inflow boundary	
Oxidizer inlet chamber interface	Plane of oxidizer injector orifice at chamber interface	

Table B.1: Specification of measurement locations and corresponding plane colors are shown in Figure B.1.

Quantity	**Method**
Pressure	Area averaged
Density	Area averaged
Temperature	Mass averaged
Velocity	Mass averaged
Mass flow	Area integral
Wall temperature	Area averaged
Heat flux	Area integral

Table B.2: Measurement techniques for various quantities.

Figure B.1: Isometric view of igniter geometry and planes at which measurement are taken.

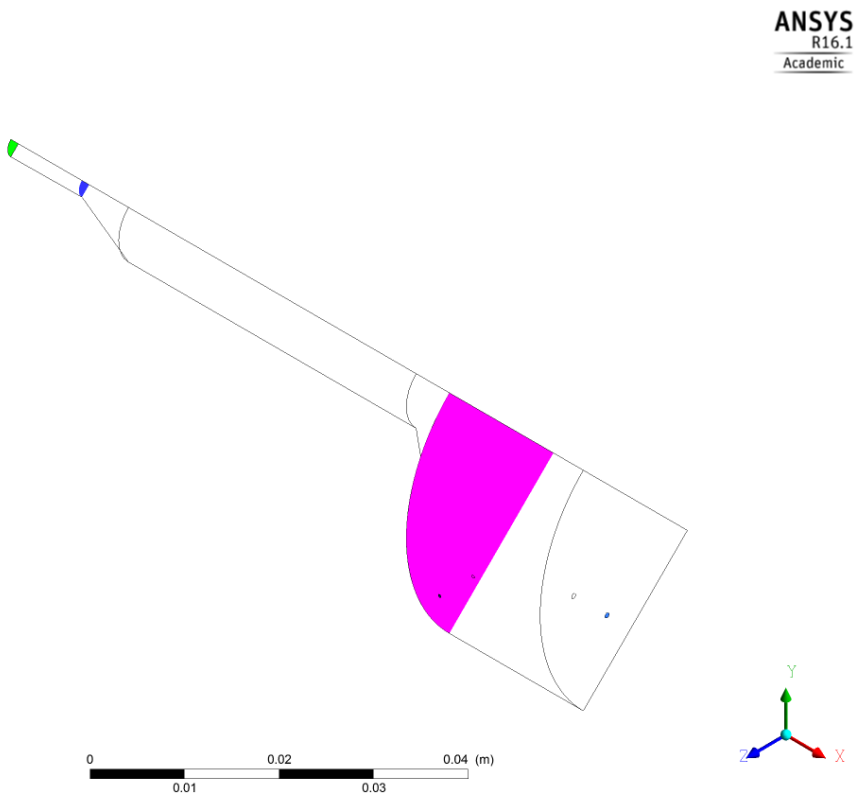

C

RPA Lite inputs and outputs

This appendix contains the input and output file for the Rocket Propulsion Analysis (RPA) program used to determine the chemical equilibrium performance of the igniter. Rocket Propulsion Analysis (RPA) is a tool for designing chemical rocket engines [36]. The use of the calculations performed using RPA is discussed in Section 3.4.2.

C.1. RPA Lite input file

```
version = 1.2;
name = "Igniter baseline design";
info = "";
generalOptions :
{
  multiphase = true;
  ions = true;
  flowSeparation = true;
};
combustionChamberConditions :
{
  pressure :
  {
    value = 4.0;
    unit = "MPa";
  };
};
nozzleFlow :
{
  calculateNozzleFlow = true;
  nozzleExitConditions :
  {
    areaRatio = 1.1;
    supersonic = true;
  };
  nozzleStations = ( );
};
propellant :
{
  components :
  {
    ratio :
    {
```

```
      value = 3.99;
      unit = "O/F";
    };
    oxidizer = (
      {
        name = "O2(L)";
        massFraction = 1.0;
        T :
        {
          value = 147.56;
          unit = "K";
        };
        p :
        {
          value = 4.0;
          unit = "MPa";
        };
      } );
    fuel = (
      {
        name = "CH4(L)";
        massFraction = 1.0;
        T :
        {
          value = 186.1;
          unit = "K";
        };
        p :
        {
          value = 4.0;
          unit = "MPa";
        };
      } );
  };
};
engineSize :
{
  chambersNo = 1;
};
propelantFeedSystem :
{
};
```

C.2. RPA Lite output file

```
# Engine name: Igniter baseline design
# Mon Aug 22 10:50:19 2016
#
#*****************************************************************************************
# Propellant Specification
#-----------------------------------------------------------------------------------------
#     Component  Temp.          Mass          Mole
#                  [K]      fraction      fraction
#-----------------------------------------------------------------------------------------
#        CH4(L)   111.6     0.2004008     0.3332923
#         O2(L)   147.6     0.7995992     0.6667077
#-----------------------------------------------------------------------------------------
```

```
#                Total:      1.0000000        1.0000000
#-------------------------------------------------------------------------------
#     Exploded formula:   (O)1.333 (C)0.333 (H)1.333
#                  O/F:      3.9900000
#                O/F 0:      3.9892635 (stoichiometric)
#                alpha:      1.0001846 (oxidizer excess coefficient)
#-------------------------------------------------------------------------------
#
# Table 1. Thermodynamic properties
#-------------------------------------------------------------------------------
#           Parameter        Injector       Nozzle inl       Nozzle thr       Nozzle exi
Unit
#-------------------------------------------------------------------------------
              Pressure          4.0000           4.0000           2.3212           1.5423
MPa
           Temperature       3509.0903        3509.0903        3352.1553        3241.6033
K
              Enthalpy      -1236.6876       -1236.6876       -1913.8680       -2396.9059
kJ/kg
               Entropy         11.9028          11.9028          11.9028          11.9028
kJ/(kg.K)
Specific heat (p=const)          8.0074           8.0074           8.0186           7.9924
kJ/(kg.K)
Specific heat (V=const)          6.7879           6.7879           6.8455           6.8578
kJ/(kg.K)
          Gas constant          0.3654           0.3654           0.3603           0.3566
kJ/(kg.K)
      Molecular weight         22.7568          22.7568          23.0783          23.3171
 Isentropic exponent          1.1254           1.1254           1.1215           1.1187
               Density          3.1199           3.1199           1.9220           1.3343
kg/m3
        Sonic velocity       1201.2085        1201.2085        1163.7745        1137.1685
m/s
              Velocity          0.0000           0.0000        1163.7745        1523.2979
m/s
           Mach number          0.0000           0.0000           1.0000           1.3396
            Area ratio          0.0000           0.0000           1.0000           1.1000
             Mass flux          0.0000           0.0000        2236.8018        2032.4801
kg/(m2.s)
#-------------------------------------------------------------------------------
#
#-------------------------------------------------------------------------------
#
# Table 2. Fractions of the combustion products
#-------------------------------------------------------------------------------
#              Species        Injector         Injector       Nozzle inl       Nozzle inl
Nozzle thr       Nozzle thr       Nozzle exi       Nozzle exi
#                                mass fract       mole fract       mass fract       mole fract
mass fract       mole fract       mass fract       mole fract
#-------------------------------------------------------------------------------
                    CO       0.1723795        0.1400497        0.1723795        0.1400497
0.1599836        0.1318151        0.1505142        0.1252961
                   CO2       0.2788876        0.1442096        0.2788876        0.1442096
0.2983778        0.1564676        0.3132625        0.1659728
                  COOH       0.0000185        0.0000093        0.0000185        0.0000093
0.0000109        0.0000056        0.0000073        0.0000038
```

```
                    H       0.0009781       0.0220836       0.0009781       0.0220836
0.0008429       0.0192995       0.0007498       0.0173451
                   H2       0.0047422       0.0535335       0.0047422       0.0535335
0.0043448       0.0497404       0.0040560       0.0469141
                  H2O       0.3618778       0.4571222       0.3618778       0.4571222
0.3709780       0.4752383       0.3774624       0.4885484
                 H2O2       0.0000381       0.0000255       0.0000381       0.0000255
0.0000243       0.0000165       0.0000173       0.0000118
     HCHO, formaldehy       0.0000002       0.0000001       0.0000002       0.0000001
0.0000000       0.0000000       0.0000000       0.0000000
                  HCO       0.0000077       0.0000060       0.0000077       0.0000060
0.0000041       0.0000033       0.0000025       0.0000020
                HCOOH       0.0000020       0.0000010       0.0000020       0.0000010
0.0000011       0.0000006       0.0000007       0.0000004
                  HO2       0.0003221       0.0002220       0.0003221       0.0002220
0.0002205       0.0001541       0.0001647       0.0001163
                    O       0.0146641       0.0208575       0.0146641       0.0208575
0.0123177       0.0177676       0.0107285       0.0156355
                   O2       0.0962657       0.0684619       0.0962657       0.0684619
0.0912013       0.0657767       0.0871012       0.0634695
                   O3       0.0000009       0.0000004       0.0000009       0.0000004
0.0000005       0.0000002       0.0000003       0.0000001
                   OH       0.0698156       0.0934174       0.0698156       0.0934174
0.0616925       0.0837144       0.0559327       0.0766839
#-------------------------------------------------------------------------------
#
#-------------------------------------------------------------------------------
#
# Table 3. Theoretical (ideal) performance
#-------------------------------------------------------------------------------
#          Parameter       Sea level       Optimum ex          Vacuum              Unit
#-------------------------------------------------------------------------------
 Characteristic velocity       0.0000       1788.2700          0.0000              m/s
 Effective exhaust velocity       2232.2600       1523.3000       2282.1100
m/s
 Specific impulse (by mass)       2232.2600       1523.3000       2282.1100
N.s/kg
 Specific impulse (by weight)        227.6300        155.3300        232.7100
s
   Thrust coefficient          1.2483          0.8518          1.2762
#-------------------------------------------------------------------------------
#
#-------------------------------------------------------------------------------
#
# Table 4. Estimated delivered performance
#-------------------------------------------------------------------------------
#          Parameter       Sea level       Optimum ex          Vacuum              Unit
#-------------------------------------------------------------------------------
 Characteristic velocity       0.0000       1736.4600          0.0000              m/s
 Effective exhaust velocity       2126.5800       1417.6200       2176.4400
m/s
 Specific impulse (by mass)       2126.5800       1417.6200       2176.4400
N.s/kg
 Specific impulse (by weight)        216.8500        144.5600        221.9300
s
   Thrust coefficient          1.2247          0.8164          1.2534
```

```
#-------------------------------------------------------------------------------------------------------------
#
#<b>Ambient condition for optimum expansion:</b>  H=0.00 km, p=15.221 atm
#
#
#-------------------------------------------------------------------------------------------------------------
#
#
#-------------------------------------------------------------------------------------------------------------
```

D

NASA CEA inputs and outputs

This appendix lists the inputs and output used for the NASA Chemical Equilibrium with Applications computer program. The theory behind and use of the individual cases is presented in Section 4.6.2. For each case the NASA CEA input script and the resulting output is listed.

D.1. 1 step

```
problem    case=1step o/f=3.99,
    hp    p,bar=70,40,1
react
  oxid=O2 moles=5   t,k=161
  fuel=CH4 moles=1   t,k=186
only
  CO2 H2O
output     trace=1.e-15
end
```

THERMODYNAMIC EQUILIBRIUM COMBUSTION PROPERTIES AT ASSIGNED

PRESSURES

CASE = 1step

	REACTANT	MOLES	ENERGY KJ/KG-MOL	TEMP K
OXIDANT	O2	5.0000000	-4000.829	161.000
FUEL	CH4	1.0000000	-78441.219	186.000

O/F= 3.99000 %FUEL= 20.040080 R,EQ.RATIO= 0.999815 PHI,EQ.RATIO= 0.999815

THERMODYNAMIC PROPERTIES

P, BAR	70.000	40.000	1.0000
T, K	5103.17	5103.17	5103.17
RHO, KG/CU M	4.4011 0	2.5149 0	6.2873-2
H, KJ/KG	-1079.85	-1079.85	-1079.85
U, KJ/KG	-2670.35	-2670.35	-2670.35
G, KJ/KG	-59386.4	-60276.5	-66143.6
S, KJ/(KG)(K)	11.4255	11.6000	12.7497

```
 M, (1/n)              26.677    26.677    26.677
 (dLV/dLP)t         -1.00000  -1.00000  -1.00000
 (dLV/dLT)p            1.0000    1.0000    1.0000
 Cp, KJ/(KG)(K)        2.3378    2.3378    2.3378
 GAMMAs                1.1538    1.1538    1.1538
 SON VEL,M/SEC         1354.7    1354.7    1354.7

 MOLE FRACTIONS

 *CO2               3.3325-1  3.3325-1  3.3325-1
 H2O                6.6675-1  6.6675-1  6.6675-1

   * THERMODYNAMIC PROPERTIES FITTED TO 20000.K
```

D.2. 2 step

```
problem    case=2step o/f=3.99,
    hp    p,bar=70,40,1
react
  oxid=O2 moles=5   t,k=161
  fuel=CH4 moles=1   t,k=186
only
  CO2 H2O CO O2
output
     trace=1.e-15 siunits
end


          THERMODYNAMIC EQUILIBRIUM COMBUSTION PROPERTIES AT ASSIGNED

                                PRESSURES

 CASE = 2step

              REACTANT                          MOLES          ENERGY        TEMP
                                                               KJ/KG-MOL        K
 OXIDANT      O2                             5.0000000       -4000.829     161.000
 FUEL         CH4                            1.0000000      -78441.219     186.000

 O/F=     3.99000  %FUEL= 20.040080  R,EQ.RATIO= 0.999815  PHI,EQ.RATIO= 0.999815

 THERMODYNAMIC PROPERTIES

 P, BAR                70.000    40.000    1.0000
 T, K                 4099.88   4049.95   3789.77
 RHO, KG/CU M      4.9119 0  2.8273 0  7.3649-2
 H, KJ/KG          -1079.85  -1079.85  -1079.85
 U, KJ/KG          -2504.96  -2494.63  -2437.64
 G, KJ/KG          -48804.2  -49012.8  -50885.2
 S, KJ/(KG)(K)      11.6404   11.8354   13.1420

 M, (1/n)              23.920    23.801    23.207
 (dLV/dLP)t         -1.01398  -1.01318  -1.00634
 (dLV/dLT)p            1.2194    1.2096    1.1083
 Cp, KJ/(KG)(K)        3.4348    3.3969    2.8685
 GAMMAs                1.1581    1.1591    1.1724
 SON VEL,M/SEC         1284.7    1280.6    1261.7
```

```
 MOLE FRACTIONS

 *CO                2.0695-1  2.1584-1  2.6040-1
 *CO2               9.1859-2  8.1479-2  2.9501-2
 H2O                5.9761-1  5.9465-1  5.7980-1
 *O2                1.0358-1  1.0803-1  1.3031-1

   * THERMODYNAMIC PROPERTIES FITTED TO 20000.K
```

D.3. 4 step

```
problem    case=4step o/f=3.99,
     hp    p,bar=70,40,1
react
  oxid=O2 moles=5   t,k=161
  fuel=CH4 moles=1   t,k=186
only
  CO2 H2O CO O2 H2
output
      trace=1.e-15 siunits
end


          THERMODYNAMIC EQUILIBRIUM COMBUSTION PROPERTIES AT ASSIGNED

                                    PRESSURES

 CASE = 4step

              REACTANT                          MOLES          ENERGY        TEMP
                                                               KJ/KG-MOL       K
 OXIDANT      O2                             5.0000000       -4000.829     161.000
 FUEL         CH4                            1.0000000      -78441.219     186.000

 O/F=     3.99000   %FUEL= 20.040080   R,EQ.RATIO= 0.999815   PHI,EQ.RATIO= 0.999815

 THERMODYNAMIC PROPERTIES

 P, BAR               70.000    40.000    1.0000
 T, K                3894.70   3822.35   3360.38
 RHO, KG/CU M     5.0553 0  2.9222 0  7.9466-2
 H, KJ/KG          -1079.85  -1079.85  -1079.85
 U, KJ/KG          -2464.53  -2448.67  -2338.25
 G, KJ/KG          -46558.2  -46476.7  -45532.0
 S, KJ/(KG)(K)      11.6770   11.8767   13.2283

 M, (1/n)             23.386    23.218    22.203
 (dLV/dLP)t        -1.02791  -1.02875  -1.03302
 (dLV/dLT)p           1.4492    1.4709    1.6116
 Cp, KJ/(KG)(K)       4.8067    4.9937    6.4341
 GAMMAs               1.1460    1.1447    1.1340
 SON VEL,M/SEC        1259.7    1251.8    1194.6

 MOLE FRACTIONS

 *CO                1.6852-1  1.7418-1  2.0034-1
```

```
 *CO2             1.2362-1 1.1586-1 7.7014-2
 *H2              7.8430-2 8.5398-2 1.3532-1
 H2O              5.0585-1 4.9467-1 4.1939-1
 *O2              1.2358-1 1.2989-1 1.6793-1

  * THERMODYNAMIC PROPERTIES FITTED TO 20000.K
```

D.4. Sandia National Flame

```
problem    case=4step o/f=3.99,
    hp    p,bar=70,40,1
react
  oxid=O2 moles=5   t,k=161
  fuel=CH4 moles=1   t,k=186
only
  CO2 H2O CO O2 H2 OH
output
     trace=1.e-15 siunits
end
```

```
          THERMODYNAMIC EQUILIBRIUM COMBUSTION PROPERTIES AT ASSIGNED

                              PRESSURES

 CASE = 4step

              REACTANT                        MOLES        ENERGY       TEMP
                                                          KJ/KG-MOL        K
 OXIDANT      O2                          5.0000000      -4000.829    161.000
 FUEL         CH4                         1.0000000     -78441.219    186.000

 O/F=     3.99000  %FUEL= 20.040080  R,EQ.RATIO= 0.999815  PHI,EQ.RATIO= 0.999815

 THERMODYNAMIC PROPERTIES

 P, BAR              70.000    40.000    1.0000
 T, K              3705.42   3633.49   3189.94
 RHO, KG/CU M   5.2470 0   3.0371 0  8.3068-2
 H, KJ/KG         -1079.85  -1079.85  -1079.85
 U, KJ/KG         -2413.95  -2396.88  -2283.69
 G, KJ/KG         -44529.3  -44420.3  -43484.7
 S, KJ/(KG)(K)     11.7259   11.9281   13.2933

 M, (1/n)            23.093    22.938    22.032
 (dLV/dLP)t       -1.03234  -1.03309  -1.03637
 (dLV/dLT)p         1.5783    1.6034    1.7534
 Cp, KJ/(KG)(K)     5.9630    6.2240    8.1054
 GAMMAs             1.1339    1.1320    1.1195
 SON VEL,M/SEC      1229.9    1221.0    1160.9

 MOLE FRACTIONS

 *CO              1.5243-1 1.5738-1 1.8220-1
 *CO2             1.3605-1 1.2917-1 9.3024-2
 *H2              6.0244-2 6.4737-2 9.6850-2
 H2O              4.6048-1 4.4995-1 3.8417-1
```

```
*OH                 1.1248-1  1.1680-1  1.3885-1
*O2                 7.8323-2  8.1962-2  1.0491-1

 * THERMODYNAMIC PROPERTIES FITTED TO 20000.K
```

E

Chemkin chemical kinetics schemes

This appendix contains printouts of the chemical kinetics schemes used in this work in Chemkin format. Chemkin is a Fortran chemical kinetics package for the analysis of gas-phase chemical kinetics which was developed at Sandia National Labs [22]. Chemkin is not directly used by itself in this work but the input format for Chemkin has become a loosely defined standard for specifying chemical kinetics schemes, often referred to as the Chemkin format. The listed Chemkin files in this chapter are thus computer readable version of the chemical kinetics schemes introduced in Section 4.6.2.

E.1. Westbrook Dryer 1 step

```
ELEMENTS
C H O N
END
SPECIE
CH4 O2 H2O CO2 N2
END
REACTIONS KCAL/MOLE MOLES
CH4 + 2O2 => CO2 + 2H2O 1.30E+8 0.0 48.40
FORD /CH4 -0.3/
FORD /O2 1.3/
END
```

E.2. Westbrook Dryer 2 step

```
ELEMENTS
C H O N
END
SPECIE
CH4 O2 CO H2O CO2 N2
END
REACTIONS KCAL/MOLE MOLES
CH4 + 1.5O2 => CO + 2H2O 2.80E+09 0.0 48.4
FORD /CH4 -0.3/
FORD /O2 1.3/
CO2 => CO + 0.5O2 5.00E+08 0.0 40
FORD /CO2 1.0 /
CO + H2O + 0.5O2 => CO2 + H2O 3.98E+14 0.0 40
FORD /CO 1.0 /
FORD /H2O 0.5 /
FORD /O2 0.25/
END
```

E.3. Jones Lindstedt 4 step

```
ELEMENTS
C H O N
END
SPECIE
CH4 O2 CO H2O CO2 H2 N2
END
REACTIONS KJOULES/MOLE MOLES
CH4 + 0.5O2 => CO + 2H2 0.44E+12 0.0 30E+3
FORD /CH4 0.5/
FORD /O2 1.25/
CH4 + H2O => CO + 3H2 0.3E+9 0.0 30E+3
FORD /CH4 1/
FORD /H2O 1/
H2 + 0.5O2 => H2O 0.25E+17 -1.0 40E+3
FORD /H2 0.5/
FORD /O2 2.25/
FORD /H2O -1.0/
CO + H2O => CO2 + H2 0.275E+10 0 20E+3
FORD /CO 1.0/
FORD /H2O 1.0/
END
```

F

Thermal power calculations

This appendix contains the detailed intermediate and final results of the calculations of the igniter thermal power based on the model outputs. The cases themselves are presented in Section 5.4 while the results of these calculations are discussed in Section 7.3.1. The methodology behind calculating the thermal power is presented in Section 3.4.

Species	**Mass flow** [kgs^{-1}]	**Molar mass** [gmol^{-1}]	H_i [kJmol^{-1}]	H_ref [kJmol^{-1}]	ΔH [kJkg^{-1}]	**Power** [kJs^{-1}]
CH4	$4.29{\cdot}10^{-5}$	16.04	308.464	26.4984	$1.76{\cdot}10^{4}$	$7.54{\cdot}10^{2}$
H2O	$1.77{\cdot}10^{-3}$	18.02	174.378	19.1032	$8.62{\cdot}10^{3}$	$1.52{\cdot}10^{4}$
CO2	$2.16{\cdot}10^{-3}$	44.01	205.583	24.2716	$4.12{\cdot}10^{3}$	$8.90{\cdot}10^{3}$
O2	$3.78{\cdot}10^{-9}$	32.00	132.122	16.792	$3.60{\cdot}10^{3}$	$1.36{\cdot}10^{-2}$
N2	$9.17{\cdot}10^{-5}$	28.01	124.058	15.9376	$3.86{\cdot}10^{3}$	$3.54{\cdot}10^{2}$
Total	$4.06{\cdot}10^{-3}$					$2.53{\cdot}10^{4}$
Igniter total	$1.63e{\cdot}10^{-2}$					$1.01{\cdot}10^{5}$
Fraction of design						80.16%

Table F.1: EDC WD 1 Step predicted exhaust flow composition and resulting heating power.

Species	**Mass flow** [kgs^{-1}]	**Molar mass** [gmol^{-1}]	H_i [kJmol^{-1}]	H_ref [kJmol^{-1}]	ΔH [kJkg^{-1}]	**Power** [kJs^{-1}]
CH4	$1.05{\cdot}10^{-4}$	16.04	307.32	26.4984	$1.75{\cdot}10^{4}$	$1.84{\cdot}10^{3}$
CO	$1.48{\cdot}10^{-5}$	28.01	124.61	16.0816	$3.87{\cdot}10^{3}$	$5.74{\cdot}10^{1}$
H2O	$1.77{\cdot}10^{-3}$	18.02	173.74	19.1032	$8.58{\cdot}10^{3}$	$1.51{\cdot}10^{4}$
CO2	$2.17{\cdot}10^{-3}$	44.01	204.89	24.2716	$4.10{\cdot}10^{3}$	$8.89{\cdot}10^{3}$
O2	$9.77{\cdot}10^{-7}$	32.00	131.66	16.792	$3.59{\cdot}10^{3}$	3.51
N2	$9.12{\cdot}10^{-6}$	28.01	123.64	15.9376	$3.85{\cdot}10^{3}$	$3.51{\cdot}10^{1}$
Total	$4.06{\cdot}10^{-3}$					$2.60{\cdot}10^{4}$
Igniter total	$1.62e{\cdot}10^{-2}$					$1.04{\cdot}10^{5}$
Fraction of design						82.45%

Table F.2: EDC WD 2 Step predicted exhaust flow composition and resulting heating power.

Species	**Mass flow** [kgs^{-1}]	**Molar mass** [$gmol^{-1}$]	H_i [$kJmol^{-1}$]	H_ref [$kJmol^{-1}$]	ΔH [$kJkg^{-1}$]	**Power** [kJs^{-1}]
CH4	$9.97{\cdot}10^{-7}$	16.04	268.462	26.4984	$1.51{\cdot}10^{4}$	$1.50{\cdot}10^{1}$
H2O	$1.83{\cdot}10^{-3}$	18.02	152.235	19.1032	$7.39{\cdot}10^{3}$	$1.35{\cdot}10^{4}$
CO2	$2.23{\cdot}10^{-3}$	44.01	181.328	24.2716	$3.57{\cdot}10^{3}$	$7.95{\cdot}10^{3}$
O2	$2.89{\cdot}10^{-7}$	3.002	116.437	16.792	$3.11{\cdot}10^{3}$	$8.99{\cdot}10^{-1}$
N2	$6.61{\cdot}10^{11}$	28.01	109.746	15.9376	$3.35{\cdot}10^{3}$	$2.21{\cdot}10^{-4}$
Total	$4.05{\cdot}10^{-3}$					$2.15{\cdot}10^{4}$
Igniter total	$1.62e{\cdot}10^{-2}$					$8.48{\cdot}10^{4}$
Fraction of design						68.10%

Table F.3: EDM Ambient predicted exhaust flow composition and resulting heating power.

Species	**Mass flow** [kgs^{-1}]	**Molar mass** [$gmol^{-1}$]	H_i [$kJmol^{-1}$]	H_ref [$kJmol^{-1}$]	ΔH [$kJkg^{-1}$]	**Power** [Js^{-1}]
CH4	$3.04{\cdot}10^{-8}$	16.04	306.384	26.4984	$1.74{\cdot}10^{4}$	$5.30{\cdot}10^{-1}$
H2O	$1.83{\cdot}10^{-3}$	18.02	173.218	19.1032	$8.55{\cdot}10^{3}$	$1.57{\cdot}10^{4}$
CO2	$2.24{\cdot}10^{-3}$	44.01	204.323	24.2716	$4.09{\cdot}10^{3}$	$9.16{\cdot}10^{3}$
O2	$7.39{\cdot}10^{-6}$	32.00	131.282	16.792	$3.58{\cdot}10^{3}$	$2.64{\cdot}10^{1}$
N2	$2.88{\cdot}10^{-6}$	28.01	123.298	15.9376	$3.83{\cdot}10^{3}$	$1.11{\cdot}10^{1}$
Total	$4.05{\cdot}10^{-3}$					$2.49{\cdot}10^{4}$
Igniter total	$1.62e{\cdot}10^{-2}$					$9.95{\cdot}10^{4}$
Fraction of design						78.95%

Table F.4: EDM Pressure predicted exhaust flow composition and resulting heating power.

Species	**Mass flow** [kgs^{-1}]	**Molar mass** [$gmol^{-1}$]	H_i [$kJmol^{-1}$]	H_ref [$kJmol^{-1}$]	ΔH [$kJkg^{-1}$]	**Power** [kJs^{-1}]
CH4	$4.08{\cdot}10^{-4}$	16.04	105	26.4984	$4.89{\cdot}10^{3}$	$1.99{\cdot}10^{3}$
CO	$2.47{\cdot}10^{-6}$	28.01	49.53	16.0816	$1.19{\cdot}10^{3}$	$2.94{\cdot}10^{0}$
CO2	$9.89{\cdot}10^{-4}$	44.01	79.44	24.2716	$1.25{\cdot}10^{3}$	$1.24{\cdot}10^{3}$
H2O	$8.03{\cdot}10^{-4}$	18.02	62.69	19.1032	$2.42{\cdot}10^{3}$	$1.94{\cdot}10^{3}$
O2	$1.81{\cdot}10^{-3}$	32.00	51.67	16.792	$1.09{\cdot}10^{3}$	$1.97{\cdot}10^{3}$
OH	$1.80{\cdot}10^{-5}$	17.01	46.9	15.7228	$1.83{\cdot}10^{3}$	$3.31{\cdot}10^{1}$
Total	$4.03{\cdot}10^{-3}$					$7.18{\cdot}10^{3}$
Igniter total	$1.61e{\cdot}10^{-2}$					$2.87{\cdot}10^{4}$
Fraction of design						22.79%

Table F.5: Equilibrium Ambient predicted exhaust flow composition and resulting heating power. Only significant species (massflow > $1{\cdot}10^{-6}$ kg/s) are included.

Species	**Mass flow** [kgs^{-1}]	**Molar mass** [gmol^{-1}]	H_i [kJmol^{-1}]	H_ref [kJmol^{-1}]	ΔH [kJkg^{-1}]	**Power** [kJs^{-1}]
CH4	$4.10{\cdot}10^{-4}$	16.04	116.268	26.4984	$5.60{\cdot}10^{3}$	$2.29{\cdot}10^{3}$
CO	$6.87{\cdot}10^{-6}$	28.01	53.9164	16.0816	$1.35{\cdot}10^{3}$	$9.28{\cdot}10^{0}$
CO2	$9.89{\cdot}10^{-4}$	44.01	86.7444	24.2716	$1.42{\cdot}10^{3}$	$1.40{\cdot}10^{3}$
H2O	$7.99{\cdot}10^{-4}$	18.02	68.8198	19.1032	$2.76{\cdot}10^{3}$	$2.20{\cdot}10^{3}$
O2	$1.81{\cdot}10^{-3}$	32.00	56.2372	16.792	$1.23{\cdot}10^{3}$	$2.23{\cdot}10^{3}$
OH	$3.33{\cdot}10^{-5}$	17.01	51.079	15.7228	$2.08{\cdot}10^{3}$	$6.91{\cdot}10^{1}$
Total	$4.05{\cdot}10^{-3}$					$8.21{\cdot}10^{3}$
Igniter total	$1.62e{\cdot}10^{-2}$					$3.28{\cdot}10^{4}$
Fraction of design						26.07%

Table F.6: Equilibrium Pressure predicted exhaust flow composition and resulting heating power. Only significant species (massflow > $1{\cdot}10^{-6}$ kg/s) are included.

Species	**Mass flow** [kgs^{-1}]	**Molar mass** [gmol^{-1}]	H_i [kJmol^{-1}]	H_ref [kJmol^{-1}]	ΔH [kJkg^{-1}]	**Power** [kJs^{-1}]
CH4	$3.88{\cdot}10^{-4}$	16.04	105	26.4984	$4.89{\cdot}10^{3}$	$1.90{\cdot}10^{3}$
CO	$3.83{\cdot}10^{-6}$	28.01	49.53	16.0816	$1.19{\cdot}10^{3}$	$4.57{\cdot}10^{0}$
CO2	$9.96{\cdot}10^{-4}$	44.01	79.44	24.2716	$1.25{\cdot}10^{3}$	$1.25{\cdot}10^{3}$
H2O	$8.07{\cdot}10^{-4}$	18.02	62.69	19.1032	$2.42{\cdot}10^{3}$	$1.95{\cdot}10^{3}$
O2	$1.82{\cdot}10^{-3}$	32.00	51.67	16.792	$1.09{\cdot}10^{3}$	$1.98{\cdot}10^{3}$
OH	$2.31{\cdot}10^{-5}$	17.01	46.9	15.7228	$1.83{\cdot}10^{3}$	$4.23{\cdot}10^{1}$
Total	$4.04{\cdot}10^{-3}$					$7.13{\cdot}10^{3}$
Igniter total	$1.62e{\cdot}10^{-2}$					$2.85{\cdot}10^{4}$
Fraction of design						22.62%

Table F.7: Equilibrium Ambient Hot Walls predicted exhaust flow composition and resulting heating power. Only significant species (massflow > $1{\cdot}10^{-6}$ kg/s) are included.

Species	**Mass flow** [kgs^{-1}]	**Molar mass** [gmol^{-1}]	H_i [kJmol^{-1}]	H_ref [kJmol^{-1}]	ΔH [kJkg^{-1}]	**Power** [kJs^{-1}]
CH4	$0.00{\cdot}10^{0}$	16.04	279.483	26.4984	$1.58{\cdot}10^{4}$	$0.00{\cdot}10^{0}$
H2O	$1.71{\cdot}10^{-3}$	18.02	158.277	19.1032	$7.72{\cdot}10^{3}$	$1.32{\cdot}10^{4}$
CO2	$2.09{\cdot}10^{-3}$	44.01	187.943	24.2716	$3.72{\cdot}10^{3}$	$7.77{\cdot}10^{3}$
O2	$2.34{\cdot}10^{-4}$	32.00	120.64	16.792	$3.25{\cdot}10^{3}$	$7.59{\cdot}10^{2}$
N2	$3.35{\cdot}10^{-5}$	28.01	113.557	15.9376	$3.49{\cdot}10^{3}$	$1.17{\cdot}10^{2}$
Total	$4.07{\cdot}10^{-3}$					$2.19{\cdot}10^{4}$
Igniter total	$1.63e{\cdot}10^{-2}$					$8.74{\cdot}10^{4}$
Fraction of design						69.37%

Table F.8: Finite Rate 1 step Start predicted exhaust flow composition and resulting heating power.

Species	**Mass flow** [kgs^{-1}]	**Molar mass** [gmol^{-1}]	H_i [kJmol^{-1}]	H_ref [kJmol^{-1}]	ΔH [kJkg^{-1}]	**Power** [kJs^{-1}]
CH4	$0.00 \cdot 10^{0}$	16.04	310.96	26.4984	$1.77 \cdot 10^{4}$	$0.00 \cdot 10^{0}$
H2O	$1.75 \cdot 10^{-3}$	18.02	175.77	19.1032	$8.69 \cdot 10^{3}$	$1.52 \cdot 10^{4}$
CO2	$2.13 \cdot 10^{-3}$	44.01	207.095	24.2716	$4.15 \cdot 10^{3}$	$8.86 \cdot 10^{3}$
O2	$1.60 \cdot 10^{-4}$	32.00	140.605	16.792	$3.87 \cdot 10^{3}$	$6.18 \cdot 10^{2}$
N2	$7.44 \cdot 10^{-6}$	28.01	124.97	15.9376	$3.89 \cdot 10^{3}$	$2.90 \cdot 10^{1}$
Total	$4.05 \cdot 10^{-3}$					$2.47 \cdot 10^{4}$
Igniter total	$1.62e \cdot 10^{-2}$					$9.88 \cdot 10^{4}$
Fraction of design						78.41%

Table F.9: Finite Rate 1 step Pressure predicted exhaust flow composition and resulting heating power.

G

Cold flow verification code

This appendix contains a printout of the Python code used to calculate the cold flow through the igniter at ambient exhaust conditions. The backing theory and use of this code is documented in Section 6.2.2.

```
# -*- coding: utf-8 -*-
"""
Created on Wed Jul 12 21:41:27 2017

@author: Christ Akkermans

Numerical simulation of cold flow using using ideal rocketry
equations and inflow.
"""

from numpy import *
from heat import *
import matplotlib.pyplot as plt

m_dot_fuel = 3.259e-3;
m_dot_ox = 1.299e-2;
Cp_fuel = 33.51; # At 200 K, 1bar, source NIST
Cp_ox = 29.11; #  At 200 K, 1bar, source NIST

M_fuel = 16.0425; # Molar mass fuel
M_ox = 31.9988; # Molar mass oxidizer
Ra = 8.314462175; # Universal gas constant

# Calculate mixture properties using mixing laws.
n_fuel = m_dot_fuel / M_fuel * 1000;
n_ox = m_dot_ox / M_ox * 1000;
M = (n_fuel * M_fuel + n_ox * M_ox) / (n_fuel + n_ox);
Cp = (n_fuel * Cp_fuel + n_ox * Cp_ox) / (n_fuel + n_ox);
m_dot_in = m_dot_fuel + m_dot_ox;

# Calculate gas properties.
R = Ra / (M * 1e-3);
Cv = Cp - Ra;
gamma = Cp / Cv;

# Calculate constants
```

```
c1 = (2 * gamma) / (gamma - 1);
c2 = 2 / gamma;
c3 = (gamma - 1) / gamma;

# Calculate fixed chamber volume
Vc = pi * pow(5e-3, 2) * 40e-3;
Vc += 1./3. * pi * pow(15e-3, 2) * 20e-3;
h_cone = 15e-3 / (10e-3 / 17.1e-3);
Vc += 1./3. * pi * (pow(5e-3, 2) + 5e-3 * 15e-3 + pow(15e-3, 2)) * h_cone;

At = 7.266e-06; # Throat area m^2
e = 1.1; # Nozzle expansion ratio

# Setup variable storage
dt = 0.0005; # Time step size s
t = arange(0, 0.1, dt);
m = empty(t.size + 1);
rho = empty(t.size);
p = empty(t.size);
pe = empty(t.size);

Tc = 200.; # Chamber temperature
Gamma = 0.6796; # vd Kerckhoven constant. Obtained from Zandbergen reader

# Initial values
p[0] = 1.01e5;
rho[0] = p[0] / (R * Tc);
m[0] = Vc * rho[0];

# Numerically approximate the current exhaust pressure from the nozzle
# area ratio. Initial guess of pressure ratio is 0.02.
np = 0.02;
while True:

    # Calculate current area ratio f. Check if we have converged.
    f = Gamma * pow((c1 * pow(np, c2) * (1. - pow(np, c3))), -0.5) - e;
    if abs(f) < 1e-7:
        break;

    df = -0.5 * Gamma * pow(c1 * pow(np, c2) * (1 - pow(np, c3)), -1.5) \
        * (c1 * c2 * pow(np, (c2 - 1)) * (1 - pow(np, c3)) \
        + c1 * pow(np, c2) * ( -c3 * pow(np, (c3 - 1))));

    # Update guess of pressure ratio. Ensure that we don't go to negative
    # values.
    np = np - f / df;
    if np < 0:
        np = 1e-5;

# Time step for the given number of steps.
for i in arange(0, t.size):

    # Calculate current chamber pressure and density.
    rho[i] = m[i] / Vc;
    p[i] = rho[i] * R * Tc;
    pe[i] = np * p[i];
```

```
    # Choked nozzle outflow.
    m_dot_out = p[i] * At * Gamma / sqrt(Tc * R);

    # Step forward in time.
    m[i + 1] = m[i] + (m_dot_in - m_dot_out) * dt;


# Plot the results.
fig = plt.figure();
plt.plot(t, p, 'darkblue');
plt.plot(t, pe, 'red');
```

H

CFD Results

This appendix contains the reported CFD results. Results are presented per case and contain a number of plots depending on the applicability of types of plots per case. Some types of plots require extra attention:

Absolute pressure contour Absolute pressure in this sense refers to the absolute static pressure. It is common in aerodynamics to define the absolute pressure as the sum of the static and dynamic pressure. Absolute static pressure refers to the static pressure as measured from the absolute zero. ANSYS Fluent internally works with relative pressures.

Temperature development Development of mass averaged temperature in the igniter flow as measured from the igniter chamber wall on the right.

Species development Development of the mass averaged species concentrations in the igniter flow as measured from the igniter chamber wall on the right.

The attentive reader will note that for some cases not the full residual or integral quantity history over all iterations is given. This is due to the functionality of saving plots of these values is found to be not completely reliable. Especially in cases where numerical instabilities necessitated restarting the simulations a few times the residual history is sometimes only partially available.

For some cases the results are omitted for brevity. The results of these cases are not considered of sufficient interest to include in the report as the plots of their results add little to no extra information. These cases are:

- Cold flow grid convergence study
- Eddy dissipation model (EDM) grid convergence study

H.1. ColdFlowStart

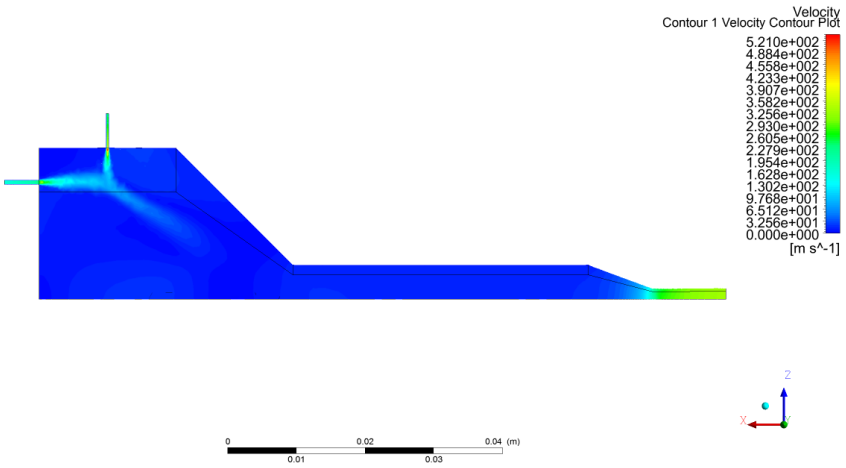

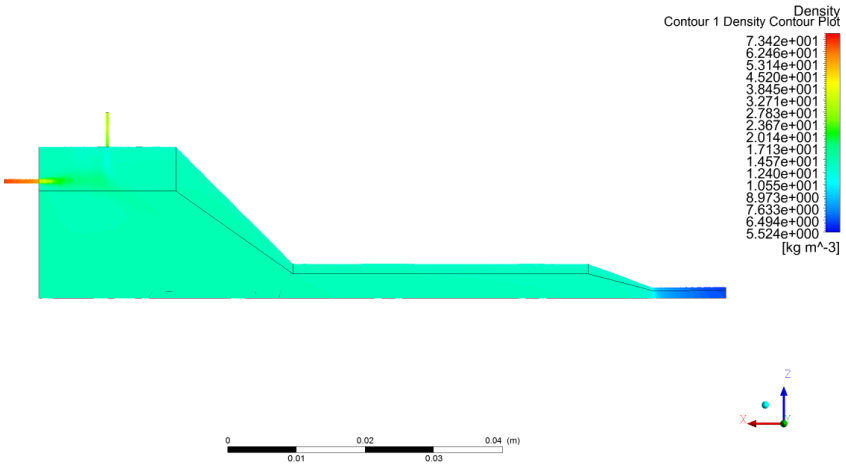

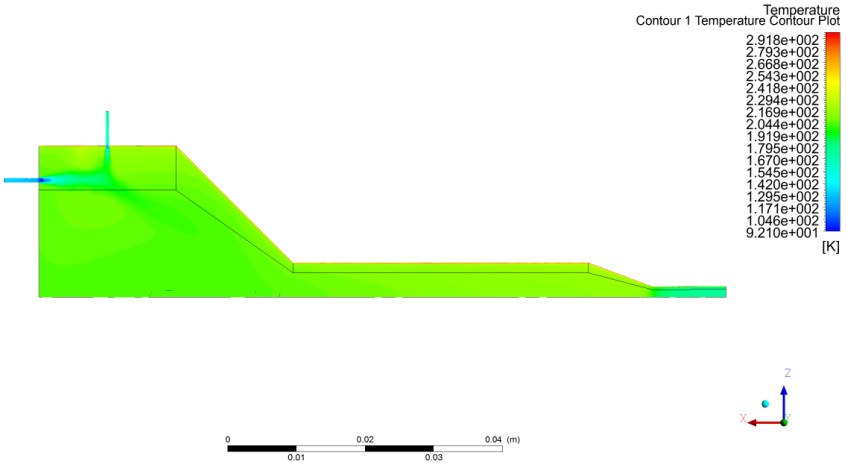

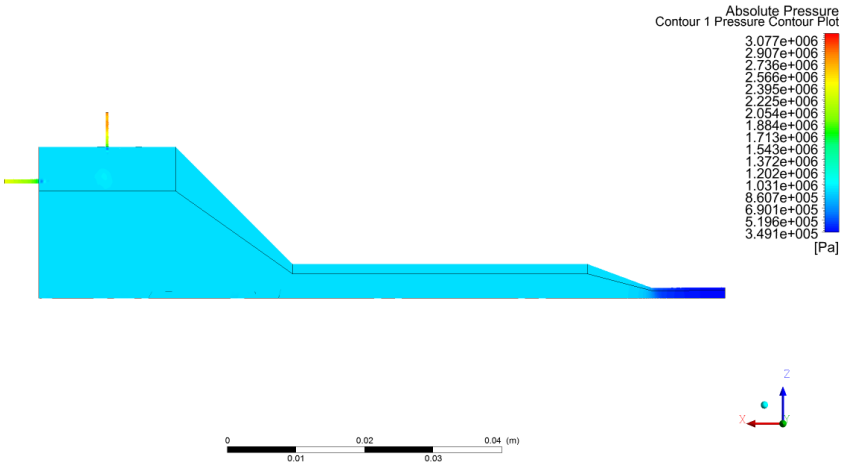
Absolute Pressure
Contour 1 Pressure Contour Plot
3.077e+006
2.907e+006
2.736e+006
2.566e+006
2.395e+006
2.225e+006
2.054e+006
1.884e+006
1.713e+006
1.543e+006
1.372e+006
1.202e+006
1.031e+006
8.607e+005
6.901e+005
5.196e+005
3.491e+005
[Pa]
Z
X
Y
0
0.02
0.04 (m)
0.01
0.03

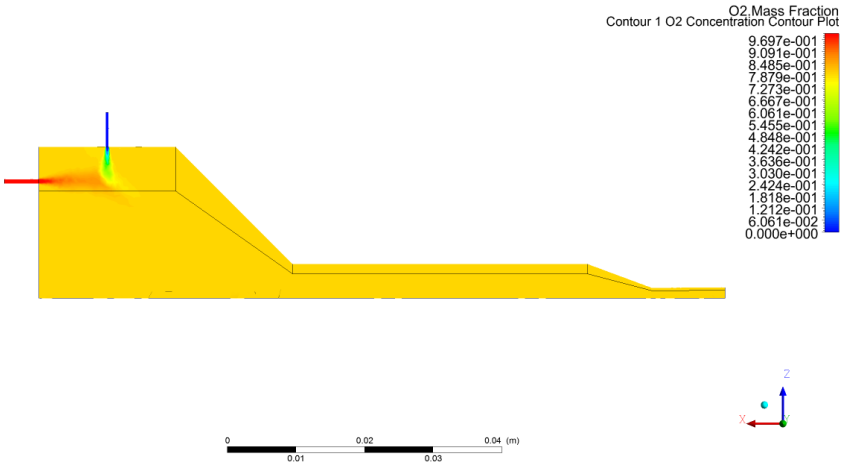
O2,Mass Fraction
Contour 1 O2 Concentration Contour Plot
9.697e-001
9.091e-001
8.485e-001
7.879e-001
7.273e-001
6.667e-001
6.061e-001
5.455e-001
4.848e-001
4.242e-001
3.636e-001
3.030e-001
2.424e-001
1.818e-001
1.212e-001
6.061e-002
0.000e+000
Z
X
Y
0
0.02
0.04 (m)
0.01
0.03

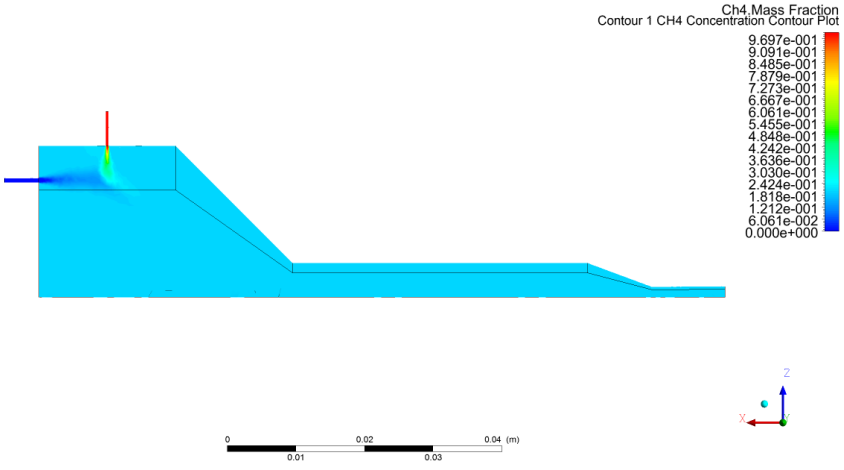
Ch4,Mass Fraction
Contour 1 CH4 Concentration Contour Plot
9.697e-001
9.091e-001
8.485e-001
7.879e-001
7.273e-001
6.667e-001
6.061e-001
5.455e-001
4.848e-001
4.242e-001
3.636e-001
3.030e-001
2.424e-001
1.818e-001
1.212e-001
6.061e-002
0.000e+000
Z
X
Y
0
0.02
0.04 (m)
0.01
0.03

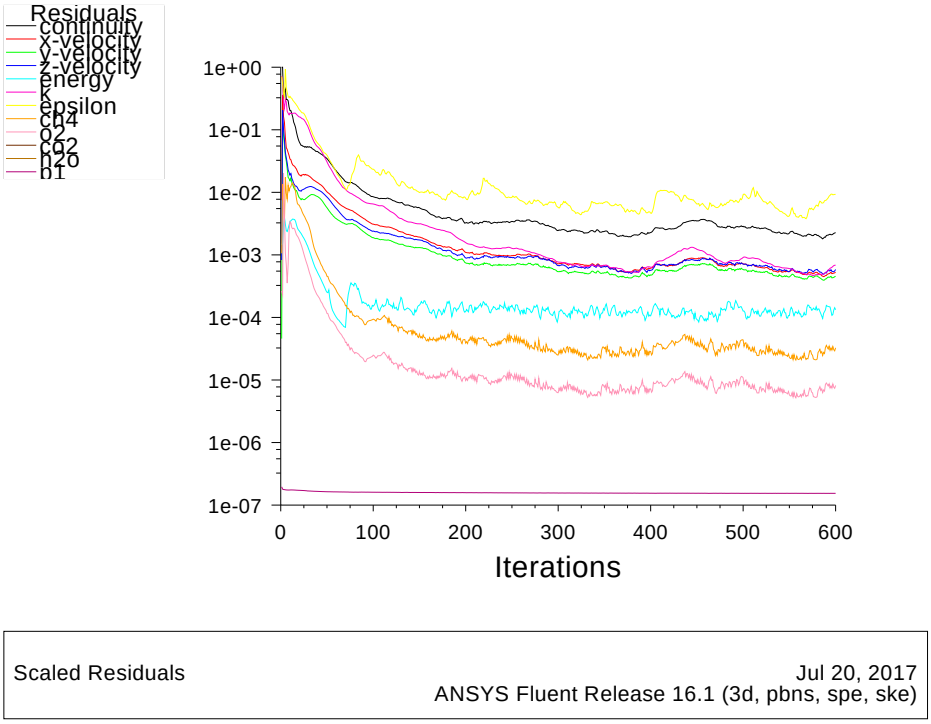

Figure H.1: Convergence history of scaled residuals for ColdFlowAmbient case.

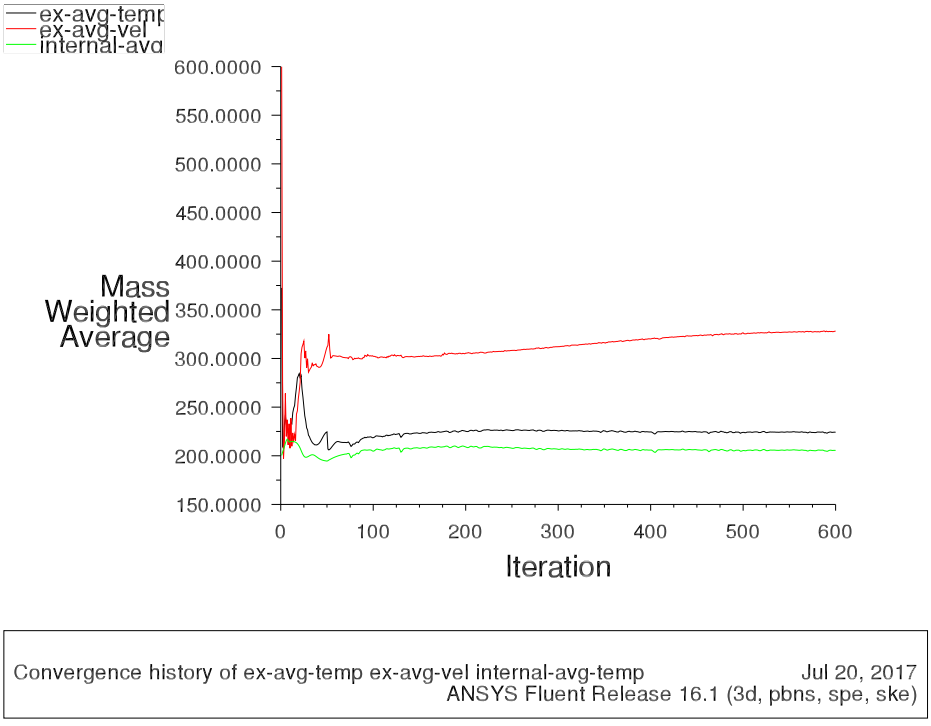

Figure H.2: Convergence history of integral quantities for ColdFlowAmbient case.

H.2. ColdFlowPressure

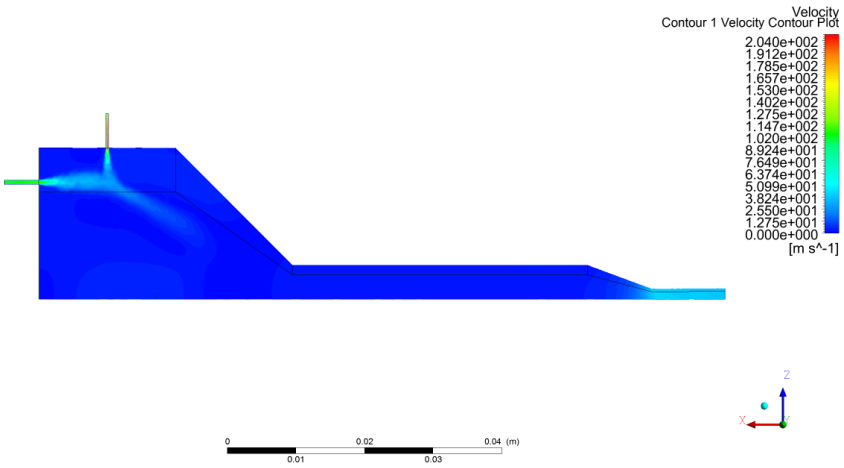

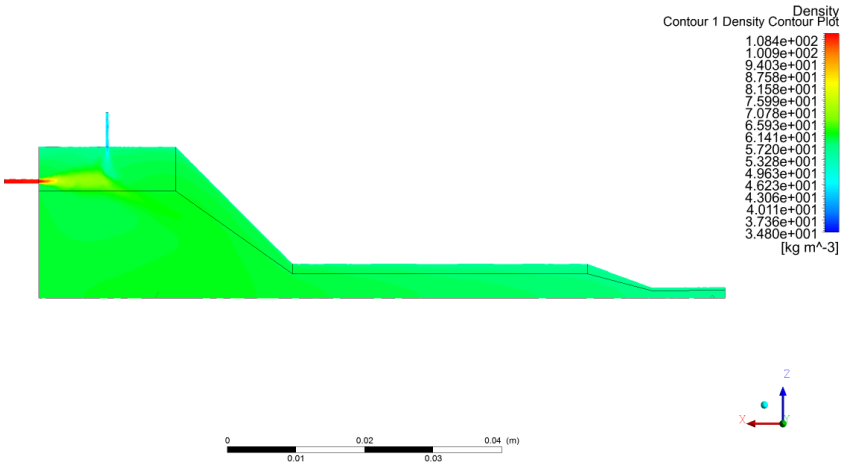

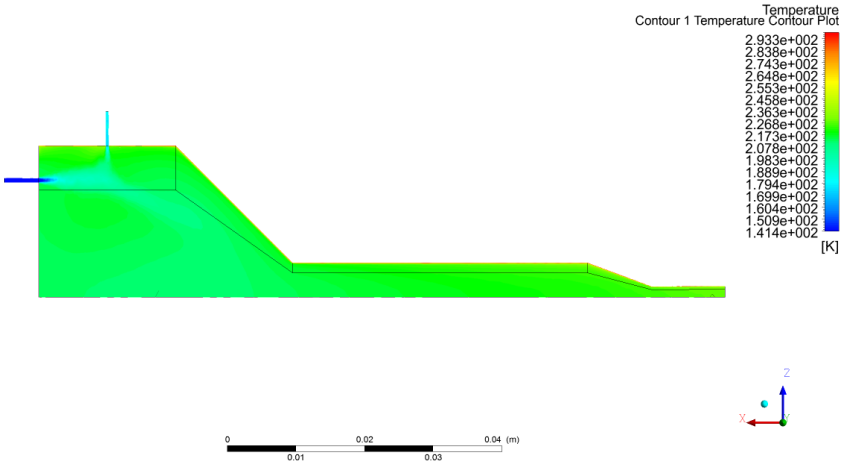

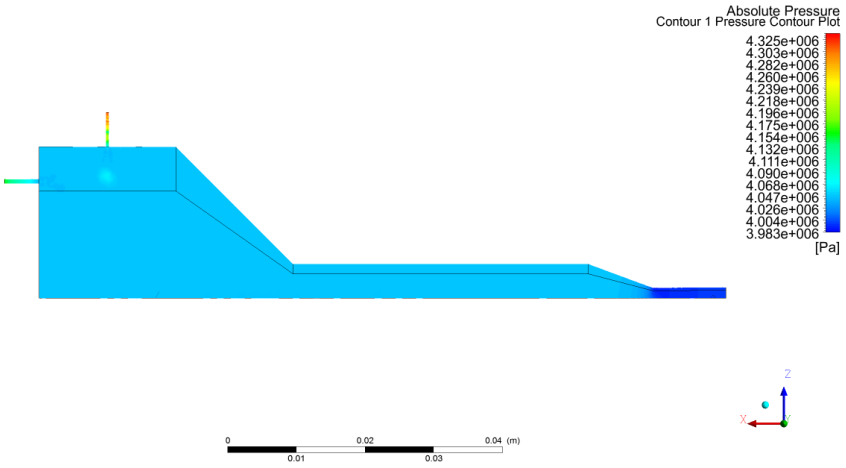
Absolute Pressure
Contour 1 Pressure Contour Plot
4.325e+006
4.303e+006
4.282e+006
4.260e+006
4.239e+006
4.218e+006
4.196e+006
4.175e+006
4.154e+006
4.132e+006
4.111e+006
4.090e+006
4.068e+006
4.047e+006
4.026e+006
4.004e+006
3.983e+006
[Pa]
Z
X
Y
0
0.02
0.04 (m)
0.01
0.03

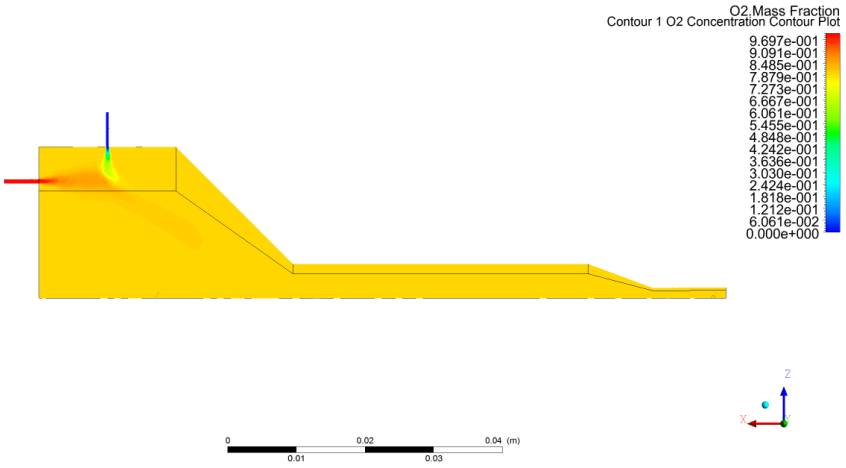
O2.Mass Fraction
Contour 1 O2 Concentration Contour Plot
9.697e-001
9.091e-001
8.485e-001
7.879e-001
7.273e-001
6.667e-001
6.061e-001
5.455e-001
4.848e-001
4.242e-001
3.636e-001
3.030e-001
2.424e-001
1.818e-001
1.212e-001
6.061e-002
0.000e+000
Z
X
Y
0
0.02
0.04 (m)
0.01
0.03

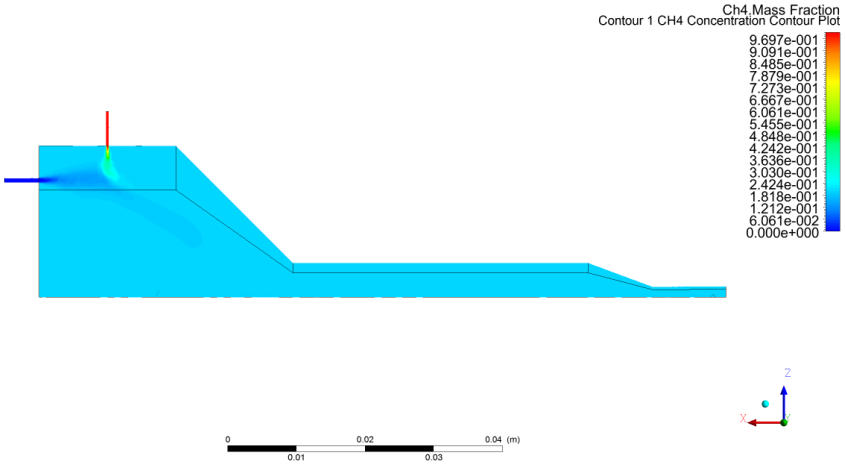
Ch4.Mass Fraction
Contour 1 CH4 Concentration Contour Plot
9.697e-001
9.091e-001
8.485e-001
7.879e-001
7.273e-001
6.667e-001
6.061e-001
5.455e-001
4.848e-001
4.242e-001
3.636e-001
3.030e-001
2.424e-001
1.818e-001
1.212e-001
6.061e-002
0.000e+000
Z
X
Y
0
0.02
0.04 (m)
0.01
0.03

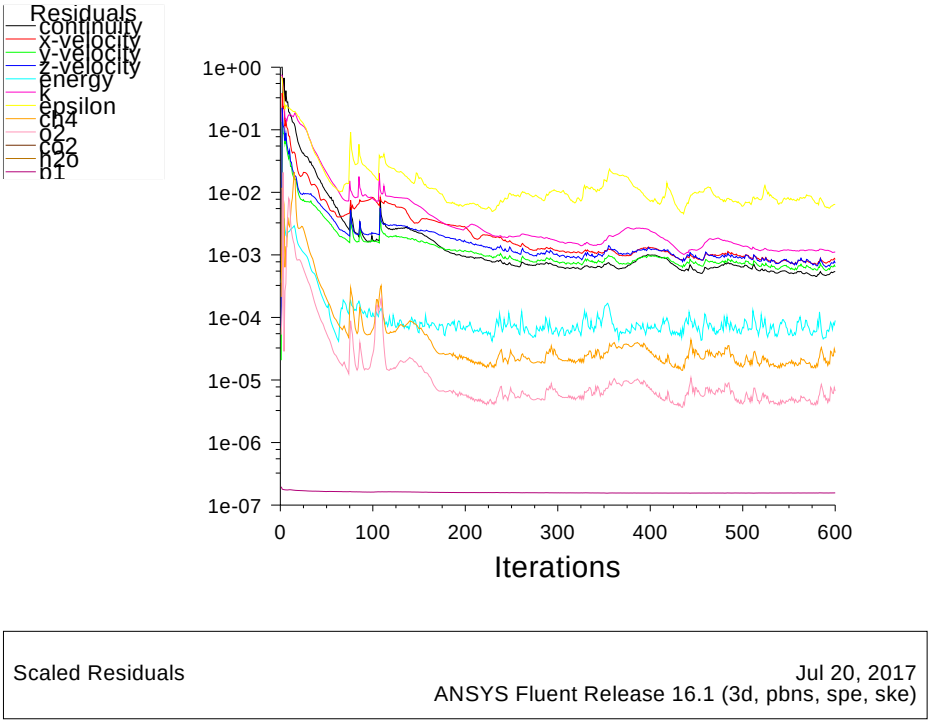

Figure H.3: Convergence history of scaled residuals for ColdFlowPressure case.

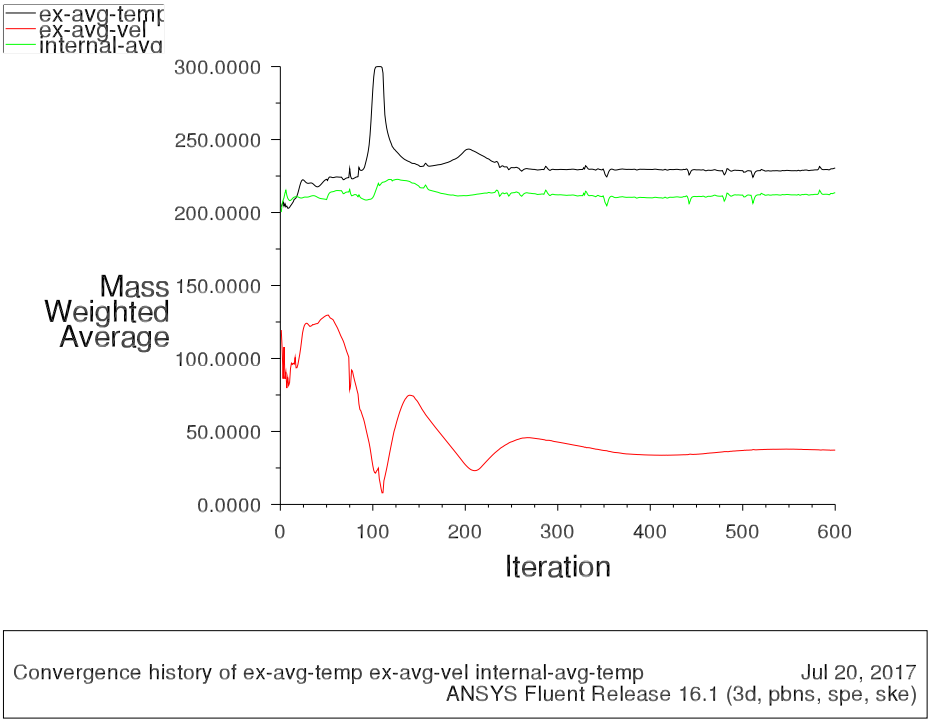

Figure H.4: Convergence history of integral quantities for ColdFlowPressure case.

H.3. FullColdFlowStart

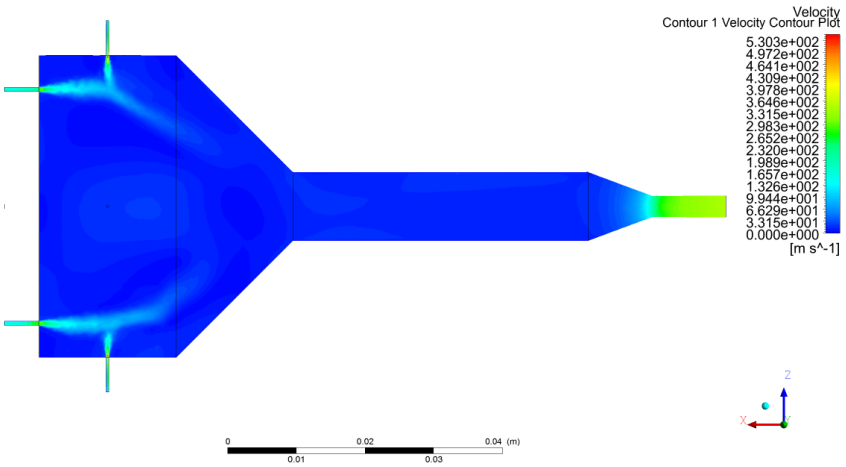

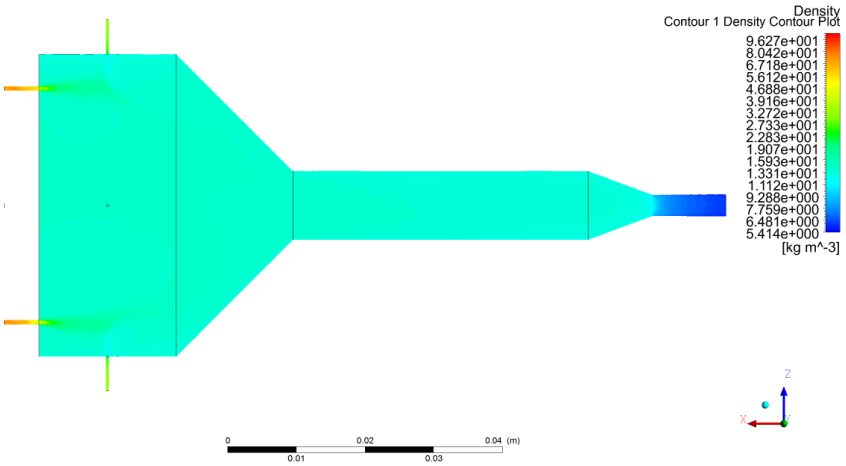

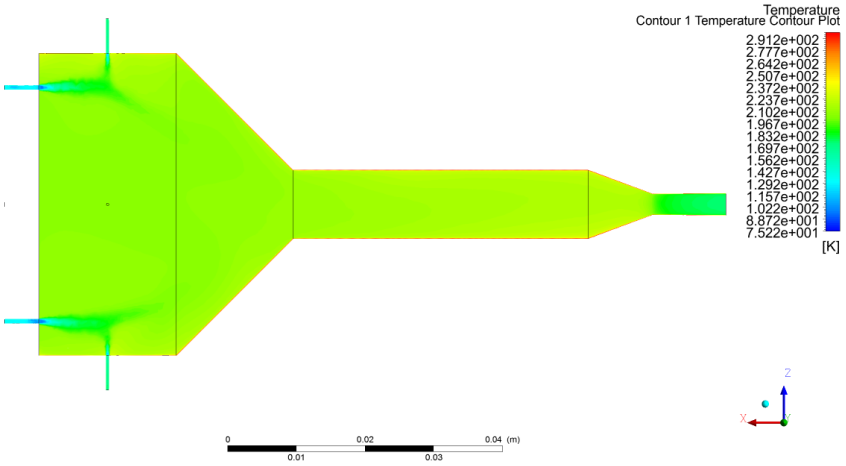

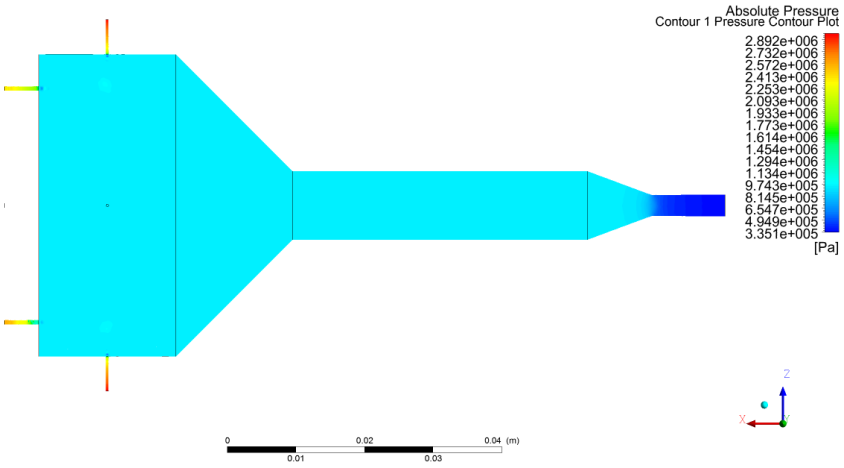
Absolute Pressure
Contour 1 Pressure Contour Plot
2.892e+006
2.732e+006
2.572e+006
2.413e+006
2.253e+006
2.093e+006
1.933e+006
1.773e+006
1.614e+006
1.454e+006
1.294e+006
1.134e+006
9.743e+005
8.145e+005
6.547e+005
4.949e+005
3.351e+005
[Pa]
0
0.02
0.04 (m)
0.01
0.03
Z
X
Y

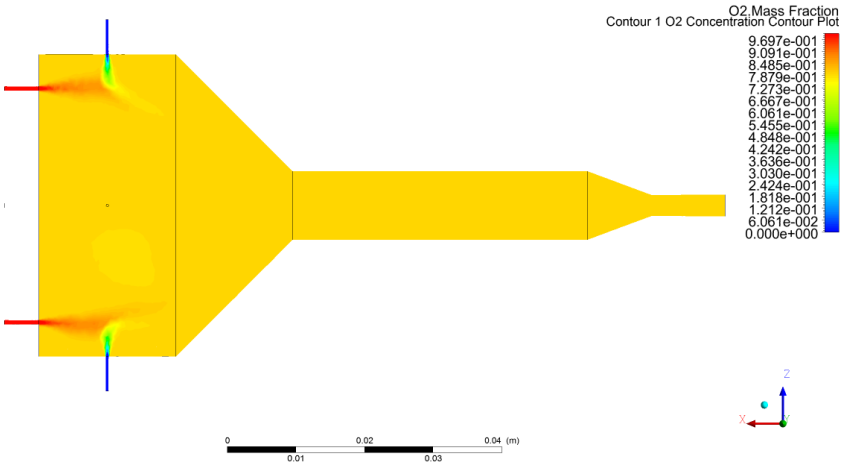
O2,Mass Fraction
Contour 1 O2 Concentration Contour Plot
9.697e-001
9.091e-001
8.485e-001
7.879e-001
7.273e-001
6.667e-001
6.061e-001
5.455e-001
4.848e-001
4.242e-001
3.636e-001
3.030e-001
2.424e-001
1.818e-001
1.212e-001
6.061e-002
0.000e+000
0
0.02
0.04 (m)
0.01
0.03
Z
X
Y

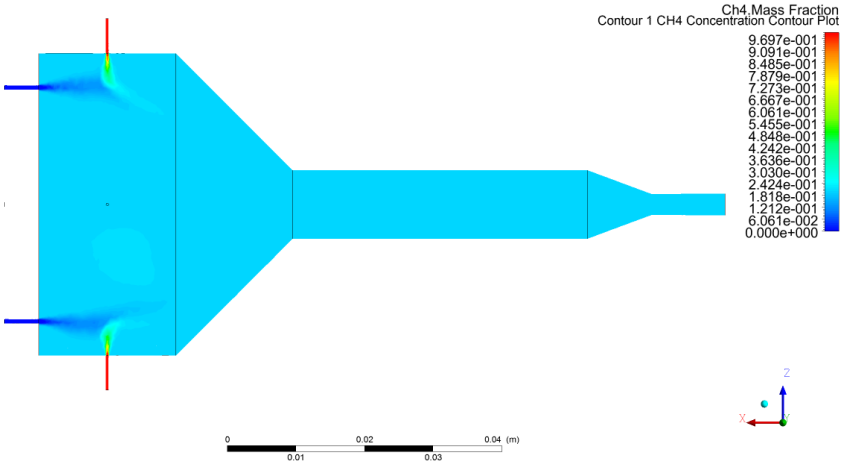
Ch4,Mass Fraction
Contour 1 CH4 Concentration Contour Plot
9.697e-001
9.091e-001
8.485e-001
7.879e-001
7.273e-001
6.667e-001
6.061e-001
5.455e-001
4.848e-001
4.242e-001
3.636e-001
3.030e-001
2.424e-001
1.818e-001
1.212e-001
6.061e-002
0.000e+000
0
0.02
0.04 (m)
0.01
0.03
Z
X
Y

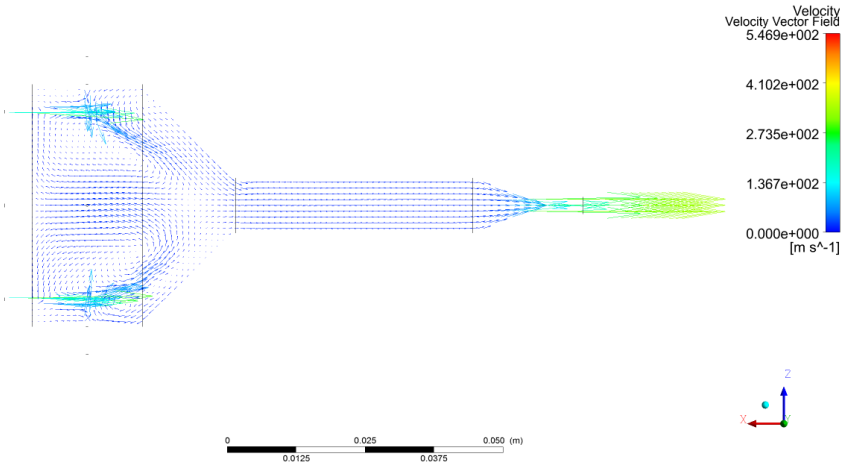
Velocity
Velocity Vector Field
5.469e+002
4.102e+002
2.735e+002
1.367e+002
0.000e+000
[m s^-1]
Z
X
Y
0
0.025
0.050 (m)
0.0125
0.0375

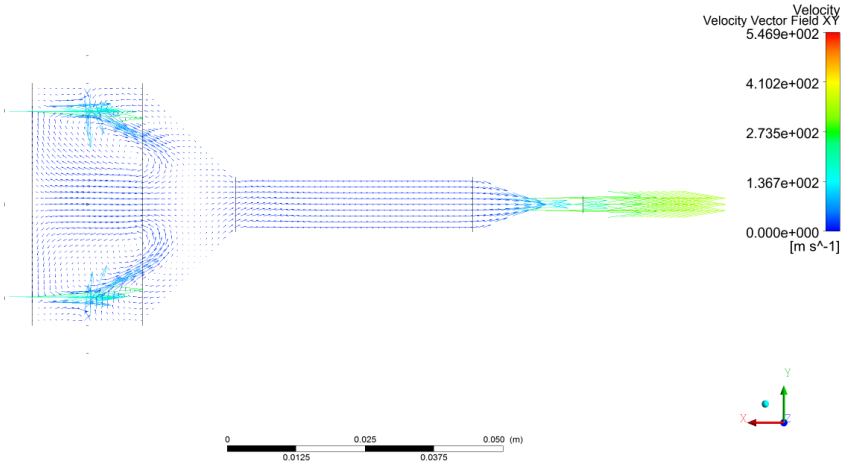
Velocity
Velocity Vector Field XY
5.469e+002
4.102e+002
2.735e+002
1.367e+002
0.000e+000
[m s^-1]
Y
X
0
0.025
0.050 (m)
0.0125
0.0375

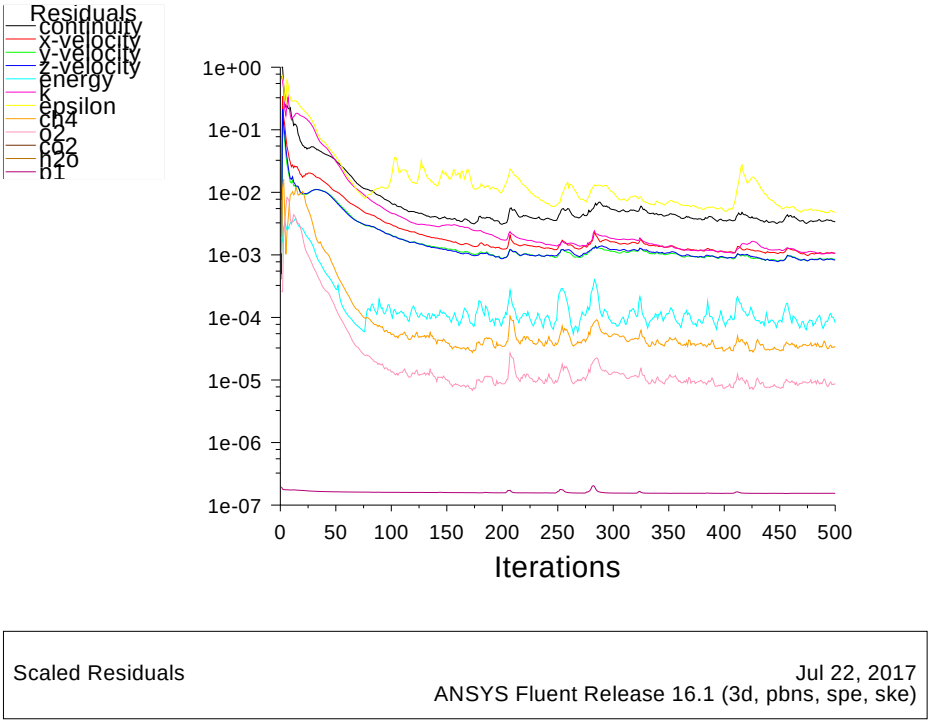

Figure H.5: Convergence history of scaled residuals for FullColdFlowStart case.

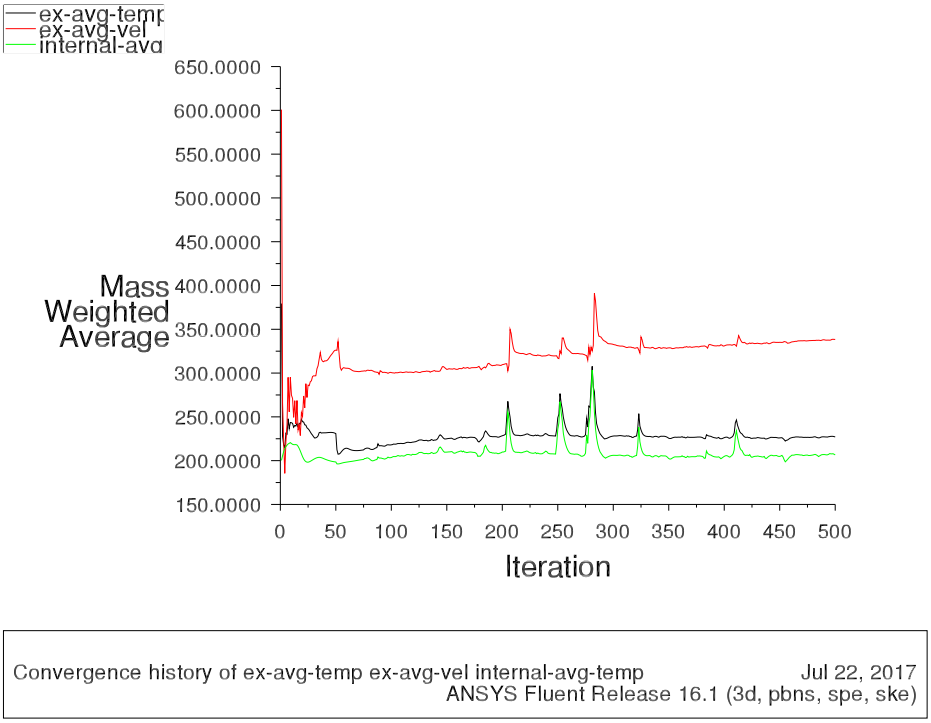

Figure H.6: Convergence history of integral quantities for FullColdFlowStart case.

H.4. InflowColdFlowMassStart

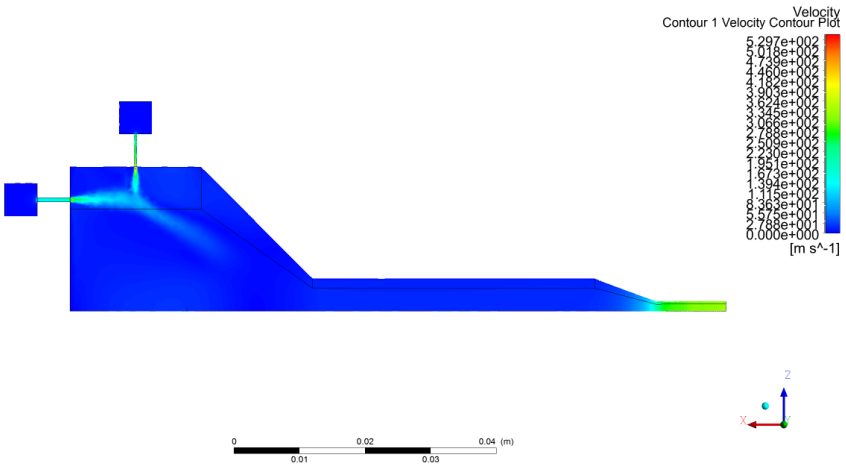

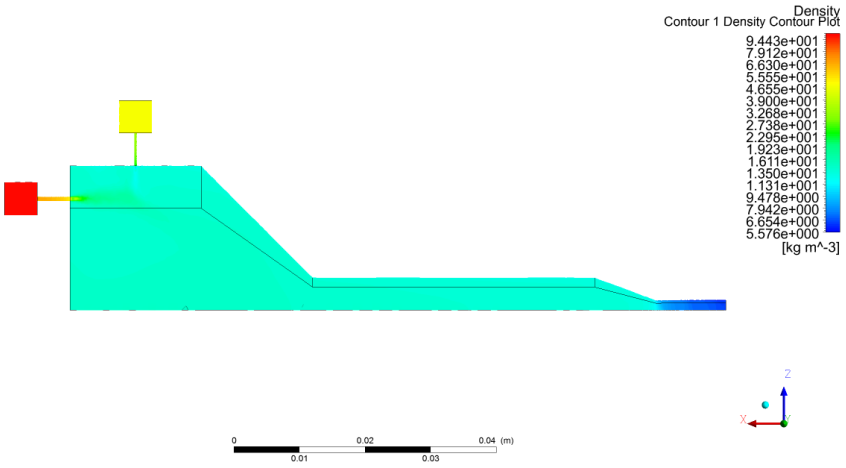

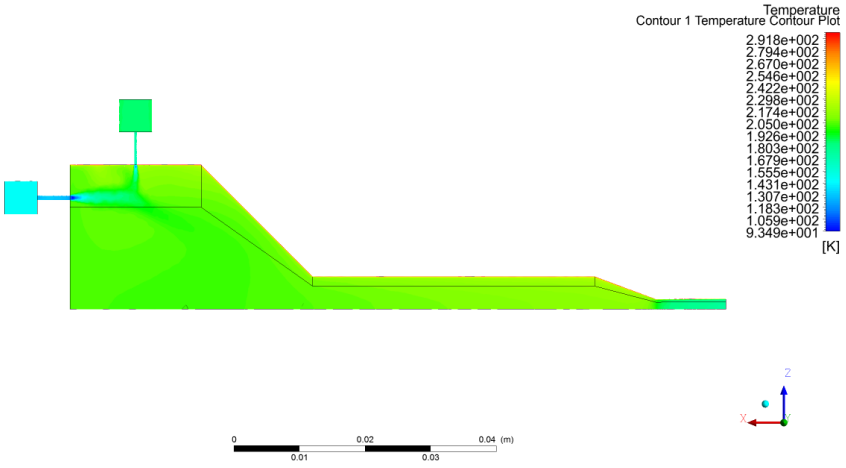

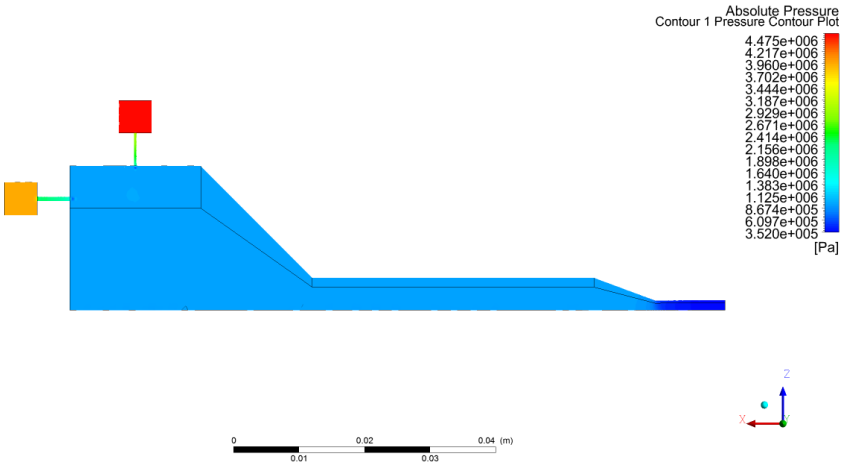
Absolute Pressure
Contour 1 Pressure Contour Plot
4.475e+006
4.217e+006
3.960e+006
3.702e+006
3.444e+006
3.187e+006
2.929e+006
2.671e+006
2.414e+006
2.156e+006
1.898e+006
1.640e+006
1.383e+006
1.125e+006
8.674e+005
6.097e+005
3.520e+005
[Pa]
0
0.02
0.04 (m)
0.01
0.03
Z
X
Y

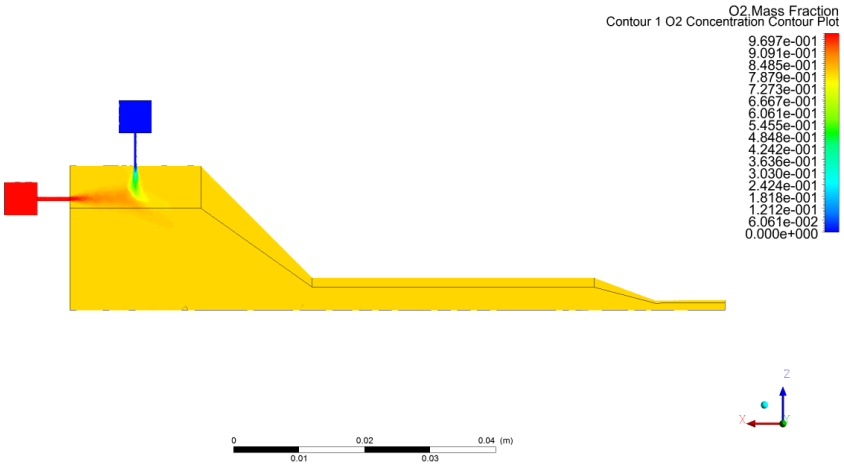
O2,Mass Fraction
Contour 1 O2 Concentration Contour Plot
9.697e-001
9.091e-001
8.485e-001
7.879e-001
7.273e-001
6.667e-001
6.061e-001
5.455e-001
4.848e-001
4.242e-001
3.636e-001
3.030e-001
2.424e-001
1.818e-001
1.212e-001
6.061e-002
0.000e+000
0
0.02
0.04 (m)
0.01
0.03
Z
X
Y

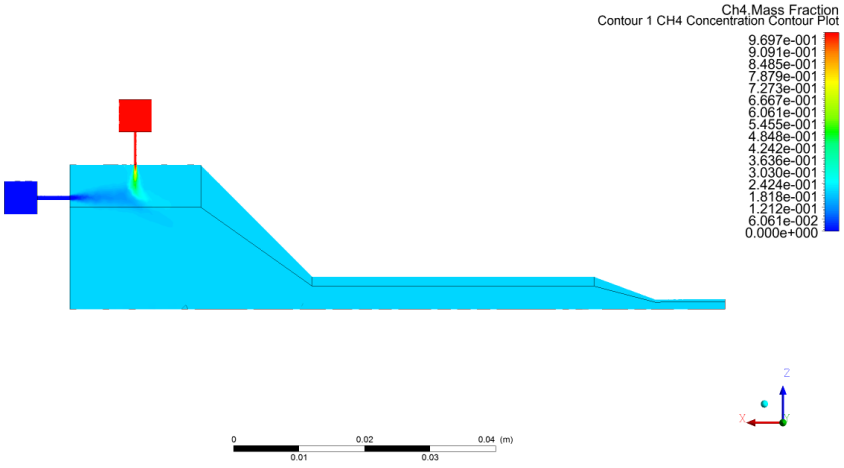
Ch4,Mass Fraction
Contour 1 CH4 Concentration Contour Plot
9.697e-001
9.091e-001
8.485e-001
7.879e-001
7.273e-001
6.667e-001
6.061e-001
5.455e-001
4.848e-001
4.242e-001
3.636e-001
3.030e-001
2.424e-001
1.818e-001
1.212e-001
6.061e-002
0.000e+000
0
0.02
0.04 (m)
0.01
0.03
Z
X
Y

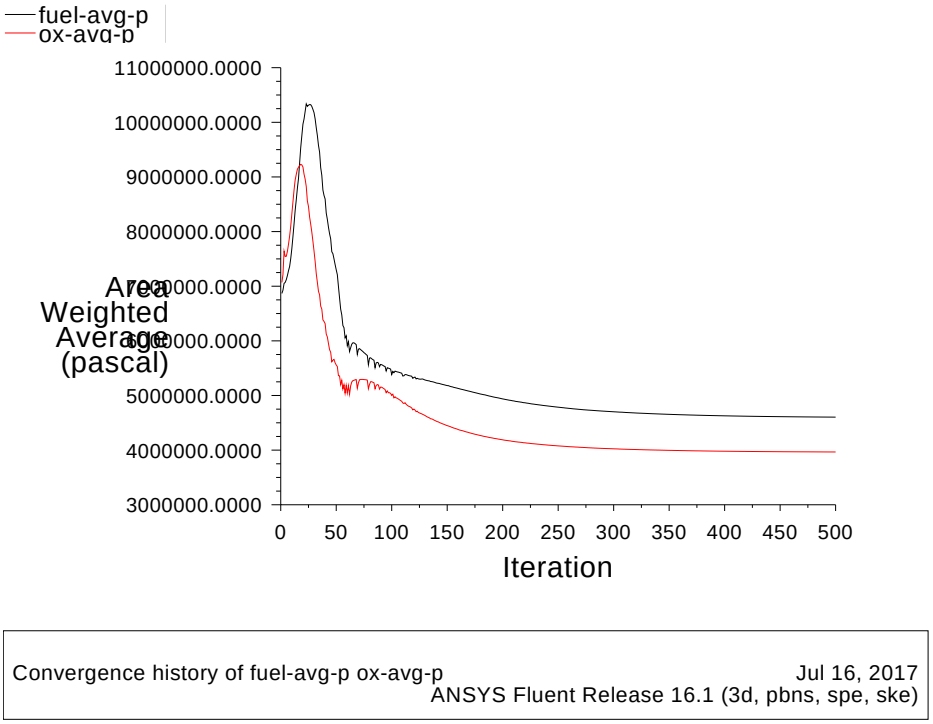

Figure H.7: Convergence history of scaled residuals for InflowColdFlowMassStart case.

H.5. InflowColdFlowPressureStart

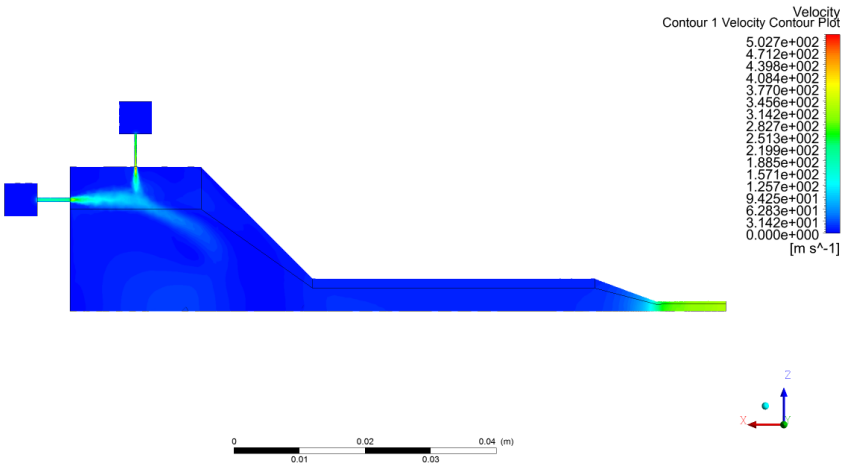

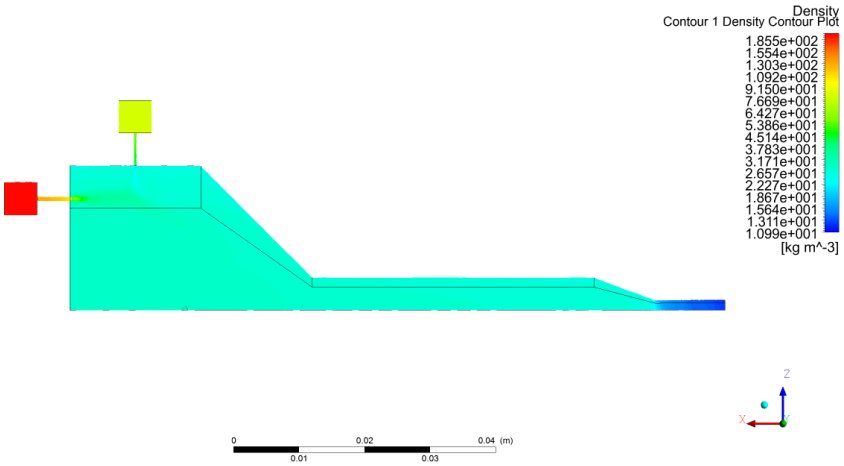
Density
Contour 1 Density Contour Plot
1.855e+002
1.554e+002
1.303e+002
1.092e+002
9.150e+001
7.669e+001
6.427e+001
5.386e+001
4.514e+001
3.783e+001
3.171e+001
2.657e+001
2.227e+001
1.867e+001
1.564e+001
1.311e+001
1.099e+001
[kg m^-3]
Z
X
Y
0
0.02
0.04 (m)
0.01
0.03

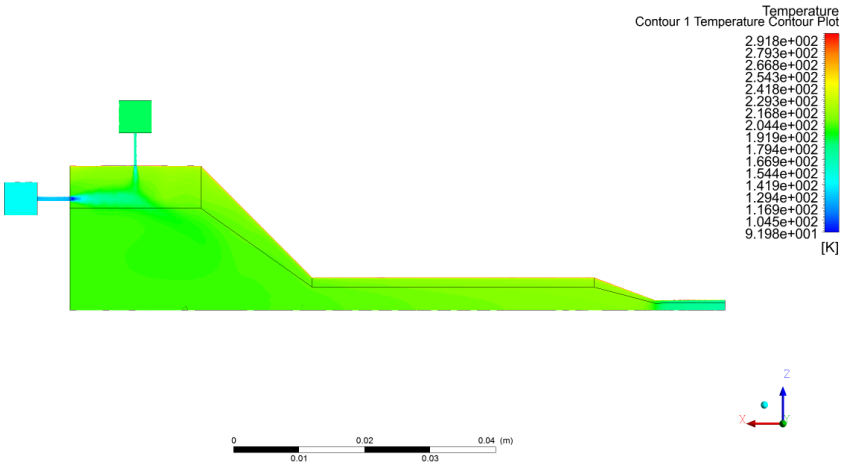
Temperature
Contour 1 Temperature Contour Plot
2.918e+002
2.793e+002
2.668e+002
2.543e+002
2.418e+002
2.293e+002
2.168e+002
2.044e+002
1.919e+002
1.794e+002
1.669e+002
1.544e+002
1.419e+002
1.294e+002
1.169e+002
1.045e+002
9.198e+001
[K]
Z
X
Y
0
0.02
0.04 (m)
0.01
0.03

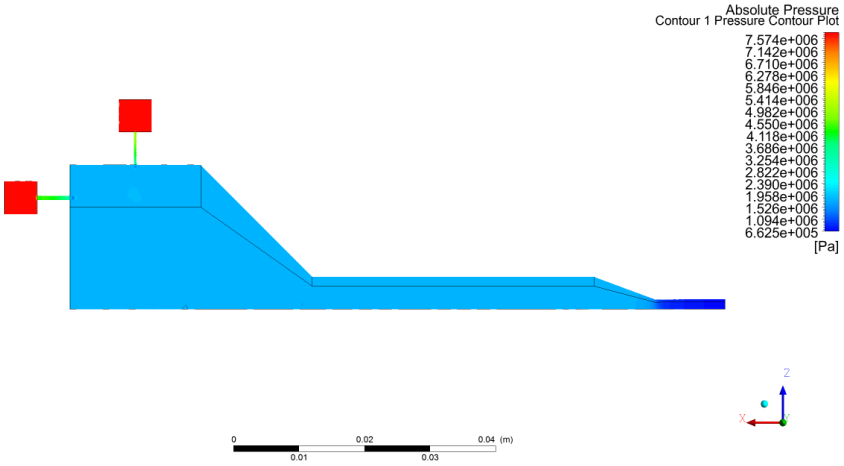
Absolute Pressure
Contour 1 Pressure Contour Plot
7.574e+006
7.142e+006
6.710e+006
6.278e+006
5.846e+006
5.414e+006
4.982e+006
4.550e+006
4.118e+006
3.686e+006
3.254e+006
2.822e+006
2.390e+006
1.958e+006
1.526e+006
1.094e+006
6.625e+005
[Pa]
Z
X
Y
0
0.02
0.04 (m)
0.01
0.03

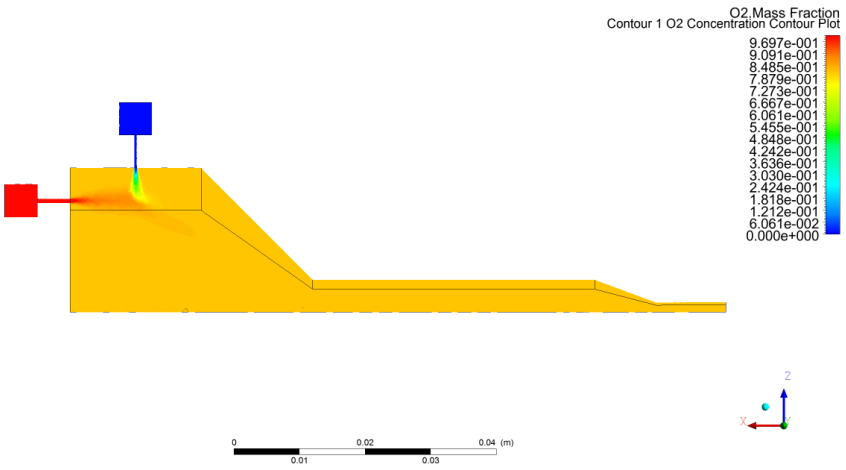
O2.Mass Fraction
Contour 1 O2 Concentration Contour Plot
9.697e-001
9.091e-001
8.485e-001
7.879e-001
7.273e-001
6.667e-001
6.061e-001
5.455e-001
4.848e-001
4.242e-001
3.636e-001
3.030e-001
2.424e-001
1.818e-001
1.212e-001
6.061e-002
0.000e+000
0
0.02
0.04 (m)
0.01
0.03
Z
X
Y

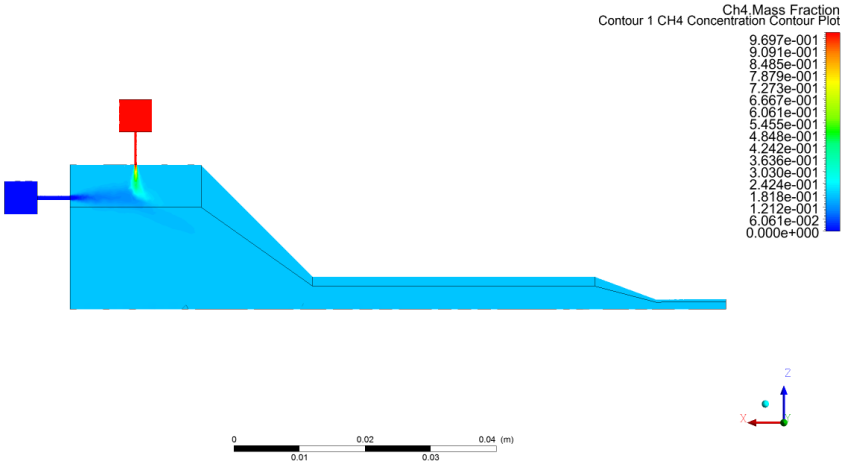
Ch4.Mass Fraction
Contour 1 CH4 Concentration Contour Plot
9.697e-001
9.091e-001
8.485e-001
7.879e-001
7.273e-001
6.667e-001
6.061e-001
5.455e-001
4.848e-001
4.242e-001
3.636e-001
3.030e-001
2.424e-001
1.818e-001
1.212e-001
6.061e-002
0.000e+000
0
0.02
0.04 (m)
0.01
0.03
Z
X
Y

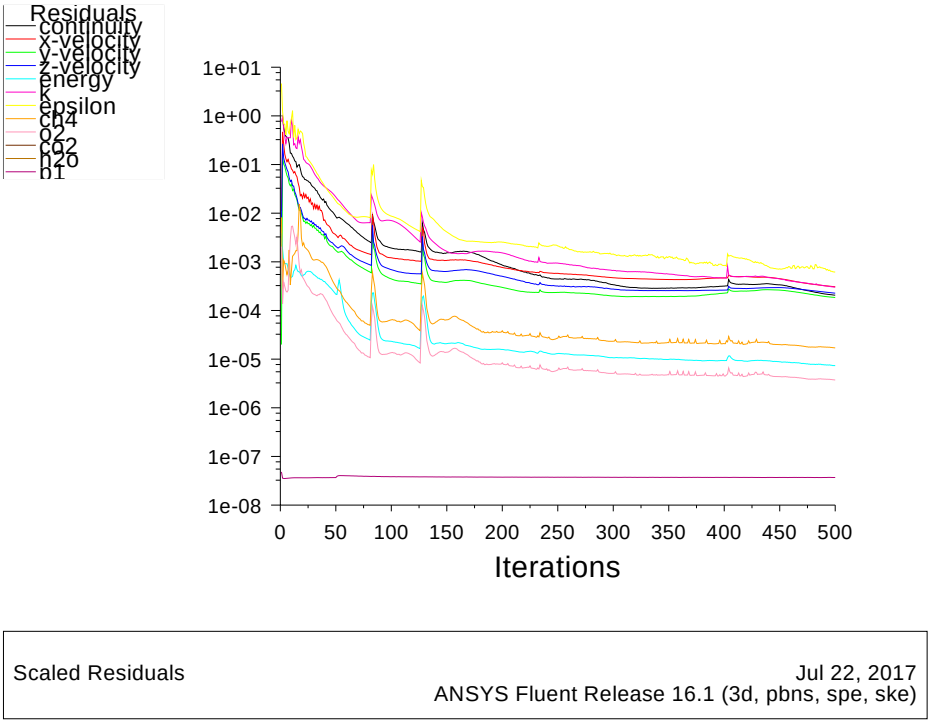

Figure H.8: Convergence history of scaled residuals of InflowColdFlowPressureStart case.

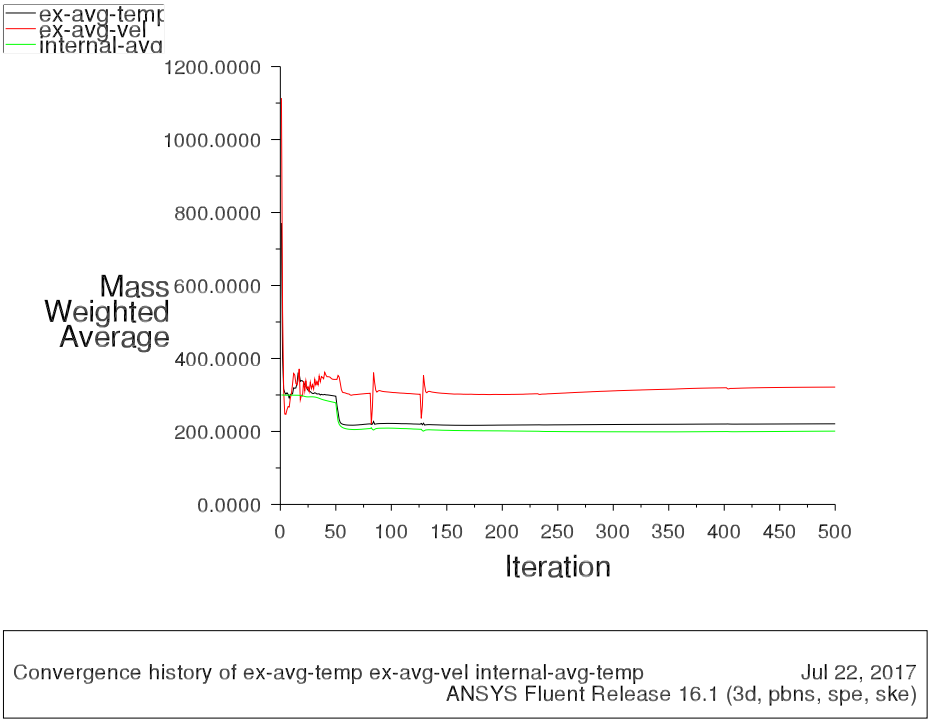

Figure H.9: Convergence history of integral quantities of InflowColdFlowPressureStart case.

H.6. EquilibriumAmbient

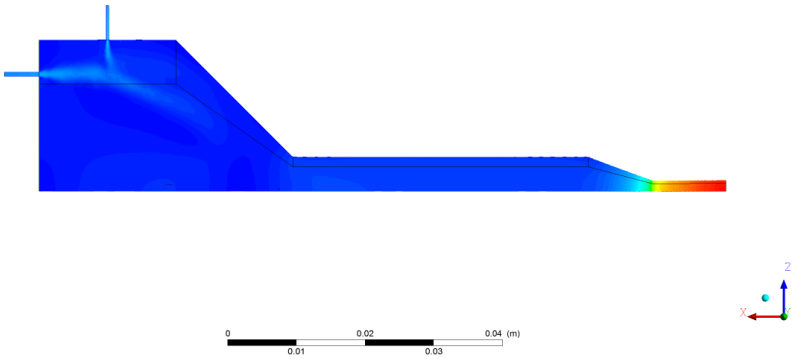

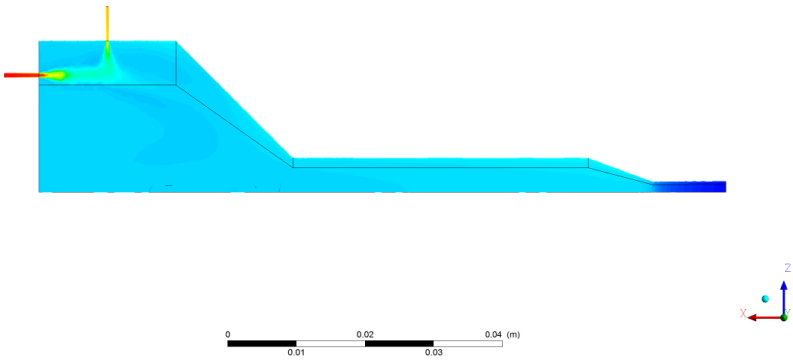

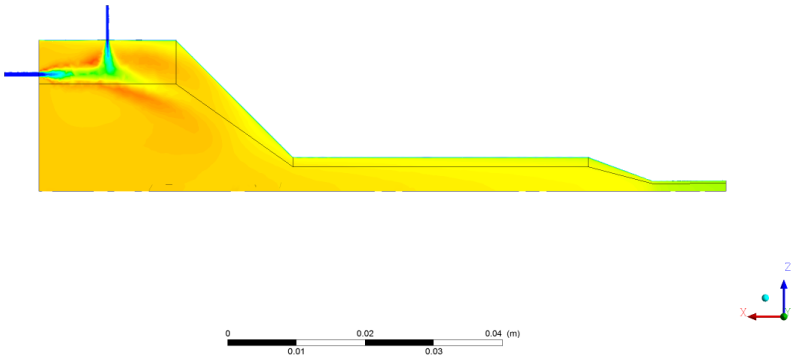

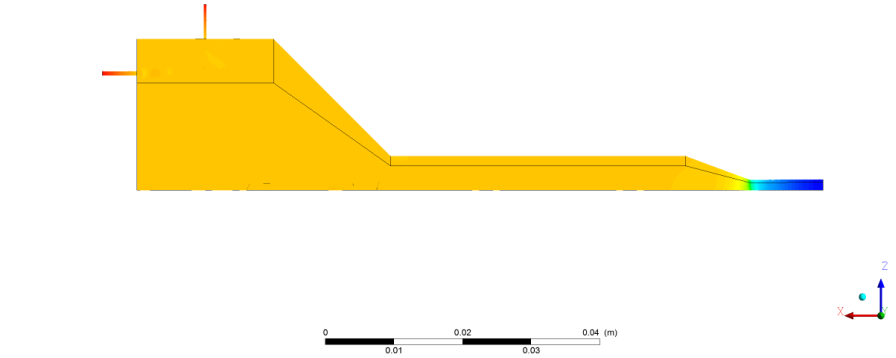

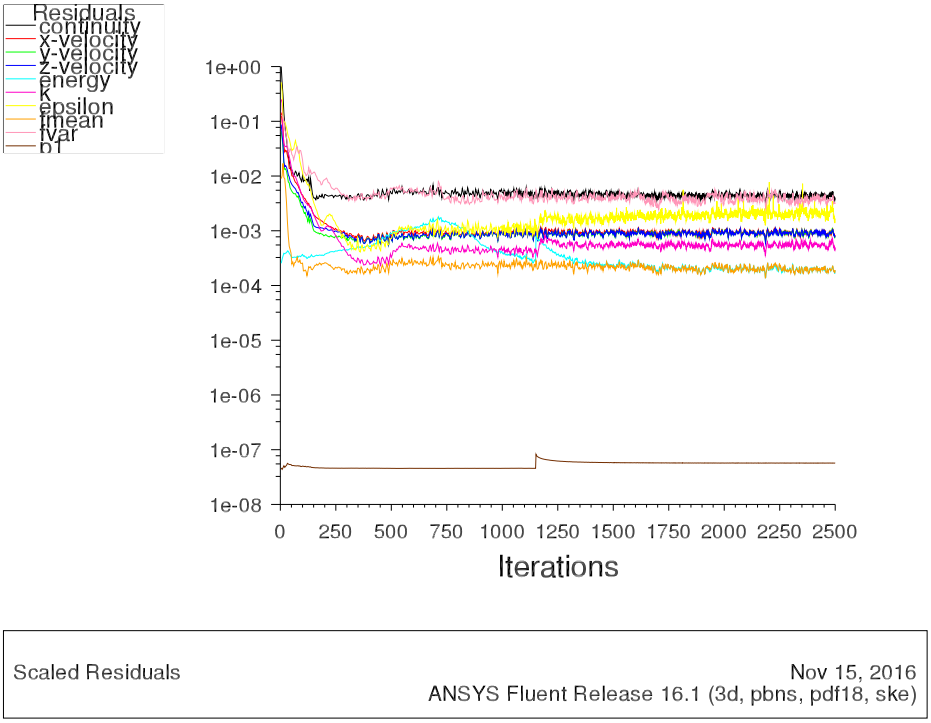

Figure H.10: Convergence history of scaled residuals for EquilibriumAmbient case.

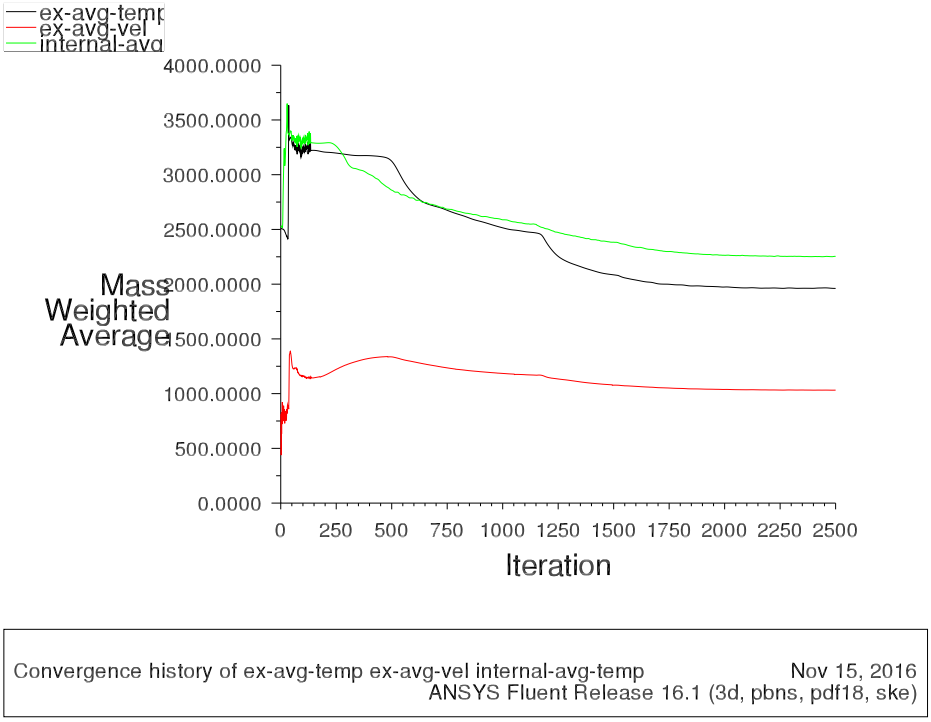

Figure H.11: Convergence history of integral quantities for EquilibriumAmbient case.

H.7. EquilibriumAmbientHotWall

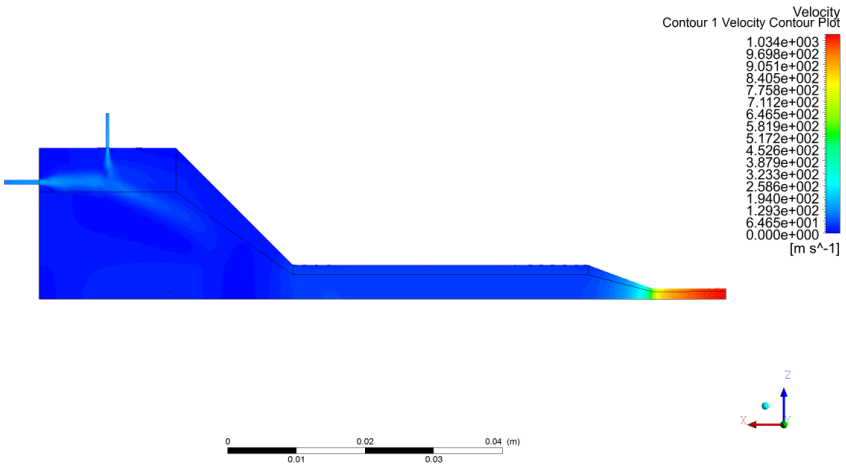

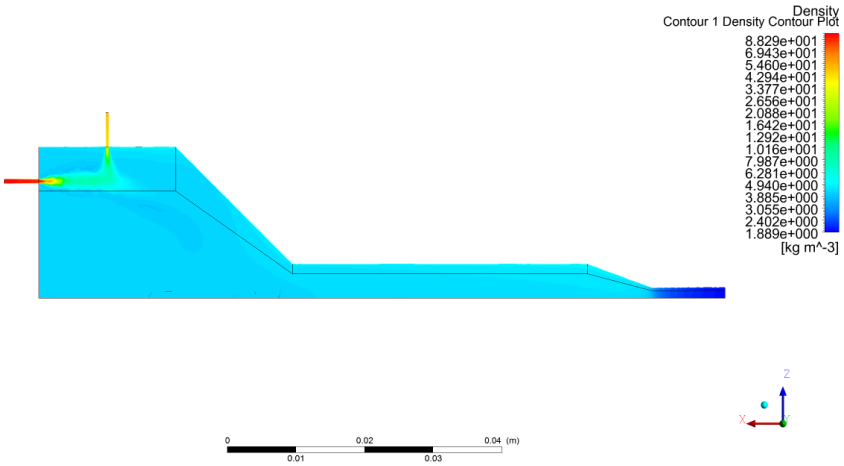
Density
Contour 1 Density Contour Plot
8.829e+001
6.943e+001
5.460e+001
4.294e+001
3.377e+001
2.656e+001
2.088e+001
1.642e+001
1.292e+001
1.016e+001
7.987e+000
6.281e+000
4.940e+000
3.885e+000
3.055e+000
2.402e+000
1.889e+000
[kg m^-3]
Z
X
Y
0
0.02
0.04 (m)
0.01
0.03

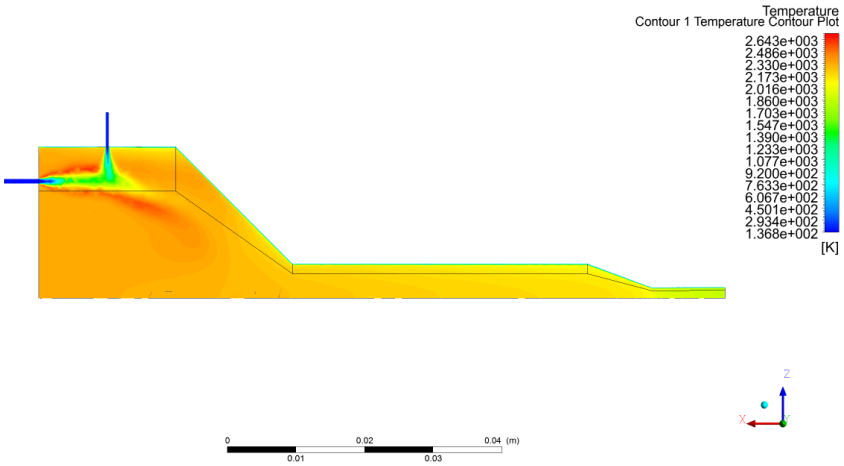
Temperature
Contour 1 Temperature Contour Plot
2.643e+003
2.486e+003
2.330e+003
2.173e+003
2.016e+003
1.860e+003
1.703e+003
1.547e+003
1.390e+003
1.233e+003
1.077e+003
9.200e+002
7.633e+002
6.067e+002
4.501e+002
2.934e+002
1.368e+002
[K]
Z
X
Y
0
0.02
0.04 (m)
0.01
0.03

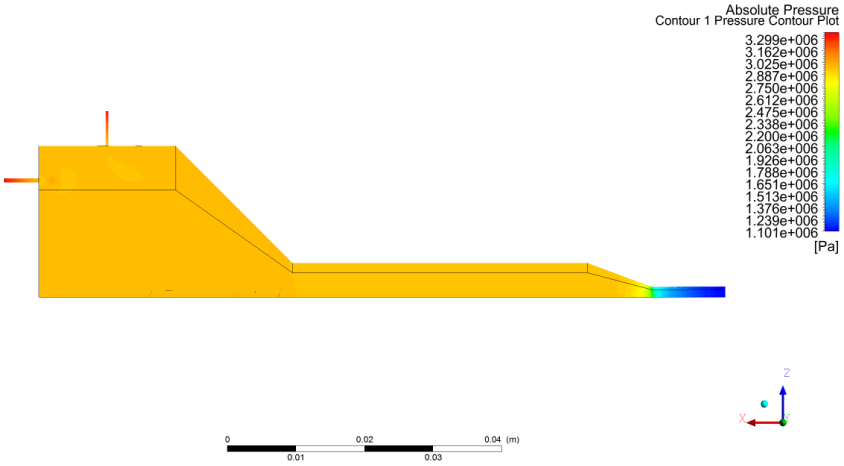
Absolute Pressure
Contour 1 Pressure Contour Plot
3.299e+006
3.162e+006
3.025e+006
2.887e+006
2.750e+006
2.612e+006
2.475e+006
2.338e+006
2.200e+006
2.063e+006
1.926e+006
1.788e+006
1.651e+006
1.513e+006
1.376e+006
1.239e+006
1.101e+006
[Pa]
Z
X
Y
0
0.02
0.04 (m)
0.01
0.03

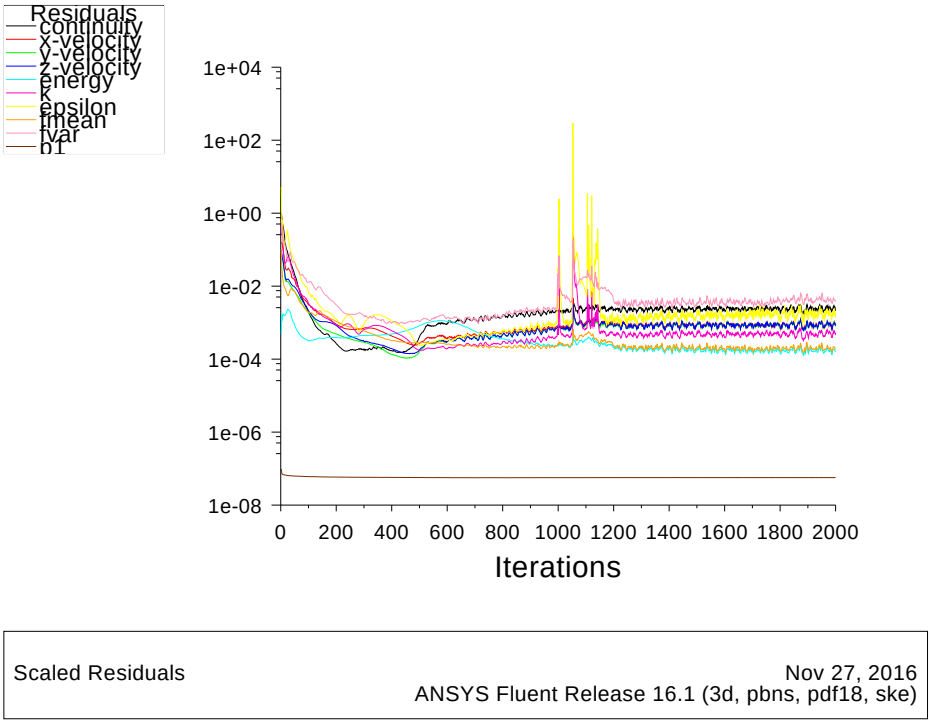

Figure H.12: Convergence history of scaled residuals for EquilibriumAmbientHotWall case.

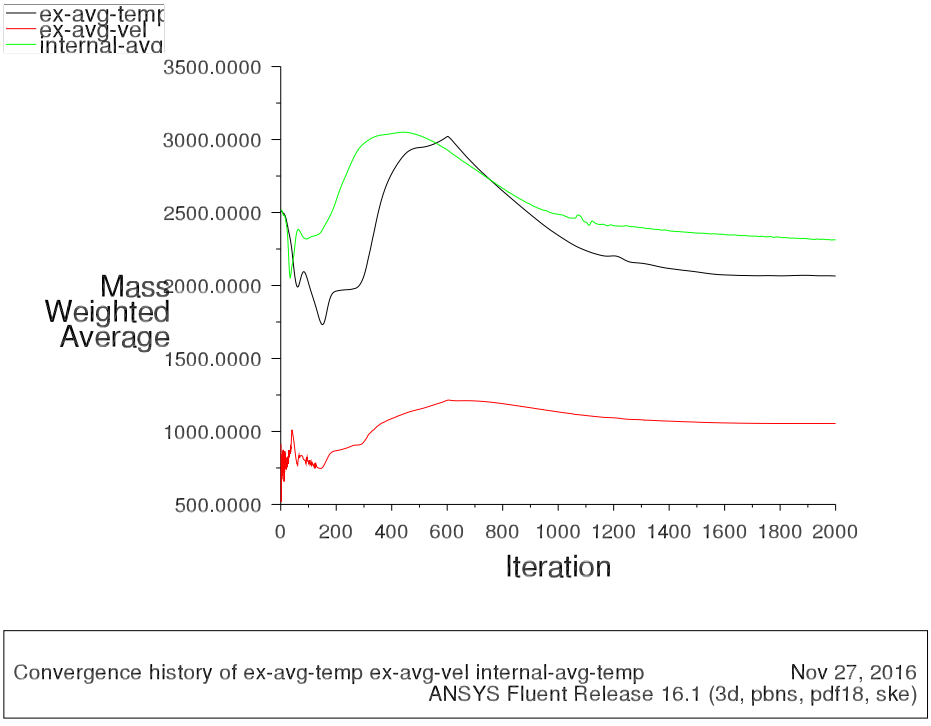

Figure H.13: Convergence history of integral quantities for EquilibriumAmbientHotWall case.

H.8. EquilibriumPressure

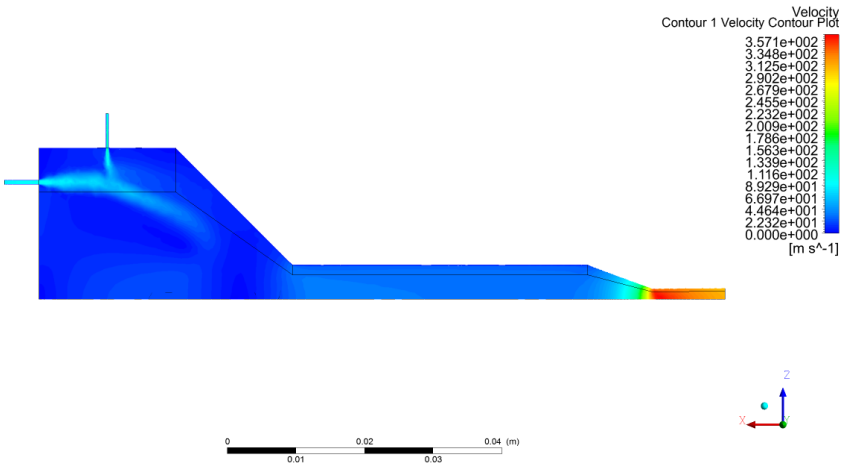

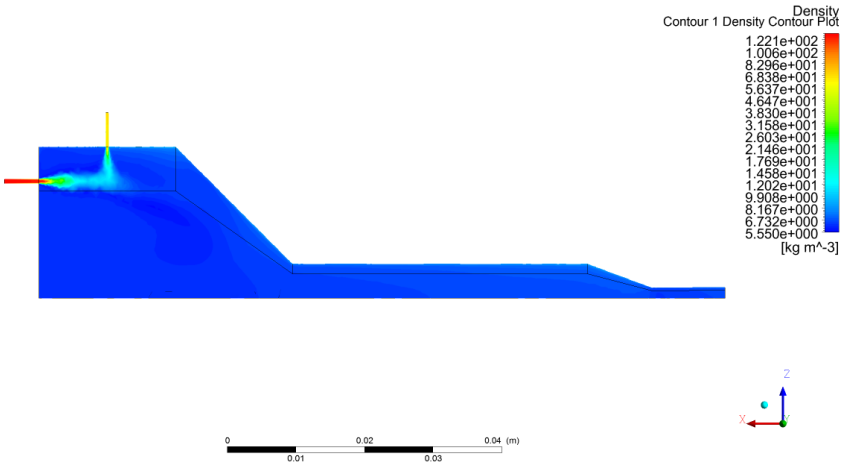

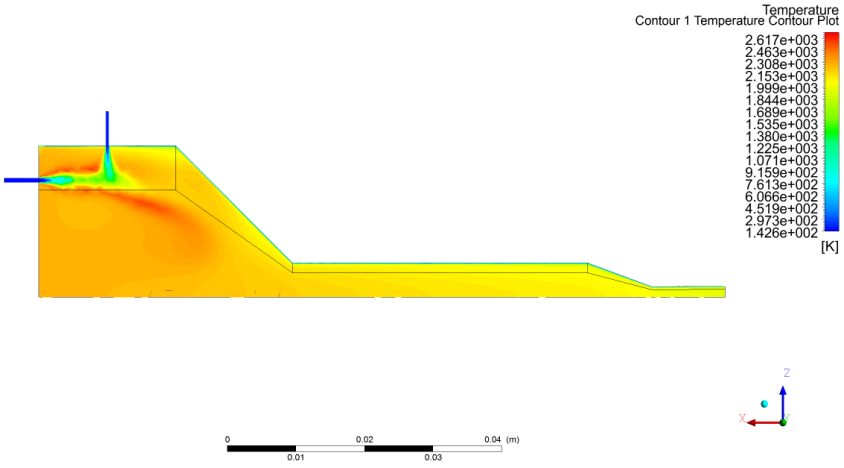

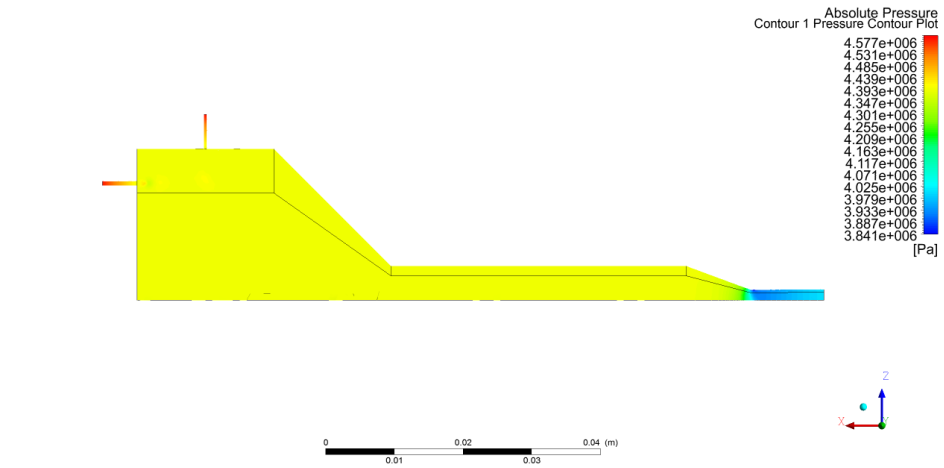

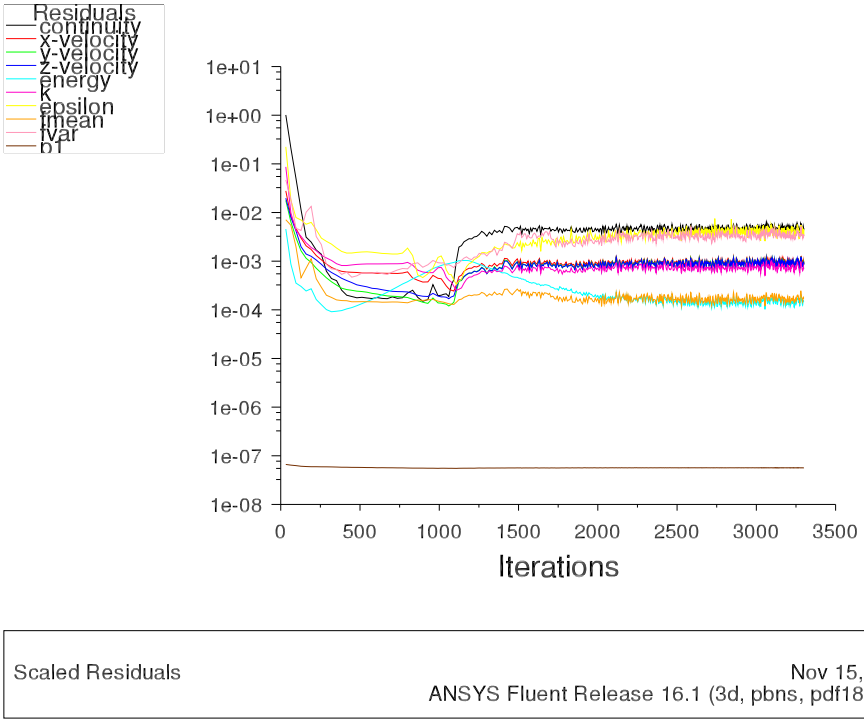

Figure H.14: Convergence history of scaled residuals for EquilibriumPressure case.

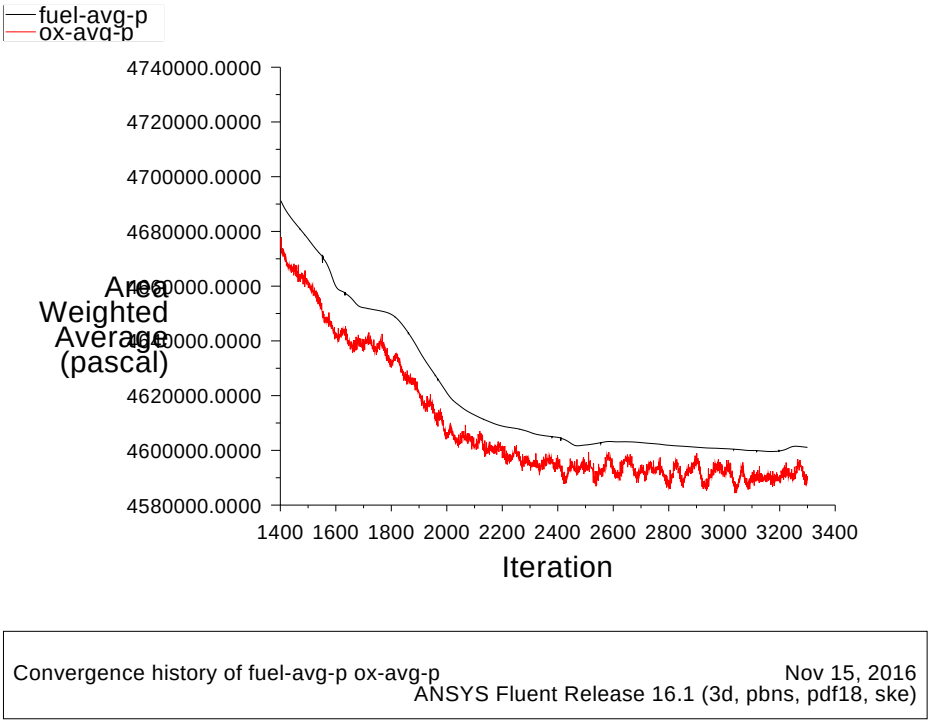

Figure H.15: Convergence history of integral quantities for EquilibriumPressure case.

H.9. FiniteRate1StepAmbient

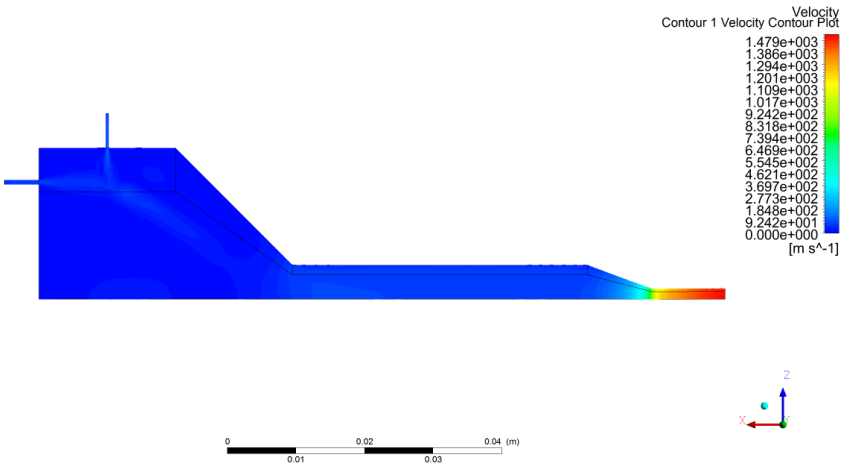

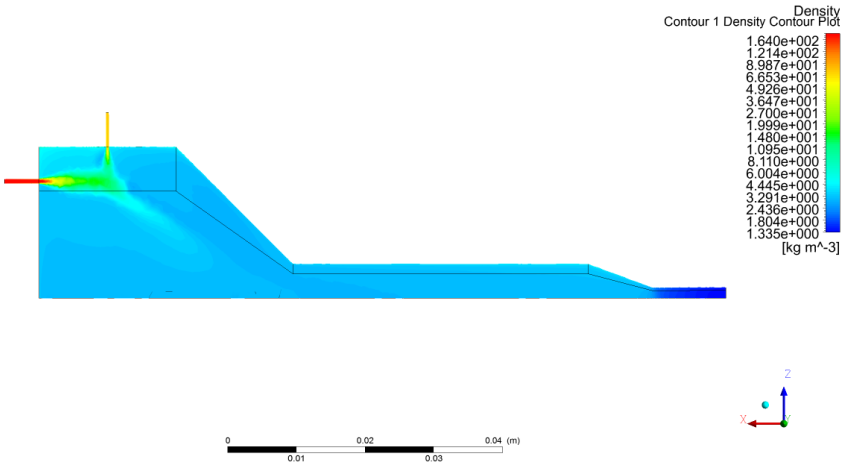
Density
Contour 1 Density Contour Plot
1.640e+002
1.214e+002
8.987e+001
6.653e+001
4.926e+001
3.647e+001
2.700e+001
1.999e+001
1.480e+001
1.095e+001
8.110e+000
6.004e+000
4.445e+000
3.291e+000
2.436e+000
1.804e+000
1.335e+000
[kg m^-3]
Z
X
Y
0
0.02
0.04 (m)
0.01
0.03

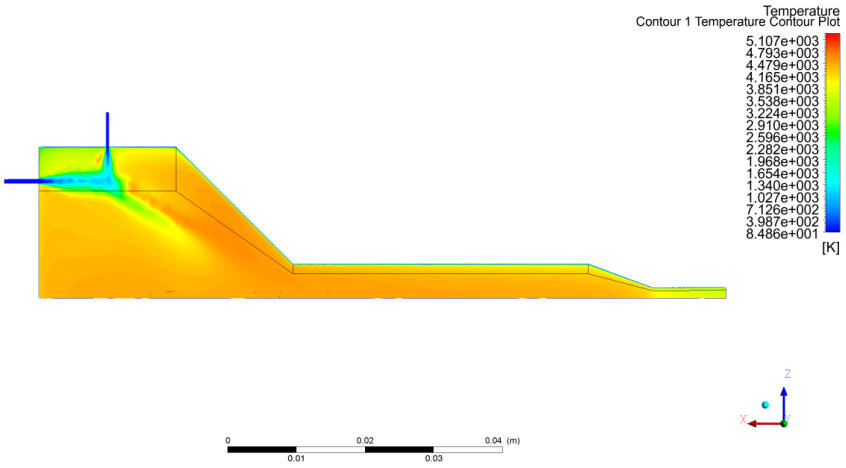
Temperature
Contour 1 Temperature Contour Plot
5.107e+003
4.793e+003
4.479e+003
4.165e+003
3.851e+003
3.538e+003
3.224e+003
2.910e+003
2.596e+003
2.282e+003
1.968e+003
1.654e+003
1.340e+003
1.027e+003
7.126e+002
3.987e+002
8.486e+001
[K]
Z
X
Y
0
0.02
0.04 (m)
0.01
0.03

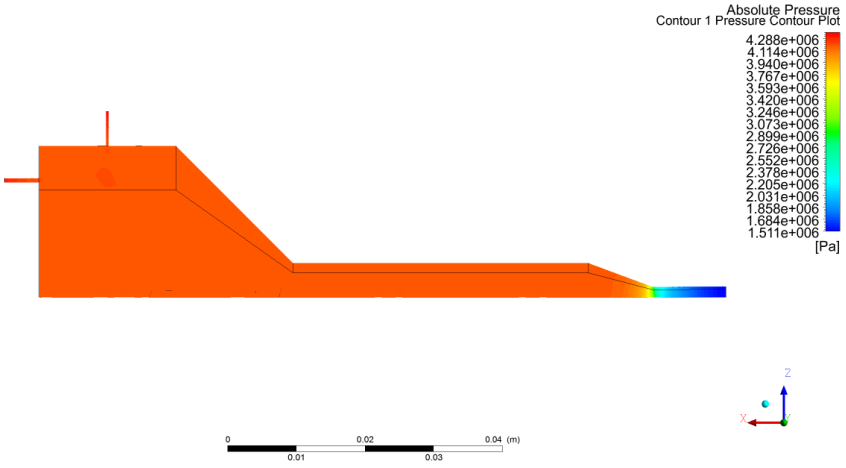
Absolute Pressure
Contour 1 Pressure Contour Plot
4.288e+006
4.114e+006
3.940e+006
3.767e+006
3.593e+006
3.420e+006
3.246e+006
3.073e+006
2.899e+006
2.726e+006
2.552e+006
2.378e+006
2.205e+006
2.031e+006
1.858e+006
1.684e+006
1.511e+006
[Pa]
Z
X
Y
0
0.02
0.04 (m)
0.01
0.03

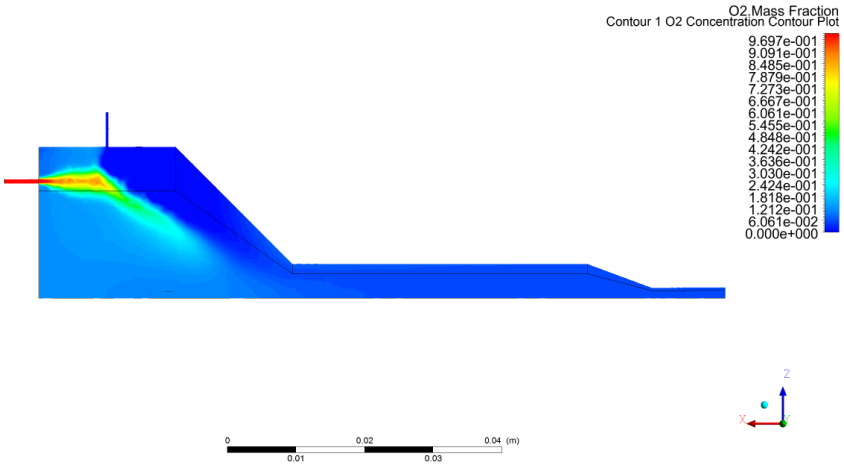
O2.Mass Fraction
Contour 1 O2 Concentration Contour Plot
9.697e-001
9.091e-001
8.485e-001
7.879e-001
7.273e-001
6.667e-001
6.061e-001
5.455e-001
4.848e-001
4.242e-001
3.636e-001
3.030e-001
2.424e-001
1.818e-001
1.212e-001
6.061e-002
0.000e+000
Z
X
Y
0
0.02
0.04 (m)
0.01
0.03

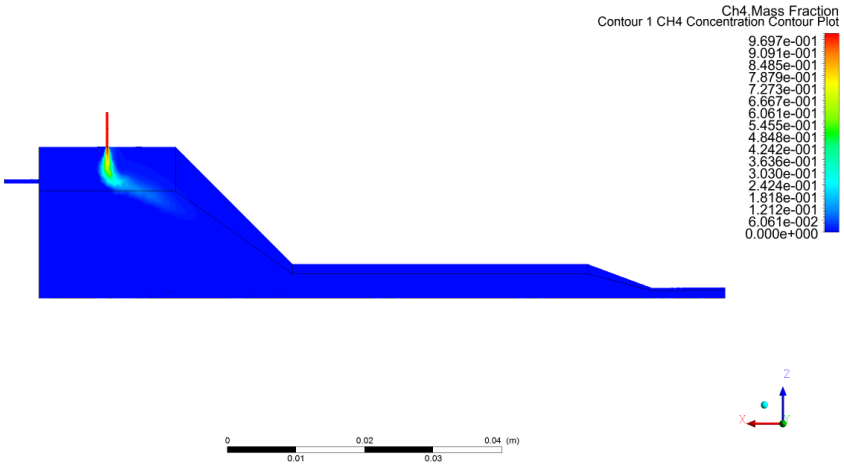
Ch4.Mass Fraction
Contour 1 CH4 Concentration Contour Plot
9.697e-001
9.091e-001
8.485e-001
7.879e-001
7.273e-001
6.667e-001
6.061e-001
5.455e-001
4.848e-001
4.242e-001
3.636e-001
3.030e-001
2.424e-001
1.818e-001
1.212e-001
6.061e-002
0.000e+000
Z
X
Y
0
0.02
0.04 (m)
0.01
0.03

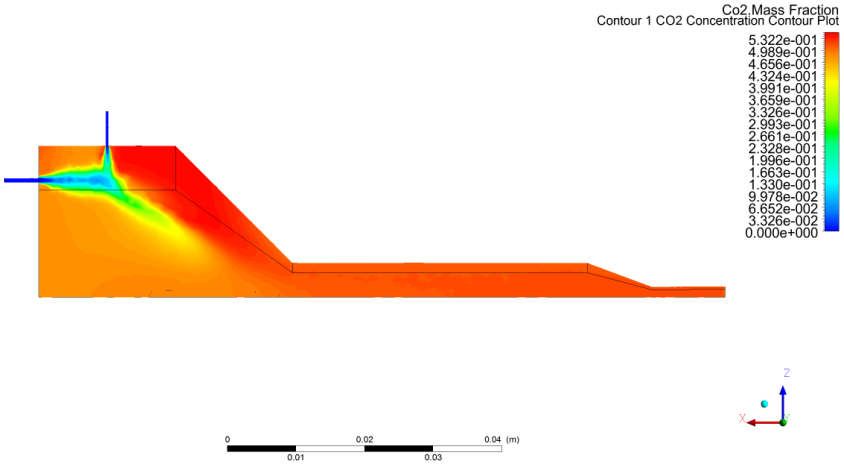
Co2.Mass Fraction
Contour 1 CO2 Concentration Contour Plot
5.322e-001
4.989e-001
4.656e-001
4.324e-001
3.991e-001
3.659e-001
3.326e-001
2.993e-001
2.661e-001
2.328e-001
1.996e-001
1.663e-001
1.330e-001
9.978e-002
6.652e-002
3.326e-002
0.000e+000
Z
X
Y
0
0.02
0.04 (m)
0.01
0.03

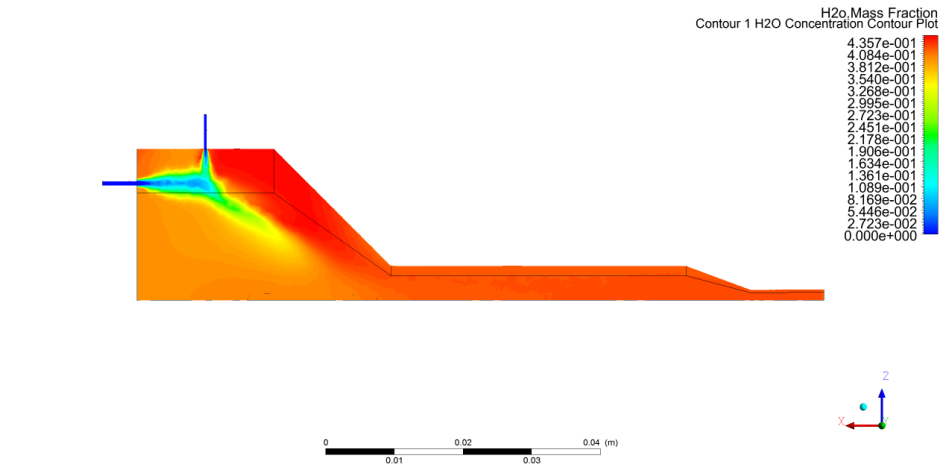

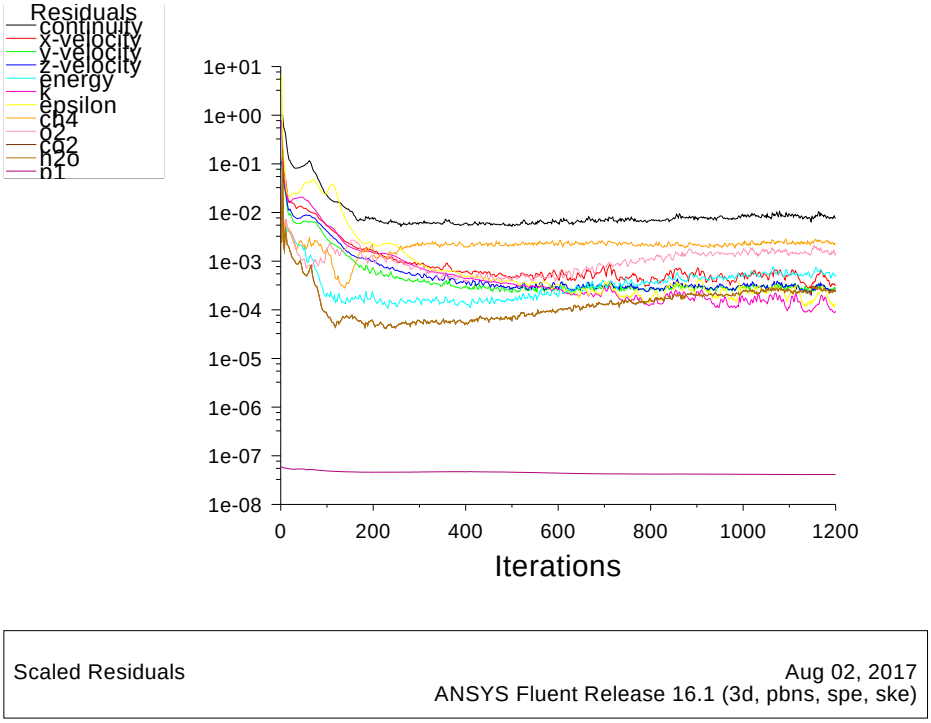

Figure H.16: Convergence history of scaled residuals for FiniteRate1StepAmbient case.

H.10. FiniteRate1StepPressure

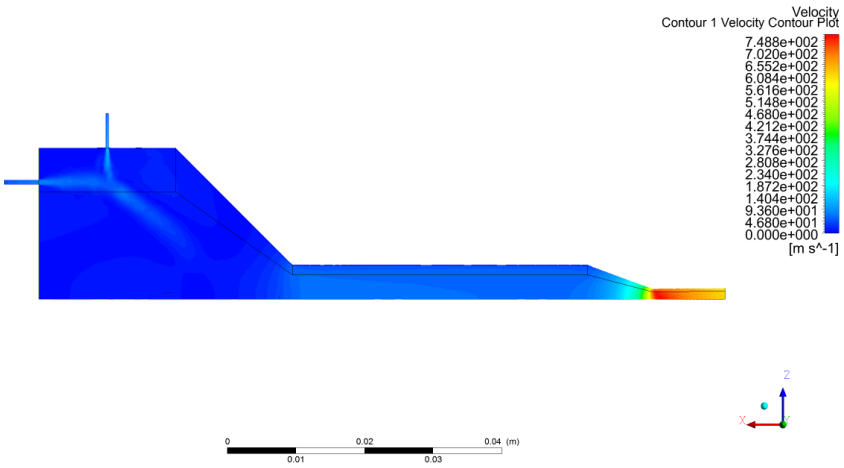

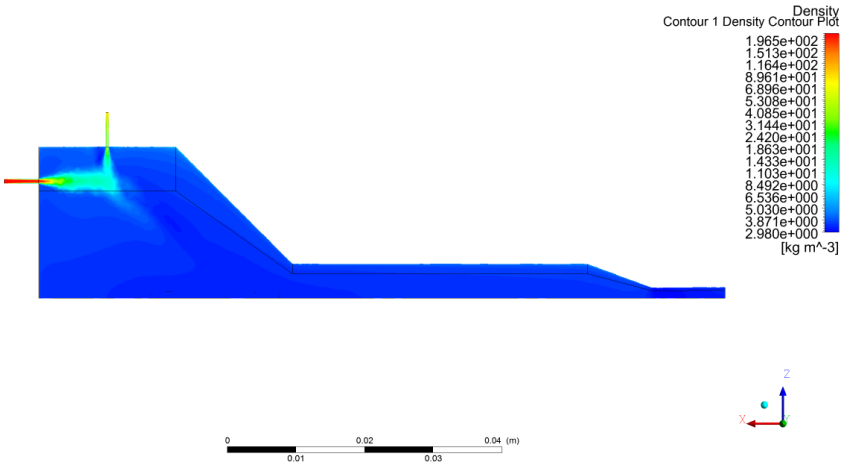

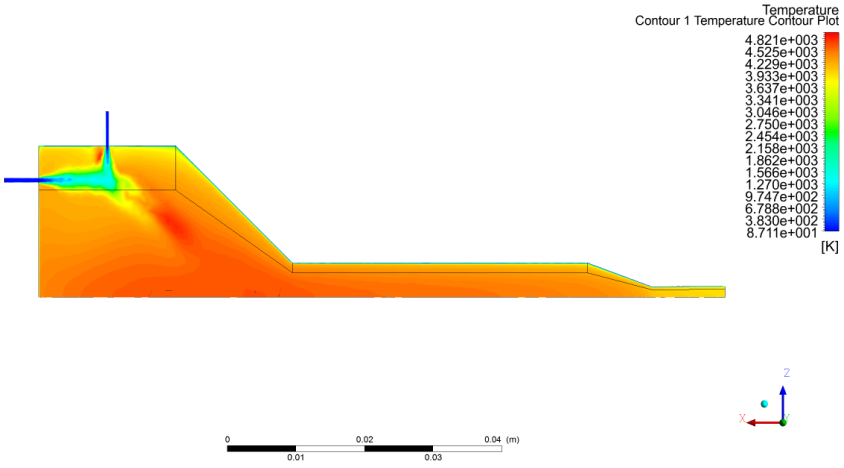

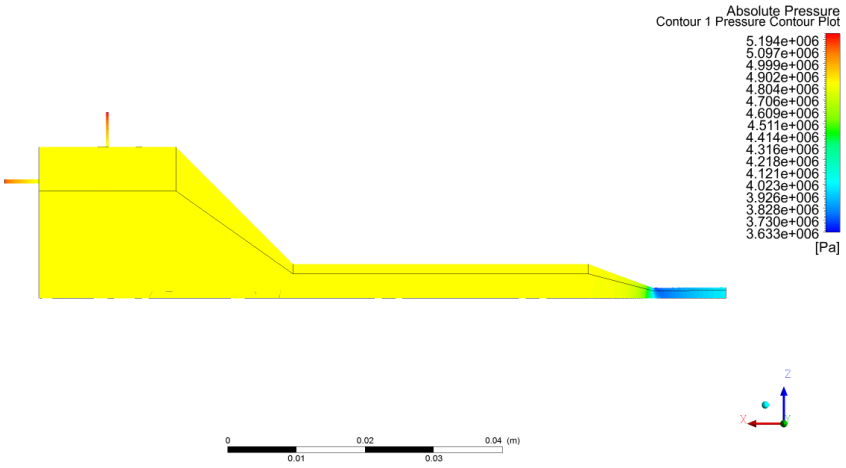
Absolute Pressure
Contour 1 Pressure Contour Plot
5.194e+006
5.097e+006
4.999e+006
4.902e+006
4.804e+006
4.706e+006
4.609e+006
4.511e+006
4.414e+006
4.316e+006
4.218e+006
4.121e+006
4.023e+006
3.926e+006
3.828e+006
3.730e+006
3.633e+006
[Pa]
Z
X
Y
0
0.02
0.04 (m)
0.01
0.03

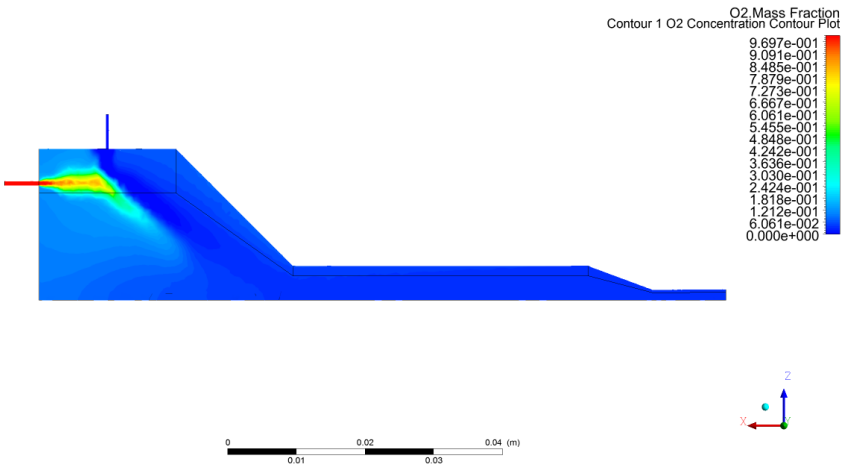
O2.Mass Fraction
Contour 1 O2 Concentration Contour Plot
9.697e-001
9.091e-001
8.485e-001
7.879e-001
7.273e-001
6.667e-001
6.061e-001
5.455e-001
4.848e-001
4.242e-001
3.636e-001
3.030e-001
2.424e-001
1.818e-001
1.212e-001
6.061e-002
0.000e+000
Z
X
Y
0
0.02
0.04 (m)
0.01
0.03

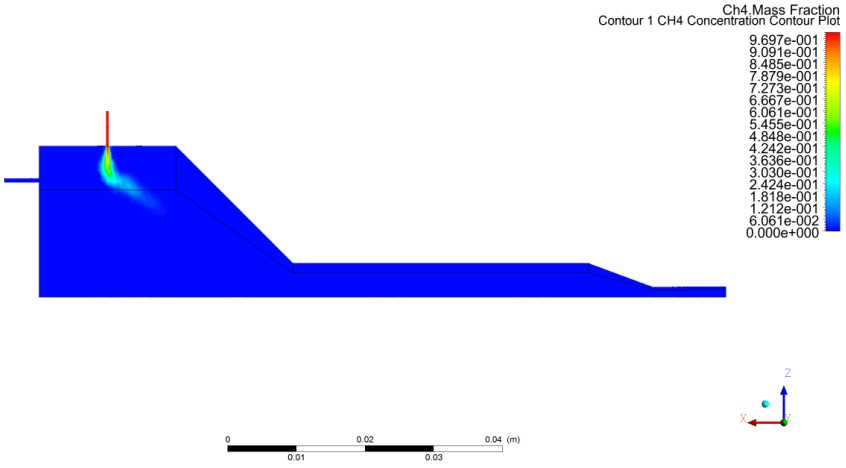
Ch4.Mass Fraction
Contour 1 CH4 Concentration Contour Plot
9.697e-001
9.091e-001
8.485e-001
7.879e-001
7.273e-001
6.667e-001
6.061e-001
5.455e-001
4.848e-001
4.242e-001
3.636e-001
3.030e-001
2.424e-001
1.818e-001
1.212e-001
6.061e-002
0.000e+000
Z
X
Y
0
0.02
0.04 (m)
0.01
0.03

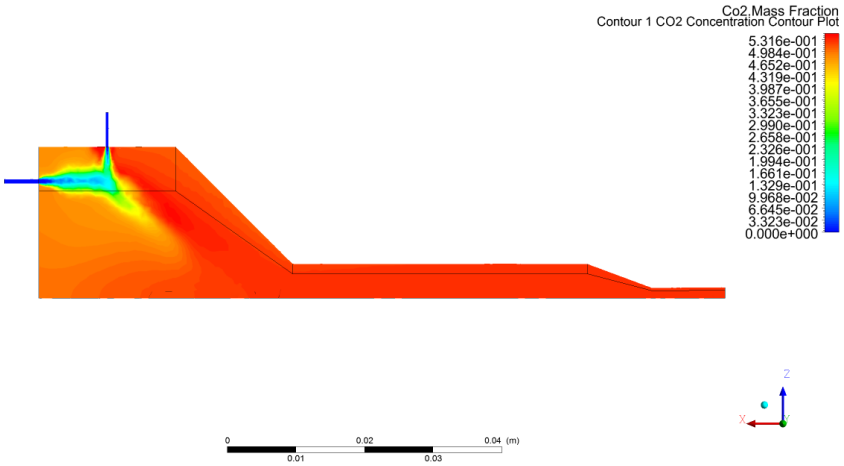
Co2,Mass Fraction
Contour 1 CO2 Concentration Contour Plot
5.316e-001
4.984e-001
4.652e-001
4.319e-001
3.987e-001
3.655e-001
3.323e-001
2.990e-001
2.658e-001
2.326e-001
1.994e-001
1.661e-001
1.329e-001
9.968e-002
6.645e-002
3.323e-002
0.000e+000
Z
X
Y
0
0.02
0.04 (m)
0.01
0.03

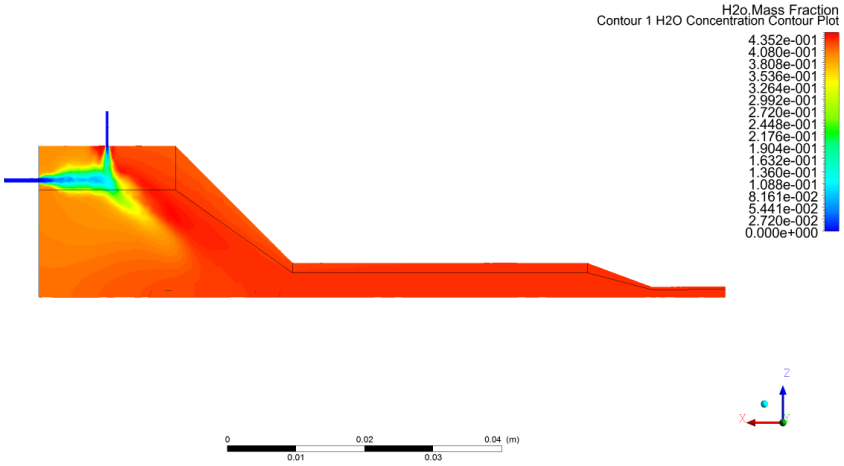
H2o,Mass Fraction
Contour 1 H2O Concentration Contour Plot
4.352e-001
4.080e-001
3.808e-001
3.536e-001
3.264e-001
2.992e-001
2.720e-001
2.448e-001
2.176e-001
1.904e-001
1.632e-001
1.360e-001
1.088e-001
8.161e-002
5.441e-002
2.720e-002
0.000e+000
Z
X
Y
0
0.02
0.04 (m)
0.01
0.03

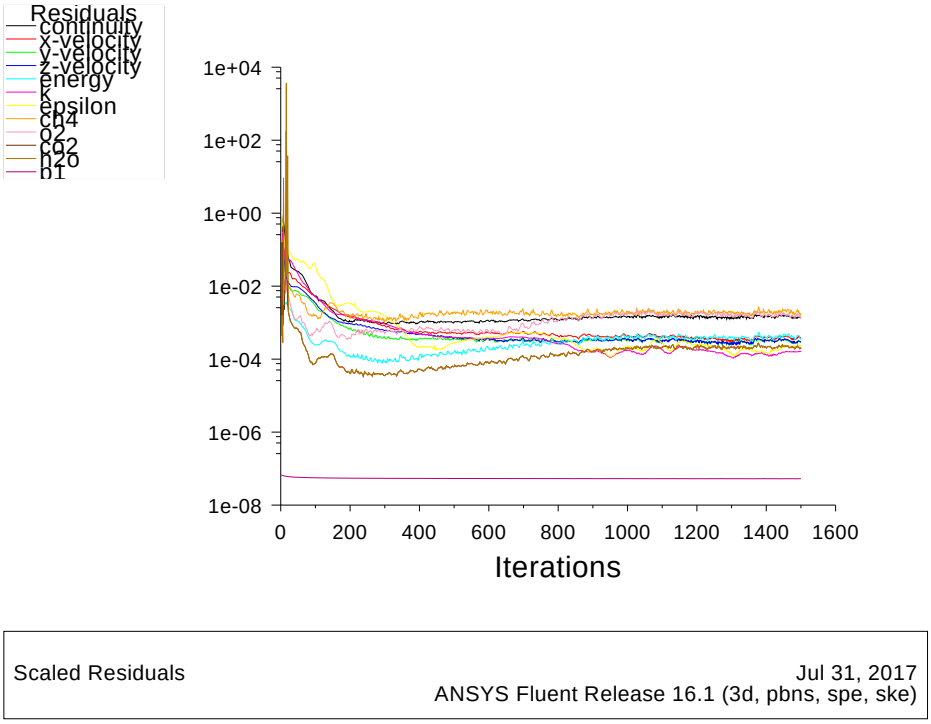

Figure H.17: Convergence history of scaled residuals for FiniteRate1StepPressure case.

H.11. FiniteRate2StepAmbient

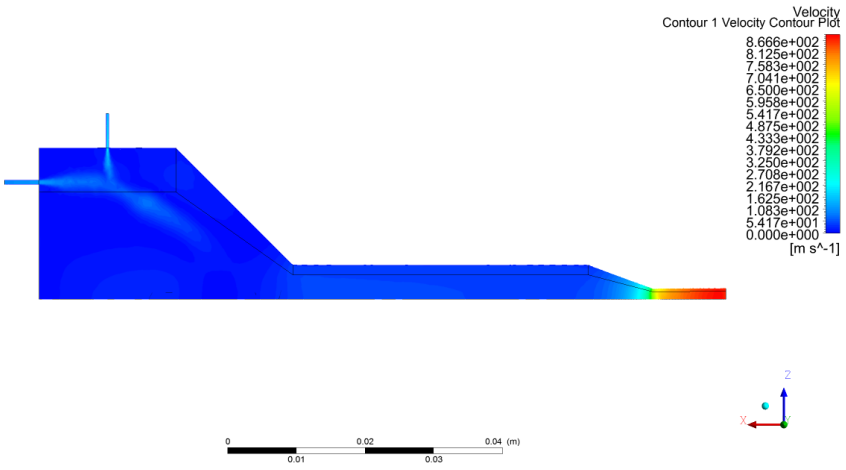

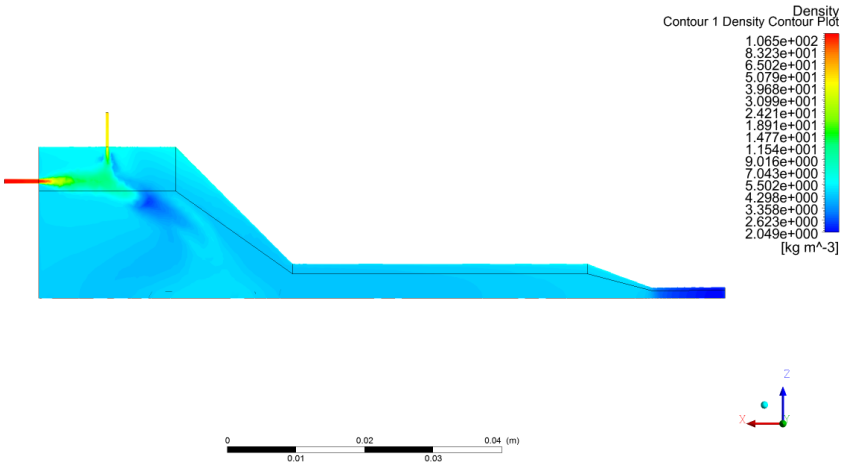
Density
Contour 1 Density Contour Plot
1.065e+002
8.323e+001
6.502e+001
5.079e+001
3.968e+001
3.099e+001
2.421e+001
1.891e+001
1.477e+001
1.154e+001
9.016e+000
7.043e+000
5.502e+000
4.298e+000
3.358e+000
2.623e+000
2.049e+000
[kg m^-3]
Z
X
Y
0
0.02
0.04 (m)
0.01
0.03

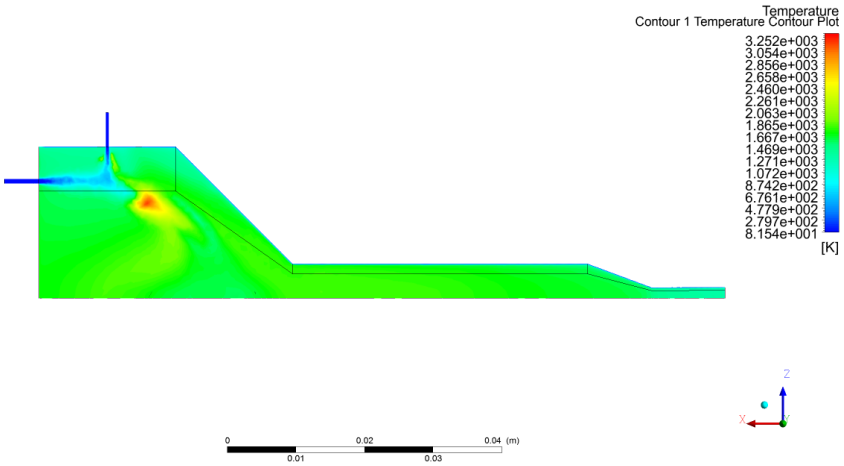
Temperature
Contour 1 Temperature Contour Plot
3.252e+003
3.054e+003
2.856e+003
2.658e+003
2.460e+003
2.261e+003
2.063e+003
1.865e+003
1.667e+003
1.469e+003
1.271e+003
1.072e+003
8.742e+002
6.761e+002
4.779e+002
2.797e+002
8.154e+001
[K]
Z
X
Y
0
0.02
0.04 (m)
0.01
0.03

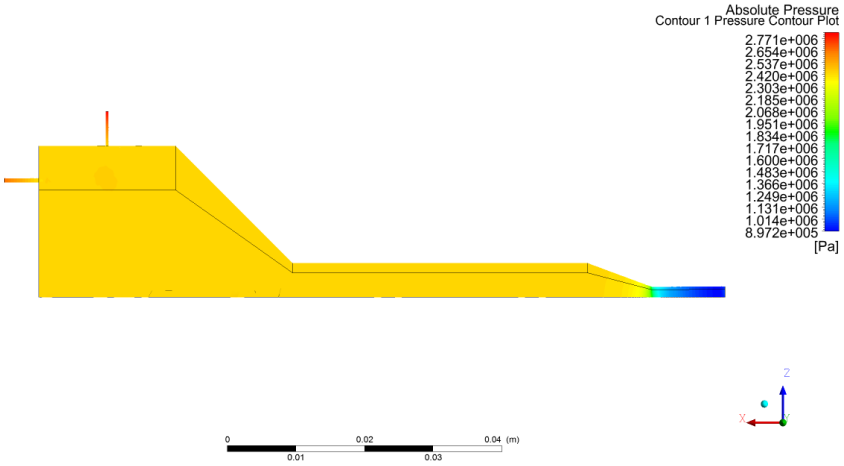
Absolute Pressure
Contour 1 Pressure Contour Plot
2.771e+006
2.654e+006
2.537e+006
2.420e+006
2.303e+006
2.185e+006
2.068e+006
1.951e+006
1.834e+006
1.717e+006
1.600e+006
1.483e+006
1.366e+006
1.249e+006
1.131e+006
1.014e+006
8.972e+005
[Pa]
Z
X
Y
0
0.02
0.04 (m)
0.01
0.03

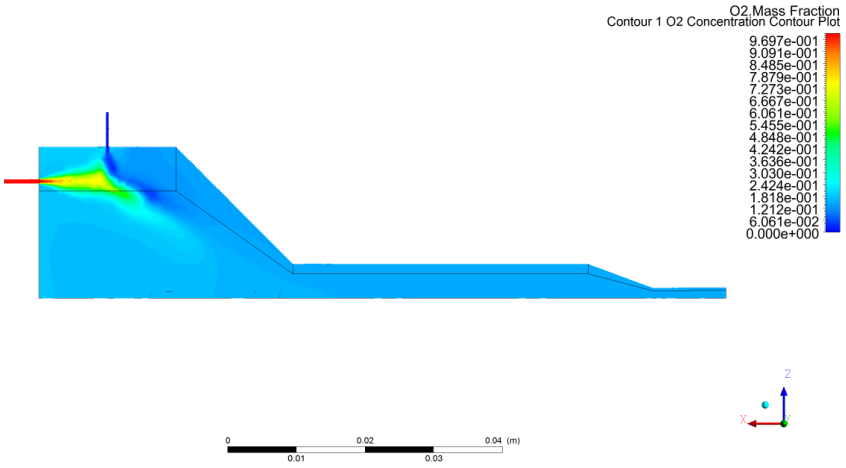
O2.Mass Fraction
Contour 1 O2 Concentration Contour Plot
9.697e-001
9.091e-001
8.485e-001
7.879e-001
7.273e-001
6.667e-001
6.061e-001
5.455e-001
4.848e-001
4.242e-001
3.636e-001
3.030e-001
2.424e-001
1.818e-001
1.212e-001
6.061e-002
0.000e+000
Z
X
Y
0
0.02
0.04 (m)
0.01
0.03

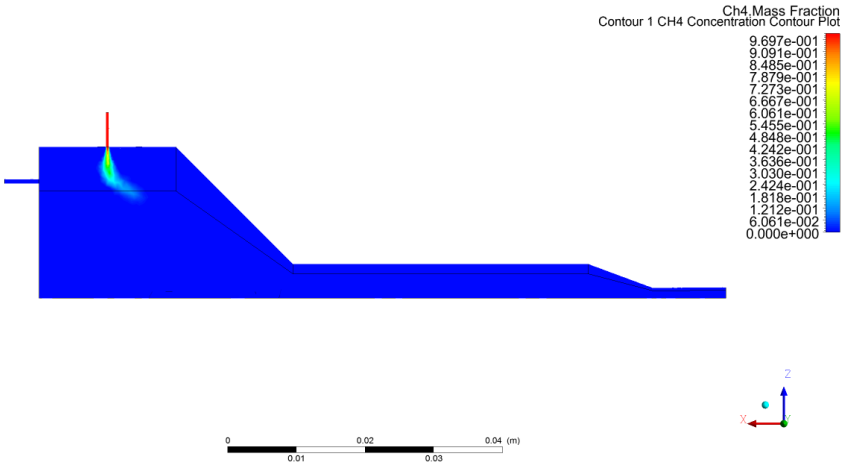
Ch4.Mass Fraction
Contour 1 CH4 Concentration Contour Plot
9.697e-001
9.091e-001
8.485e-001
7.879e-001
7.273e-001
6.667e-001
6.061e-001
5.455e-001
4.848e-001
4.242e-001
3.636e-001
3.030e-001
2.424e-001
1.818e-001
1.212e-001
6.061e-002
0.000e+000
Z
X
Y
0
0.02
0.04 (m)
0.01
0.03

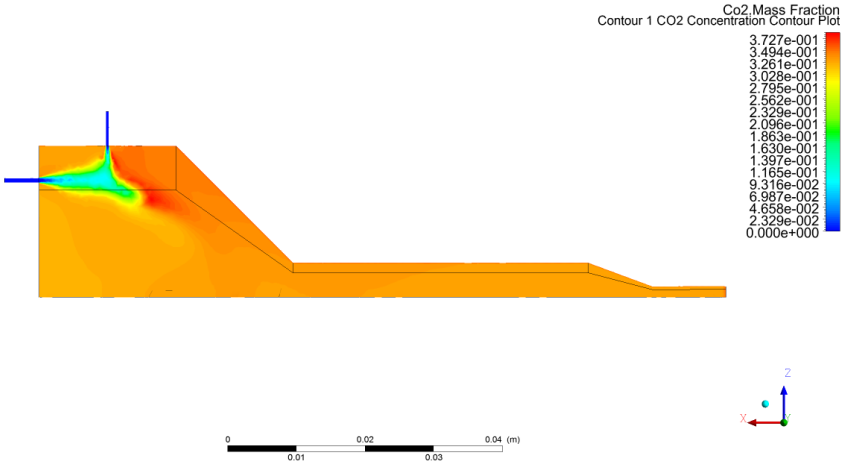
Co2.Mass Fraction
Contour 1 CO2 Concentration Contour Plot
3.727e-001
3.494e-001
3.261e-001
3.028e-001
2.795e-001
2.562e-001
2.329e-001
2.096e-001
1.863e-001
1.630e-001
1.397e-001
1.165e-001
9.316e-002
6.987e-002
4.658e-002
2.329e-002
0.000e+000
Z
X
Y
0
0.02
0.04 (m)
0.01
0.03

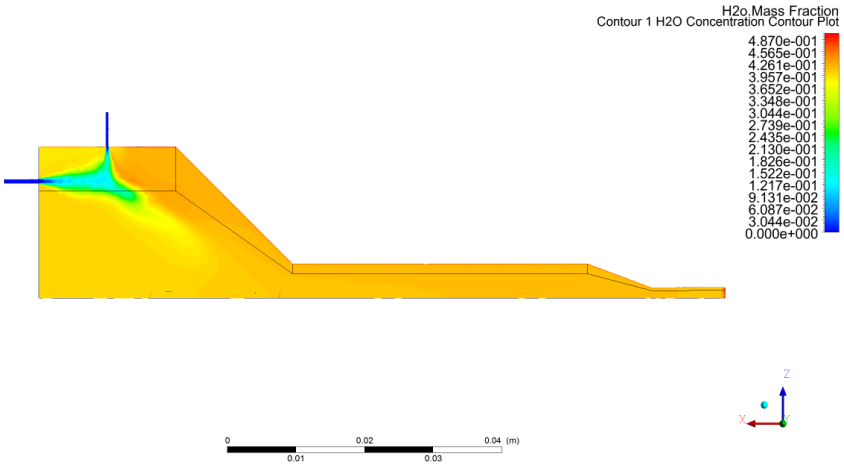

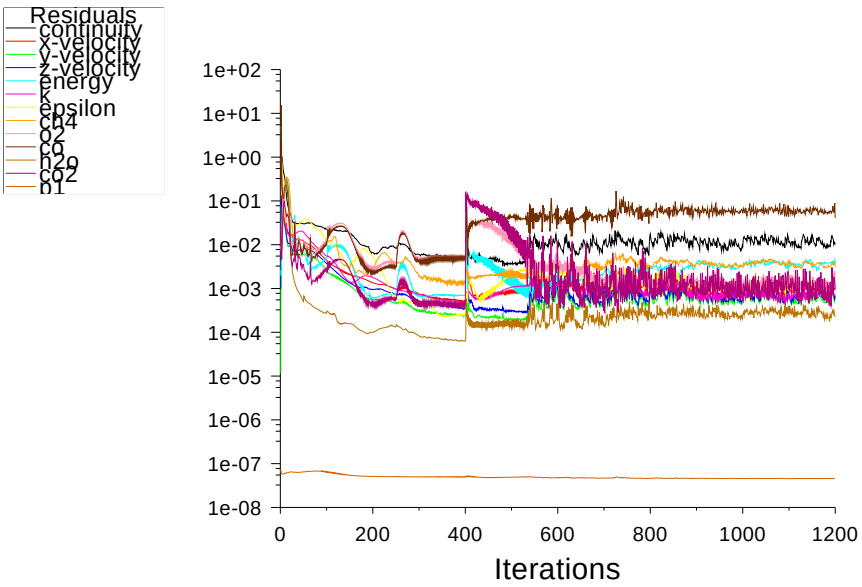

Scaled Residuals

Aug 03, 2017
ANSYS Fluent Release 16.1 (3d, pbns, spe, ske)

Figure H.18: Convergence history of scaled residuals for FiniteRate2StepAmbient case.

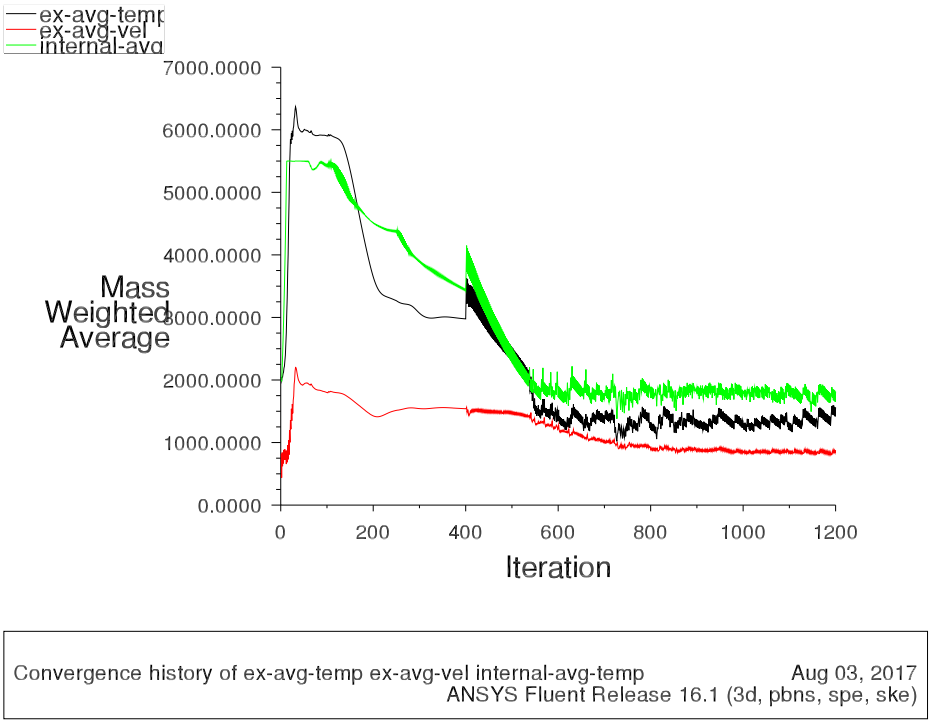

Figure H.19: Convergence history of integral quantities for FiniteRate2StepAmbient case.

H.12. FiniteRate4StepAmbient

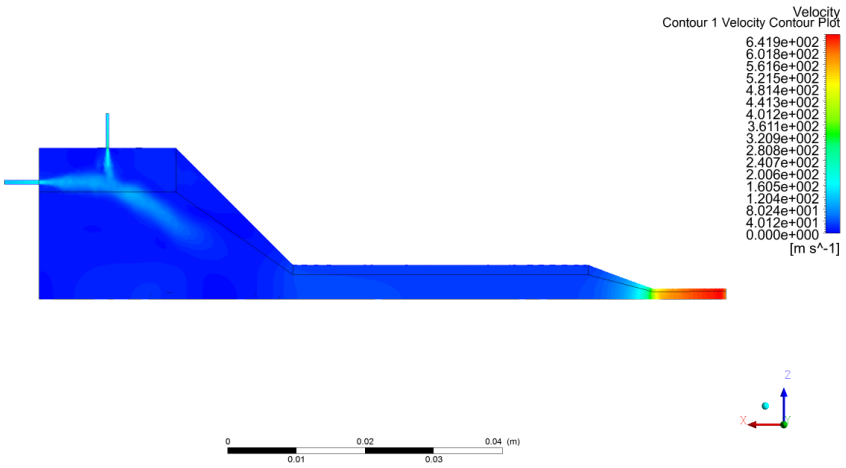

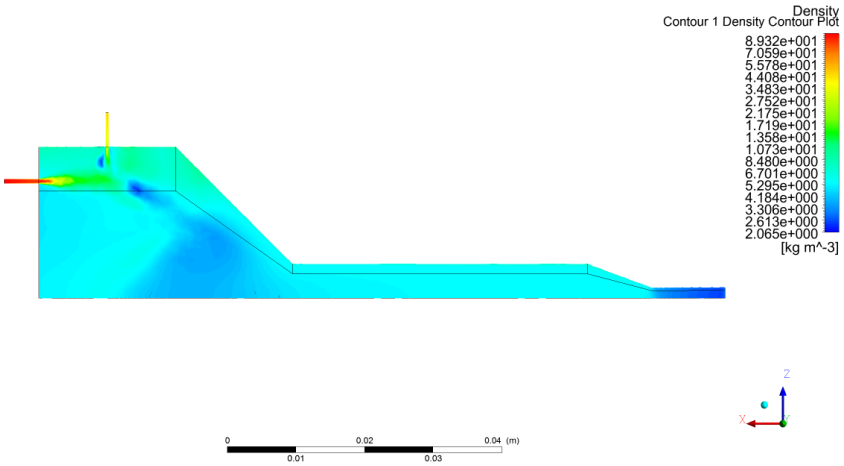
Density
Contour 1 Density Contour Plot
8.932e+001
7.059e+001
5.578e+001
4.408e+001
3.483e+001
2.752e+001
2.175e+001
1.719e+001
1.358e+001
1.073e+001
8.480e+000
6.701e+000
5.295e+000
4.184e+000
3.306e+000
2.613e+000
2.065e+000
[kg m^-3]
Z
X
Y
0
0.02
0.04 (m)
0.01
0.03

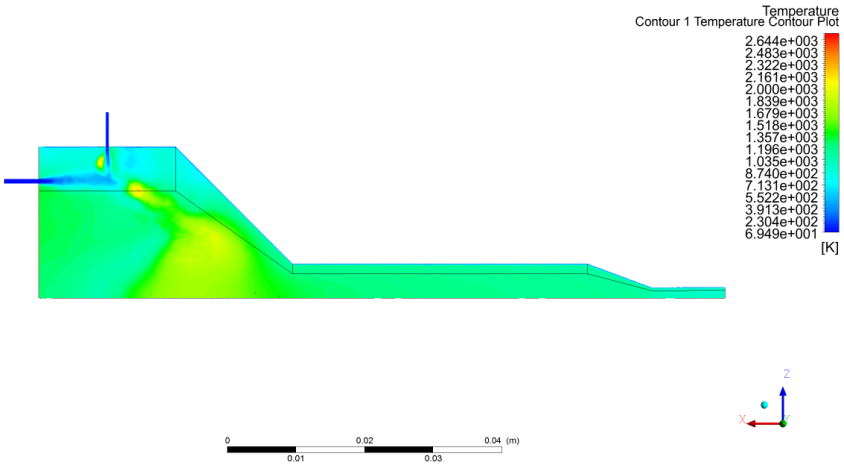
Temperature
Contour 1 Temperature Contour Plot
2.644e+003
2.483e+003
2.322e+003
2.161e+003
2.000e+003
1.839e+003
1.679e+003
1.518e+003
1.357e+003
1.196e+003
1.035e+003
8.740e+002
7.131e+002
5.522e+002
3.913e+002
2.304e+002
6.949e+001
[K]
Z
X
Y
0
0.02
0.04 (m)
0.01
0.03

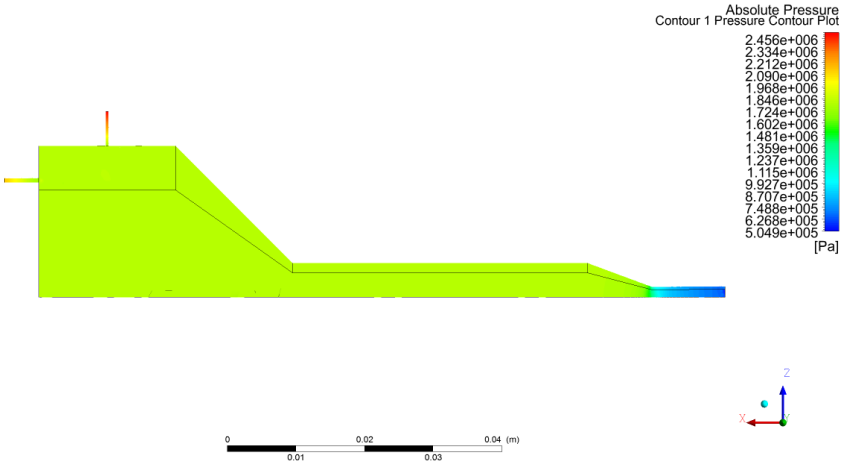
Absolute Pressure
Contour 1 Pressure Contour Plot
2.456e+006
2.334e+006
2.212e+006
2.090e+006
1.968e+006
1.846e+006
1.724e+006
1.602e+006
1.481e+006
1.359e+006
1.237e+006
1.115e+006
9.927e+005
8.707e+005
7.488e+005
6.268e+005
5.049e+005
[Pa]
Z
X
Y
0
0.02
0.04 (m)
0.01
0.03

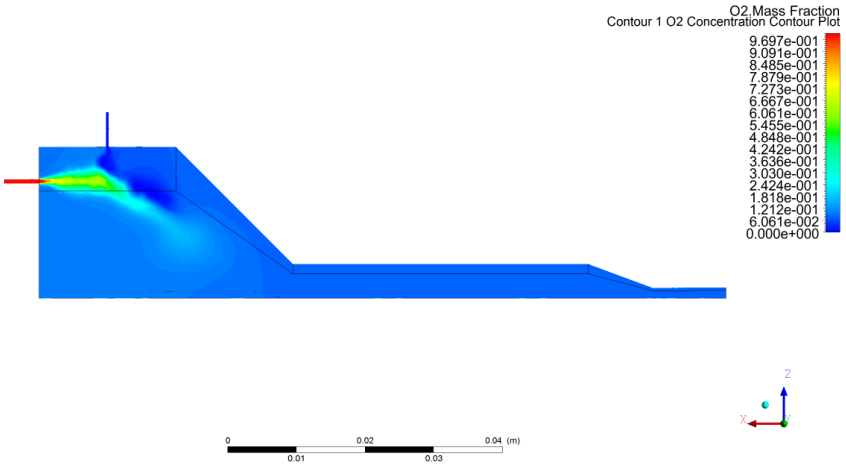
O2.Mass Fraction
Contour 1 O2 Concentration Contour Plot
9.697e-001
9.091e-001
8.485e-001
7.879e-001
7.273e-001
6.667e-001
6.061e-001
5.455e-001
4.848e-001
4.242e-001
3.636e-001
3.030e-001
2.424e-001
1.818e-001
1.212e-001
6.061e-002
0.000e+000
Z
X
Y
0
0.02
0.04 (m)
0.01
0.03

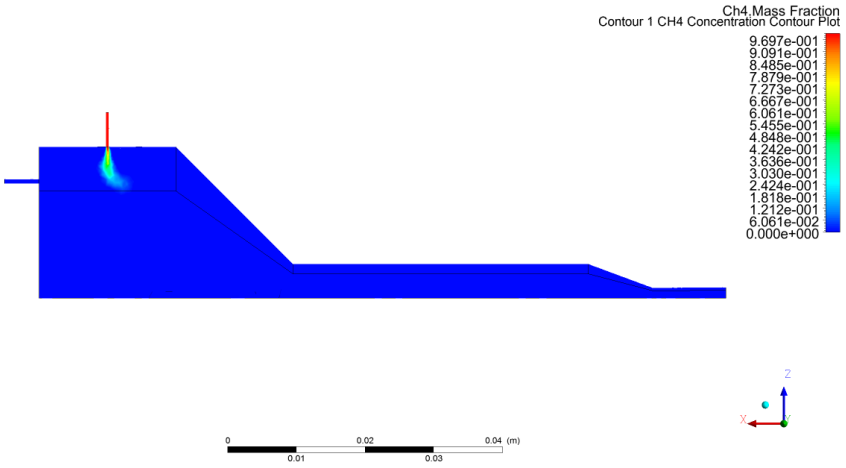
Ch4.Mass Fraction
Contour 1 CH4 Concentration Contour Plot
9.697e-001
9.091e-001
8.485e-001
7.879e-001
7.273e-001
6.667e-001
6.061e-001
5.455e-001
4.848e-001
4.242e-001
3.636e-001
3.030e-001
2.424e-001
1.818e-001
1.212e-001
6.061e-002
0.000e+000
Z
X
Y
0
0.02
0.04 (m)
0.01
0.03

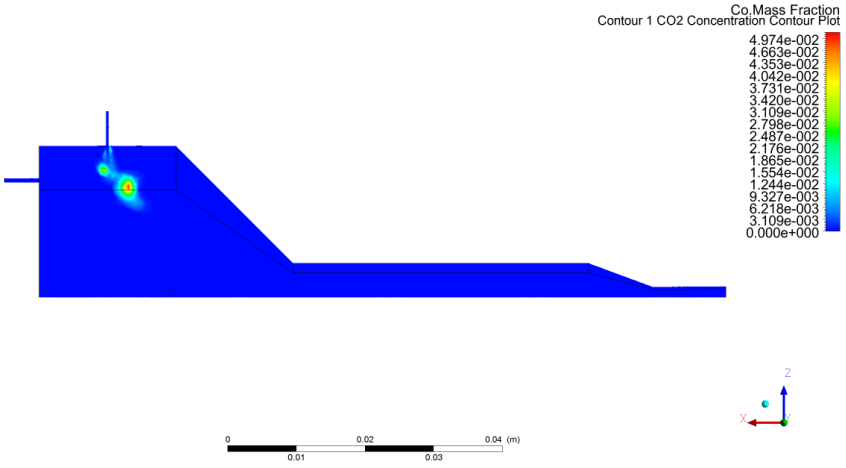
Co.Mass Fraction
Contour 1 CO2 Concentration Contour Plot
4.974e-002
4.663e-002
4.353e-002
4.042e-002
3.731e-002
3.420e-002
3.109e-002
2.798e-002
2.487e-002
2.176e-002
1.865e-002
1.554e-002
1.244e-002
9.327e-003
6.218e-003
3.109e-003
0.000e+000
Z
X
Y
0
0.02
0.04 (m)
0.01
0.03

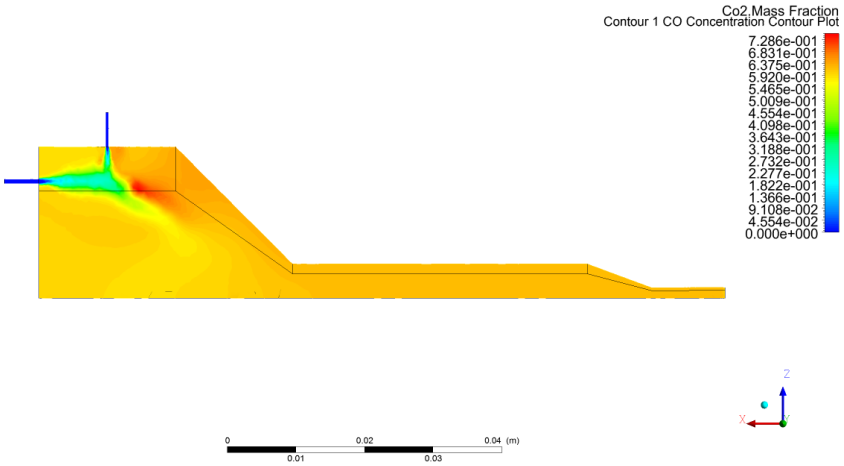
Co2,Mass Fraction
Contour 1 CO Concentration Contour Plot
7.286e-001
6.831e-001
6.375e-001
5.920e-001
5.465e-001
5.009e-001
4.554e-001
4.098e-001
3.643e-001
3.188e-001
2.732e-001
2.277e-001
1.822e-001
1.366e-001
9.108e-002
4.554e-002
0.000e+000
Z
X
Y
0
0.02
0.04 (m)
0.01
0.03

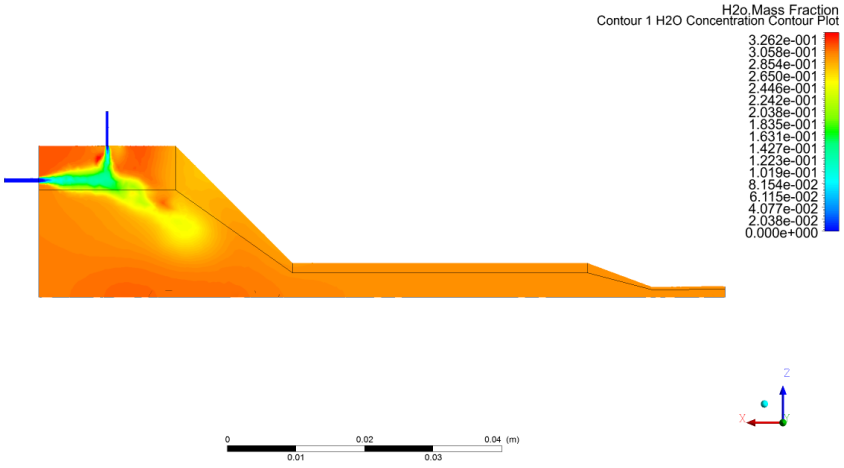
H2o,Mass Fraction
Contour 1 H2O Concentration Contour Plot
3.262e-001
3.058e-001
2.854e-001
2.650e-001
2.446e-001
2.242e-001
2.038e-001
1.835e-001
1.631e-001
1.427e-001
1.223e-001
1.019e-001
8.154e-002
6.115e-002
4.077e-002
2.038e-002
0.000e+000
Z
X
Y
0
0.02
0.04 (m)
0.01
0.03

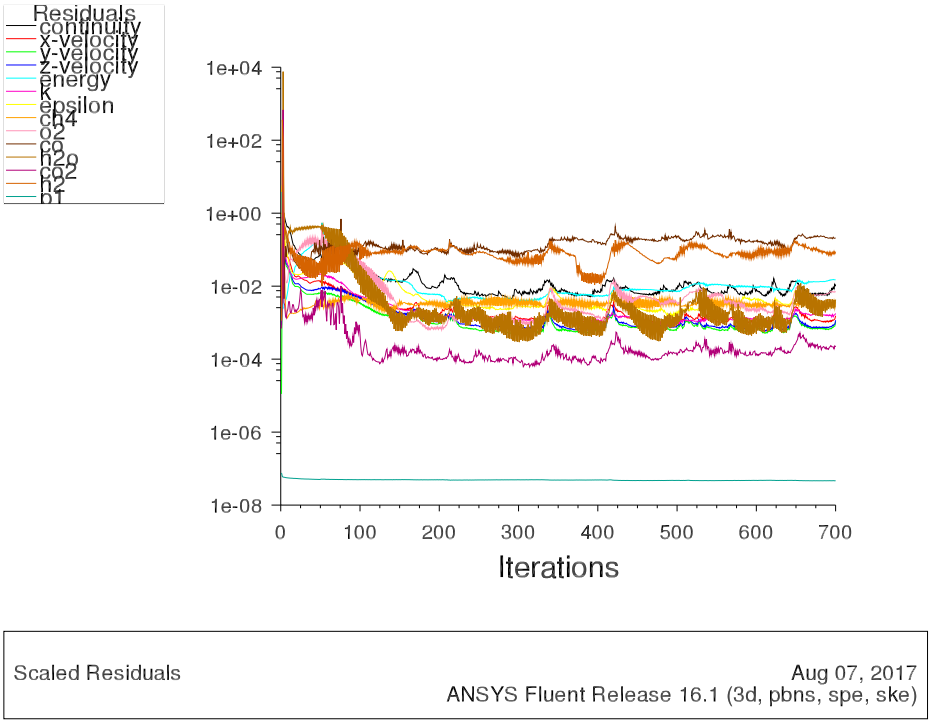

Figure H.20: Convergence history of scaled residuals for FiniteRate4StepAmbient case.

H.13. EDMAmbient

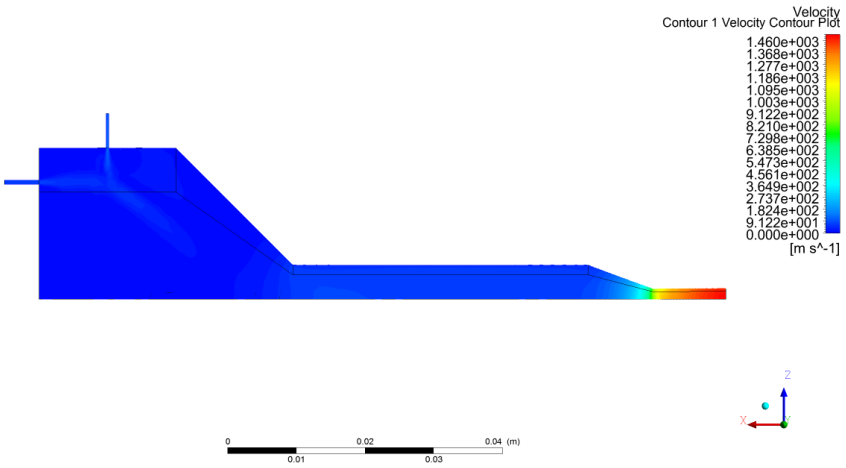

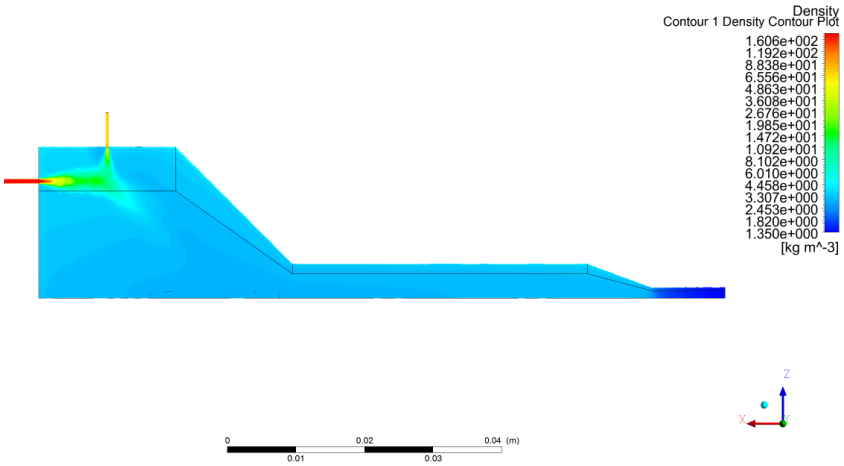
Density
Contour 1 Density Contour Plot
1.606e+002
1.192e+002
8.838e+001
6.556e+001
4.863e+001
3.608e+001
2.676e+001
1.985e+001
1.472e+001
1.092e+001
8.102e+000
6.010e+000
4.458e+000
3.307e+000
2.453e+000
1.820e+000
1.350e+000
[kg m^-3]
Z
X
Y
0
0.02
0.04 (m)
0.01
0.03

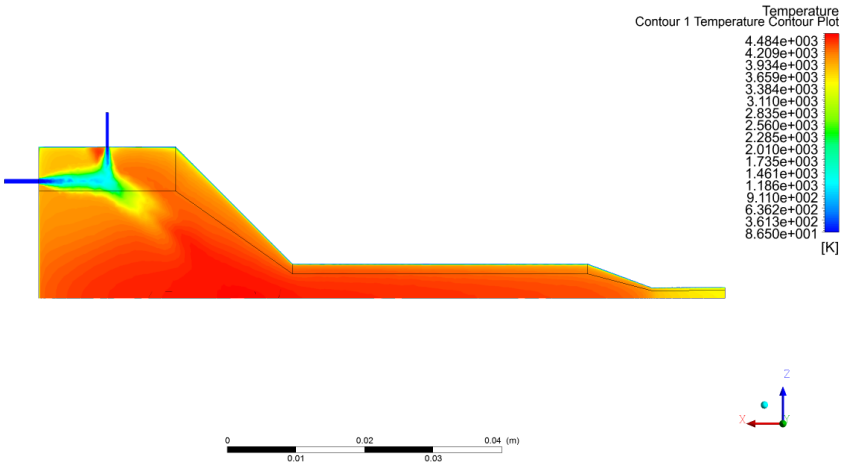
Temperature
Contour 1 Temperature Contour Plot
4.484e+003
4.209e+003
3.934e+003
3.659e+003
3.384e+003
3.110e+003
2.835e+003
2.560e+003
2.285e+003
2.010e+003
1.735e+003
1.461e+003
1.186e+003
9.110e+002
6.362e+002
3.613e+002
8.650e+001
[K]
Z
X
Y
0
0.02
0.04 (m)
0.01
0.03

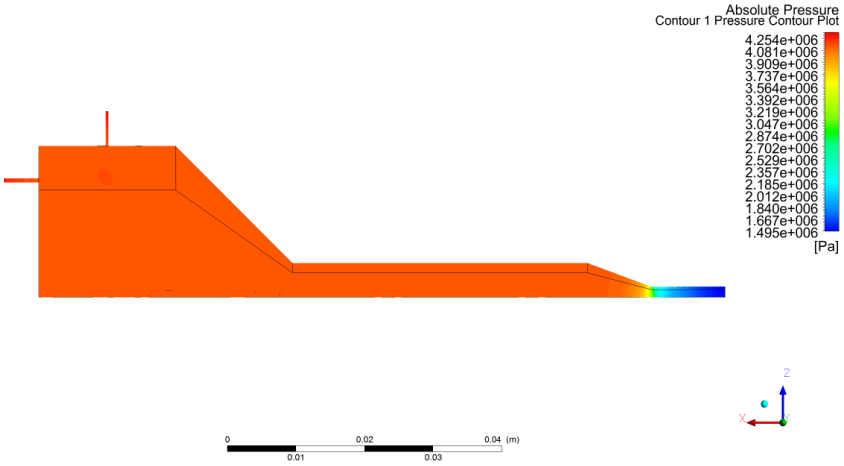
Absolute Pressure
Contour 1 Pressure Contour Plot
4.254e+006
4.081e+006
3.909e+006
3.737e+006
3.564e+006
3.392e+006
3.219e+006
3.047e+006
2.874e+006
2.702e+006
2.529e+006
2.357e+006
2.185e+006
2.012e+006
1.840e+006
1.667e+006
1.495e+006
[Pa]
Z
X
Y
0
0.02
0.04 (m)
0.01
0.03

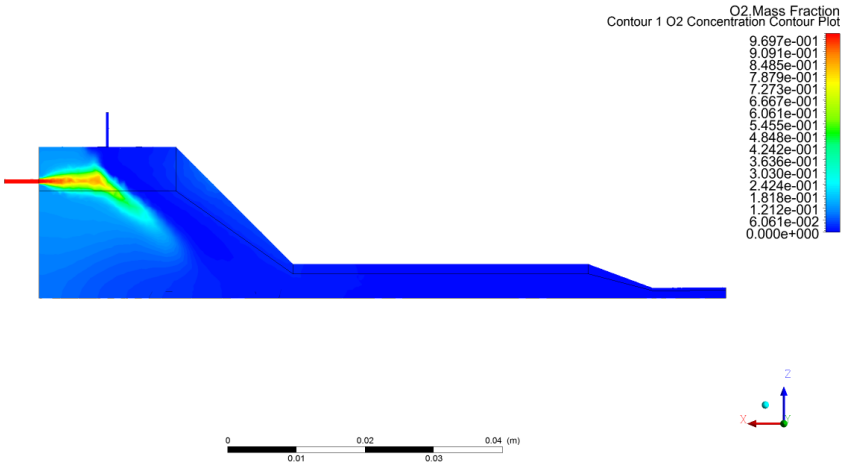
O2.Mass Fraction
Contour 1 O2 Concentration Contour Plot
9.697e-001
9.091e-001
8.485e-001
7.879e-001
7.273e-001
6.667e-001
6.061e-001
5.455e-001
4.848e-001
4.242e-001
3.636e-001
3.030e-001
2.424e-001
1.818e-001
1.212e-001
6.061e-002
0.000e+000
Z
X
Y
0
0.02
0.04 (m)
0.01
0.03

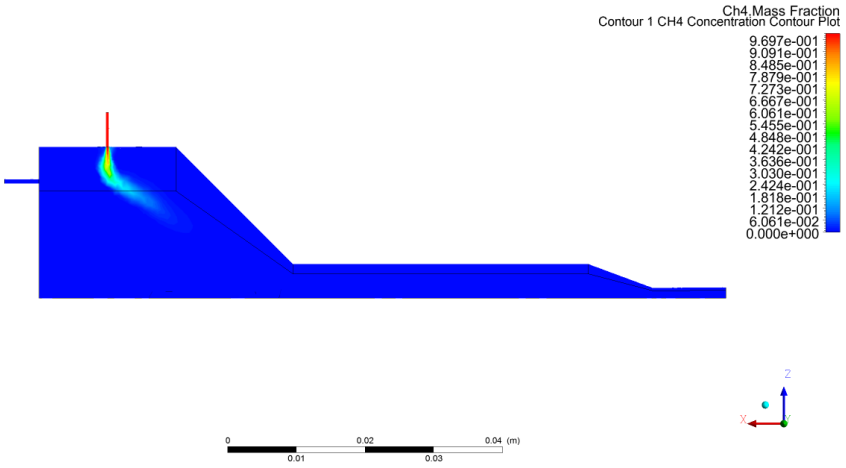
Ch4.Mass Fraction
Contour 1 CH4 Concentration Contour Plot
9.697e-001
9.091e-001
8.485e-001
7.879e-001
7.273e-001
6.667e-001
6.061e-001
5.455e-001
4.848e-001
4.242e-001
3.636e-001
3.030e-001
2.424e-001
1.818e-001
1.212e-001
6.061e-002
0.000e+000
Z
X
Y
0
0.02
0.04 (m)
0.01
0.03

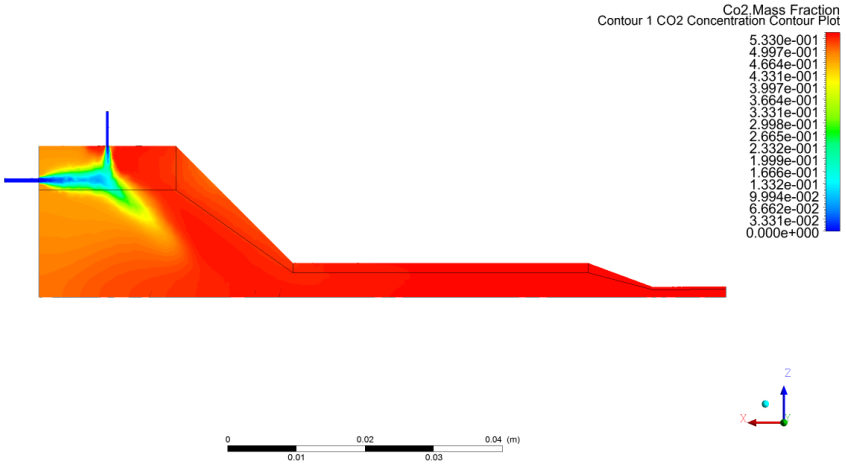
Co2.Mass Fraction
Contour 1 CO2 Concentration Contour Plot
5.330e-001
4.997e-001
4.664e-001
4.331e-001
3.997e-001
3.664e-001
3.331e-001
2.998e-001
2.665e-001
2.332e-001
1.999e-001
1.666e-001
1.332e-001
9.994e-002
6.662e-002
3.331e-002
0.000e+000
Z
X
Y
0
0.02
0.04 (m)
0.01
0.03

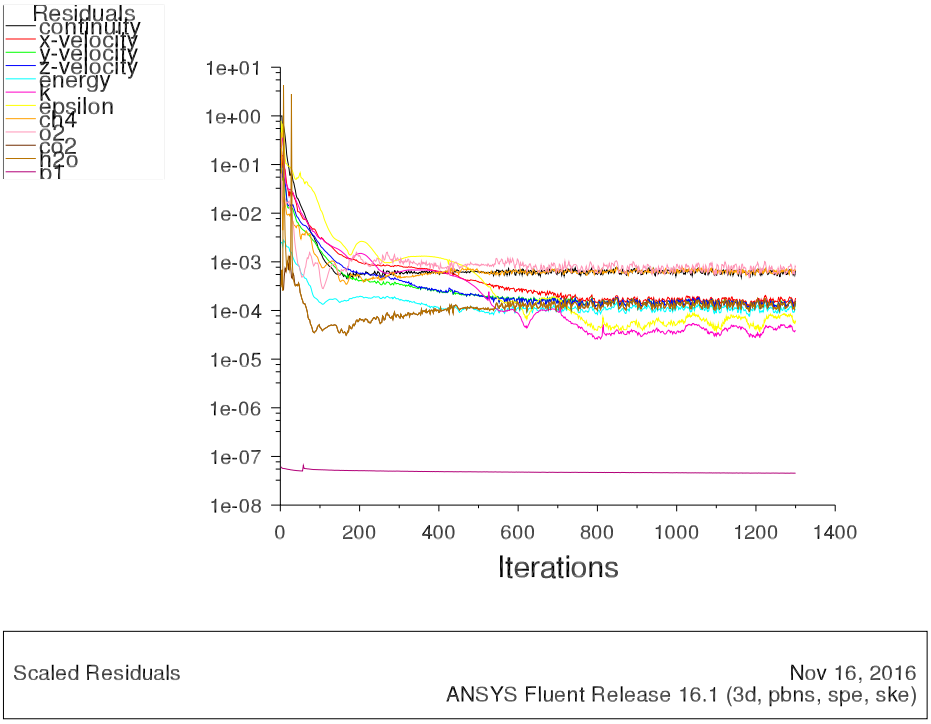

Figure H.21: Convergence history of scaled residuals for EDMAmbient case.

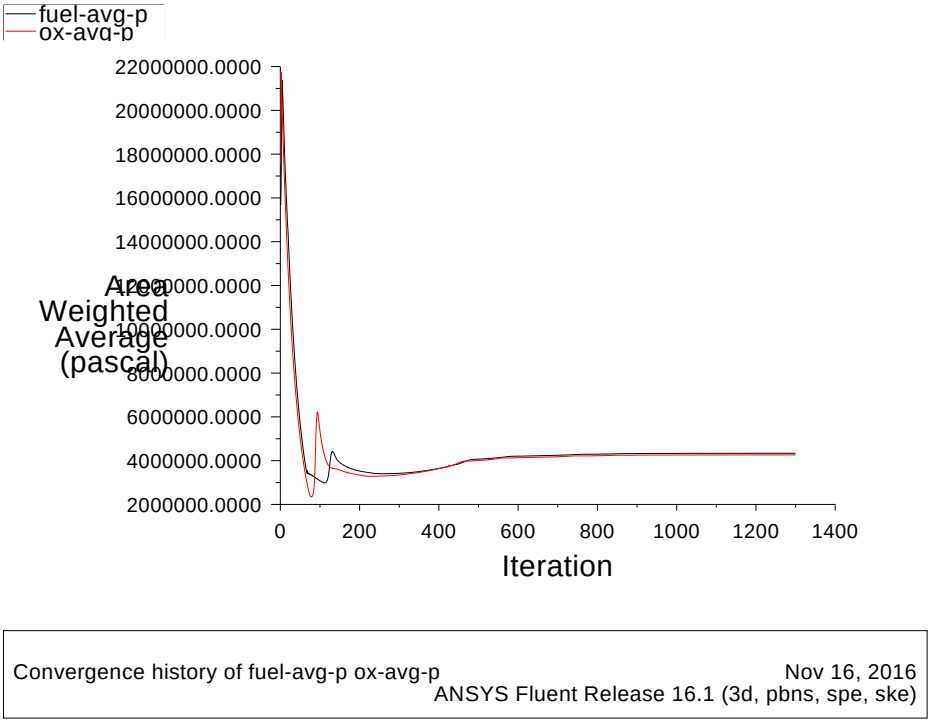

Figure H.22: Convergence history of integral quantities for EDMAmbient case.

H.14. EDMAmbientNoRadiation

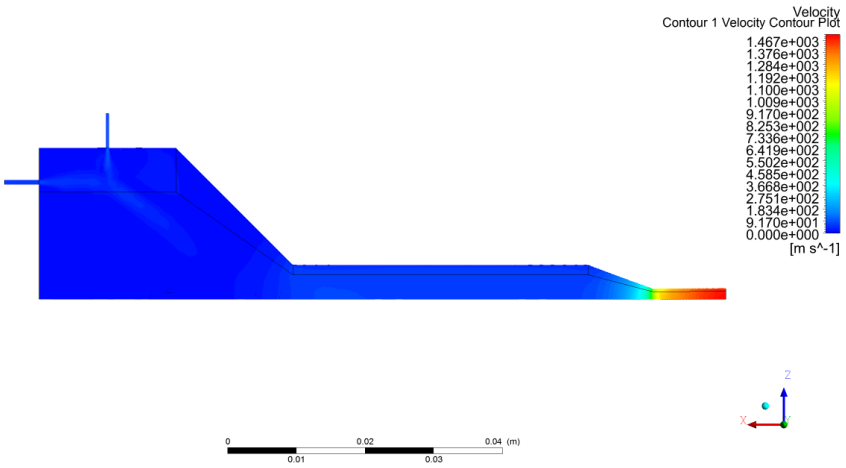

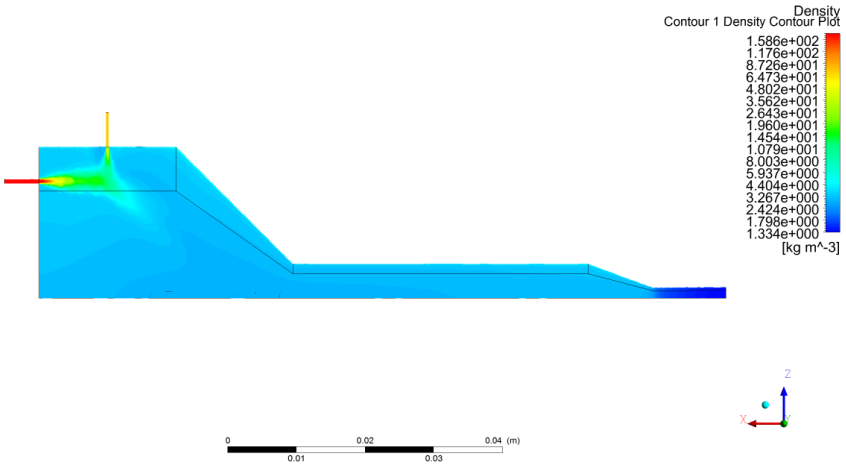

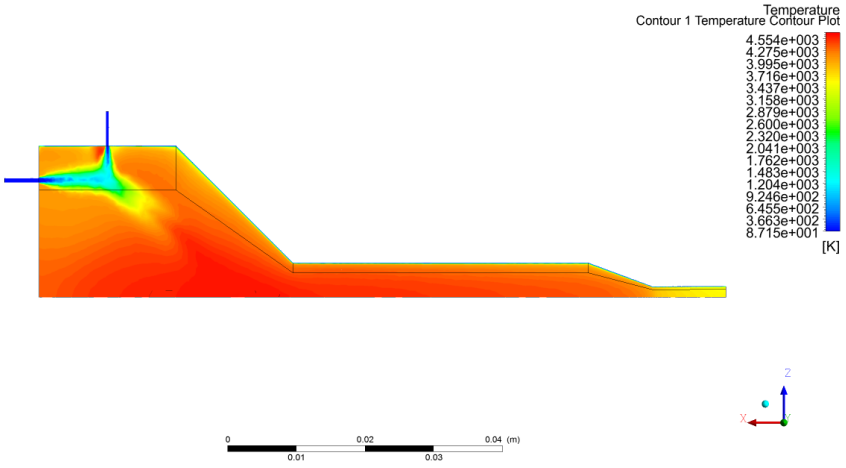

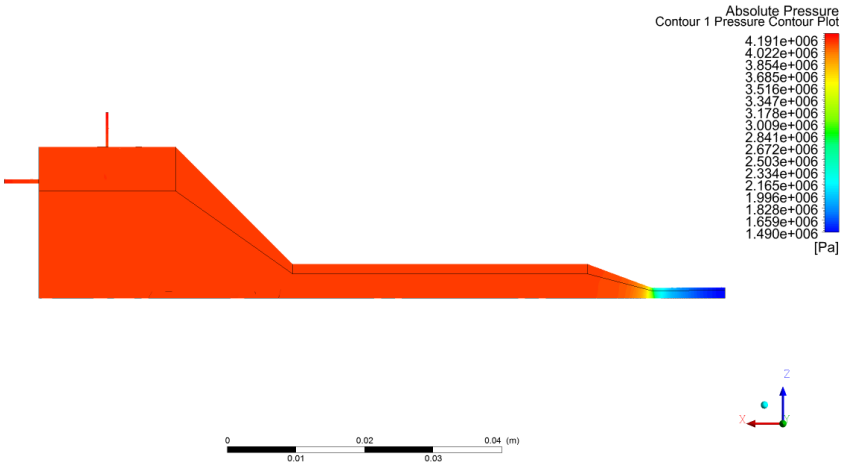
Absolute Pressure
Contour 1 Pressure Contour Plot
4.191e+006
4.022e+006
3.854e+006
3.685e+006
3.516e+006
3.347e+006
3.178e+006
3.009e+006
2.841e+006
2.672e+006
2.503e+006
2.334e+006
2.165e+006
1.996e+006
1.828e+006
1.659e+006
1.490e+006
[Pa]
0
0.02
0.04 (m)
0.01
0.03

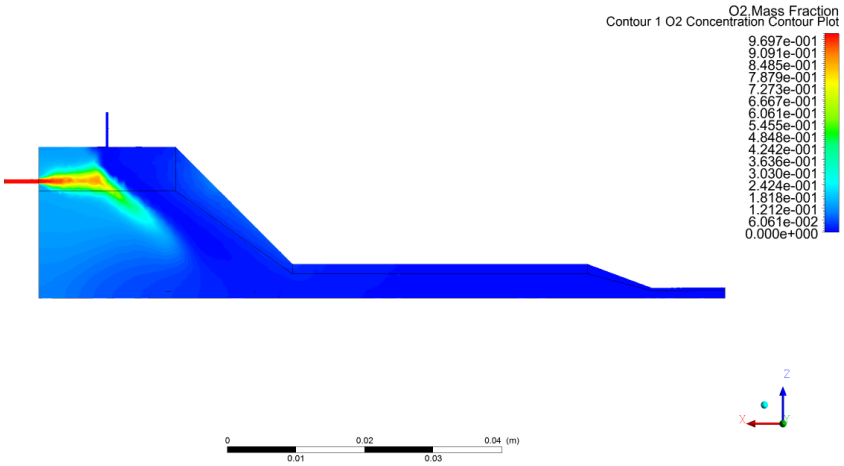
O2.Mass Fraction
Contour 1 O2 Concentration Contour Plot
9.697e-001
9.091e-001
8.485e-001
7.879e-001
7.273e-001
6.667e-001
6.061e-001
5.455e-001
4.848e-001
4.242e-001
3.636e-001
3.030e-001
2.424e-001
1.818e-001
1.212e-001
6.061e-002
0.000e+000
0
0.02
0.04 (m)
0.01
0.03

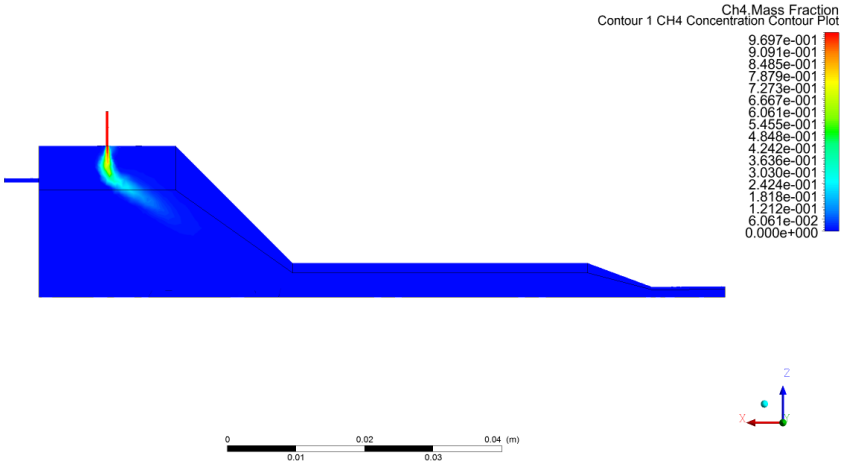
Ch4.Mass Fraction
Contour 1 CH4 Concentration Contour Plot
9.697e-001
9.091e-001
8.485e-001
7.879e-001
7.273e-001
6.667e-001
6.061e-001
5.455e-001
4.848e-001
4.242e-001
3.636e-001
3.030e-001
2.424e-001
1.818e-001
1.212e-001
6.061e-002
0.000e+000
0
0.02
0.04 (m)
0.01
0.03

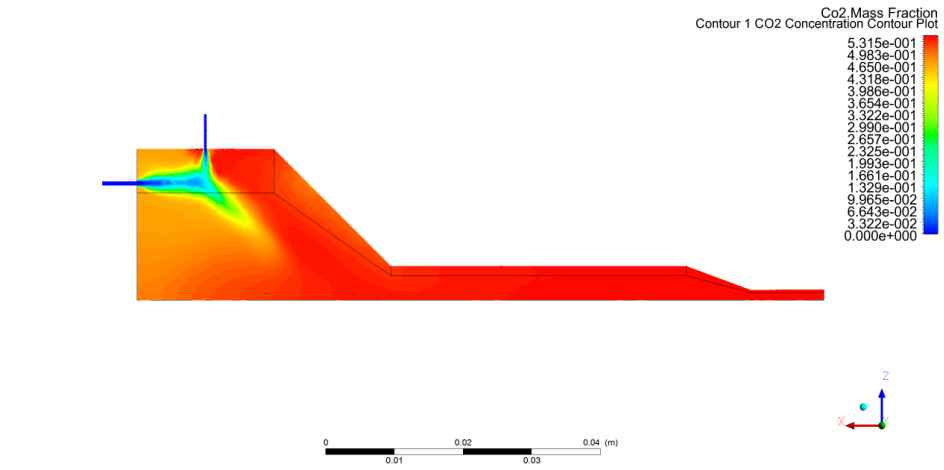

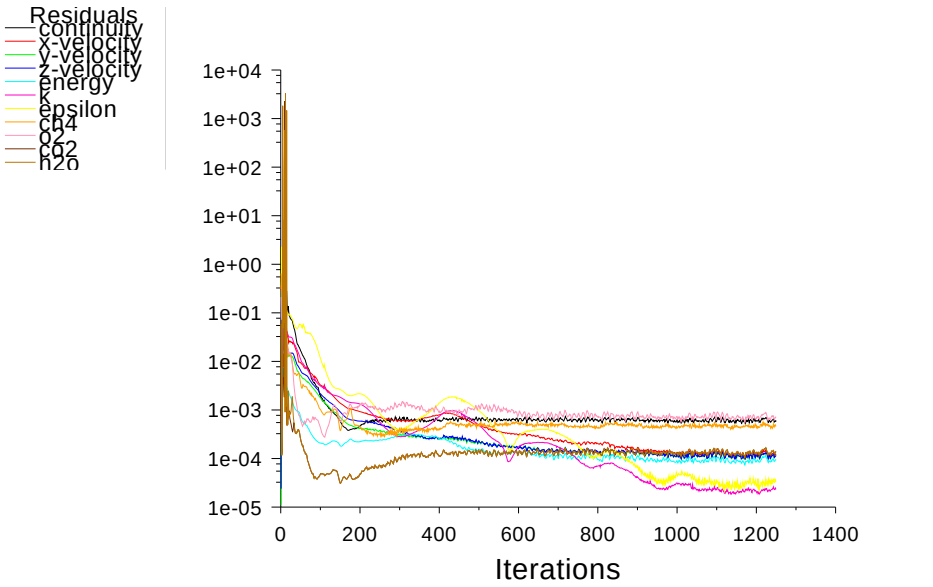

Scaled Residuals

Jun 11, 2017
ANSYS Fluent Release 16.1 (3d, pbns, spe, ske)

Figure H.23: Convergence history of scaled residuals for EDMAmbientNoRad case.

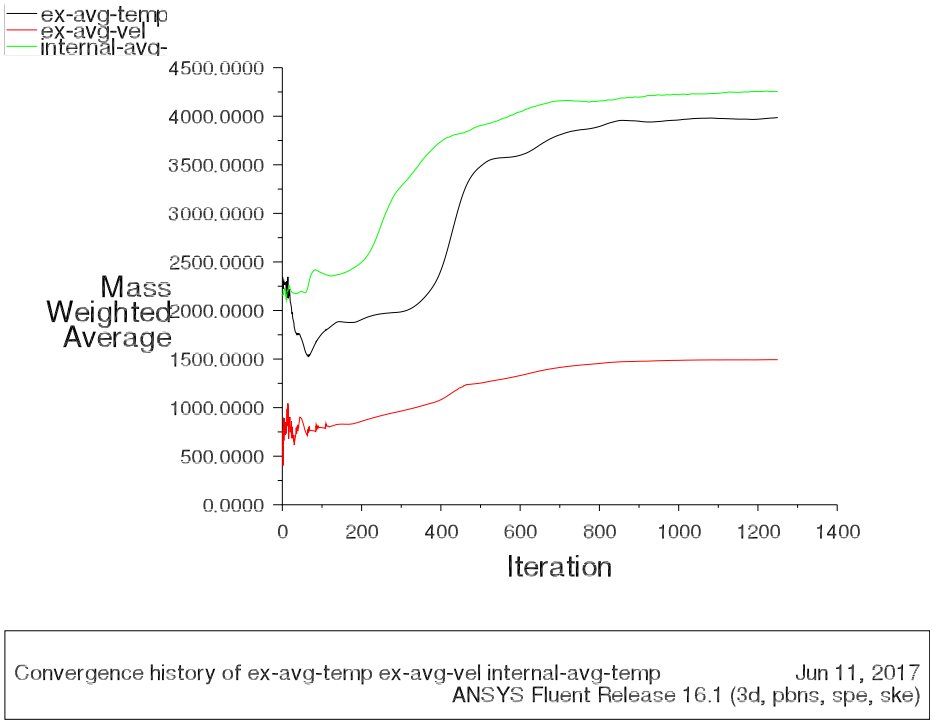

Figure H.24: Convergence history of integral quantities for EDMAmbientNoRad case.

H.15. EDMPressure

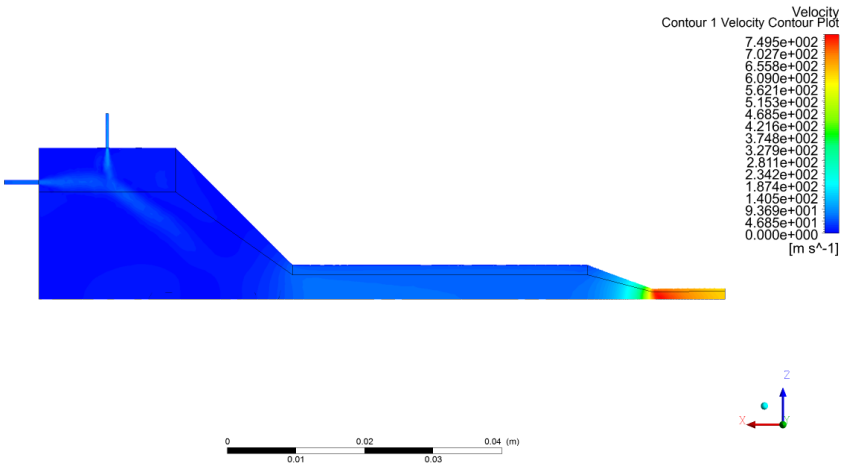

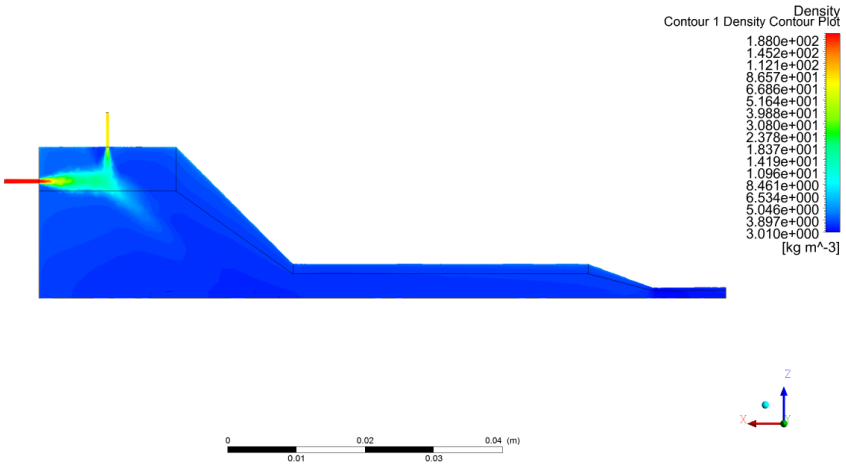
Density
Contour 1 Density Contour Plot
1.880e+002
1.452e+002
1.121e+002
8.657e+001
6.686e+001
5.164e+001
3.988e+001
3.080e+001
2.378e+001
1.837e+001
1.419e+001
1.096e+001
8.461e+000
6.534e+000
5.046e+000
3.897e+000
3.010e+000
[kg m^-3]
Z
X
Y
0
0.02
0.04 (m)
0.01
0.03

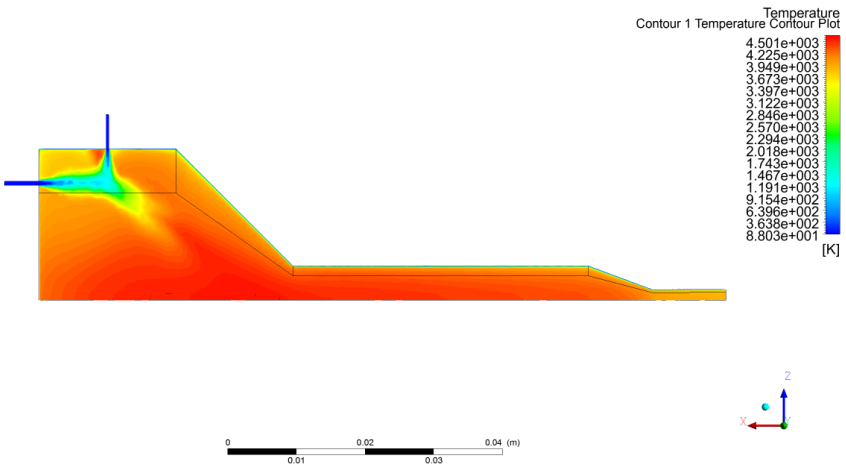
Temperature
Contour 1 Temperature Contour Plot
4.501e+003
4.225e+003
3.949e+003
3.673e+003
3.397e+003
3.122e+003
2.846e+003
2.570e+003
2.294e+003
2.018e+003
1.743e+003
1.467e+003
1.191e+003
9.154e+002
6.396e+002
3.638e+002
8.803e+001
[K]
Z
X
Y
0
0.02
0.04 (m)
0.01
0.03

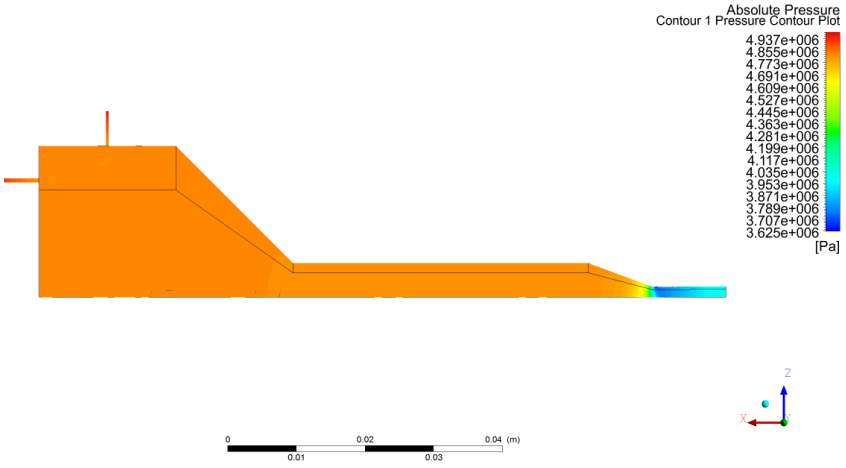
Absolute Pressure
Contour 1 Pressure Contour Plot
4.937e+006
4.855e+006
4.773e+006
4.691e+006
4.609e+006
4.527e+006
4.445e+006
4.363e+006
4.281e+006
4.199e+006
4.117e+006
4.035e+006
3.953e+006
3.871e+006
3.789e+006
3.707e+006
3.625e+006
[Pa]
Z
X
Y
0
0.02
0.04 (m)
0.01
0.03

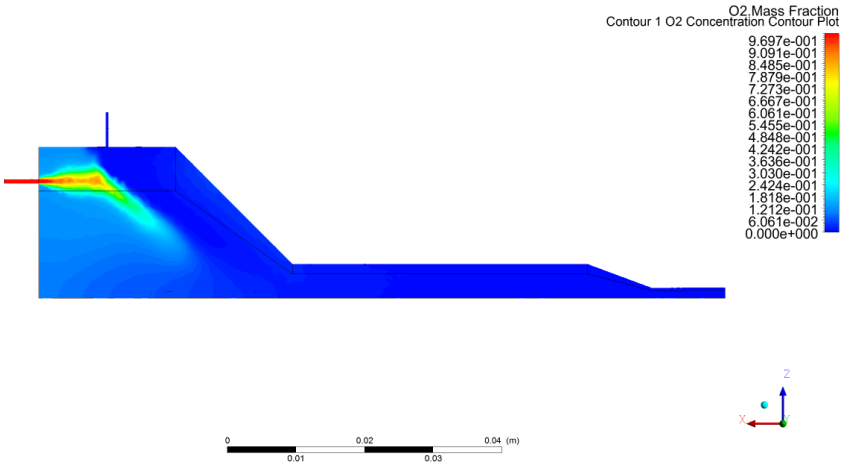
O2,Mass Fraction
Contour 1 O2 Concentration Contour Plot
9.697e-001
9.091e-001
8.485e-001
7.879e-001
7.273e-001
6.667e-001
6.061e-001
5.455e-001
4.848e-001
4.242e-001
3.636e-001
3.030e-001
2.424e-001
1.818e-001
1.212e-001
6.061e-002
0.000e+000
Z
X
Y
0
0.02
0.04 (m)
0.01
0.03

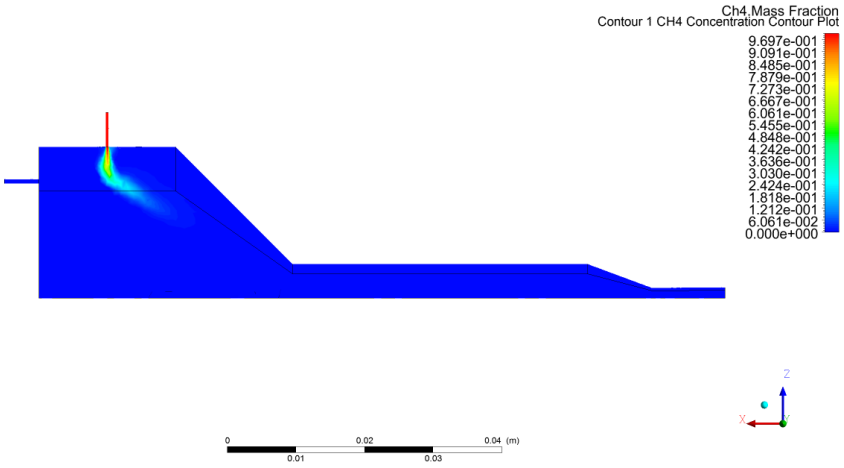
Ch4,Mass Fraction
Contour 1 CH4 Concentration Contour Plot
9.697e-001
9.091e-001
8.485e-001
7.879e-001
7.273e-001
6.667e-001
6.061e-001
5.455e-001
4.848e-001
4.242e-001
3.636e-001
3.030e-001
2.424e-001
1.818e-001
1.212e-001
6.061e-002
0.000e+000
Z
X
Y
0
0.02
0.04 (m)
0.01
0.03

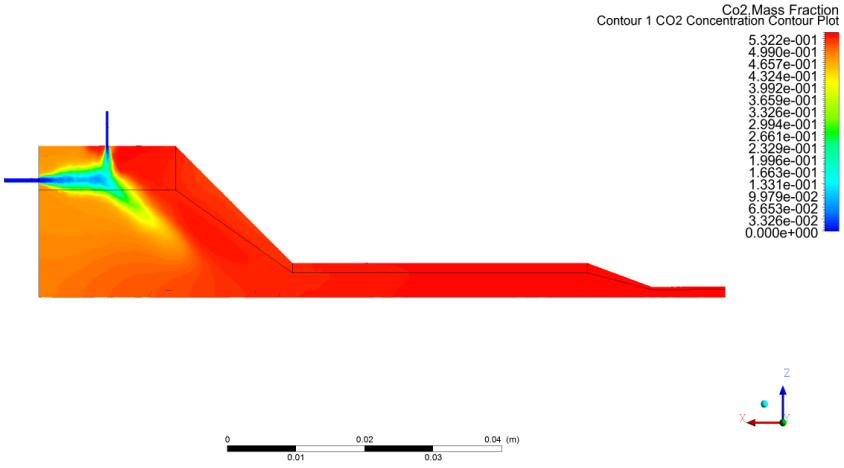
Co2,Mass Fraction
Contour 1 CO2 Concentration Contour Plot
5.322e-001
4.990e-001
4.657e-001
4.324e-001
3.992e-001
3.659e-001
3.326e-001
2.994e-001
2.661e-001
2.329e-001
1.996e-001
1.663e-001
1.331e-001
9.979e-002
6.653e-002
3.326e-002
0.000e+000
Z
X
Y
0
0.02
0.04 (m)
0.01
0.03

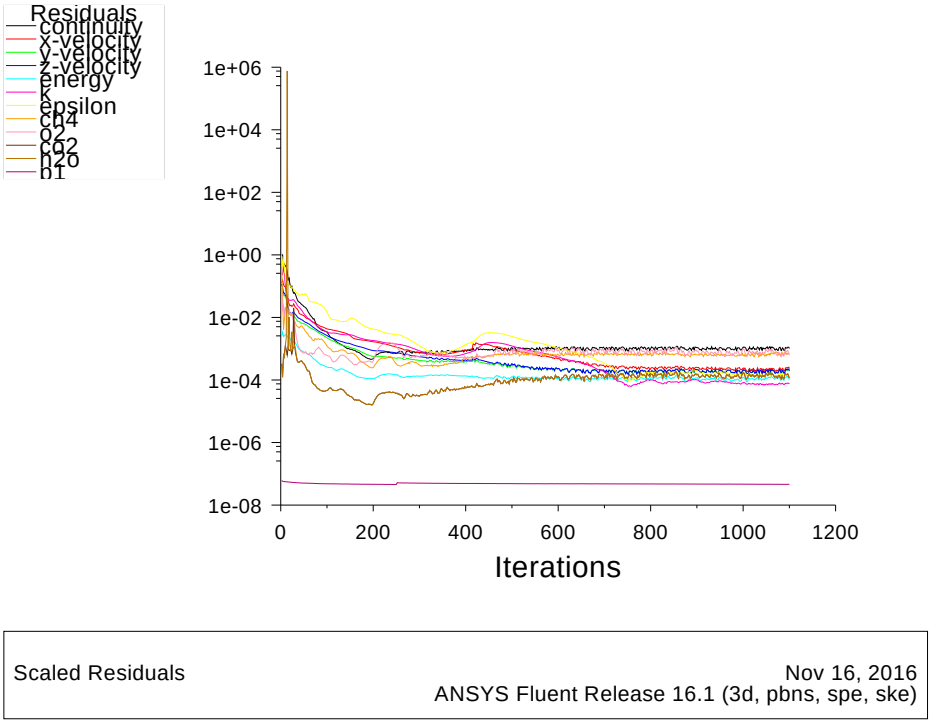

Figure H.25: Convergence history of scaled residuals for EDMPressure case.

H.16. EdcWd1StepAmbient

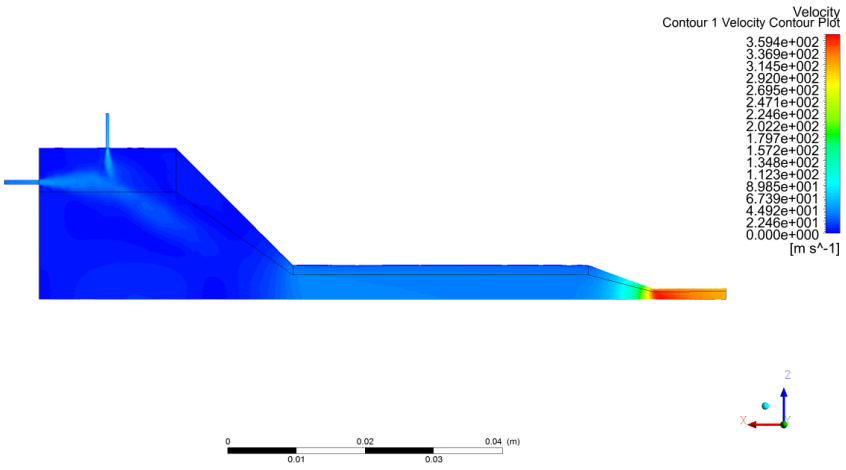

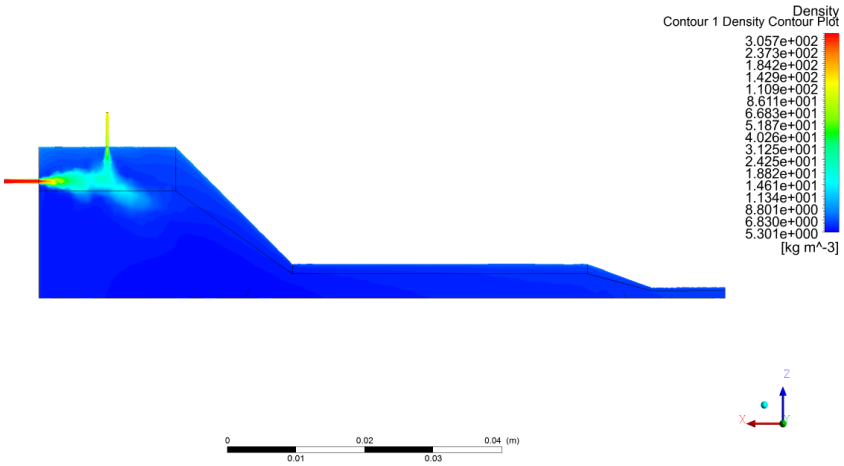
Density
Contour 1 Density Contour Plot
3.057e+002
2.373e+002
1.842e+002
1.429e+002
1.109e+002
8.611e+001
6.683e+001
5.187e+001
4.026e+001
3.125e+001
2.425e+001
1.882e+001
1.461e+001
1.134e+001
8.801e+000
6.830e+000
5.301e+000
[kg m^-3]
Z
X
Y
0
0.02
0.04 (m)
0.01
0.03

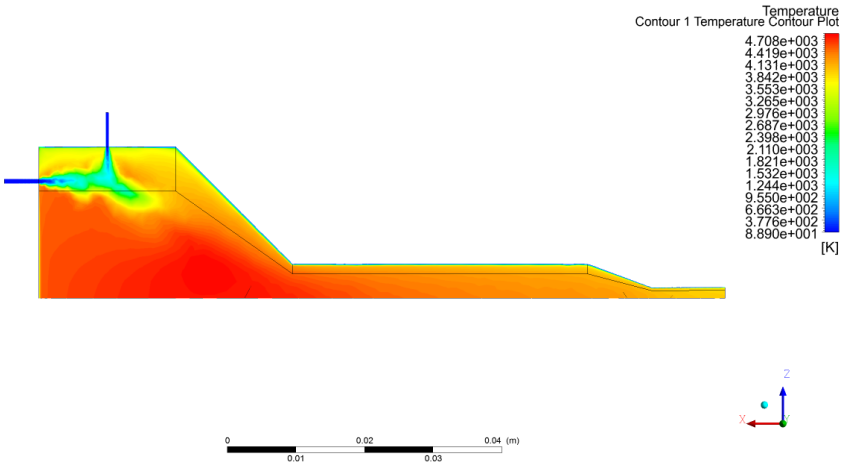
Temperature
Contour 1 Temperature Contour Plot
4.708e+003
4.419e+003
4.131e+003
3.842e+003
3.553e+003
3.265e+003
2.976e+003
2.687e+003
2.398e+003
2.110e+003
1.821e+003
1.532e+003
1.244e+003
9.550e+002
6.663e+002
3.776e+002
8.890e+001
[K]
Z
X
Y
0
0.02
0.04 (m)
0.01
0.03

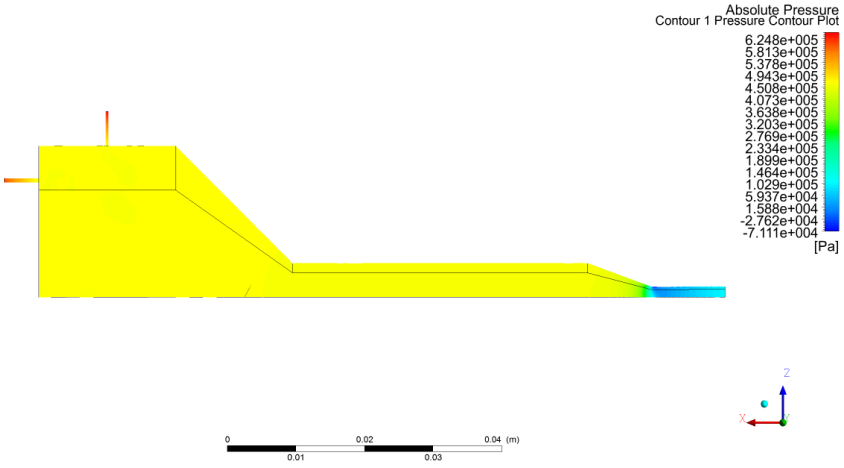
Absolute Pressure
Contour 1 Pressure Contour Plot
6.248e+005
5.813e+005
5.378e+005
4.943e+005
4.508e+005
4.073e+005
3.638e+005
3.203e+005
2.769e+005
2.334e+005
1.899e+005
1.464e+005
1.029e+005
5.937e+004
1.588e+004
-2.762e+004
-7.111e+004
[Pa]
Z
X
Y
0
0.02
0.04 (m)
0.01
0.03

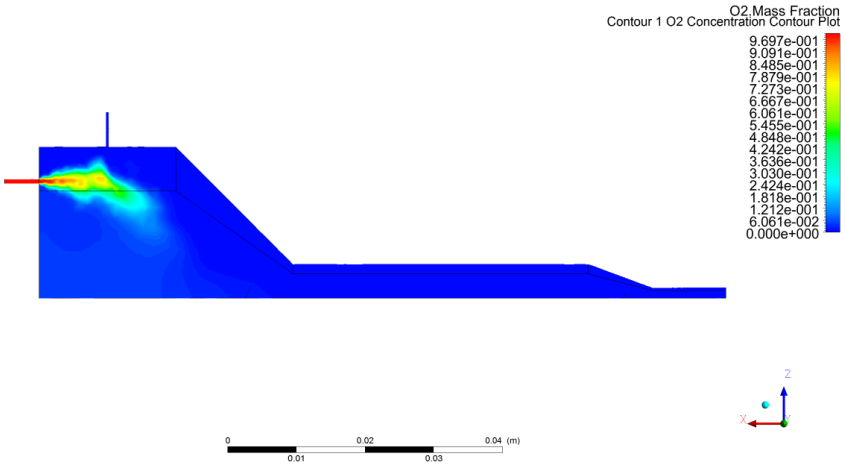
O2.Mass Fraction
Contour 1 O2 Concentration Contour Plot
9.697e-001
9.091e-001
8.485e-001
7.879e-001
7.273e-001
6.667e-001
6.061e-001
5.455e-001
4.848e-001
4.242e-001
3.636e-001
3.030e-001
2.424e-001
1.818e-001
1.212e-001
6.061e-002
0.000e+000
Z
Y
X
0
0.02
0.04 (m)
0.01
0.03

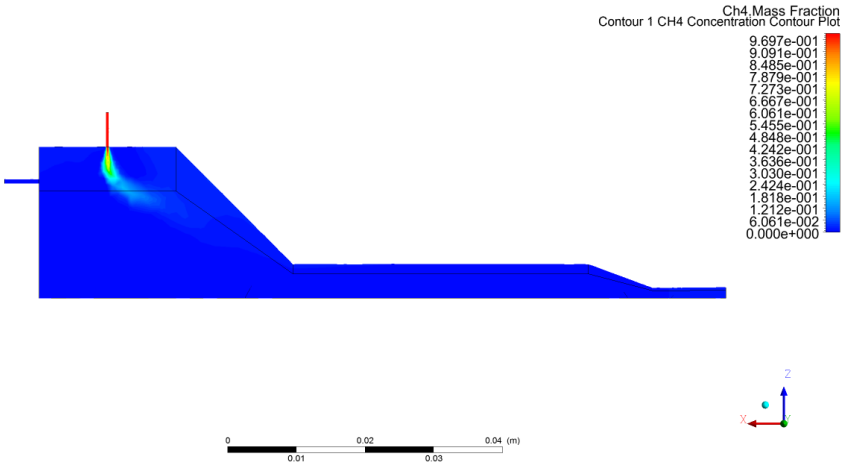
Ch4.Mass Fraction
Contour 1 CH4 Concentration Contour Plot
9.697e-001
9.091e-001
8.485e-001
7.879e-001
7.273e-001
6.667e-001
6.061e-001
5.455e-001
4.848e-001
4.242e-001
3.636e-001
3.030e-001
2.424e-001
1.818e-001
1.212e-001
6.061e-002
0.000e+000
Z
Y
X
0
0.02
0.04 (m)
0.01
0.03

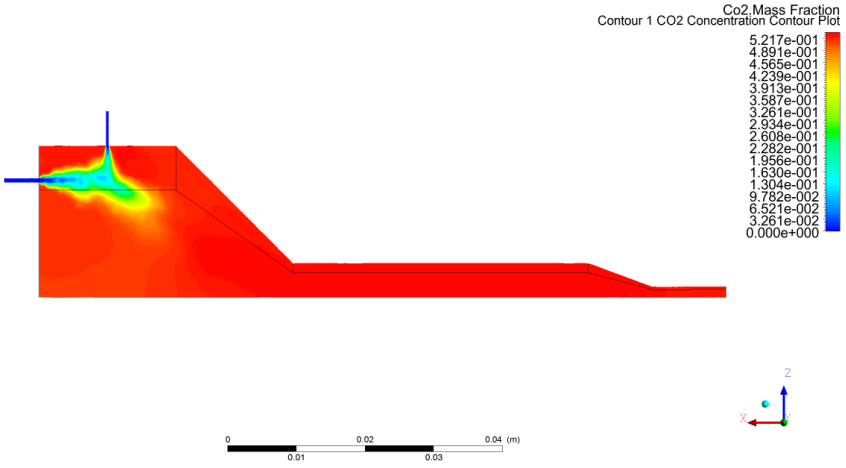
Co2.Mass Fraction
Contour 1 CO2 Concentration Contour Plot
5.217e-001
4.891e-001
4.565e-001
4.239e-001
3.913e-001
3.587e-001
3.261e-001
2.934e-001
2.608e-001
2.282e-001
1.956e-001
1.630e-001
1.304e-001
9.782e-002
6.521e-002
3.261e-002
0.000e+000
Z
Y
X
0
0.02
0.04 (m)
0.01
0.03

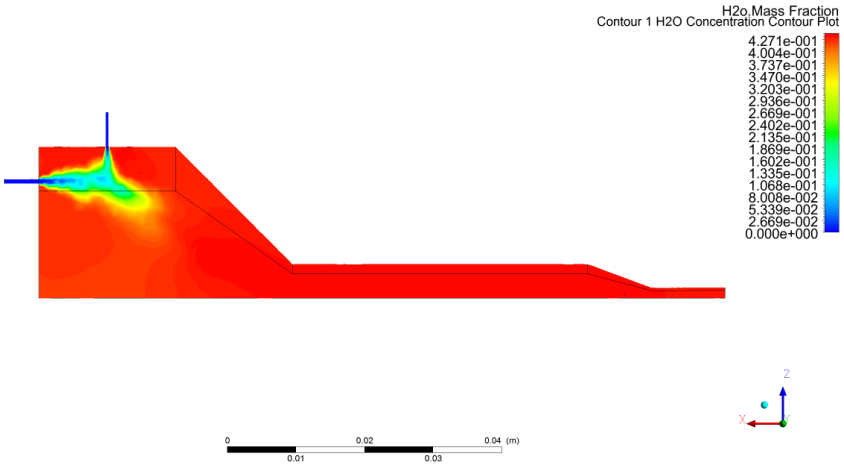
H2o.Mass Fraction
Contour 1 H2O Concentration Contour Plot
4.271e-001
4.004e-001
3.737e-001
3.470e-001
3.203e-001
2.936e-001
2.669e-001
2.402e-001
2.135e-001
1.869e-001
1.602e-001
1.335e-001
1.068e-001
8.008e-002
5.339e-002
2.669e-002
0.000e+000
Z
X
Y
0
0.02
0.04 (m)
0.01
0.03

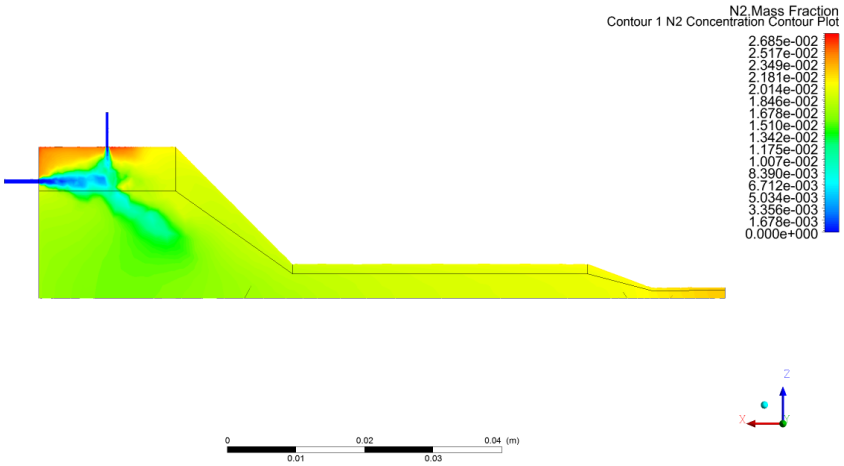
N2.Mass Fraction
Contour 1 N2 Concentration Contour Plot
2.685e-002
2.517e-002
2.349e-002
2.181e-002
2.014e-002
1.846e-002
1.678e-002
1.510e-002
1.342e-002
1.175e-002
1.007e-002
8.390e-003
6.712e-003
5.034e-003
3.356e-003
1.678e-003
0.000e+000
Z
X
Y
0
0.02
0.04 (m)
0.01
0.03

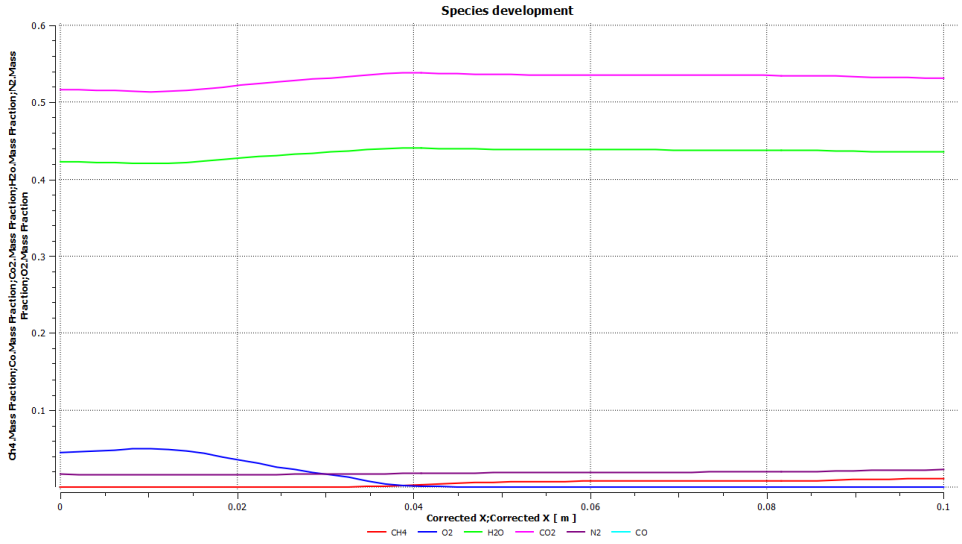
Species development
Ch4.Mass Fraction;Co.Mass Fraction;Co2.Mass Fraction;H2o.Mass Fraction;N2.Mass Fraction;O2.Mass Fraction
0.6
0.5
0.4
0.3
0.2
0.1
0
0.02
0.04
0.06
0.08
0.1
Corrected X;Corrected X [m]
CH4
O2
H2O
CO2
N2
CO

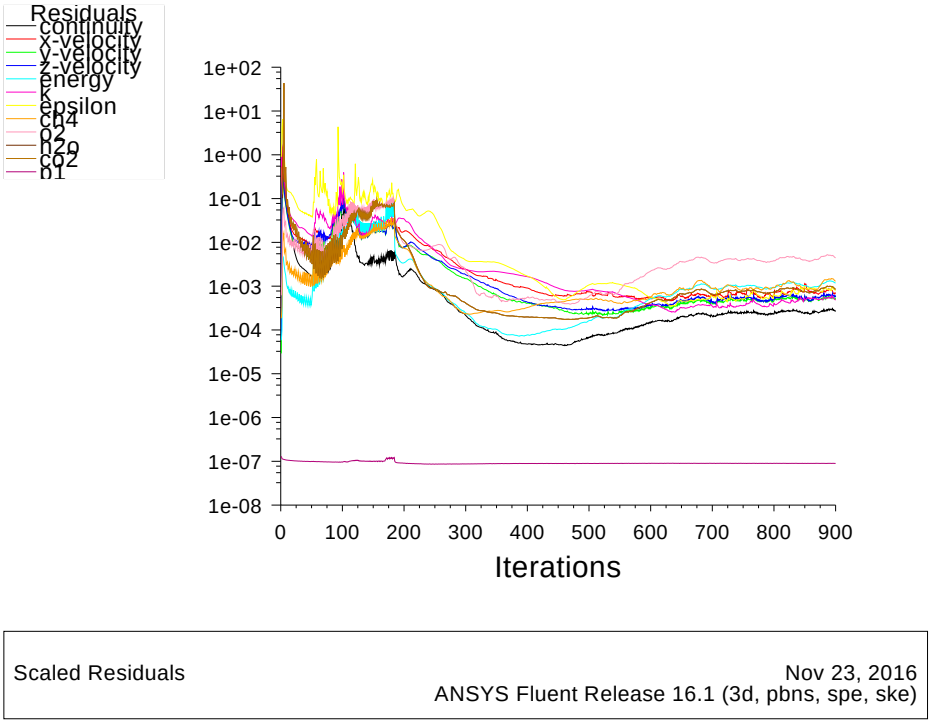

Figure H.26: Convergence history of scaled residuals for EdcWd1StepAmbient case.

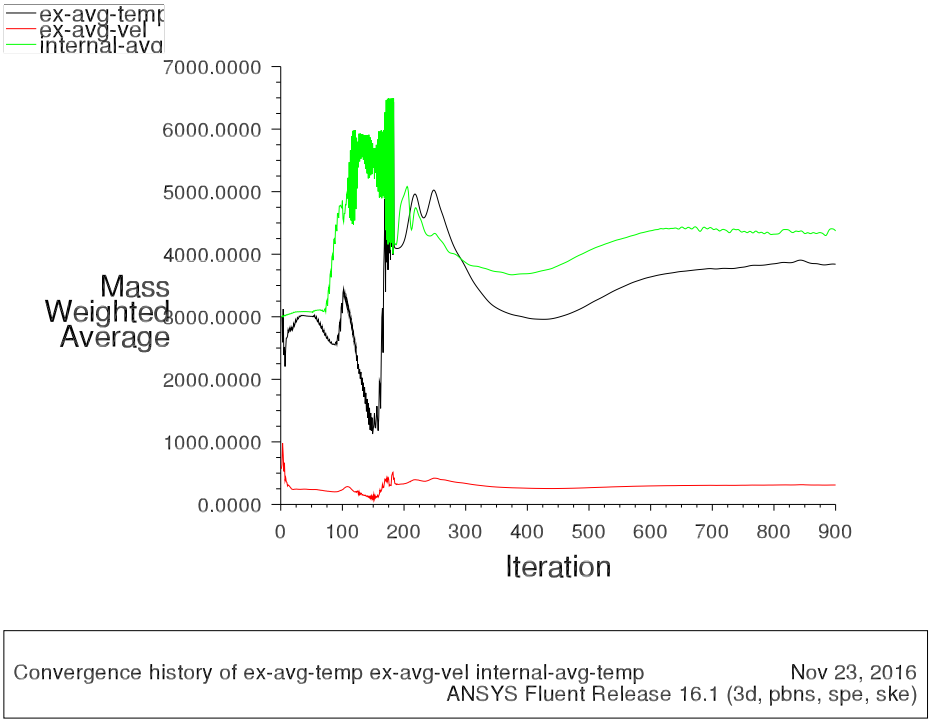

Figure H.27: Convergence history of integral quantities for EdcWd1StepAmbient case.

H.17. EdcWd2StepAmbient

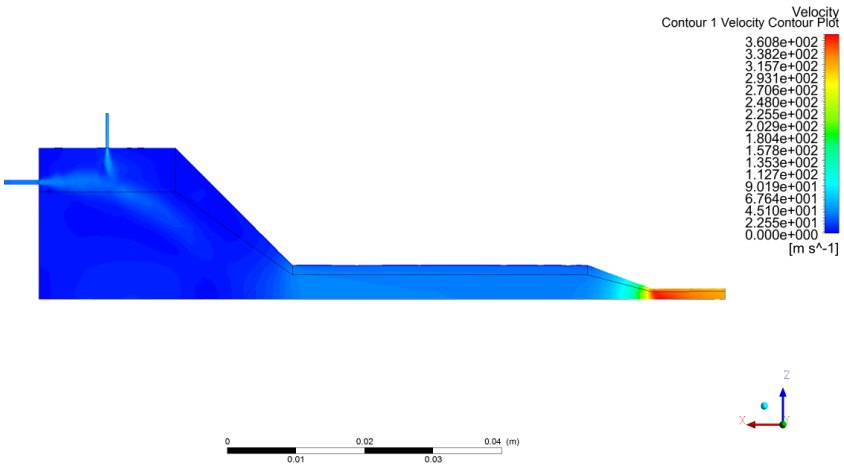

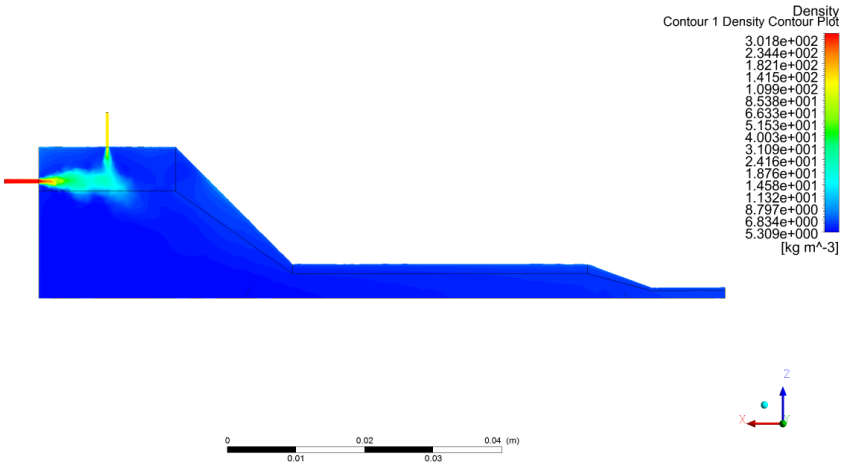

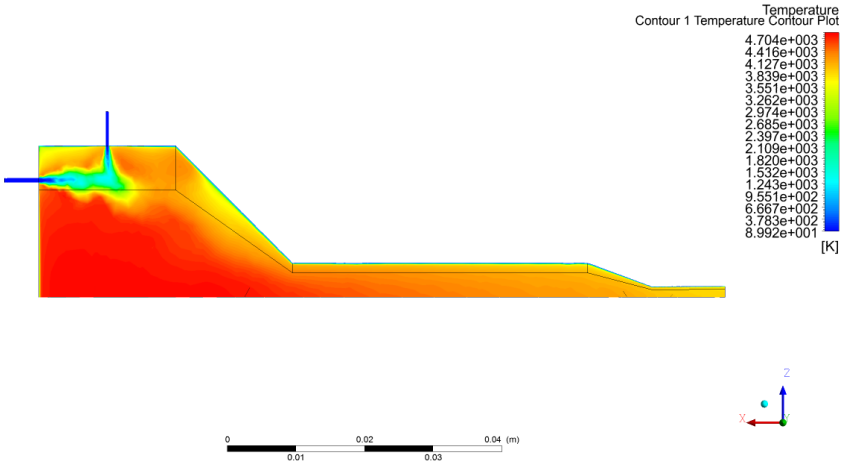

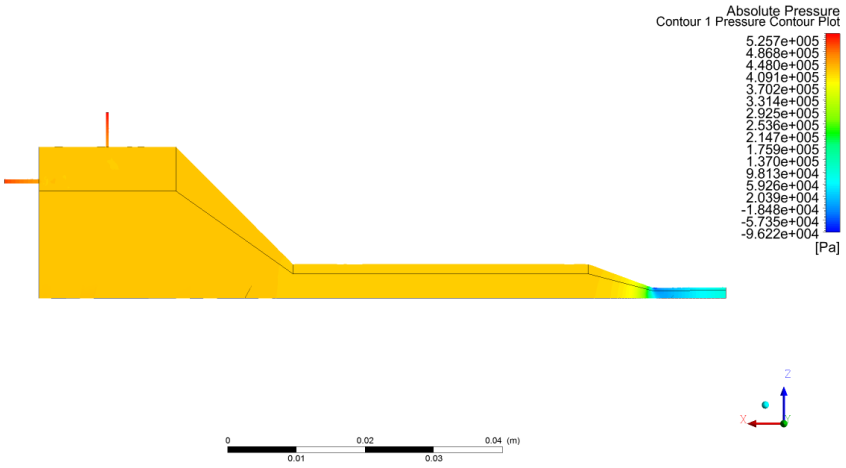
Absolute Pressure
Contour 1 Pressure Contour Plot
5.257e+005
4.868e+005
4.480e+005
4.091e+005
3.702e+005
3.314e+005
2.925e+005
2.536e+005
2.147e+005
1.759e+005
1.370e+005
9.813e+004
5.926e+004
2.039e+004
-1.848e+004
-5.735e+004
-9.622e+004
[Pa]
Z
X
Y
0
0.02
0.04 (m)
0.01
0.03

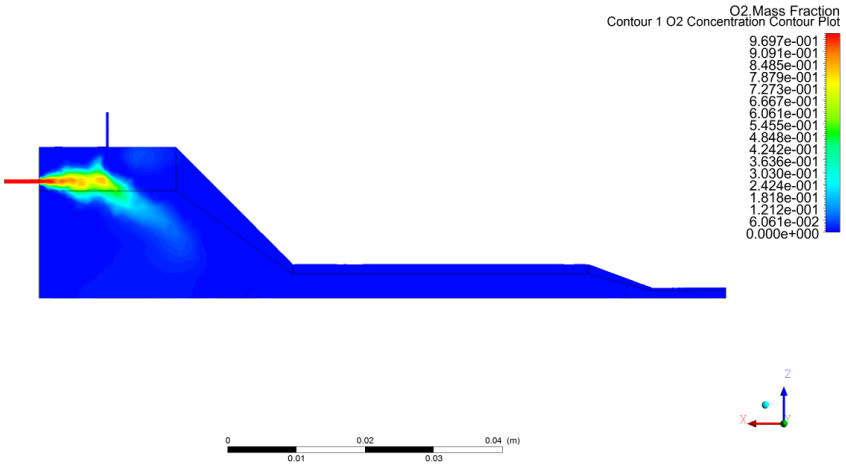
O2.Mass Fraction
Contour 1 O2 Concentration Contour Plot
9.697e-001
9.091e-001
8.485e-001
7.879e-001
7.273e-001
6.667e-001
6.061e-001
5.455e-001
4.848e-001
4.242e-001
3.636e-001
3.030e-001
2.424e-001
1.818e-001
1.212e-001
6.061e-002
0.000e+000
Z
X
Y
0
0.02
0.04 (m)
0.01
0.03

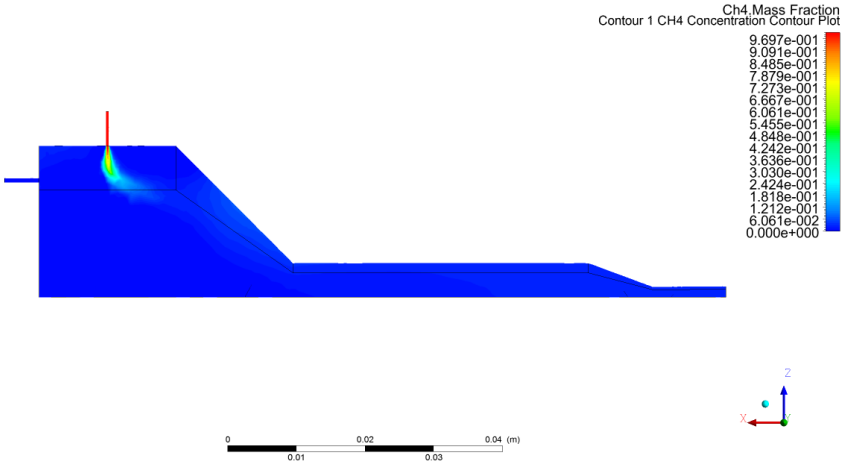
Ch4.Mass Fraction
Contour 1 CH4 Concentration Contour Plot
9.697e-001
9.091e-001
8.485e-001
7.879e-001
7.273e-001
6.667e-001
6.061e-001
5.455e-001
4.848e-001
4.242e-001
3.636e-001
3.030e-001
2.424e-001
1.818e-001
1.212e-001
6.061e-002
0.000e+000
Z
X
Y
0
0.02
0.04 (m)
0.01
0.03

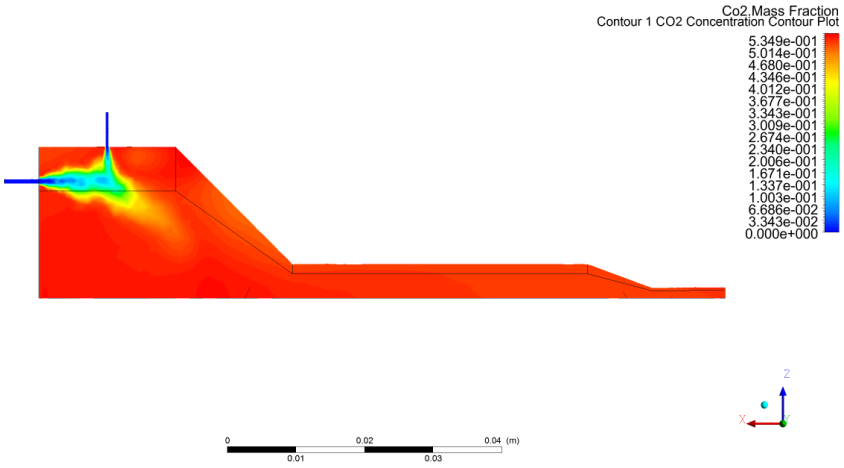
Co2,Mass Fraction
Contour 1 CO2 Concentration Contour Plot
5.349e-001
5.014e-001
4.680e-001
4.346e-001
4.012e-001
3.677e-001
3.343e-001
3.009e-001
2.674e-001
2.340e-001
2.006e-001
1.671e-001
1.337e-001
1.003e-001
6.686e-002
3.343e-002
0.000e+000
Z
X
Y
0
0.02
0.04 (m)
0.01
0.03

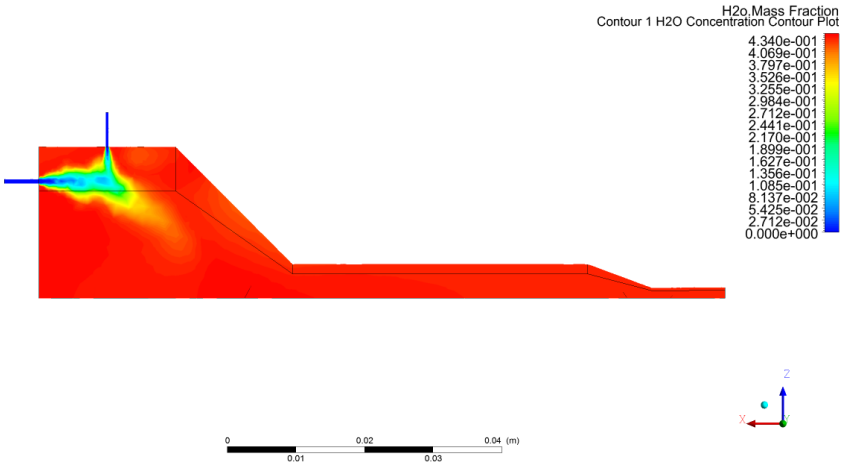
H2o,Mass Fraction
Contour 1 H2O Concentration Contour Plot
4.340e-001
4.069e-001
3.797e-001
3.526e-001
3.255e-001
2.984e-001
2.712e-001
2.441e-001
2.170e-001
1.899e-001
1.627e-001
1.356e-001
1.085e-001
8.137e-002
5.425e-002
2.712e-002
0.000e+000
Z
X
Y
0
0.02
0.04 (m)
0.01
0.03

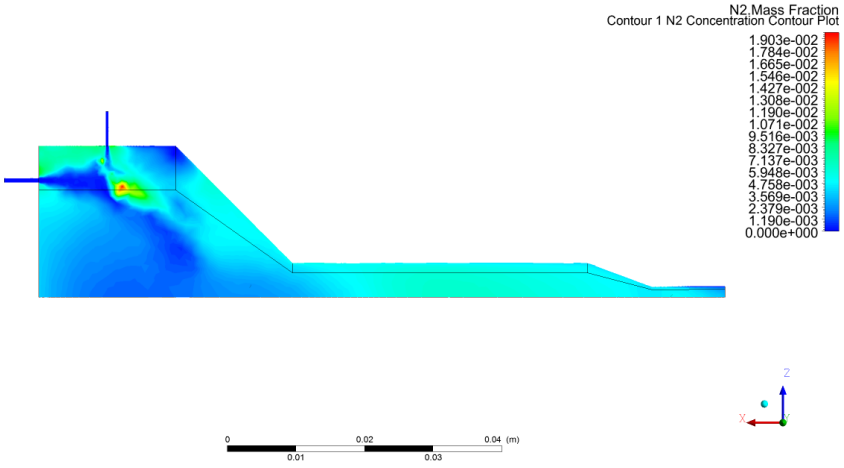
N2,Mass Fraction
Contour 1 N2 Concentration Contour Plot
1.903e-002
1.784e-002
1.665e-002
1.546e-002
1.427e-002
1.308e-002
1.190e-002
1.071e-002
9.516e-003
8.327e-003
7.137e-003
5.948e-003
4.758e-003
3.569e-003
2.379e-003
1.190e-003
0.000e+000
Z
X
Y
0
0.02
0.04 (m)
0.01
0.03

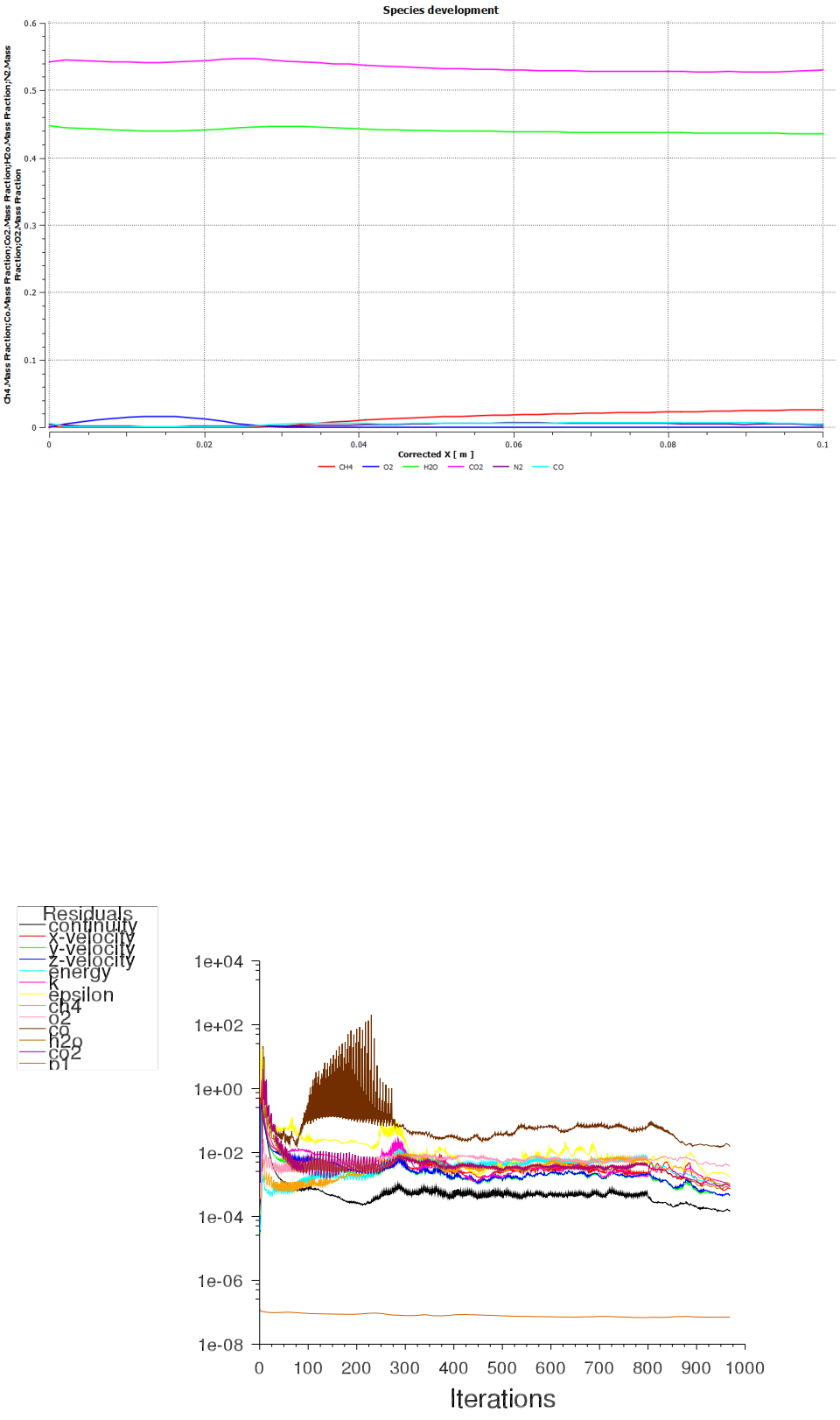

Figure H.28: Convergence history of scaled residuals for EdcWd2StepAmbient case.

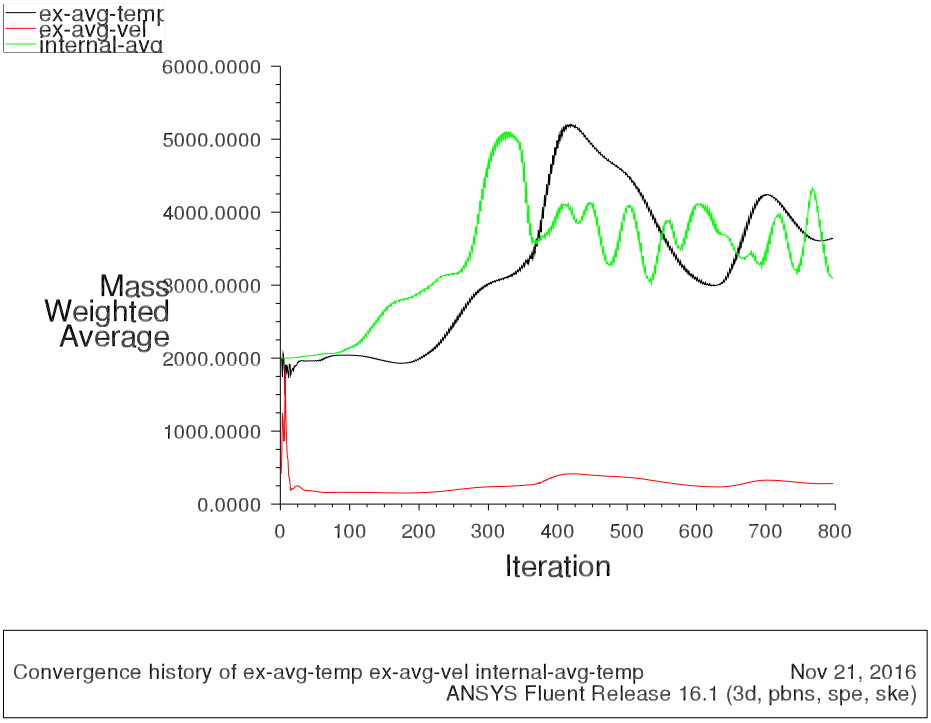

Figure H.29: Convergence history of integral quantities for EdcWd2StepAmbient case.

H.18. OutflowEquilibriumPressure

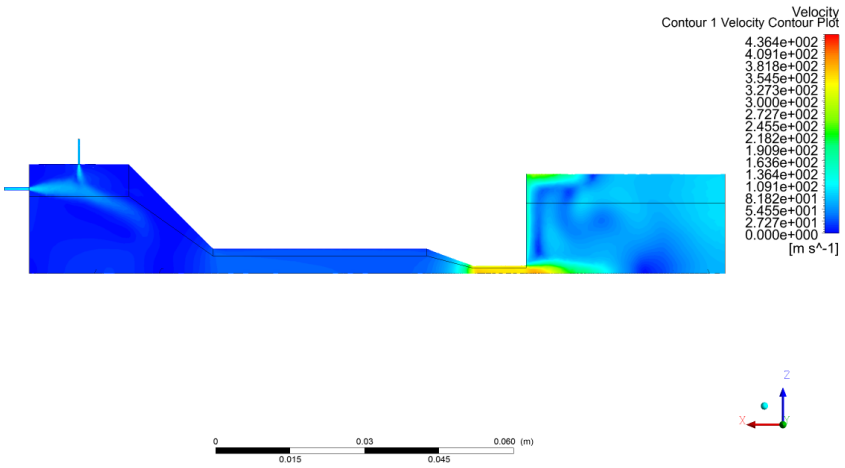

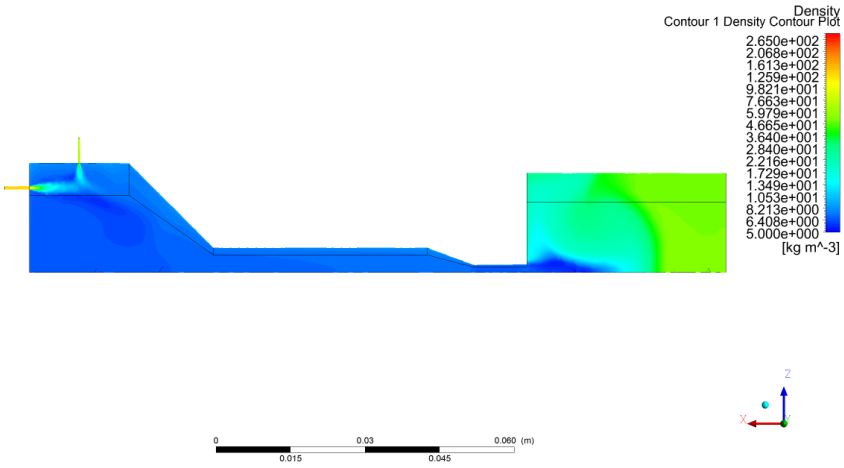
Density
Contour 1 Density Contour Plot
2.650e+002
2.068e+002
1.613e+002
1.259e+002
9.821e+001
7.663e+001
5.979e+001
4.665e+001
3.640e+001
2.840e+001
2.216e+001
1.729e+001
1.349e+001
1.053e+001
8.213e+000
6.408e+000
5.000e+000
[kg m^-3]
Z
X
Y
0
0.03
0.060 (m)
0.015
0.045

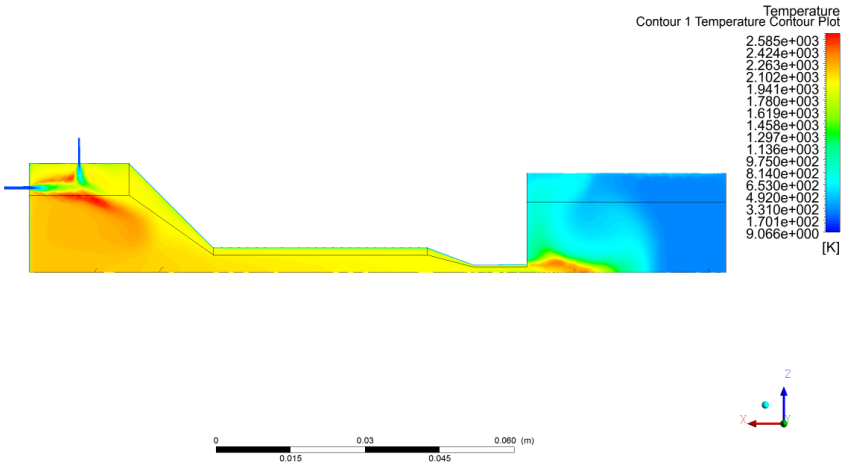
Temperature
Contour 1 Temperature Contour Plot
2.585e+003
2.424e+003
2.263e+003
2.102e+003
1.941e+003
1.780e+003
1.619e+003
1.458e+003
1.297e+003
1.136e+003
9.750e+002
8.140e+002
6.530e+002
4.920e+002
3.310e+002
1.701e+002
9.066e+000
[K]
Z
X
Y
0
0.03
0.060 (m)
0.015
0.045

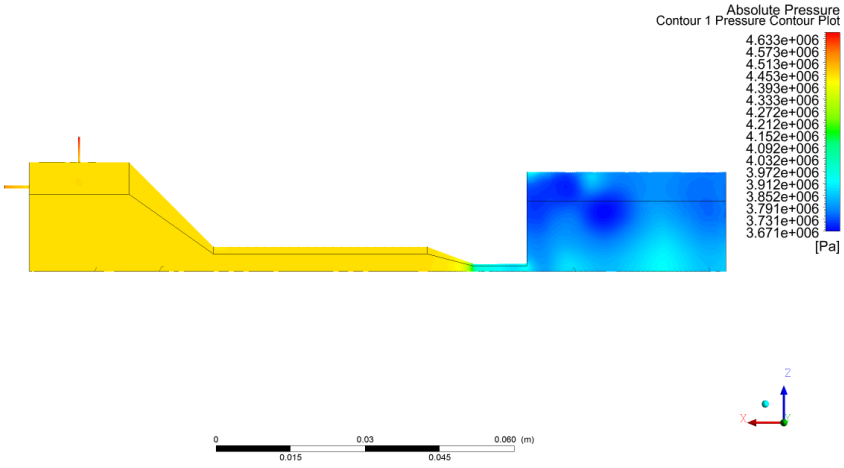
Absolute Pressure
Contour 1 Pressure Contour Plot
4.633e+006
4.573e+006
4.513e+006
4.453e+006
4.393e+006
4.333e+006
4.272e+006
4.212e+006
4.152e+006
4.092e+006
4.032e+006
3.972e+006
3.912e+006
3.852e+006
3.791e+006
3.731e+006
3.671e+006
[Pa]
Z
X
Y
0
0.03
0.060 (m)
0.015
0.045

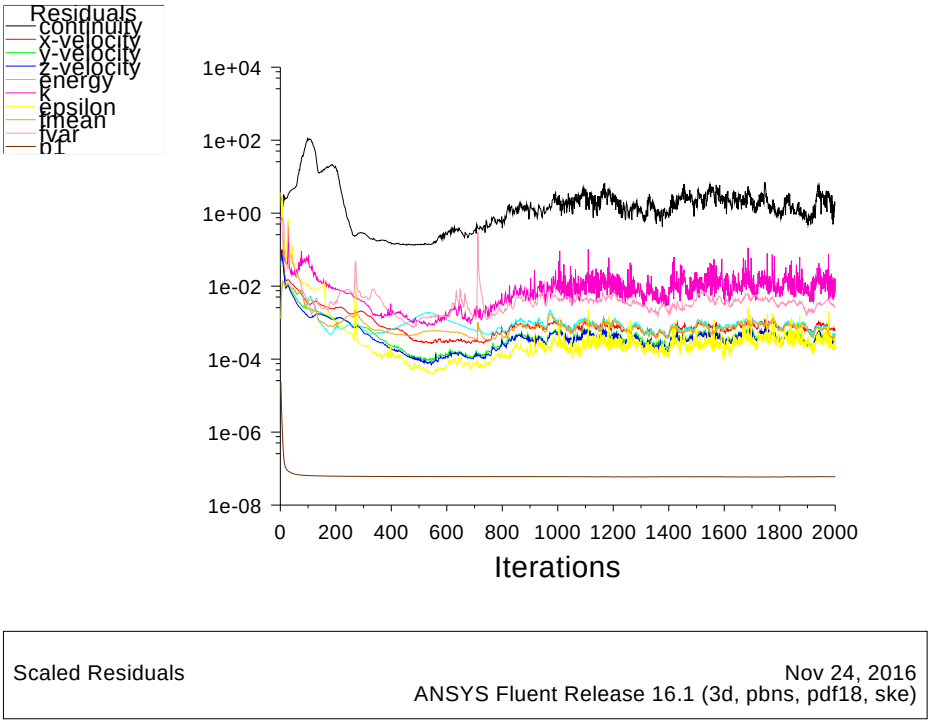

Figure H.30: Convergence history of scaled residuals for OutflowEquilibriumPressure case.

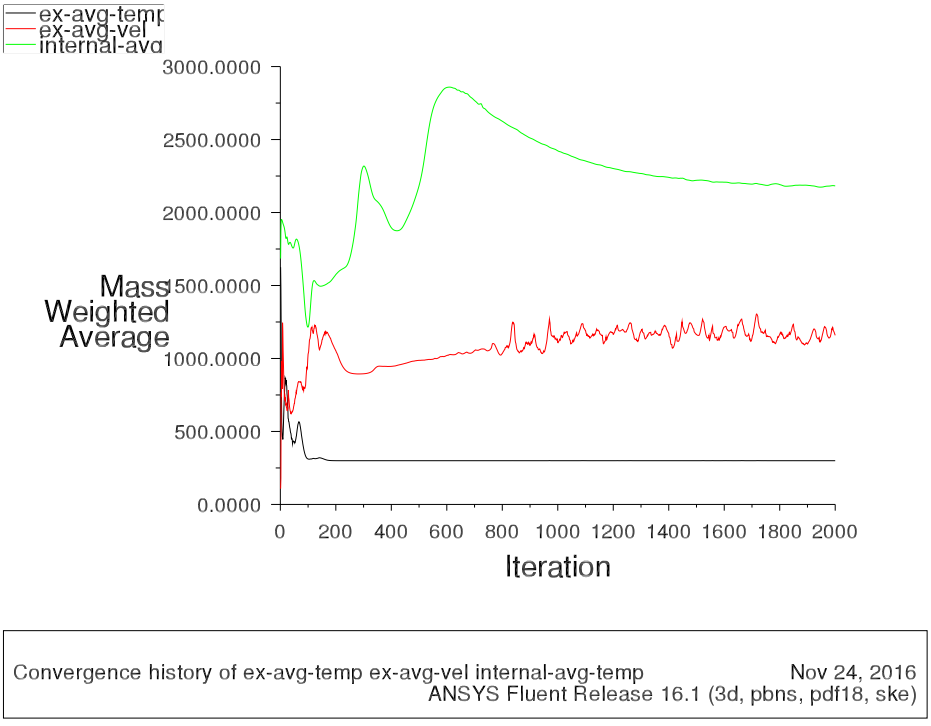

Figure H.31: Convergence history of integral quantities for OutflowEquilibriumPressure case.

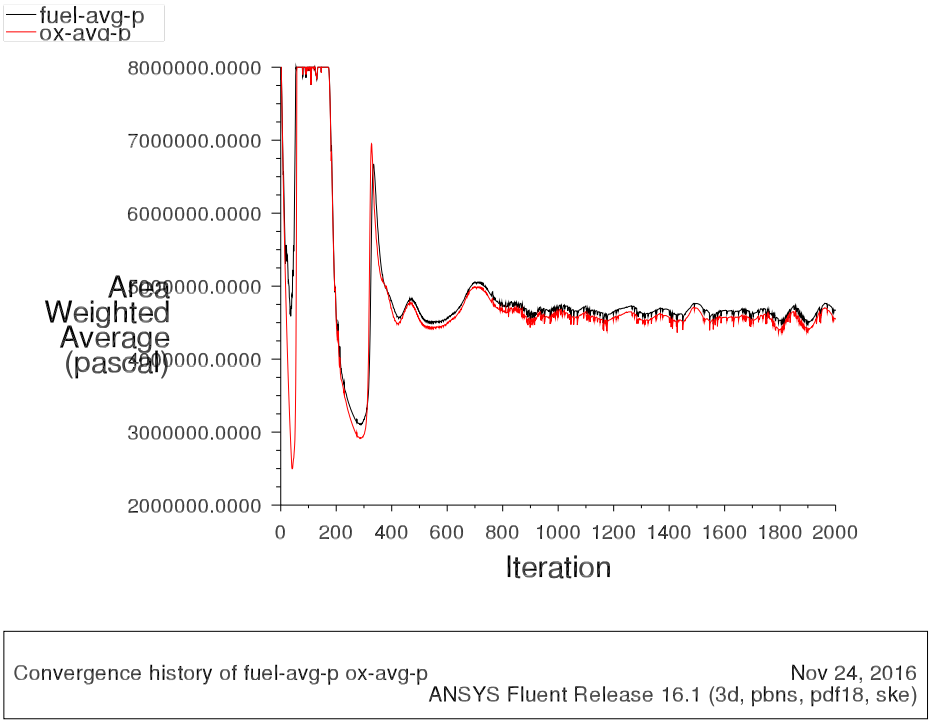

Figure H.32: Convergence history of secondary integral quantities for OutflowEquilibriumPressure case.